Amphibian skin peptides which inhibit nNOS: Structure and binding studies using heteronuclear NMR

A thesis submitted for the degree of Doctor of Philosophy

by

Margit Anneliese Apponyi B.Sc. (Hons)

from
The Department of Chemistry
The University of Adelaide

February, 2006

Table of contents

Abstract……... i
Statement of originality……...ii
Acknowledgements…….iii
List of figures……...v
List of tables……ix

Chapter 1 Introduction 12

1.1 Amphibian skin secretions as drugs..... 2
1.2 Antibacterial frog skin peptides..... 6
1.3 Anticancer frog skin peptides 7
1.4 Amphibian pheromones..... 8
1.5 Edmundson helical wheel representation of peptides..... 9

Chapter 2 Introduction to nuclear magnetic resonance spectroscopy of proteins and peptides..... 11

2.1 Nuclear magnetic resonance spectroscopy (NMR) 12
2.2 NMR of biological molecules..... 12
2.3 Random coil shifts 14
2.4 Secondary chemical shifts 15
2.5 The chemical shift index..... 16
2.6 Structure determination using molecular dynamics calculations 18
2.7 Restrained molecular dynamics and simulated annealing calculations..... 19
2.8 Ambiguous and stereo-specific assignments 20
2.9 Structure quality: Distance restraints and violations 21
2.10 Structure quality: Ramachandran plots..... 21
2.11 Solvent systems for NMR structure determination of peptides..... 22
2.12 Two dimensional NMR spectroscopy..... 22

2.13 TOCSY (TOtal Correlation SpectroscopY) 23
2.14 COSY (COrrelated SpectroscopY) 23
2.15 NOESY (Nuclear Overhauser Effect SpectroscopY) 24
2.16 HMBC (Heteronuclear Multiple Bond Coherence spectroscopy) 27
2.17 HSQC (Heteronuclear Single Quantum Coherence spectroscopy) 27
2.18 Three dimensional NMR of proteins: HNCACB 28
2.19 Three dimensional NMR of proteins: CBCA(CO)NH 30
2.20 Sequential assignment strategy 32
2.21 Main chain directed assignment strategy 33

Chapter 3 The structure determination of the sex pheromone of Litoria splendida 34

3.1 Litoria splendida 35
3.2 Splendipherin 39
3.3 Aims 40
3.4 Edmudson helical wheel analysis of splendipherin 41
3.5 Comparison of splendipherin with frenatin 3 42
3.6 NMR spectroscopy of splendipherin 43
3.7 Assignment of the NMR spectra of splendipherin 43
3.8 Secondary shift data 46
3.9 CSI Data 50
3.10 Nuclear overhauser effect data 51
3.11 Restrained molecular dynamics and simulated annealing calculations 52
3.12 Structure quality analysis 56
3.13 Summary 57
3.13.1 The nature of the structure of splendipherin 57
3.13.2 The movement of splendipherin on the surface of water 58

Chapter 4 Peptides which inhibit neuronal nitric oxide synthase 60

4.1 Nitric oxide synthases 61

4.2 Calmodulin 62

4.3 Peptides which bind to calmodulin – "baa" peptides 63

4.4 Peptides which bind to calmodulin – consensus hydrophobic residue sequences 64

4.5 Binding modes of peptides to calmodulin 65

4.6 Litoria lesueuri 66

4.7 nNOS active Australian amphibian peptides 67

4.8 Aims: 68

4.9 Bacterial protein expression systems 69

4.10 Transcription of genes using the T7 promoter system 69

4.11 Bacterial cell lines suitable for protein expression 71

4.12 Fusion proteins 71

4.13 Bacterial expression of isotopically labelled proteins 72

4.14 Preparation of ^{15}N labelled calmodulin for titration studies 73

4.15 Titrations of Australian amphibian skin peptides with calmodulin 77

4.16 Preparation of peptides for titration 77

4.17 Titration of calmodulin with splendipherin 78

4.18 Titration of a citropin 1.1 analogue with calmodulin 82

4.19 Titration of calmodulin with caerin 1.8 87

4.20 Summary 91

Chapter 5 Expression of ^{15}N labelled caerin 1.8 peptide for NMR complex studies 92

5.1 Aims 93

5.2 NMR studies of peptide-protein complexes 93

5.3 Construction of a vector to express caerin 1.8 as a fusion protein 94
5.4 Post-translational C-terminal amidation of synthetic caerin 1.8..... 96
5.5 Expression tests with the caerin 1.8-GST fusion..... 96
5.6 Summary..... 97

Chapter 6 Preparation and analysis of the calmodulin–caerin 1.8 complex 98

6.1 Aims..... 99
6.2 Preparation of ^{15}N and ^{13}C doubly labelled calmodulin 99
6.3 3D NMR spectroscopy of the calmodulin-caerin 1.8 complex 100
6.4 Co-assignment of the bound and unbound forms of calmodulin..... 105
6.5 Chemical shift analysis and discussion of structural implications 117
6.6 Summary..... 127

Chapter 7 Summary and future directions 128

7.1 The structure and movement of splendipherin 129
7.2 Titration of amphibian skin peptides with calmodulin..... 129
7.3 3D NMR studies of the complex between caerin 1.8 and calmodulin 130

Chapter 8 Experimental..... 131

8.1 Materials 132
8.2 Protein and peptide sample preparation..... 132
8.2.1 Buffers, solutions and growth media 132
8.2.2 Protein gels 133
8.2.3 DNA analysis..... 133
8.2.4 Bacterial cell lines..... 134
8.2.5 Bacterial expression of calmodulin..... 134
8.2.6 Anion exchange chromatography 135

8.2.7 Size exclusion chromatography 135
8.3 NMR spectroscopy 136
8.3.1 2D NMR Spectroscopy of splendipherin 136
8.3.2 Homonuclear NMR spectra of splendipherin 137
8.3.3 Heteronuclear NMR spectra of splendipherin 137
8.3.4 Structure Calculations 137
8.3.5 NMR sample preparation for titration studies 138
8.3.6 2D ^{15}N-HSQC titration experiments 139
8.3.7 HSQC conversion file 139
8.3.8 HSQC processing file 140
8.3.9 3D NMR spectroscopy 140
8.3.10 HNCACB conversion file 141
8.3.11 HNCACB processing file 141
8.3.12 CBCA(CO)NH conversion file 142
8.3.13 CBCA(CO)NH processing file 143

References 144

Abstract

Using 2-D NMR spectroscopy, the structure of the sex pheromone from *Litoria splendida* has been determined, in order to elucidate its mode of transport through the aquatic environment. The peptide was found form an α-helical structure, with a central flexible hinge region. The mode of transport through the aquatic environment has been discussed in relation to the structure.

Previous work indicated that the Australian amphibian host defence skin peptides that inhibit neuronal nitric oxide synthase (nNOS) were likely to act indirectly on the enzyme, by binding to the co-enzyme of nNOS, calmodulin. ^{15}N labelled calmodulin was expressed and purified *via* a bacterial protein expression system and a series of 2-D NMR ^{15}N-HSQC titrations was performed with Australian amphibian host defence skin peptides. in order to determine whether these peptides bind to calmodulin. The three peptides tested were found to bind, and with differing strengths of interaction. One of these was selected for further study.

^{15}N and ^{13}C doubly labelled calmodulin was then prepared in order to study the complex between this protein and the selected peptide, caerin 1.8, an Australian amphibian skin peptide isolated from *Litoria chloris*. A series of 3-D NMR spectra has been recorded on this complex. The backbone atom resonances have been assigned for free calmodulin and for the calmodulin-peptide complex, using a combination of main chain directed and sequential assignment strategies. By analysing the changes in chemical shift that occur upon binding the peptide, it was determined that the mode of binding involves a stronger interaction with the C-terminal domain than the N-terminal domain..

Statement of originality

This thesis contains no material that has been accepted for the award of any other degree or diploma in any other university or tertiary institution and, to the best of my knowledge and belief, contains no material, previously published or written by another person, except where due reference has been made in the text.

I give consent for a copy of my thesis, when deposited in the University of Adelaide library, to be available for loan and photocopying.

Margit Anneliese Apponyi

Acknowledgements

I wish to thank my supervisor, Professor John Bowie, for giving me the opportunity to undertake this project. His advice and guidance over the last four years have been greatly appreciated. I would also like to thank him for sending me overseas and interstate on a number of occasions to present my work at conferences and to collaborate with other researchers, where I gained a great deal of valuable experience and insight into my own and others' work.

I would like to acknowledge the Australian Postgraduate Award Scholarship and the Departmental Supplementary Scholarship which enabled me to undertake this body of work.

I owe a huge debt of thanks to Dr Horst Joachim Schirra of the University of Queensland, whose advice on my 3D NMR data has proven invaluable.

Thanks to the members of the Bowie group, past and present, especially Tara Pukala, Dr Mark Fitzgerald, Daniel Bilusich, Dr Kate Wegener and Dr Craig Brinkworth, for helpful chats on NMR and many other interesting topics.

Thanks also to Dr Grant Booker of the Biochemistry Department who allowed me to use his laboratory to express and purify my protein and to all the members of the Booker lab who were very willing to teach a chemist how to become a biochemist.

I wish especially to thank Dr Anita Merkel for teaching me how to undertake protein expression and Dr Kasper Kowalski for his help with my isotopically labelled NMR samples and assistance with NMRPipe.

Thanks also must go to the academic and technical staff at the Department of Chemistry, especially to Philip Clements, for teaching me how to drive the 600.

To all of my friends, especially Mark Egelstaff, Heidi Holzknecht, Emily Heylen, Tomais Byrt, Andrew Wilkins, Jonathan Webb and Dr Samuel Mickan, thanks for

your friendship, thesis-writing camaraderie and discussions about the nonsensical, which all helped me through the more difficult parts of my project.

Thank you to my sister Katalin for constant encouragement, and to the rest of my family, especially my Mum and Dad, whose love and support have really kept me going. I couldn’t have done it without you!

List of figures

Figure 1: Construction of the Edmundson helical wheel diagram..... 9
Figure 2: Spacing between residues which appear adjacent on the Edmundson helical wheel diagram is either 7 or 11 residues. 10
Figure 3: A 1D spectrum of splendipherin. 13
Figure 4: NOESY interactions expected in an α-helix. 25
Figure 5: NOE interaction intensity diagram for a typical α-helix and a typical β-sheet, the strength of interaction is indicated by the thickness of the bands. 26
Figure 6: A typical strip in an HNCACB spectrum, with two α-carbon correlations (blue) and two β-carbon correlations (green). 29
Figure 7: A typical strip from a CBCA(CO)NH spectrum, with correlations to Cα-1 and Cβ-1 only. 30
Figure 8: Overlaid view of a strip from an HNCACB spectrum and a CBCA(CO)NH spectrum, peaks which appear in both spectra can therefore be identified as arising from correlations with the preceding residue. 31
Figure 9: A typical specimen of *Litoria splendida.* 36
Figure 10: Location map for populations of *Litoria splendida*, distribution shaded in grey. 36
Figure 11: Partial HPLC traces of male (a) and female (b) *L. splendida.* 37
Figure 12: Splendipherin levels in male *L. splendida* secretions (averaged over a 3 year period). 38
Figure 13: Behavioural testing of female *L. splendida* with splendipherin: (a) initial conditions in the tank, the sample of splendipherin is indicated (b) after seven minutes the female frog rests on the sample (c) the path taken by the frog to reach the swab. 39
Figure 14: The EHW representation of splendipherin. Hydrophobic residues are shown in red and hydrophilic residues are shown in blue. 41
Figure 15: Overlaid 20 lowest energy structures for frenatin 3. 43

Figure 16: The assigned HN-HN region of the NOESY spectrum..... 45
Figure 17: Hα secondary shift plot for splendipherin. 46
Figure 18: Cα secondary shift plot for splendipherin. 46
Figure 19: HN secondary shift plot for splendipherin. 48
Figure 20: CSI data for splendipherin, negative CSI values indicating α-helical regions extending between residues 3 - 10 and 14 - 21. 50
Figure 21: NOE intensity diagram for splendipherin. Peak intensity is indicated by band height. Overlapped peaks are indicated by shaded areas. Peaks overlapped on the diagonal have been omitted..... 51
Figure 22: Low energy ensemble fitted over residues 3 - 10(a), fitted over residues 12 - 21(b) and over the entire well-defined regions (c). 54
Figure 23: Averaged and energy minimised structure of splendipherin (a) and superimposition of three low energy structures (b). 55
Figure 24: Ramachandran plot of psi and phi angles for <SA>. 57
Figure 25: Box diagram of the general nitric oxide synthase structure. Variations occur in each of the three isoforms. (Adapted from Kone, 2003 [85].) 61
Figure 26: Box diagram of the calmodulin sequence, showing the eight helical regions and the four calcium binding loops..... 62
Figure 27: The model calmodulin binding peptide designed by DeGrado and co-workers with clearly defined amphipathicity and a high positive charge from basic lysine residues..... 64
Figure 28: The protein encoding sequence of the inserted calmodulin gene..... 73
Figure 29: SDS-page gel of fractions 39 - 47 from a typical anion exhange column of unpurified calmodulin..... 75
Figure 30: SDS gel of fractions 40 - 56 of a typical superdex 75 column of calmodulin. 76
Figure 31: An Edmundson helical wheel representation of splendipherin. 78
Figure 32: The two helices of splendipherin, presented as Edmundson helical wheel diagrams..... 79
Figure 33: A section of the overlaid ^{15}N-HSQC spectra of the titration of calmodulin with splendipherin. Assigned residues in the unbound spectrum are labelled. The legend is shown below the spectrum. 81
Figure 34: An Edmundson helical wheel projection of citropin 1.1 showing the good delineation between hydrophobic and hydrophilic zones..... 83

Figure 35: An Edmundson helical wheel projection of the citropin 1.1 analogue (7) used to titrate with calmodulin. Hydrophobic residues are shown in red, hydrophilic residues are shown in blue and basic residues in green. 84
Figure 36: A region of the overlaid ^{15}N-HSQC spectra from the titration of calmodulin with the citropin analogue. 86
Figure 37: An Edmundson helical wheel projection of caerin 1.8. Hydrophobic residues are shown in red, hydrophilic residues in blue and basic residues in green. 87
Figure 38: Edmundson helical wheel diagrams of the first half (a) and second half (b) of caerin 1.8. 88
Figure 39: A region of the titration spectra of calmodulin bound to caerin 1.8. 90
Figure 40: The oligonucleotides encoding the caerin 1.8 sequence. 94
Figure 41: Translation of the oligonucleotide sequence inserted into the vector for expression of caerin 1.8. 95
Figure 42: Strip plots of the overlaid HNCACB(blue (Cα) and green(Cβ)) and CBCA(CO)NH (red) spectra, showing the correlations between HN and N of A102 with S101, in the calmodulin-caerin 1.8 complex (a) and in free calmodulin (b)..... 101
Figure 43: Strip plots of the overlaid HNCACB(blue (Cα) and green(Cβ)) and CBCA(CO)NH (red) spectra, showing the correlations between HN and N of T29 with T28, in the calmodulin-caerin 1.8 complex (a) and in free calmodulin (b)..... 102
Figure 44: Strip plot of the overlaid HNCACB (blue and green) and CBCA(CO)NH (red) spectra showing the bound (left) and unbound (right) peaks for T44. 103
Figure 45: A region of the overlaid ^{15}N-HSQC spectra of singly ^{15}N labelled free calmodulin (orange), ^{15}N labelled calmodulin bound to caerin 1.8 (purple) and the ^{15}N and ^{13}C doubly labelled calmodulin in complex with caerin 1.8 (green)..... 104
Figure 46: Cross sections of the HNCACB and CBCA(CO)NH spectra illustrating the sequential connectivites from residues D58 - T62 in the bound species. The HNCACB spectrum is shown in blue (Cα) and green (Cβ), the CBCA(CO)NH spectrum is shown in red. 107
Figure 47: CSI plot derived from Cα chemical shifts of free calmodulin. 118

Figure 48: CSI plot derived from Cα chemical shifts of calmodulin bound to caerin 1.8. 118
Figure 49: CSI plot derived from Cβ chemical shifts of free calmodulin. 119
Figure 50: CSI plot derived from Cβ chemical shifts of calmodulin bound to caerin 1.8. 119
Figure 51: Plot of the changes in calmodulin chemical shift which occur upon complexation with caerin 1.8 for ^{15}N. 121
Figure 52: Plots of change in calmodulin chemical shift which occur upon complexation with caerin 1.8 for CA. 122
Figure 53: Changes in calmodulin HN chemical shift upon complexation with caerin 1.8. 123
Figure 54: Changes in HN chemical shift experienced by calmodulin upon binding to caerin 1.8 and C20W peptide..... 124
Figure 55: Changes in HN chemical shift experienced by calmodulin upon binding to caerin 1.8 and M13 peptide. 125
Figure 56:Weighted average of the chemical shift changes over all three backbone atoms. 126

List of tables

Table 1: Alphabetical listing of some selected biologically active amphibian skin peptides 4
Table 2: Experimentally determined random coil shifts for Hα , HN and Cα, when followed by alanine, in the 20 commonly occurring amino acids. 14
Table 3: The chemical shift values used in the CSI method. 16
Table 4: CSI values used for α- and β-carbon chemical shift analysis 17
Table 5: Chemical shift assignments from NOESY and HSQC spectra for splendipherin 44
Table 6: Hα secondary shift data for splendipherin 47
Table 7: Cα secondary shift data for splendipherin. 47
Table 8: HN secondary shift data for splendipherin. 49
Table 9: Summary of restraints generated from the NOESY spectrum of splendipherin 52
Table 10: X-PLOR energies and violation statistics for <SA> (ensemble of twenty lowest energy structures) and $(SA)_r$ (energy minimised averaged structure). 53
Table 11: RMSD comparison for structures fitted over the separate well defined regions, and over the entire molecule. 56
Table 12: nNOS active peptides, their activity levels and species of origin. (Adapted from Apponyi et al, [10]) 68
Table 13: Quantities of splendipherin used for titration with calmodulin. 80
Table 14: Quantities of the citropin 1.1 analogue used in the titration with calmodulin. 85
Table 15: Quantities of caerin 1.8 used in the titration with calmodulin. 89
Table 16: Distribution of assigned chemical shift residues of bound and unbound calmodulin. 109
Table 17: N, HN, Cα, and Cβ chemical shifts for free calmodulin at pH 6.3, 25˚C, 31mM KCl and 6.3mM $CaCl_2$. 110

Table 18: N, HN, Cα, and Cβ chemical shifts for calmodulin bound to caerin 1.8 at pH 6.3, 25˚C, 31mM KCl and 6.3mM $CaCl_2$. 114
Table 19: Location of α-helices and β-sheets in bound and free calmodulin determined by CSI methods..... 120

Chapter 1 Introduction

1.1 Amphibian skin secretions as drugs

New drugs are constantly being developed as the need for better, cheaper and safer drugs increases. The two most popular approaches to designing new drugs are that of structural analysis of the drug target, in order to design specific inhibitors [1, 2] and that of natural product isolation, from analysis of traditional medicines or observation of particular animal species and the purification and characterisation of the active ingredients from such sources.

With bacteria becoming increasingly resistant to the classic array of antibiotics [3], the search for novel antibacterial agents has been intense [4]. Animals which appear to have a natural immunity to infection have become prime candidates for study.

Included in this group are amphibians, which generally live in dirty and stagnant water where bacteria and other contaminants are rife. This observation led to the discovery of the magainin peptides from *Xenopus laevis* by Zasloff, after he noticed that frogs returned to an unclean and stagnant tank after surgery remained healthy and that their wounds did not become infected by bacteria [5].

The discovery of these peptides has triggered the study of frog skin secretions by many other researchers intent on finding naturally occurring antibacterial peptides [6]. Thus, the skin secretions of other species of frog have been shown to contain a rich arsenal of biologically active compounds. These include alkaloids, such as those toxins produced by poison dart frogs [7], biogenic amines which function as neurotransmitter molecules [8, 9], steroidal compounds and many more biologically active peptides with a wide range of activities [10].

More than 25 species of Australian frogs have been studied fully by our group in the last decade, yielding over 150 bioactive peptides. Amongst these are analgesics which display orders of magnitude more powerful than morphine and compounds affecting muscle action, heart rate, blood pressure and capillary permeability [10, 11].

Although peptides are generally unsuitable for use as drugs by oral delivery, some of these compounds are already in medical use or being developed for medical usage today, for the treatment of conditions such as gastrointestinal infections, conjunctivitis and foot ulcers [12-16]. Some of these peptides, such as the magainins, are even active against the human immunodeficiency virus and show potential for use in combined contraceptive and infection prevention devices [17].

The peptide caerulein, isolated from the Australian frog *Litoria caerulea* in 1999, has clinical applications resulting from its ability to stimulate the gut and gall bladder [11, 18]. This peptide has also been found to occur in the skin secretions of a number of other species of frogs [19].

A list of selected biologically active peptides isolated by our group from Australian frogs appears in Table 1, (modified from [10]).

Table 1: Alphabetical listing of some selected biologically active amphibian skin peptides

Name	Sequence	MW	Species	Activity
Aurein 1.1	GLFDIIKKIAESI-NH_2	1444	a	1,2
Aurein 1.2	GLFDIIKKIAESF-NH_2	1478	a	1,2
Aurein 2.1	GLLDIVKKVVGAFGSL-NH_2	1613	a	1,2
Aurein 2.2	GLFDIVKKVVGALGSL-NH_2	1613	a	1,2,4
Aurein 2.3	GLFDIVKKVVGAIGSL-NH_2	1613	a	1,2,4
Caerin 1.1	GLLSVLGSVAKHVLPHVVPVIAEHL-NH_2	2582	b,c,d	1,2,3,4
Modification 1	GLLSVLGSVAKHVL**G**HVV**G**VIAEHL-NH_2	2502		1,2
Caerin 1.3	GLLSVLGSVAQHVLPHVVPVIAEHL-NH_2	2582	c	1,2
Caerin 1.4	GLLSSLGSVAKHVLPHVVPVIAEHL-NH_2	2600	c,d	1
Caerin 1.5	GLLSVLGSVVKHVIPHVVPVIAEHL-NH_2	2610	c	1,2
Caerin 2.1	GLVSSIGRALGGLLADVVKSKGQPA-OH	2392	b	1,4
Caerin 2.2	GLVSSIGRALGGLLADVVKSKEQPA-OH	2464	c	1,4
Caerin 2.4	GLVSSIGKALGGLLADVVKTKEQPA-OH	2450	c	4
Caerin 2.5	GLVSSIGRALGGLLADVVKSKEQPA-OH	2448	d	1,4
Caerin 3.1	GLWQKIKDKASELVSGIVEGVK-NH_2	2382	b,c	1
Caerin 3.2	GLWEKIKEKASELVSGIVEGVK-NH_2	2397	c	1
Caerin 3.3	GLWEKIKEKANELVSGIVEGVK-NH_2	2424	c	1
Caerin 3.4	GLEWKIREKANELVSGIVEGVK-NH_2	2452	c	1
Caerin 4.1	GLWQKIKSAAGDLASGIVEGIKS-NH_2	2326	c	1
Caerin 4.2	GLWQKIKSAAGDLASGIVEAIKS-NH_2	2340	c	1
Caerin 4.3	GLWQKIKQAAGDLASGIVEGIKS-NH_2	2353	c	1
Caerulein 1.1	pEQDY(SO_3)TGWMDF-NH_2	1351	h	5
Caerulein 1.2	pEQDY(SO_3)TGWFDF-NH_2	1367	b,i	5
Caerulein 2.1	pEQDY(SO_3)TGAHMDF-NH_2	1373	i	5
Citropin 1.1	GLFDVIKKVASVIGGL-NH_2	1613	i	1,2,3,4
Modification 1	GLF**A**VIKKVASVIGGL-NH_2	1569		1,2,3,4
Modification 14	GLFDVI**A**KVASVI**KK**L-NH_2	1699		1,2,3,4
Citropin 1.2	GLFDIIKKVASVVGGL-NH_2	1613	i	1,2,3,4
Citropin 1.3	GLFDIIKKVASVIGGL-NH2	1627	i	1,2,3,4

Name	Sequence	MW	Species	Activity
Dahlein 1.1	GLFDIIKNIVSTL-NH_2	1430	j	1
Dahlein 1.2	GLFDIIKNIFSGL-NH_2	1434	j	1
Dahlein 4.1	GLWQLIKDKIKDAATGLVTGIQS-NH_2	2486	j	
Dahlein 5.1	GLLGSIGNAIGAFIANKLKP-OH	1952	j	4
Frenatin 3	GLMSVLGHAVGNVLGGLFKPKS-OH	2180	q	4
Lesueurin	GLLDILKKVGKVA-NH_2	1352	r	4
Maculatin 1.1	GLFGVLAKVAAHVVPAIAEHF-NH_2	2145	s	1,2,3,4
Maculatin 1.2	GLFGVLAKVASHVVAAIAEHFQA-NH_2	2360	s	1,2
Maculatin 1.3	GLLGLLGSVVSHVVPAIVGHF-NH_2	2068	g	1,2
Maculatin 1.4	GLLGLLGSVVSHVLPAITQHL-NH_2	2121	g	1,2
Maculatin 2.1	GFVDFLKKVAGTIANVVT-NH_2	1878	s	1,2
Signiferin 1	RLC*IPYIIPC*-OH	1187	v	5
Splendipherin	GLVSSIGKALGGLLADVVKSKGQPA-OH	2364	b,c	4,6
Tryptophyllin L 1.4	FPFPWL-NH_2	805	t	5
Uperin 1.1	pEADPNAFYGLM-NH_2	1208	w	5
Uperolein	pEPDPNAFYGLM-NH_2	1232	x	5

Activities : (1) antibiotic ; (2) anticancer ; (3) fungicidal ; (4) nNOS inhibitor ; (5) smooth muscle active neuropeptide ; (6) sex pheromone ; *indicates a disulphide bridge.

Species : (a) *L. aurea, L. raniformis*[20] ; (b) *L. splendida*[21] ; (c) *L. caerulea*[22] ; (d) *L. gilleni*[23] ; (h) various *Litoria* species [12]; (i) *L. citropa* [24]; (j) *L. dahlii* [25]; (q) *L. infrafrenata*[26] ; (r) *L. lesueuri* [27]; (s) *L. genimaculata*[28] ; (t) *L. rubella*[29] ; (u) *L. rothii*[25]; (v) *C. signifera*[10] ; (w) *U. inundata* [19]; (x) various *Uperoleia* species[12]

1.2 Antibacterial frog skin peptides

The majority of Australian frog species have at least one antibacterial peptide present in their skin secretions. Good examples of potent antibiotic peptides are caerin 1.1, citropin 1.1 and aurein 1.2. (See Table 1.)

Whilst they are generally more active against Gram positive bacteria (at concentrations as low as 3 μg/mL) some are also active against Gram negative bacteria, for example caerins 1.1, 1.4 and 1.5 which are active at 25 μg/mL against *Pastuerella multocida* [10].

These peptides are thought to act on bacteria by disrupting their cell membranes, so that small molecules and ions begin to travel unchecked through the cell walls, disrupting their ionic potential and eventually causing cell lysis. The exact mechanism is still under discussion [17, 30, 31].

Two main models which are thought to be correct, are the "barrel-stave" mechanism, and the "carpet" mechanism. In the former, peptides aggregate at the cell surface. They eventually insert into the membrane and generate a pore [32]. The latter involves the assembly of the peptides in a carpet-like monolayer on the cell surface, causing strain on the curvature of the membrane, such that it is eventually dismantled into a series of micelles [33].

The charge of the peptides has a significant influence on the strength of the antibiotic effect. The first stage of both mechanisms discussed above involves attraction by electrostatic interactions to the negatively charged cell surface. Peptides with an overall positive charge are generally much more active than those which are anionic, although a few examples of anionic antibacterial peptides have been reported [17].

The degree of amphipathicity and the propensity to form an α-helix also significantly influence the antibacterial activity of these peptides [34].

Many antibacterial peptides also feature post-translational modifications that are necessary to maintain their activity. Amongst the most common modifications are disulphide bridges and C-terminal amidation, the latter being present on the majority of the antibacterial peptides isolated from Australian amphibian skin secretions [17, 35].

1.3 Anticancer frog skin peptides

Many amphibian skin peptides have also tested positive for anticancer activity. For example, the magainins from *Xenopus laevis*, and maculatin 1.1 and aurein 1.1 from Australian frogs [36]. The mechanism of action of these peptides against cancer cells is thought to be similar to the mechanism of action on bacterial cells, that is, the cell membranes are disrupted to a point where structural integrity of the cell is lost, causing cell lysis [20].

Many peptides exhibit both antibiotic and anticancer activity. This is not surprising considering that the mechanisms are very similar. Examples of peptides which display both activities are maculatin 1.1 and also many members of the caerin and aurein families [10].

What is surprising is that these peptides are highly selective in targeting cancerous cells over healthy cells. This is surmised to be because of slight changes in cellular potentials between cancerous cells and normal differentiated cells, due to the higher metabolism levels of the former [36]. Cytoskeletal modifications and alterations of the extracellular matrix surrounding these cells have also been suggested as possible indicators of their cancerous nature which cause the peptides to bind more favourably [17].

1.4 Amphibian pheromones

Pheromones are chemical messenger molecules which cause a behavioural response in an animal and are commonly involved in mating and courtship. Although alarm responses had been characterised in *Bufo bufo* tadpoles upon exposure to crushed tadpoles as early as 1949 [37], the first pheromone identified from a vertebrate was only discovered quite recently, only a decade ago, in 1995 [38].

This female-attractant sex pheromone came from the *Urodela* family of animals, more specifically from the Japanese fire-bellied newt, *Cynops pyrrhogaster*. Sodefrin (1), a 10-residue peptide, was isolated by Kikayuma and co-workers and was named by them for the Japanese word "to solicit". The sequence is shown below.

(1) Sodefrin: SIPSK DALLK-OH

Tests for the species specificity of sodefrin were performed using another species of newt, *Cynops ensicauda*, the sword-tailed newt. The pheromone had no effect on these animals. However, it was discovered during these tests that *C. ensicauda* also had a female attractant aquatic sex pheromone. This 10 residue peptide (2) was finally isolated in 2000 by Yamamoto and co-workers and was named silefrin [39]. Silefrin differs from sodefrin at positions 3 and 8, having the sequence shown below.

(2) Silefrin: SILSK DAQLK-OH

Both peptide hormones are secreted from the abdominal glands in the cloacae of the animals. Both pheromones are species-specific female attractants. The male newts send the pheromone through the water in their aquatic environment by vigorously shaking their tails to disperse the water from around their cloacae [38, 39].

A 22kD proteinaceous courtship pheromone has also been discovered in a terrestrial salamander, *Plethodon jardani*. This protein hormone is deposited directly onto the skin of the female by the male from his mental glands, located under his chin, which provides a very simple means of direct transportation to the female by physical

contact between the animals [40]. This pheromone is thought to shorten the courtship process.

More recently, the first anuran sex pheromone was discovered by members of our group; this will be discussed more fully in section 3.2.

1.5 Edmundson helical wheel representation of peptides

In 1967, Schiffer and Edmundson devised a method of displaying an end-on view of a peptide, which has since become known as the Edmundson helical wheel [41]. This technique is particularly useful in analysing the propensity or potential of a peptide to form an amphipathic α-helix. An amphipathic α-helix is one in which all hydrophobic residues are on one face and all hydrophilic residues are on the other.

Construction of an Edmundson helical wheel involves plotting the residues of a peptide about a "wheel" diagram. Each residue takes 100º of a circle, with a full turn of the helix completed in 3.6 residues. Therefore the residues are plotted around a circle as shown below in Figure 1, to give the helical wheel diagram.

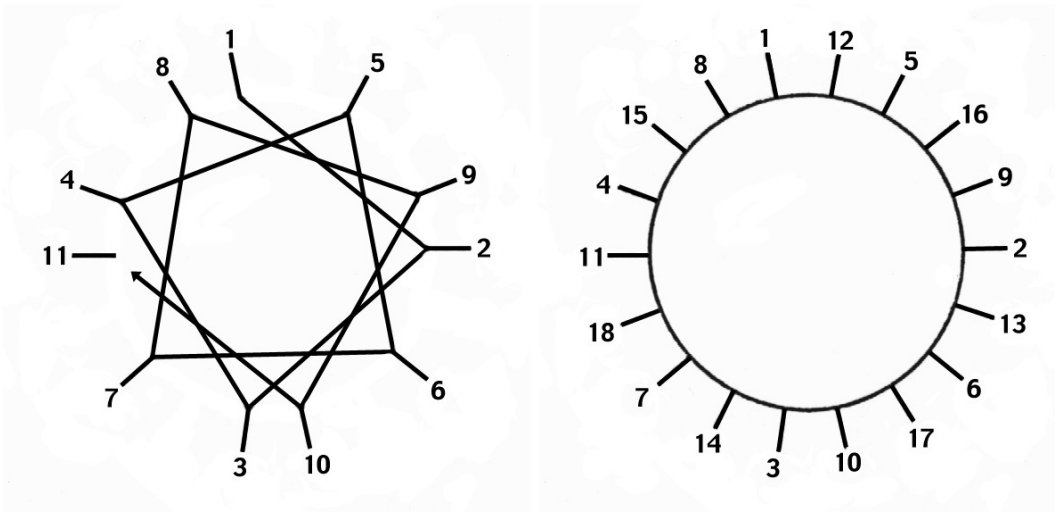

Figure 1: Construction of the Edmundson helical wheel diagram.

Using this methodology, peptide sequences can be quickly characterised as to whether they are amphipathic or not, without the need for complicated analysis. Also, due to the continuous nature of the helical structure, many residues sitting adjacent on the diagram have the same spacing relationship.

Amino acids which are 7 residues apart in the protein sequence lie in adjacent positions when the sequence is transferred to the Edmundson helical wheel diagram. Positioning large aliphatic or aromatic amino acids 7 residues apart in the sequence places them along the same face of the peptide, when in an α-helical conformation. This can be seen in Figure 2.

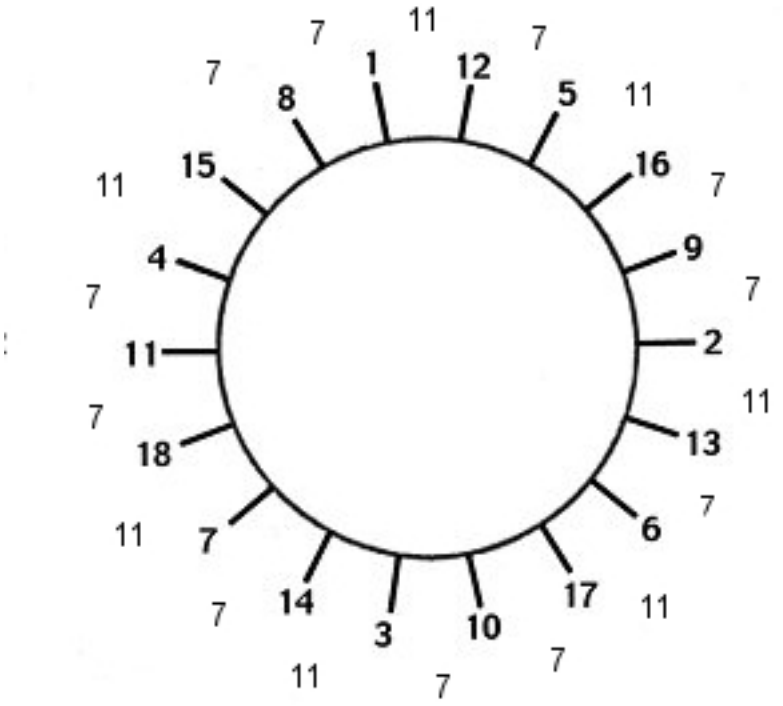

Figure 2: Spacing between residues which appear adjacent on the Edmundson helical wheel diagram is either 7 or 11 residues.

Chapter 2 Introduction to nuclear magnetic resonance spectroscopy of proteins and peptides

2.1 Nuclear magnetic resonance spectroscopy (NMR)

"The determination of the 3D structure of a biological molecule is the starting point in the understanding of molecular mechanisms involved in its complex biochemical reactions. The molecular architecture of multi-molecular systems such as membranes and chromosomes provides the key to the fascinating field of molecular biology. Stereochemical details of biological macro-molecules and their interactions with pharmacological agents form the basis of drug design" Govil and Hosur, 1982 [42].

NMR is an extremely powerful tool in structure determination. Because the technical details of NMR have been well documented and are readily available [43-48], only a brief introduction to NMR in the context of biological molecules will be given here, followed by a discussion of the data obtained using each NMR experiment applied in these studies.

2.2 NMR of biological molecules

The elements that are of most interest when studying biomolecules are hydrogen, carbon and nitrogen. ^{1}H is the most commonly occurring isotope of hydrogen, and conveniently is also spin active. Usually when considering small organic molecules, a ^{1}H NMR spectrum is enough to identify the compound and to identify its stereochemistry [46]. However, when a molecule becomes more complicated, more complicated spectroscopy must then be used.

Carbon and nitrogen both have naturally occurring isotopes that are spin active. The bulk of carbon atoms are ^{12}C, which is not spin active, however, approximately 1.1% of natural isotopic abundance is ^{13}C, which is spin active. This means that with long acquisition times, a carbon spectrum can be obtained on an unenriched natural ^{13}C abundance sample. The most commonly occurring isotope of nitrogen is ^{14}N, which is also not spin active, but ^{15}N comprises approximately 0.37% of natural nitrogen, and is spin active. Because the proportion of ^{15}N is so small, acquisition times for generating a ^{15}N spectrum from an unenriched sample are prohibitively long, and so

compounds in which the nitrogen spectrum is to be studied must be made specially using a ^{15}N enriched nitrogen source, as is the case in this work. [44] The most common method for doing this is by using bacterial protein expression, as will be discussed in section 4.9.

As the size of the molecules being studied increases, it becomes more difficult to assign the peaks in a 1D NMR spectrum. More and more atoms will coincide at the same chemical shift. For example, a 1D spectrum of the male sex pheromone of *Litoria splendida*, splendipherin, is shown in Figure 3. The spectrum is extremely overlapped. Attempting to assign this spectrum would prove futile as there are more than 150 ^{1}H nuclei in a splendipherin molecule, but there are clearly fewer than that number of well defined peaks. 2D NMR experiments make this unnecessary.

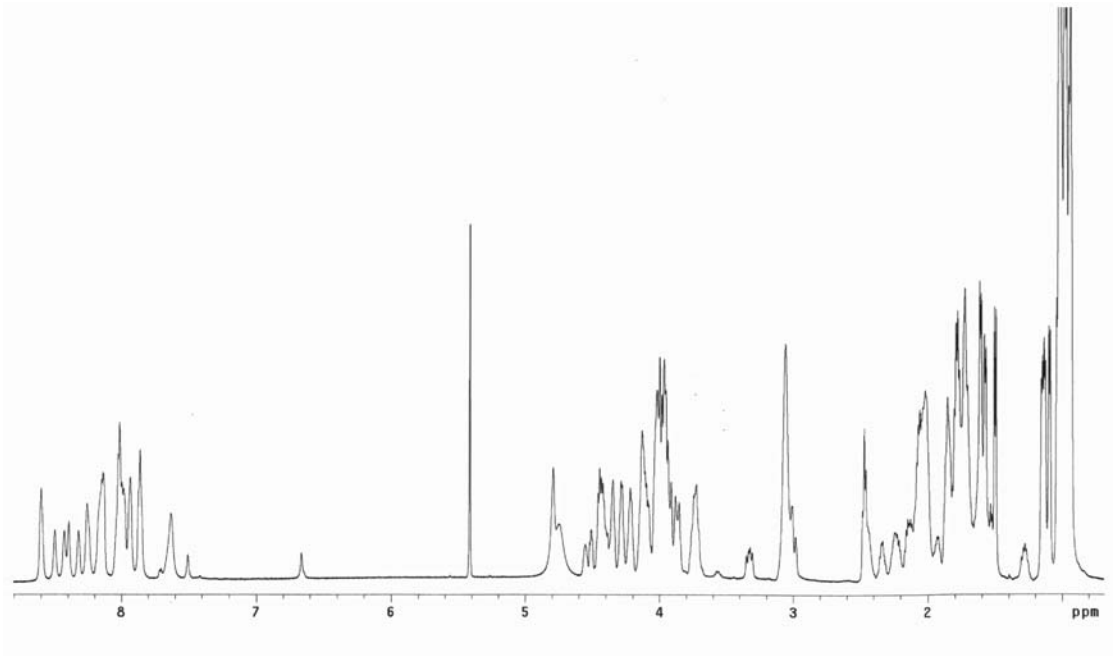

Figure 3: A 1D spectrum of splendipherin.

2.3 Random coil shifts

Even before any structure calculations have been performed, a lot of information can be gleaned from a series of fully assigned NMR spectra and their chemical shift information. When a protein or peptide exists in an unstructured form, its amino acid constituents follow certain trends in terms of chemical shifts.

These chemical shifts are known as "random coil" shifts and have been determined both experimentally and statistically. The experimentally derived random coil shifts for α-protons published by Wishart and Sykes are given in Table 2. These shifts were determined using the hexapeptide GGXAGG, in denaturing conditions. This hexapeptide was designed to minimise secondary structure formation in order to give a true random conformation [49].

Table 2: Experimentally determined random coil shifts for Hα , HN and Cα, when followed by alanine, in the 20 commonly occurring amino acids.

Amino acid	Hα shift	HN proton shift	N shift	Cα shift
Ala	4.32	8.24	123.8	52.5
Cys	4.55	8.32	118.7	58.2
Asp	4.64	8.34	120.4	54.2
Glu	4.35	8.42	120.2	56.6
Phe	4.62	8.3	120.3	57.7
Gly	3.96	8.33	108.8	45.1
His	4.73	8.42	118.2	55
Ile	4.17	8	119.9	61.1
Lys	4.32	8.29	120.4	56.2
Leu	4.34	8.16	121.8	55.1
Met	4.48	8.28	119.6	55.4
Asn	4.74	8.4	118.7	53.1
Pro	4.42	n/a	n/a	63.3
Gln	4.34	8.32	119.8	55.7
Arg	4.34	8.23	120.5	56
Ser	4.47	8.31	115.7	58.3
Thr	4.35	8.15	113.6	61.8
Val	4.12	8.03	119.2	62.2
Trp	4.66	8.25	121.3	57.5
Tyr	4.55	8.12	120.3	57.9

Statistically determined random coil shifts agree well with the experimentally determined set. A general trend which is well documented is that protons which are folded in an α-helical peptide tend to experience an upfield shift, and those in a β-sheet tend to experience a downfield shift. The reverse is true for α-carbons. In an alpha helical fold all α-carbons experience a downfield shift and those α-carbons which are part of a β-sheet experience upfield shifts [49].

2.4 Secondary chemical shifts

To put chemical shifts to use in structure determination, the secondary shifts of a molecule of interest must be found; these values are referred to also as Δδ values. This simply means finding their differences from the random coil shifts, as described in Equation 1, where δ_{obs} is the observed chemical shift, δ_{RC} is the random coil chemical shift for that residue and $\Delta\delta$ is the secondary shift.

$$\Delta\delta = \delta_{obs} - \delta_{RC}$$

Equation 1

For example, an Alanine α-proton with a chemical shift of 4.2 ppm has a secondary shift of -0.12 ppm. This corresponds to an upfield shift, which would indicate that this residue is likely to be part of a β-sheet. Plotting the secondary shifts of a structured protein gives a curved graph. The shape of the curve indicates which regions have secondary structure and which type of secondary structure is present.

Smoothing the data, or averaging over a window of n ± 2 residues, enables otherwise confusing data to be interpreted easily, as it makes trends in the data more obvious [50].

2.5 The chemical shift index

Another way to analyse the secondary shift data is to use the chemical shift index (CSI) method developed by Wishart and Sykes [51]. This method of data analysis involves "digitisation" of the secondary shift data. Each shift obtained is compared with a set range of values. These values differ slightly from the random coil values, and are shown in Table 3.

Table 3: The chemical shift values used in the CSI method.

Amino acid	Hα range
Ala	4.35 ± 0.10
Cys	4.65 ± 0.10
Asp	4.76 ± 0.10
Glu	4.29 ± 0.10
Phe	4.66 ± 0.10
Gly	3.97 ± 0.10
His	4.63 ± 0.10
Ile	3.95 ± 0.10
Lys	4.36 ± 0.10
Leu	4.17 ± 0.10
Met	4.52 ± 0.10
Asn	4.75 ± 0.10
Pro	4.44 ± 0.10
Gln	4.37 ± 0.10
Arg	4.38 ± 0.10
Ser	4.5 ± 0.10
Thr	4.35 ± 0.10
Val	3.95 ± 0.10
Trp	4.7 ± 0.10
Tyr	4.6 ± 0.10

A shift value which falls within the given range is assigned a value of zero. A shift value which is greater than the given range is assigned a value of one. Any shift value which falls below the given range is assigned a value of negative one. Secondary structure is indicated by four or more of the same value (1 or –1) not interrupted by an opposite value, with no two consecutive zero values [49]. A helical region is indicated by a series of negative values; β-sheet is indicated by a series of positive values.

The CSI method can also be applied to α-carbons and β-carbons. The trends caused by secondary structure formation in the carbon data are opposite to those in proton data. A series of positive values indicates an α-helix with α-carbon CSI data, however β-carbon data can only accurately be used to definitively identify β-sheet structure [52].

The values used for α- and β-carbon analysis are shown in Table 4.

Table 4: CSI values used for α- and β-carbon chemical shift analysis

Amino acid	Cα range	Cβ range
Ala	52.5 ± 0.70	19.0 ± 0.70
Cys	58.3 ± 0.70	28.6 ± 0.70
Asp	54.1 ± 0.70	40.8 ± 0.70
Glu	56.7 ± 0.70	29.7 ± 0.70
Phe	57.9 ± 0.70	39.3 ± 0.70
Gly	45.0 ± 0.70	Use CSI of Hα
His	55.8 ± 0.70	32.0 ± 0.70
Ile	62.6 ± 0.70	37.5 ± 0.70
Lys	56.7 ± 0.70	32.3 ± 0.70
Leu	55.7 ± 0.70	41.9 ± 0.70
Met	56.6 ± 0.70	32.8 ± 0.70
Asn	53.6 ± 0.70	39.0 ± 0.70
Pro	62.9 ± 0.70	31.7 ± 0.70
Gln	56.2 ± 0.70	30.1 ± 0.70
Arg	56.3 ± 0.70	30.3 ± 0.70
Ser	58.3 ± 0.70	62.7 ± 0.70
Thr	63.1 ± 0.70	68.1 ± 0.70
Val	63.0 ± 0.70	31.7 ± 0.70
Trp	57.8 ± 0.70	28.3 ± 0.70
Tyr	58.6 ± 0.70	38.7 ± 0.70

2.6 Structure determination using molecular dynamics calculations

When the NOESY (see section 2.15) spectrum of a peptide has been fully assigned, the volumes of the cross-peaks are determined by integration. The intensity of these peaks is inversely proportional to the distance between the interacting atoms. They are related mathematically by Equation 2, where r_{ij} is the distance between the interacting nuclei i and j, I_{ij} is the intensity of the peak and A(I) is an intensity independent proportionality factor. This is determined using the ten weakest (I_w) and ten strongest (I_s) NOE cross-peaks in the spectrum according to Equation 3 [53].

$$ri_j = \left[\frac{A(I)}{I_{ij}}\right]^{1/6}$$

Equation 2

$$A(I) = \left[\frac{I - I_s}{I_w - I_s}\right]\left[A(I_w) - A(I_s)\right] + A(I_s)$$

where $A(I_w) = (5.0\text{Å})^6 I_w$ and $A(I_s) = (1.8\text{Å})^6 I_s$

Equation 3

Therefore, by determination of the intensity of the NOESY cross-peaks, the distance between the atoms can be estimated. This gives rise to a set of distance restraints. The distance restraints can then be used as part of the molecular dynamics calculations.

2.7 Restrained molecular dynamics and simulated annealing calculations

In a molecular dynamics calculation, the initial geometry of the molecule being studied is assigned empirically [54]. The calculations simulate the atoms moving according to classical laws of motion. In Restrained Molecular Dynamics (RMD) calculations, the distance data derived from the NOESY spectrum are included as restraints according to the method of Xu *et al* [53]. These data are given as ranges rather than definite distances, due to a number of factors which can affect the intensity of peaks such as spin diffusion, internal motion and chemical exchange [44].

The system is allowed to evolve for a set number of steps. The forces acting on each atom are evaluated after each step and their trajectories are updated [55]. Excess potential energy is converted to kinetic energy during the calculations and a theoretical heat bath "absorbs" this kinetic energy [56].

RMD calculations used for this project were combined with Simulated Annealing (SA). That is, the simulated system is heated to high temperature and cooled slowly to overcome any possible local energy minima, allowing it to reach the global energy minimum, or most stable conformation [54].

These calculations are repeated a number of times to give rise to a set of structures which satisfy the restraints of the distance data and have stable psi and phi torsion angles about the amide bonds. When an ensemble of sixty structures has been calculated and ranked in order of energy, the twenty lowest energy structures are assessed and averaged to give the final structure.

2.8 Ambiguous and stereo-specific assignments

Where chemical shifts overlap and two peaks coincide in the NOESY spectrum, the peaks cannot be integrated according to the usual manner. The contribution of both sets of interacting atoms must be considered. For this reason, the volumes of ambiguously assigned peaks are treated as the sum of the volumes of each contributing peak.

Although this is less accurate than integration of individual peaks, this method allows inclusion of ambiguous peak data into the calculations. This is known as sum averaging, and increases the quality of the overall assembly of structures. An improvement in the accuracy of the calculated structures is caused by including the maximum number of NOE peaks as distance restraints [40, 57].

When prochiral centres such as methyl and methylene groups give rise to degenerate signals, stereospecific assignment is necessary to allow the maximum amount of information to be derived from the spectrum. This can be performed using coupling constants, but this is tedious and not always possible. Coupling constants must be obtained from analysis of a well dispersed 1D NMR spectrum of the protein or peptide of interest, such ideal spectra are rarely obtained, except when studying very small systems.

To overcome this problem, the floating chirality method is used. Protons are arbitrarily assigned at the beginning of the calculation and allowed to "float" between the pro-R and pro-S orientations. This allows movement into the lowest energy conformation, which is then retained at the end of the calculation. Although not completely accurate, this method allows retention of restraints which may otherwise have been discarded and gives results which agree well with experimentally derived results [58].

2.9 Structure quality: Distance restraints and violations

Assessment of the low energy subset is necessary to ensure that the averaged structure will be a true representation of the molecule of interest. This is monitored using the Root Mean Square Deviation (RMSD). The RMSD is a measure of how close the structures are to each other. The generally accepted upper limit for the RMSD is 2Å. Another method for assessing structure quality is the analysis of NOE violations. These occur when the distances between the atoms in the calculated structures disagree with the restraint data derived from the NOE spectrum. Because the NOE restraints are given as ranges, some small violations are acceptable. Ideally, they should be less than 0.3Å in size [44].

2.10 Structure quality: Ramachandran plots

Another way to assess the quality of the structure obtained is to generate a Ramachandran plot. This involves plotting the psi and phi angles of the amide bonds for each amino acid against one another. Only certain combinations of psi and phi angles are allowed, and correspond to stable secondary structural motifs. Cross peaks fall into three main regions, indicating stable formation of left-handed or right-handed α-helices or β-sheets. Left-handed α-helices are rarely seen. The majority of peaks fall into the negative psi half of the plot, with negative phi values indicating α-helical structure and positive phi values indicating β-sheet [59].

2.11 Solvent systems for NMR structure determination of peptides

The solvent system chosen for NMR studies of peptides is very important, as it plays a major role in determining the extent of secondary structure formation. For example, most amphibian skin peptides remain unstructured when dissolved in water, but when dissolved in a 1:1 mixture of water and trifluoroethanol, a membrane surface mimicking solvent, they are able to fold into the conformation they would adopt in a membrane surface environment. The 1:1 mixture of trifluoroethanol can be described as a structure promoting solvent. When there is a tendency for a peptide to form a secondary structure, this solvent system will enhance the formation of such a structure; however, it will not cause a secondary structure to form which is not already inherently programmed into the sequence [60-62].

As this solvent system is designed to mimic a membrane surface, in which there is a polar zone and an apolar zone, we can also reasonably use it to describe the interface between an aqueous surface and a gaseous phase, as the aqueous surface is a polar zone and the gaseous phase will not generate any polar interactions with the molecule at the interfacial site [63].

2.12 Two dimensional NMR spectroscopy

A two dimensional NMR experiment is essentially a set of one dimensional NMR experiment collected as a function of a variable time interval [44]. The data is processed with two Fourier transform functions at right angles to one another to give rise to a 2D experiment. Those experiments which apply to biomolecules and were utilised in this study are discussed in sections 2.13 to 2.17.

2.13 TOCSY (TOtal Correlation SpectroscopY)

TOCSY spectra are particularly useful in protein and peptide NMR studies. A TOCSY spectrum allows correlation between all atoms within a single spin system. A spin system is defined as a group of atoms that can pass magnetisation between themselves. Conveniently in a peptide or a protein, each spin system corresponds to one individual amino acid. This is because, using this pulse sequence, the magnetisation cannot be transferred across the amide bond linkage [48].

In a TOCSY experiment, magnetisation is passed between the atoms by through-bond cross-polarisation, which occurs during a process called spin-lock mixing. As there are only 20 naturally occurring amino acids, assigning TOCSY spectra in terms of residue identity is relatively straightforward. The orientation of a given atom in each amino acid remains relatively constant. That is, the magnetic environments surrounding α-protons in any leucine residue will be roughly the same as in all others, as will those surrounding the other atoms in the residue. Therefore, each amino acid has a general fingerprint or signature pattern of resonances in a TOCSY spectrum. These signature patterns have been determined for each amino acid and are useful for structure determination as well as residue identification. The fingerprint patterns have been published by Evans [44].

2.14 COSY (COrrelated SpectroscopY)

COSY spectra are useful where there is more than one atom with the same chemical shift. The employment of a COSY experiment can remove ambiguity associated with chemical shift overlap. Cross-peaks in a COSY spectrum only occur between atoms that are 2 or 3 bonds apart. This usually means that only protons on adjacent carbons will show up. For example, two peaks close to δ 1.5 in a TOCSY spectrum could be coupling with peaks at either δ 4.2 or 4.3. The COSY spectrum will elucidate which atom is coupling to which [48].

In a COSY spectrum of a peptide, all protons on adjacent carbons should give rise to cross-peaks. Lack of a cross-peak is often an indicator of incorrect assignment in another spectrum.

2.15 NOESY (Nuclear Overhauser Effect SpectroscopY)

The NOESY spectrum makes use of through-space interactions, unlike the TOCSY and COSY experiments which rely on through-bond effects. The NOESY spectrum therefore is what provides information about secondary and tertiary structure. Once the chemical shifts of all nuclei of interest have been determined using TOCSY and COSY spectra, the NOESY experiment is employed.

When a specific proton signal is irradiated with an electromagnetic radiation pulse which serves to cancel its signal, all nearby nuclei with which it is interacting will be affected. Their signal strength will change. The original spectrum is then subtracted from the irradiated spectrum to yield a difference spectrum. Interactions are indicated by the presence of peaks in the difference spectrum.

Certain NOESY interactions are indicative of particular secondary structural motifs. Due to the geometry of the folding in an α-helix, certain peaks are expected. These are illustrated in Figure 4, modified from Tanford (1961) [64]. Interactions between the α_i and N_{i+1}, N_{i+3} and N_{i+4} are indicated in purple. Peaks are also expected between N_i and N_{i+1},N_{i+2}, and N_{i+4}, shown in red, as well as α_i and β_{i+3} (green) and β_i and N_{i+1} (blue).

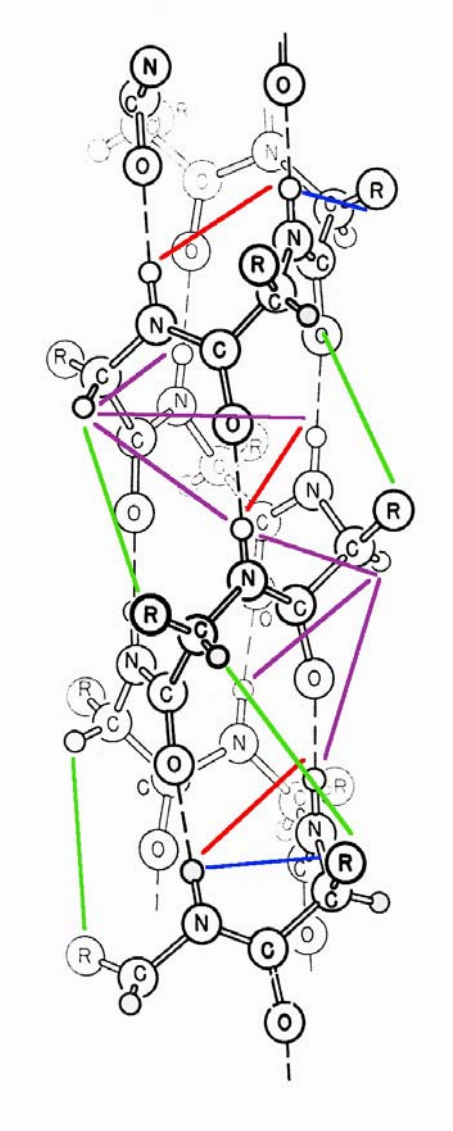

Figure 4: NOESY interactions expected in an α-helix.

In a β-sheet, the long range NOE interactions are much less extensive, occurring mainly between N_i and N_{i+1} and α_i and N_{i+1}. An intensity diagram is shown in Figure 5. Construction of an intensity diagram of cross-peak data from a fully assigned spectrum can give immediate information on possible structural elements present in a peptide sample.

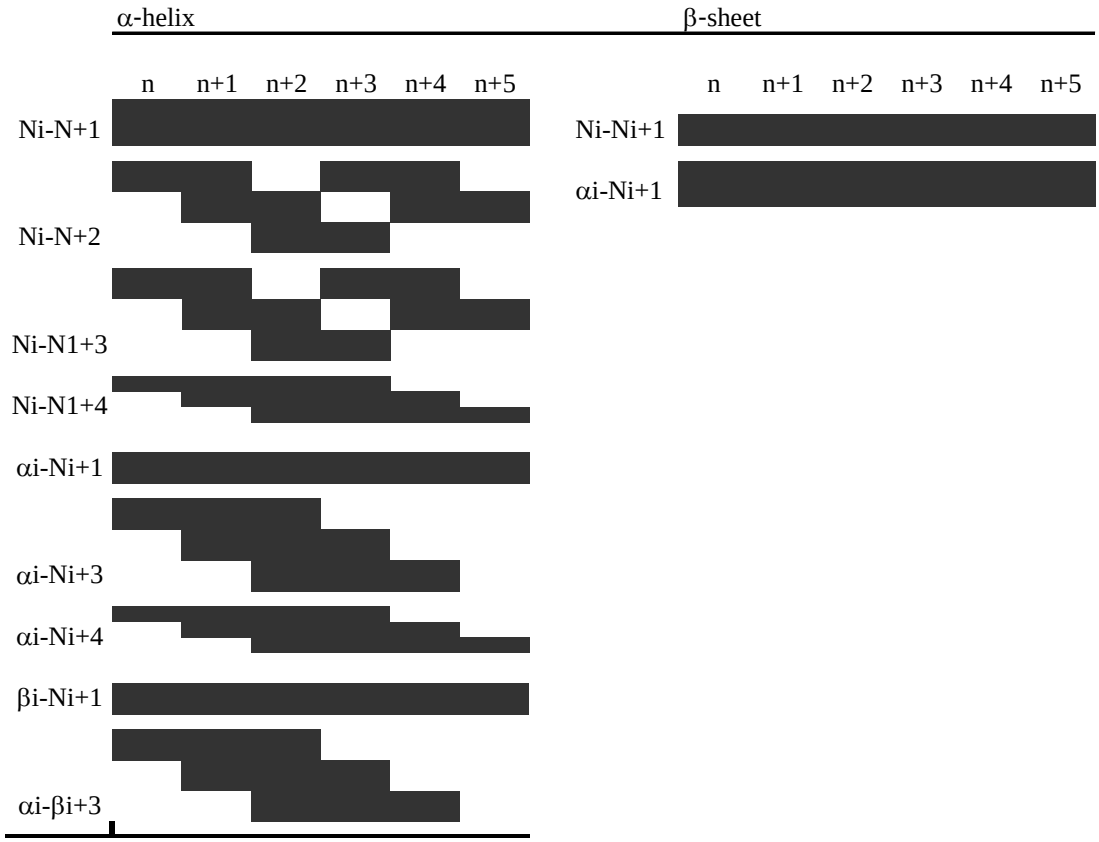

Figure 5: NOE interaction intensity diagram for a typical α-helix and a typical β-sheet, the strength of interaction is indicated by the thickness of the bands.

2.16 HMBC (Heteronuclear Multiple Bond Coherence spectroscopy)

The HMBC experiment shows only 2- and 3-bond coupling information, and gives information on carbon-proton interactions. As such it is a very powerful tool as it can allow identification of quaternary carbons which do not appear in proton correlated spectra, providing data useful in determining connectivity. In peptide studies, it is especially vital when identifying the carbonyl carbons and the nitrogen atoms of the peptide linkages if there is ambiguity in the HSQC [44].

2.17 HSQC (Heteronuclear Single Quantum Coherence spectroscopy)

The 2D HSQC is arguably the most important spectrum which can be recorded on either a protein or a peptide sample. It provides a fingerprint of the overall state of the protein, and can be interpreted very rapidly. It can be recorded either to show correlations between ^{15}N or ^{13}C with ^{1}H. In an HSQC experiment, only one-bond coupling information is shown [65].

For a peptide or protein, the side-chain carbon signals can be assigned using the ^{13}C-HSQC, as they are correlated with each of the side-chain protons, assigned previously with the use of TOCSY, COSY and NOESY.

With the use of a ^{15}N enriched sample, the backbone amide nitrogen resonances can also be identified. For the ^{15}N experiment one peak per backbone amide nitrogen is expected, along with two peaks per side chain $-NH_2$ group, which have degenerate nitrogen chemical shifts. These characteristic signals arise from every glutamine and asparagine residue [48].

The ^{15}N-HSQC also forms the backbone of the pulse sequences of many of the 3D experiments used for structure determination of larger proteins and of protein-peptide complexes, acting as a "top-view" of the 3D data cube. Each peak in the HSQC corresponds to one strip in the 3D spectrum. As such, the HSQC is an extremely important tool in both determining that the correct number of resonances is appearing

in the 3D experiment, but also as an overall guide to changes in the fold of the peptide or protein of interest [48].

As there is always one peak per backbone carbon atom in a ^{13}C-HSQC, and one peak per backbone amide nitrogen atom in a ^{15}N-HSQC, a simple peak count is useful to ascertain whether the protein has a single conformation or whether more than one structural form is present.

The backbone amide nitrogen and proton resonances are particularly good indicators of change in tertiary structure, and as such are generally solely used for titrations and binding studies. Upon addition of a ligand, chemical shift changes greater than 0.25 ppm in the nitrogen dimension and greater than 0.025 ppm in the hydrogen dimension of the HSQC experiment can be considered significant. Depending on the number of peaks whose chemical shifts change above these threshold levels the significance cut-off can be placed higher, for example at 0.5ppm in the nitrogen dimension and 0.05ppm in the proton dimension [66].

2.18 Three dimensional NMR of proteins: HNCACB

The HNCACB experiment is essential in the assignment of backbone chemical shifts when studying large proteins. The HNCACB experiment correlates HN with Cα, Cβ and N chemical shifts, of the intra-residue Cα and Cβ, and also the preceding Cα and Cβ. There are therefore four peaks in each strip, corresponding to these four correlations.

Due to the pulse sequence of the experiment, the Cα and Cβ peaks appear 180 degrees out of phase with each other, which allows quick distinction between atom identities, especially important in residues like glycine, which has no α-carbon, and serine and threonine, whose β-carbon shifts are more downfield than their α-carbon shifts [48].

Each vertical strip in the HNCACB experiment corresponds to one cross-peak in the ^{15}N-HSQC experiment, which can be considered as a "top-view" of the HNCACB data cube. A typical strip is illustrated in Figure 6.

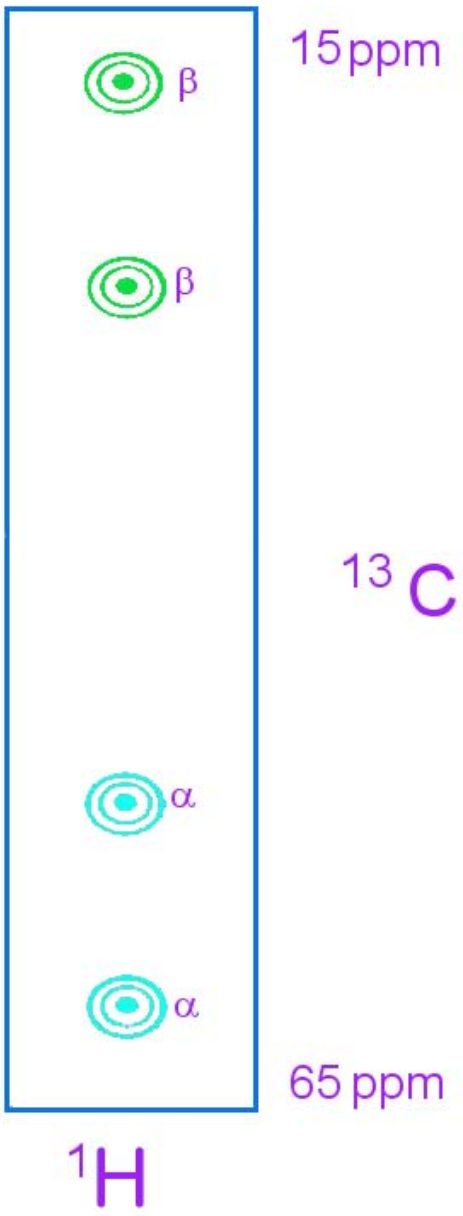

Figure 6: A typical strip in an HNCACB spectrum, with two α-carbon correlations (blue) and two β-carbon correlations (green).

2.19 Three dimensional NMR of proteins: CBCA(CO)NH

The data given by the CBCA(CO)NH experiment are very similar to those given by the HNCACB experiment, except that the carbonyl carbon of the backbone amide bond is utilised to transfer magnetisation. For this reason the N and HN resonances of each residue are correlated only with the Cα and Cβ of the preceding residue. Each strip plot (Figure 7) of the CBCA(CO)NH spectrum therefore only contains two cross-peaks [48].

Figure 7: A typical strip from a CBCA(CO)NH spectrum, with correlations to Cα-1 and Cβ-1 only.

Overlaying the HNCACB and CBCA(CO)NH allows immediate identification of which peaks in the HNCACB are due to correlations between intra-residue side chain carbons and which to inter-residue side chains. Those peaks which overlap between the two spectra arise from the correlation of the amide nitrogen with the preceding residue side chain; those for which there is only a peak in the HNCACB arise from the intra-residue side chain correlations. A typical strip from a CBCA(CO)NH spectrum, overlaid with the corresponding HNCACB strip, is illustrated in Figure 8. The ^{15}N-HSQC can again be likened to a "top-view" of the CBCA(CO)NH spectrum; using these three spectra in concert allows assignment of the majority of backbone atom resonances [48].

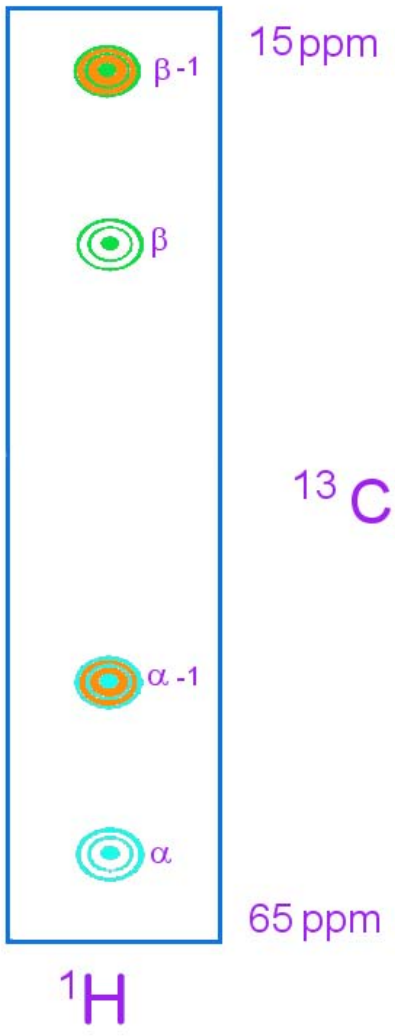

Figure 8: Overlaid view of a strip from an HNCACB spectrum and a CBCA(CO)NH spectrum, peaks which appear in both spectra can therefore be identified as arising from correlations with the preceding residue.

2.20 Sequential assignment strategy

The sequential assignment strategy has been developed by Wuthrich and co-workers [47] and depends on the identification of spin system types from the 3D spectra. First, strips are classified according to their spin systems and consequently, amino acid type.

Similarly to the TOCSY 2D spectrum, there are a number of residues which have a typical "fingerprint" of chemical shifts. However, most of the residues which have no heteroatoms in the carbon chain sidechains have similar α-carbon and β-carbon chemical shifts, with the majority of α-carbons appearing around 53 - 58 ppm and most β carbons appearing either between 28 - 33 or 38 - 42 ppm [49].

The exceptions are serine and threonine, in which the chemical shift of the β-carbon appears more downfield than the α-carbon; valine, isoleucine and proline, whose α-carbons generally appear higher than 60 ppm; alanine, with its particularly upfield α-carbon chemical shift about 16 ppm and glycine, with no β-carbon shift. These amino acid types are therefore easily identified and separated from the bulk and can provide a good starting point for sequential assignments [48].

Once each strip has been classified as to amino acid type, the protein sequence is used to identify unique sequence regions.

For example, there is only one incidence of two adjacent threonines (T28 and T29) and two adjacent alanines (A102 and A103) in the calmodulin sequence and only one incidence of a serine and alanine adjacent (S101 and A102); sequences such as these should therefore be relatively simple to unambiguously assign. This can be achieved using either NOE data or data from the HNCACB and CBCA(CO)NH spectra.

2.21 Main chain directed assignment strategy

The main chain directed approach to sequence specific assignments was developed by Wand and co-workers [67, 68]. This method involves the use of inter-residue correlations to find sequential amino acids without attempting to analyse their chemical shift signatures.

The main chain assignment strategy differs from the sequential strategy in that the resonances are connected prior to amino acid classification. Once the residues have all been connected into chains, the known amino acid sequence is aligned with the resonances. This strategy is especially useful when the sequence contains a large number of residues with similar spin system signatures, such as glutamic acid, glutamine, histidine, methionine, lysine and arginine; the Cα resonances of these residues all appear between 55 and 57 ppm and the Cβ resonances all appear between 29 and 33 ppm.

Chapter 3 The structure determination of the sex pheromone of Litoria splendida

3.1 Litoria splendida

It is possible to differentiate between frog species by analysing their skin secretions. Waugh and co-workers put this into practice in order to end the debate over whether *Litoria gilleni* and *Litoria caerulea* were the same species. Their skin secretions were found to be significantly different to the extent that they could not have arisen from the same species of frog [23].

In order to ascertain whether the skin secretions of each species of frog remain constant throughout the year, and therefore can serve as a definitive way to identify the species of an unknown specimen, members of our group studied the secretions of *Litoria splendida*. This species was chosen for the large average size and generous secretion volumes of typical specimens, making characterisation of the secretions relatively easy due to large quantities of material [21].

L. splendida, also known as the magnificent tree frog, was first identified in 1977 by Tyler, Davies and Martin [69]. This species is immediately characterised by the presence of enlarged parotid glands at the rear of the head and the pale sulphur coloured spots with dark edging scattered over the entire dorsal surface. *L. splendida,* averaging 10 cm in length, has large discs on the end of its slightly webbed fingers, extensively webbed toes and orange or yellow flanks. A typical specimen is illustrated in Figure 9.

Figure 9: A typical specimen of *Litoria splendida.*

Litoria splendida is found in a reasonably small geographical area, in the north-western parts of the Northern Territory, and in the north-eastern parts of Western Australia [70, 71], see Figure 10. Specimens collected for these studies were obtained from the Kimberley region of Western Australia.

Figure 10: Location map for populations of *Litoria splendida*, distribution shaded in grey.

Secretions were collected each month from both male and female specimens over a period of three years [72]. The chromatograms of the secretions from male frogs indicated the presence of a component in small quantities which was not present in the secretions from female frogs. Partial HPLC traces are shown in Figure 11.

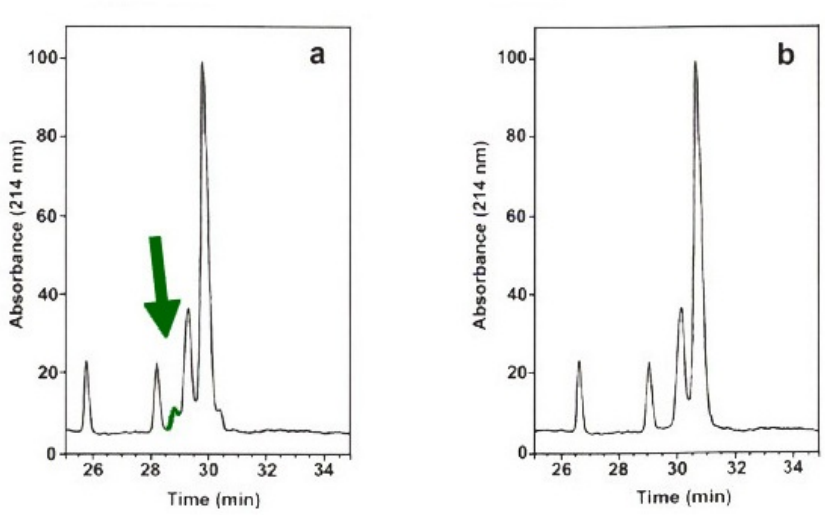

Figure 11: Partial HPLC traces of male (a) and female (b) *L. splendida.*

Comparison of the chromatograms from the three-year period show that this 25 residue peptide is produced in the highest levels during the mating season. The levels of peptide collected are shown in Figure 12. Clearly, the skin secretion does not remain constant throughout the year, however a much more interesting phenomenon was found to be occurring.

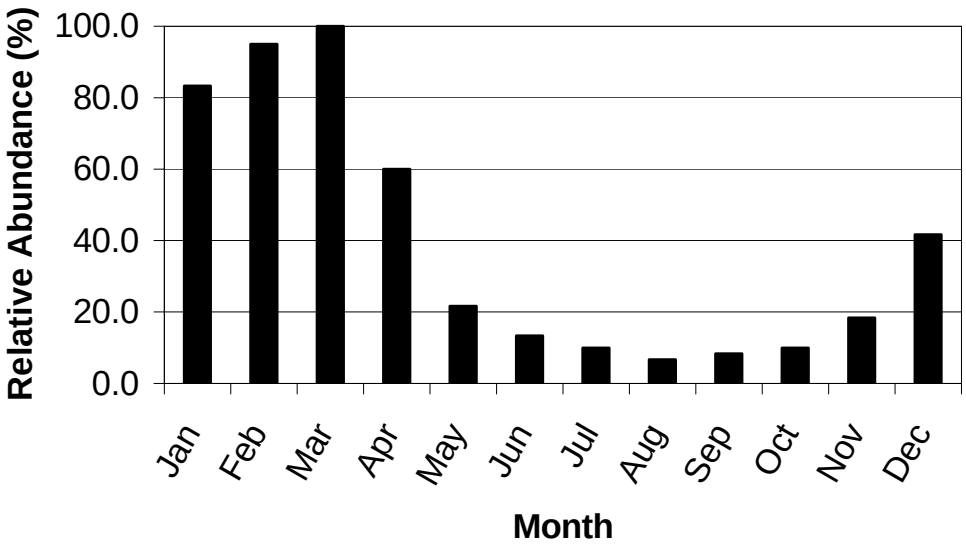

Figure 12: Splendipherin levels in male *L. splendida* secretions (averaged over a 3 year period).

The level of the peptide present in male secretions peaks in February and March. At this point it constitutes up to 1% of the total secretion material, dropping to as low as 0.1% from June through to November, when the animals are inactive. It was therefore investigated for a possible role in the breeding cycle of this species. The sequence was determined using mass spectrometry and is shown below (3).

(3) Splendipherin: GLVSS IGKAL GGLLA DVVKS KGQPA-OH

3.2 Splendipherin

The pheromone identified from *L. splendida*, named splendipherin, does not have as obvious a delivery method as do the previously discussed pheromones from species such as salamanders and newts, which involve direct contact or agitation of the water between the animals [73].

Behavioural tests were conducted in a 2 m glass tank containing a 2 cm depth of water totalling 1600 mL. The female frog was remote from the source of the pheromone, and the water was not disturbed upon addition of the peptide sample. These tests were recorded photographically; the images are shown in Figure 13.

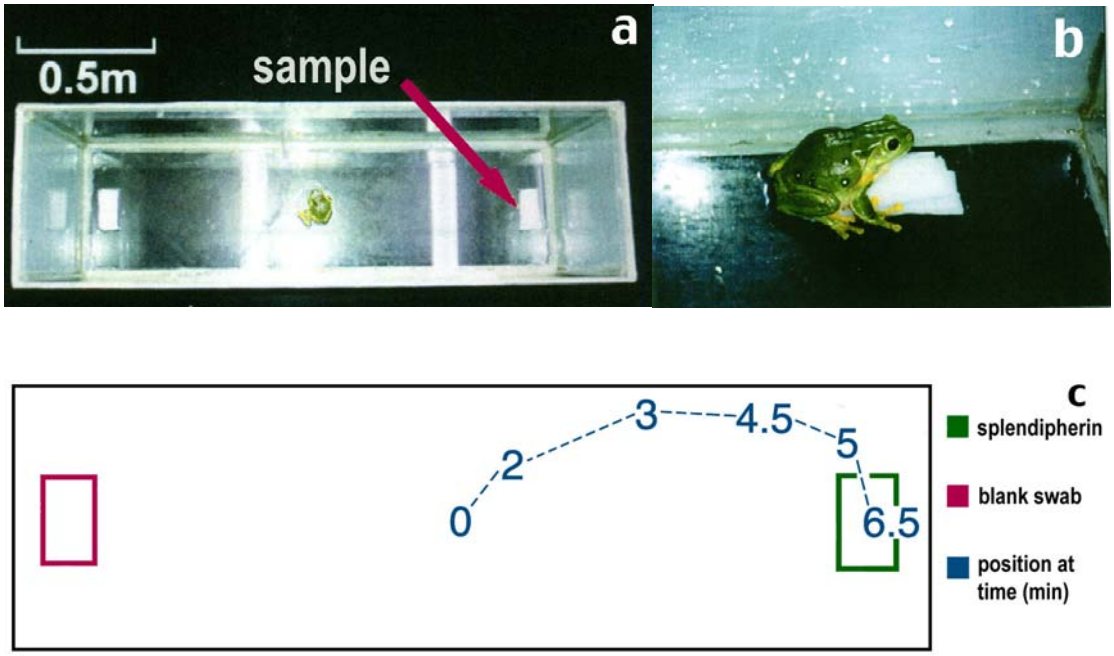

Figure 13: Behavioural testing of female *L. splendida* with splendipherin: (a) initial conditions in the tank, the sample of splendipherin is indicated (b) after seven minutes the female frog rests on the sample (c) the path taken by the frog to reach the swab.

Females of the species exposed to the hormone at a concentration of approximately 10 pM, were attracted to the source with remarkably rapid response times [21, 72].

During behavioural tests, recognition of the hormone was visible in the female within twenty seconds, made apparent by her change in posture and increased awareness. Considering that the peptide was not being moved toward the female by agitation of the water, as with the newt hormones sodefrin and silefrin, nor being directly applied, as with the terrestrial salamander, we were interested in discovering how the peptide moves through the aquatic environment.

Diffusion across the distance of approximately one metre would take hours [64, 74], however the female frogs found the source of the pheromone in a matter of minutes [21].

As the molecular weight of the peptide rules out volatility and travel through the air, this infers that the molecule is likely to be moving across the surface of the water with a surfactant-like action.

3.3 Aims

Using NMR, to determine the structure of splendipherin in an interface mimicking solvent. To analyse the structure of the peptide to ascertain how it moves across the surface of the water so rapidly.

3.4 Edmudson helical wheel analysis of splendipherin

Initial investigation of the secondary structure of splendipherin was undertaken using the Edmundson helical wheel (EHW) representation, displayed in Figure 14 [41].

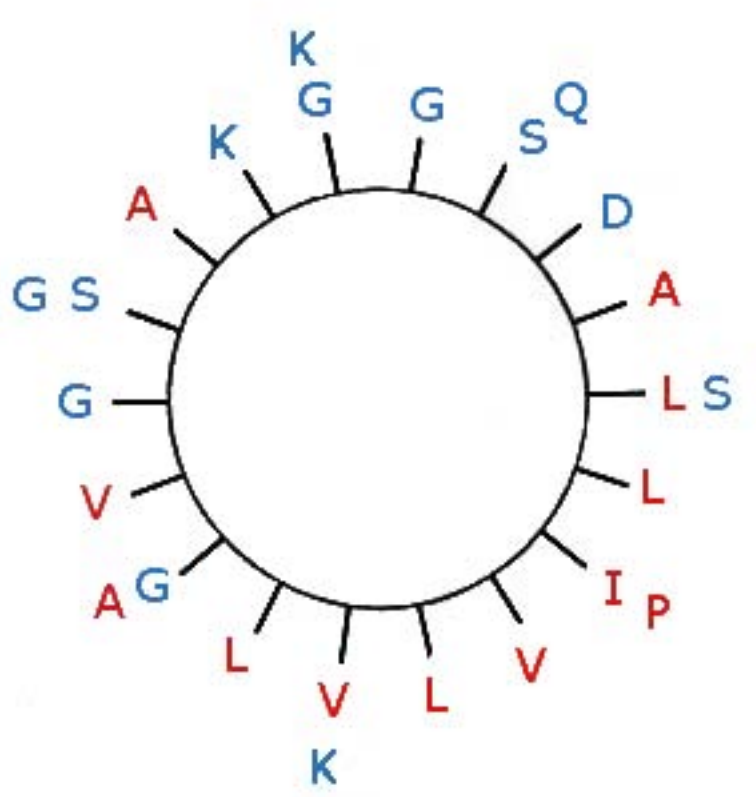

Figure 14: The EHW representation of splendipherin. Hydrophobic residues are shown in red and hydrophilic residues are shown in blue.

The Edmundson helical wheel diagram of splendipherin does not indicate a simple amphipathic helix. An amphipathic helix is one in which all hydrophobic residues are on one face of the wheel and all hydrophilic residues are on the other.

The diagram of splendipherin indicates that the hydrophobic and hydrophilic regions are not well defined. There is significant overlap, especially between residues in the first half and second half of the sequence. So, splendipherin is not a simple amphipathic helix.

3.5 Comparison of splendipherin with frenatin 3

Inspection of the sequence of splendipherin reveals a sequence motif also present in another amphibian peptide, frenatin 3. Frenatin 3 (4) was isolated from *L. infrafrenata* in 1995 [26]. It is a 22-residue peptide; the sequence is shown below.

(4) Frenatin 3: GLMSV LGHAV GNVLG GLFKP KS-OH

Both frenatin 3 and splendipherin contain a Gly-Gly motif. Glycine has been classified as a "helix-breaking" residue. That is, presence of glycine in a peptide causes increased flexibility and there is a distinct trend for glycine to be present at the end of an α-helix, in the C-terminal "cap" position [75]. The presence of two adjacent glycines in frenatin 3 at positions 15 and 16 causes a huge degree of flexibility in the molecule such that the helix is broken at that point, giving an extremely flexible "tail" region. A similar effect is expected in splendipherin at residues 13 and 14. The NMR structure of frenatin 3 has been determined and is shown in Figure 15.

Splendipherin dissolved in pure water has no secondary structure, 2D NOESY experiments recorded on such a sample lacked any significant cross-peaks indicative of either α-helical or β-sheet structure. It is unreasonable to suggest that the random conformation of the peptide could drive motion across the surface of water. Therefore a different effect must be occurring with structure being induced at the air/water interface. Whilst the mechanism by which TFE/water mixtures induce latent structure to form is still poorly understood, this mixed solvent system is the most appropriate to study the peptide conformation at the air/water interface. [1-4]

1. Reiersen, H., Rees, A. R. (2000) Trifluoroethanol may form a solvent matrix for assisted hydrophobic interactions between peptide side chains, *Protein Eng. 13*, 739-743.

2. Otting, G. (1997) NMR studies of water bound to biological molecules, *Prog. NMR. 31*, 259-285.

3. Gast, K., Siemer, A., Zirwer, D., Damaschun, G. (2001) Fluoro-alcohol-induced structural changes of proteins: some aspects of cosolvent-protein interactions, *European Biophysical Journal. 30*, 273-283.

4. Gerig, J. T. (2004) Structure and solvation of melittin in 1,1,1,3,3,3-hexafluoro-2-propanol/water, *Biophys. J. 86*, 3166-3175.

Figure 15: Overlaid 20 lowest energy structures for frenatin 3.

3.6 NMR spectroscopy of splendipherin

0.63 g of the peptide was dissolved in a 1:1 mixture of D_3-tri-fluoroethanol and water, with a total volume of 0.7 mL; trimethylsilane was used as the referencing standard. The pH was recorded to be 2.11, and was not corrected. Using this sample, TOCSY, NOESY, COSY, HMBC and ^{13}C-HSQC spectra were recorded.

3.7 Assignment of the NMR spectra of splendipherin

Complete assignment of the NOESY and TOCSY spectra was achieved using standard methodology [47]. Because of the trend of chemical shifts towards random coil values in the centre of the peptide, conclusive assignment of the spectra was made considerably difficult.

The N_i-N_{i+1} cross-peaks in the NOESY spectrum which are usually important in sequential assignment were overlapped to a large degree, to the extent that there were no cross peaks between the N-H protons of residues 3 - 4, 4 - 5, 5 - 6, 8 - 9, 15 - 16 or 20 - 21. In these cases, the α_i-N_{i+n}, β_i-N_{i+1} and α_i-β_{i+3} cross-peaks were used to assign

residues in sequence. There were also no cross-peaks for residues 23 - 34 and 24 - 25 as residue 24 is a proline, with no NH proton.

A large number of Hα and Hβ shifts were also overlapped, especially about the region between residues 10 - 14, which was problematic for peak assignment and led to a higher than usual proportion of ambiguous assignments. This was because residues 10, 13 and 14 are leucine residues, with relatively large sidechains, each with very similar Hβ, Hδ and Hγ chemical shifts, so many long-range NOE interactions could not be ruled out.

However, assignment of all sidechain protons, Cα and HN resonances was finally completed and the resultant chemical shift data is presented in Table 5. The assigned HN-HN section of the NOESY spectrum is shown in Figure 16.

Table 5: Chemical shift assignments from NOESY and HSQC spectra for splendipherin.

Residue	Cα shift	NH shift	Hα shift	Hβ shift	Hγ shift	Hδ shift
G1	42.209		3.943/3.869			
L2	56.881	8.452	4.285	1.673	1.666	0.958/0.918
V3	63.831	7.954	3.897	2.089	1.036/0.976	
S4	58.978	8.073	4.354	4.019/3.294		
S5	60.127	8.098	4.393	4.07/3.97		
I6	63.112	8.108	3.947	1.94	1.659/1.216/0.946	0.876
G7	45.958	8.259	3.878/3.811			
K8	57.718	7.88	4.157	1.951	1.487	1.73/1.607
A9	53.692	7.945	4.223	1.55		
L10	53.362	8.529	4.218	1.792/1.647	1.787	0.913/0.879
G11	45.96	8.186	3.898/3.841			
G12	45.456	7.976	3.952/3.887			
L13	56.328	7.789	4.289	1.863/1.796	1.709	0.951/0.912
L14	57.002	8.334	4.066	1.787/1.648	1.777	0.901/0.876
A15	54.086	7.867	4.055	1.515		
D16	54.763	7.802	4.488	3.261/2.93		
V17	65.762	8.367	3.654	2.378	1.086/0.933	
V18	65.536	8.436	3.762	2.185	1.067/0.955	
K19	57.711	8.199	4.147	1.985	1.529	1.65
S20	59.228	7.938	4.371	4.072/4.037		
K21	55.708	7.931	4.33	1.973	1.562	1.7
G22	44.197	8.081	3.965			
Q23	52.355	7.807	4.69	2.152/2.016	2.402	7.442/6.601(ε)
P24	62.095	49.321(Cδ)	4.447	2.275/2.008	2.059/1.902	3.793/3.693
A25	50.224	7.96	4.387	1.438		

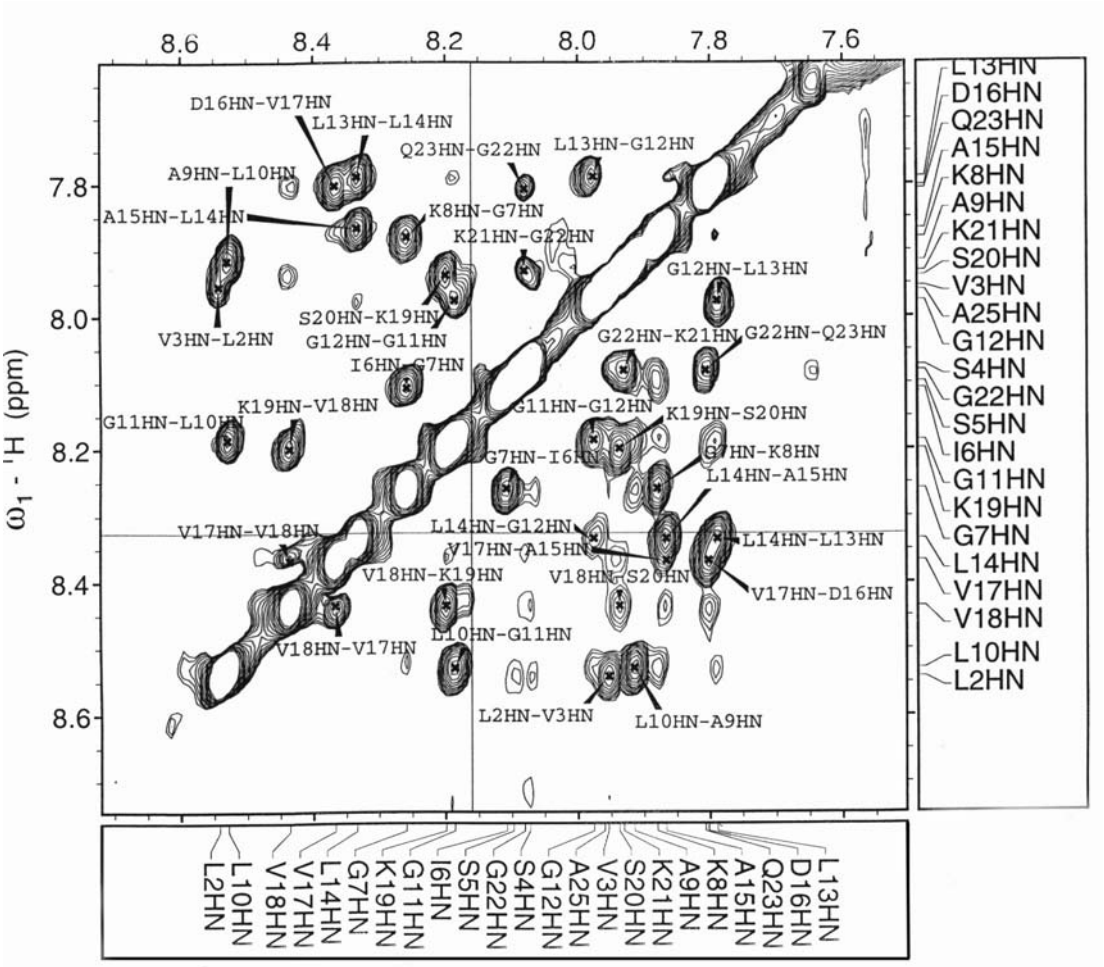

Figure 16: The assigned HN-HN region of the NOESY spectrum.

3.8 Secondary shift data

The plots of smoothed α-proton and α-carbon secondary shifts (see section 2.4) for splendipherin are shown in Figure 17 and Figure 18; the corresponding secondary shift data are shown in Table 6 and Table 7 respectively.

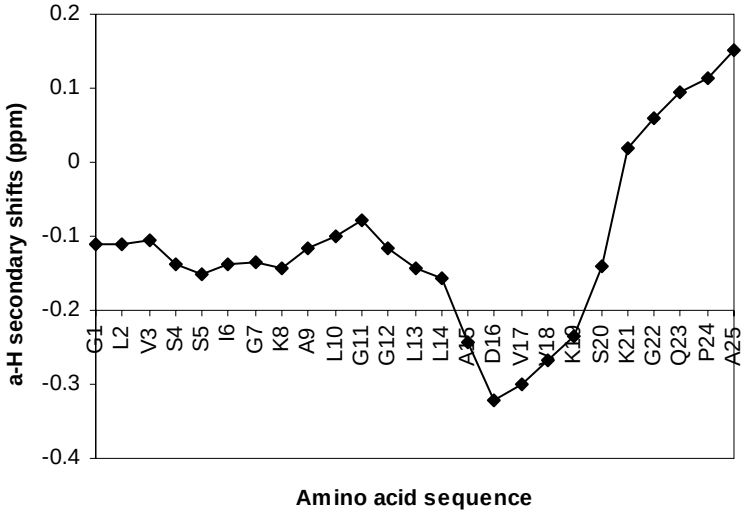

Figure 17: Hα secondary shift plot for splendipherin.

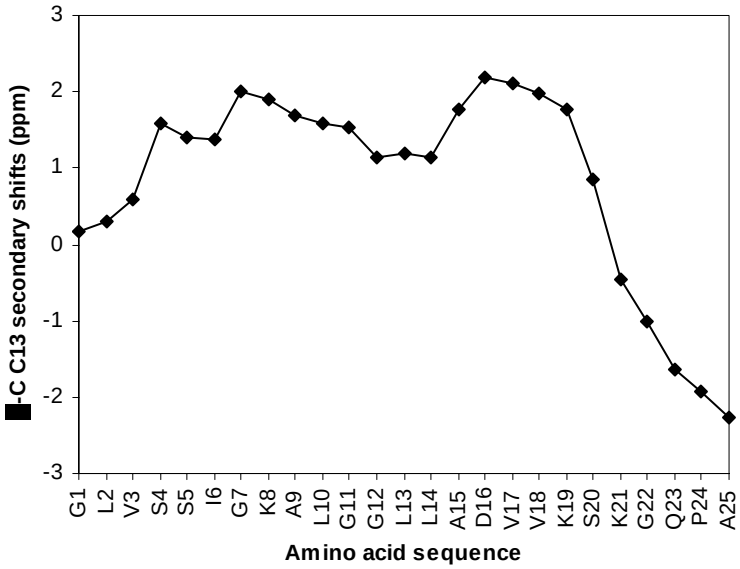

Figure 18: Cα secondary shift plot for splendipherin.

Table 6: Hα secondary shift data for splendipherin

sequence	Hα shift	random coil	secondary shift	smoothed
G1	3.906	3.96	-0.054	-0.1103
L2	4.29	4.34	-0.054	-0.11175
V3	3.90	4.12	-0.223	-0.1048
S4	4.35	4.47	-0.116	-0.1386
S5	4.39	4.47	-0.077	-0.1509
I6	3.95	4.17	-0.223	-0.1383
G7	3.84	3.96	-0.1155	-0.1345
K8	4.16	4.32	-0.16	-0.1435
A9	4.22	4.32	-0.097	-0.117
L10	4.22	4.34	-0.122	-0.1013
G11	3.87	3.96	-0.0905	-0.0795
G12	3.92	3.96	-0.037	-0.1153
L13	4.29	4.34	-0.051	-0.1441
L14	4.06	4.34	-0.276	-0.1564
A15	4.054	4.32	-0.266	-0.2422
D16	4.49	4.64	-0.152	-0.3216
V17	3.65	4.12	-0.466	-0.301
V18	3.67	4.12	-0.448	-0.2676
K19	4.15	4.32	-0.173	-0.2352
S20	4.37	4.47	-0.099	-0.141
K21	4.33	4.32	0.01	0.0202
G22	3.97	3.96	0.005	0.0602
Q23	4.70	4.34	0.358	0.0934
P24	4.45	4.42	0.027	0.11425
A25	4.39	4.32	0.067	0.1507

Table 7: Cα secondary shift data for splendipherin.

sequence	Cα shift	random coil	secondary shift	smoothed
G1	42.2	45.1	-2.9	0.167
L2	56.9	55.1	1.8	0.3
V3	63.8	62.2	1.6	0.6
S4	59	58.3	0.7	1.58
S5	60.1	58.3	1.8	1.4
I6	63.1	61.1	2.0	1.38
G7	46	45.1	0.9	2
K8	57.7	56.2	1.5	1.9
A9	56.3	52.5	3.8	1.68
L10	56.4	55.1	1.3	1.58
G11	46	45.1	0.9	1.52
G12	45.5	45.1	0.4	1.14
L13	56.3	55.1	1.2	1.2
L14	57	55.1	1.9	1.14
A15	54.1	52.5	1.6	1.78
D16	54.8	54.2	0.6	2.2
V17	65.8	62.2	3.6	2.12
V18	65.5	62.2	3.3	1.98
K19	57.7	56.2	1.5	1.76
S20	59.2	58.3	0.9	0.86
K21	55.7	56.2	-0.5	-0.46
G22	44.2	45.1	-0.9	-1
Q23	52.4	55.7	-3.3	-1.64
P24	62.1	63.3	-1.2	-1.9
A25	50.2	52.5	-2.3	-2.3

Clearly the α-protons in splendipherin are shifted downfield to a large extent in the region L13 - S20 and to a slightly lesser extent in the region S4 - L10. This indicates two α-helical regions. The shifts of G11 - 12 are closer to random coil values suggesting increased flexibility. This was expected due to the helix breaking nature of these residues. The shifts from K21 onwards are slightly positive indicating definite lack of α-helical structure, and possible β-sheet conformation.

The secondary shift plot for α-carbon resonances supports this information. Upfield shifts are strong in the regions from S4 - L10 and A15 - S20, with G11 - L14 close to random coil and residues from K21 onwards closer to β-sheet structure values.

Random coil shifts for NH protons have also been determined; plotting the secondary shifts for NH protons gives information about possible amphipathicity and helix formation. A pronounced "zig-zag" trend appears in amphipathic helices due to the differences in hydrogen bond lengths between hydrophobic and hydrophilic residues [76]. The secondary shift plot and data for splendipherin HN protons are shown in Figure 19 and Table 8 respectively.

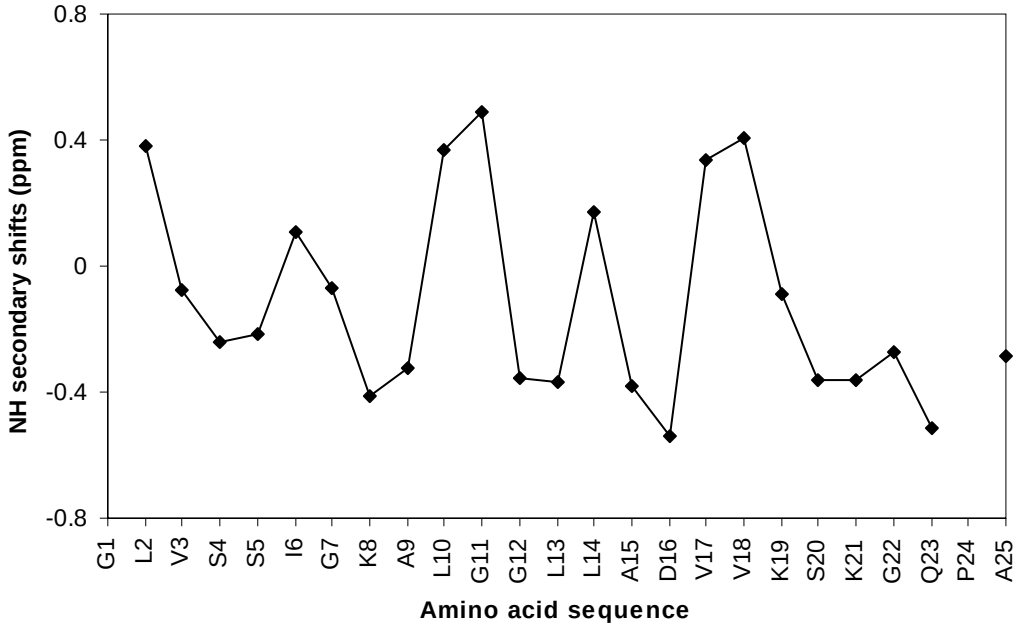

Figure 19: HN secondary shift plot for splendipherin.

Table 8: HN secondary shift data for splendipherin.

sequence	HN shift	random coil	secondary shift	smoothed
G1				
L2	8.54	8.16	0.38	0.021
V3	7.95	8.03	-0.077	-0.03825
S4	8.07	8.31	-0.24	-0.0094
S5	8.09	8.31	-0.216	-0.0996
I6	8.11	8	0.106	-0.1664
G7	8.26	8.33	-0.071	-0.1836
K8	7.88	8.29	-0.411	-0.067
A9	7.91	8.24	-0.326	0.0092
L10	8.53	8.16	0.367	-0.0474
G11	8.82	8.33	0.487	-0.0392
G12	7.98	8.33	-0.354	0.0606
L13	7.79	8.16	-0.37	-0.0884
L14	8.33	8.16	0.173	-0.2934
A15	7.86	8.24	-0.378	-0.1554
D16	7.80	8.34	-0.538	-0.0002
V17	8.37	8.03	0.336	-0.053
V18	8.44	8.03	0.406	-0.0504
K19	8.20	8.29	-0.091	-0.0148
S20	7.95	8.31	-0.365	-0.1364
K21	7.93	8.29	-0.36	-0.3202
G22	8.06	8.33	-0.272	-0.3775
Q23	7.81	8.32	-0.513	-0.35725
P24				-0.3563
A25	7.96	8.24	-0.284	-0.3985

The “zig-zag” trend in the graph of NH secondary shifts clearly drops off after residue 21, even though there is no data point for proline as it has no NH proton. This indicates that the N-terminal end and central region of the peptide are amphipathic and helical, but the C-terminal end is neither.

3.9 CSI Data

The chemical shifts of the α-protons of splendipherin were subjected to analysis using the CSI method. The CSI data and the secondary shift graphs for splendipherin both indicate two defined α-helices separated by a more flexible region. Both sets of data also indicate a lower level of structure at the C-terminal end, but neither indicates the formation of a β-sheet type conformation. The central region of flexibility was expected due to the Gly-Gly motif at residues 11 and 12. The data, shown in Figure 20, is consistent therefore with expectation.

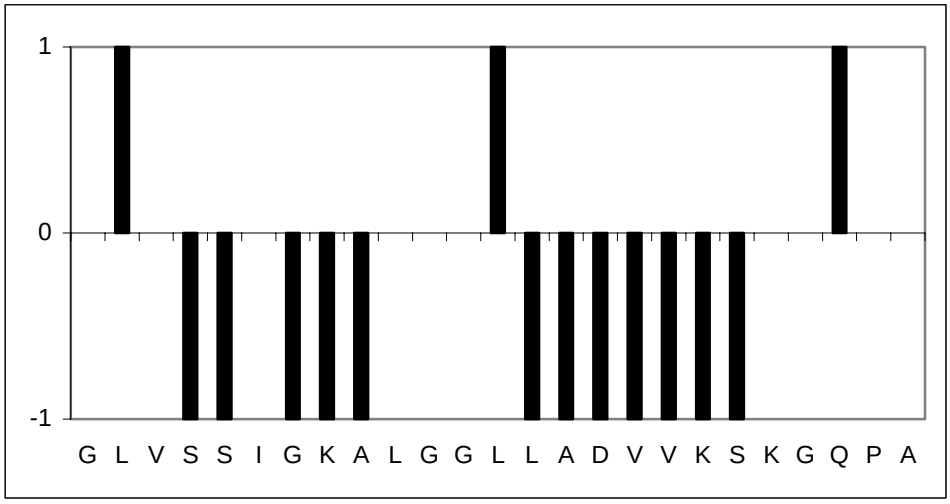

Figure 20: CSI data for splendipherin, negative CSI values indicating α-helical regions extending between residues 3 - 10 and 14 - 21.

3.10 Nuclear overhauser effect data

The NOE intensity diagram for splendipherin has been constructed and is shown in Figure 21. Although a large proportion of the peaks are overlapped, the NOE intensity diagram for splendipherin indicates that the majority of the peptide is α-helical, however there are large numbers of peaks which are typically present in an α-helix missing towards the C-terminus, indicating less rigid structure. The increased strength of dαN(i, i+1) interactions suggests that this region may have a β-sheet-like conformation. The dNN(i, i+3) peaks are also missing in the central Gly-Gly region, which also indicates less α-helical nature.

Figure 21: NOE intensity diagram for splendipherin. Peak intensity is indicated by band height. Overlapped peaks are indicated by shaded areas. Peaks overlapped on the diagonal have been omitted.

3.11 Restrained molecular dynamics and simulated annealing calculations

The distance restraints for splendipherin are summarised in Table 9.

Table 9: Summary of restraints generated from the NOESY spectrum of splendipherin.

Type of Restraint	Number of Restraints	Percentage
Sequential	56	19.72
Medium-Range	40	14.08
Long-Range	0	0
Intra-Residue	123	43.31
Ambiguous	65	22.89
Total	284	100

As discussed in section 3.7, a larger than usual percentage of assignments are ambiguous. This was countered by use of the sum averaging method described in section 2.8. Analysis of the psi and phi angles for the ensemble of twenty structures shows that there are two well-defined regions, from V3 - L10 and from G12 - K21. The first and last four residues were not expected to be well structured, as the terminal residues in any peptide are less able to form rigid secondary structure as they lack the appropriate hydrogen-bonding network.

There is no evidence of any dimerisation of splendipherin as there are no long-range NOE interactions, that is, between residues more than five positions apart in the sequence. Analysis of the energies of the ensemble of twenty lowest energy structures and of the averaged structure of splendipherin was also performed. The data from this analysis are shown in Table 10.

Table 10: X-PLOR energies and violation statistics for <SA> (ensemble of twenty lowest energy structures) and $(SA)_r$ (energy minimised averaged structure).

X-PLOR energies (kcal.mol^{-1})	<SA>	$(SA)_r$
E_{tot}	56.4794	36.3243
E_{bond}	3.99934	2.16372
E_{angle}	21.0906	15.9554
$E_{improper}$	3.29073	1.63992
E_{vdw}	4.42456	2.4844
E_{NOE}	23.674	14.0809
E_{cdih}	0	0
Violations		
No. of NOES violated >0.3Å	3	0
Maximum violation	0.448 Å	0

Analysis of the angular order parameters (S, psi and phi) of the final ensemble of twenty structures indicated that 18 of the 25, or 72%, of the residues were well defined (S>0.9 for psi and phi). This corresponds to the regions 3 - 10 and 12 - 21, indicating that the central Gly-Gly region is indeed more flexible than the rest of the peptide.

The maximum violation from the ensemble was 0.448Å. However, only three violations were present in the ensemble, which indicates that the structures fit the NMR data very well. The averaged structure therefore provides an accurate representation of the true structure of splendipherin in an interfacial environment.

Fitting the structures over the two well defined regions shows that each region forms an α-helix and that the twenty structures agree well with each other over these stretches. Fitting over the peptide including residue 11 indicates less agreement. This supports the idea of a flexible region in the centre of the molecule. The overlaid structures were generated using the MOLMOL program and are shown in Figure 22.

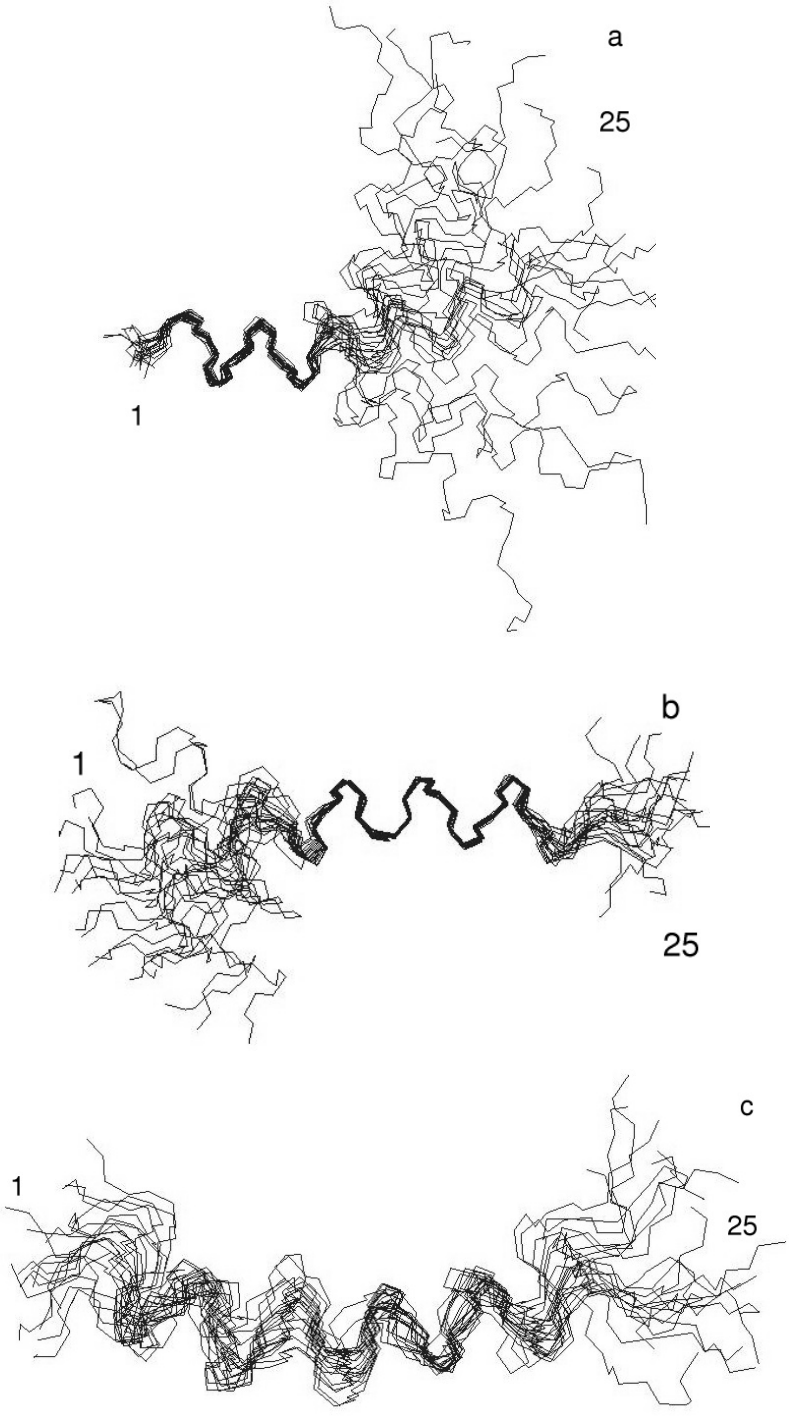

Figure 22: Low energy ensemble fitted over residues 3 - 10(a), fitted over residues 12 - 21(b) and over the entire well-defined regions (c).

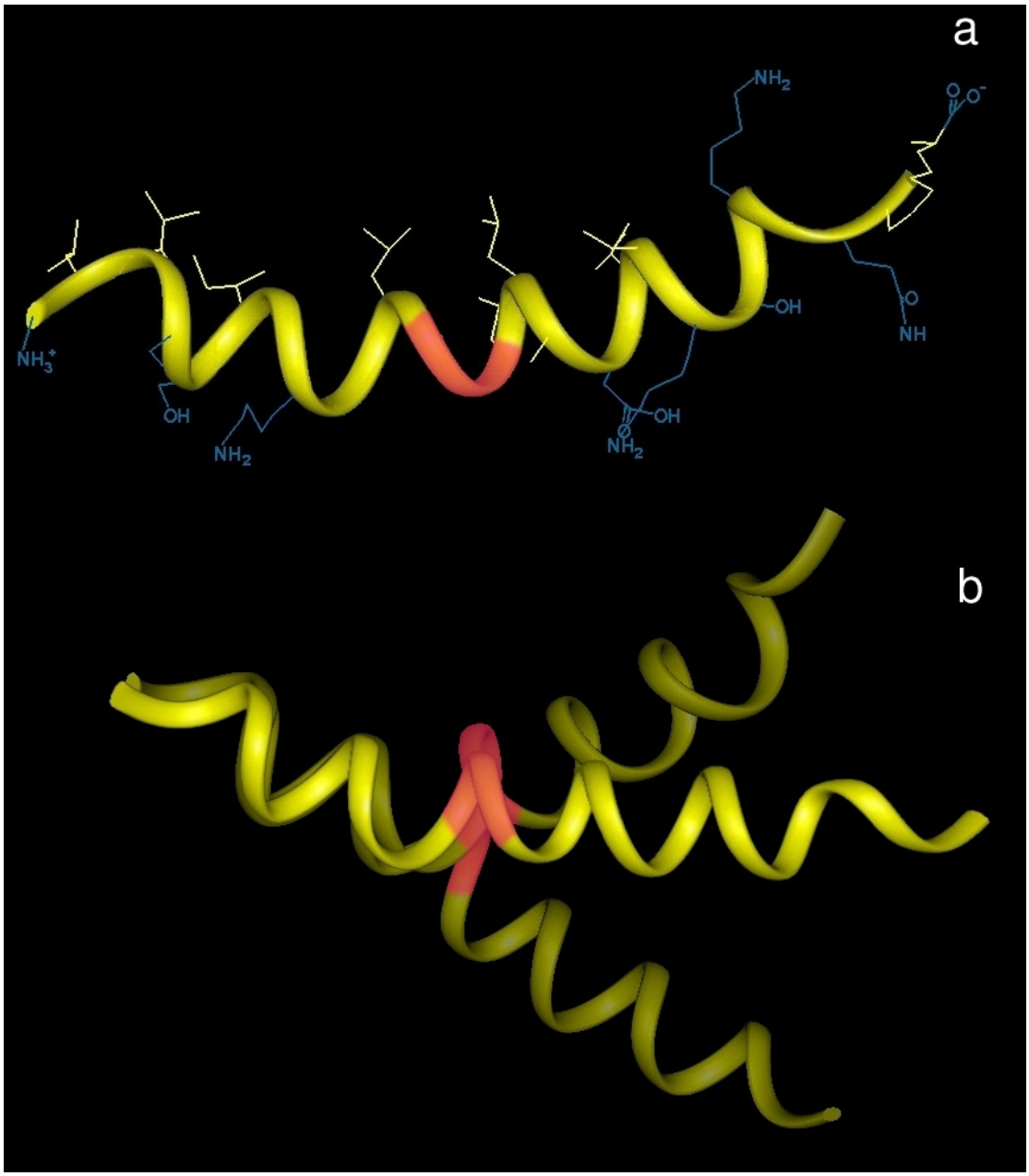

Figure 23: Averaged and energy minimised structure of splendipherin (a) and superimposition of three low energy structures (b).

The averaged structure generated from the ensemble of twenty is shown in Figure 23a. This diagram indicates clearly that the peptide is bent in the centre, about the Gly-Gly region, shaded in red. Three of the structures from the low energy ensemble have been overlaid to generate Figure 23b, demonstrating the flexibility in the centre of the molecule.

3.12 Structure quality analysis

The root mean square deviations were calculated over both well-defined regions, from residue V3 to K21. The RMSD for this region is reasonably high, due to the inclusion of the poorly defined residue G11. Calculating the RMSD for the region V3 - L10 only gives a much lower RMSD; the region from G12 - K21 gives an even lower value. These data indicate that the two well defined regions agree very well with each other, but that the structure has more deviation overall. This provides further evidence for the model of two rigid α-helices separated by a flexible linker region. The RMSD data are shown in Table 11.

Table 11: RMSD comparison for structures fitted over the separate well defined regions, and over the entire molecule.

	RMSD from mean geometry (Å)	
region	backbone atoms	heavy atoms
entire backbone	2.40 ± 0.87	2.72 ± 0.76
3-21	1.18 ± 0.51	1.62 ± 0.49
3-10	0.36 ± 0.11	0.91 ± 0.27
12-21	0.23 ± 0.06	0.91 ± 0.1

The psi and phi angle data have also been plotted on a Ramachandran plot. The distribution of cross peaks indicates that the largest portion of psi and phi angles falls into the favoured region for α-helical structure. Glycine and proline residues are not included in the Ramachandran plot due to their propensity for psi and phi angles which are not allowed in other residues. Residue Q23 falls into the β-sheet region however, which is evidence for a slightly β-sheet-like conformation at the C-terminal end. This may be because this residue is bordered on one side by a glycine and on the other by a proline; the psi and phi angles for Q23 will be influenced by the glycine and proline angle preferences. The Ramachandran plot is shown in Figure 24 [59].

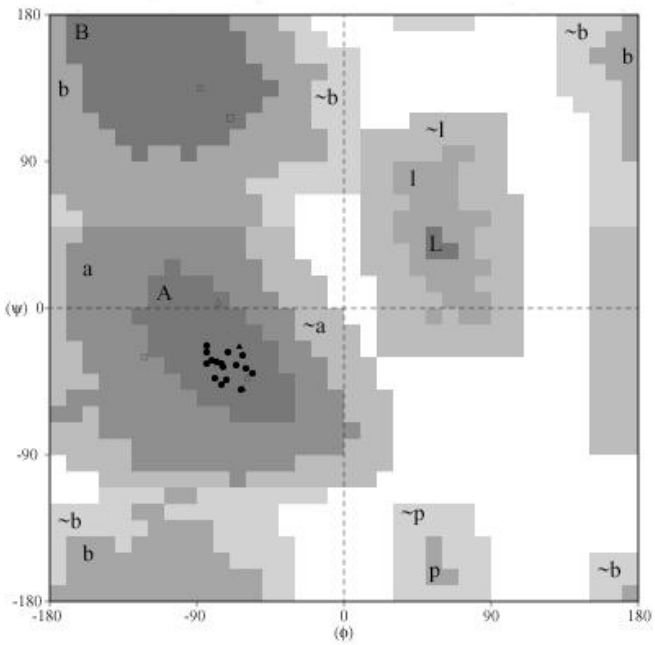

Figure 24: Ramachandran plot of psi and phi angles for <SA>.

3.13 Summary

3.13.1 The nature of the structure of splendipherin

Splendipherin is a flexible peptide with two α-helical regions spanning residues 3 - 10 and 12 - 21. The N- and C-termini are less structured, especially at the C-terminus, due to the presence of two helix-breaking residues at positions 22 and 24 and due to the lack of hydrogen bonding between the terminal residues. The C-terminal region exhibits partial β-sheet characteristics. There is no evidence of dimerisation between molecules, as there are no NOE interactions between residues more than five positions apart in the sequence.

Examination of the 3D structure of splendipherin shows that the majority of hydrophobic residues are on one face of the peptide, however this pseudo amphipathic separation breaks down towards the C-terminus. This is further underlined by the HN secondary shift plot, in which the “zig-zag” trend indicative of amphipathicity is also lost at the C-terminus. The MOLMOL visualisations of the

overlaid ensemble of structures indicate that the structure is also much more flexibility in this region.

3.13.2 The movement of splendipherin on the surface of water

Consideration of the rapid movement by splendipherin in water leads to proposals of a limited number of possible mechanisms. The peptide must move across the surface of the water as its molecular weight is much too high to allow volatility to be considered. Bulk diffusion through the body of still water would take days rather than seconds [74].

The phenomenon of molecules or particles moving across the surface of water is not unknown. Drops of oil have been shown to move across the surface of water, driven by a surface tension imbalance [77, 78]; indeed this property has even been exploited to drive a micropump [79].

In order to test the theory that the peptide moves across the surface of the water, a series of behavioural tests were carried out. A female specimen of *L. splendida* was placed in the same testing tank as was used in the original study [72], but with a partial glass barrier fitted to break the surface of the water. This allowed water to pass beneath from either side of the barrier, but prevented surface diffusion. When splendipherin was introduced on the other side of the glass barrier from the female frog, she had no response whatsoever. Had the peptide been travelling through the body of water, contact with the female would have been possible. This experiment confirms the deduction that the peptide travels across the surface of the water.

If the peptide is considered to be a charged surface active molecule, it is reasonable to suggest that its movement is a result of a surface effect. A proposed explanation is that when the sample is initially introduced to the tank, there is a high concentration of the peptide at the introduction site. If the material is surface active, then this gives rise by definition to a surface tension gradient, since a reduction in surface tension is a necessary corollary of adsorption. This therefore also gives rise to a driving force for the spreading of the peptide [63].

Splendipherin, a water soluble molecule, has clearly defined amphipathicity at the N-terminus; both are properties required by surface active agents. Water soluble amphiphiles are strongly adsorbed at interphase surfaces [74]. At the surface of water, the hydrophilic portion can be submerged whilst the hydrophobic region sits in the vapour phase [63].

The difference in surface tension between water, and water with surface active material adsorbed at the surface, is often referred to as a "surface pressure". The units of surface tension are Jm^{-2} or Nm^{-1} and thus the surface tension gradient can be thought of as a pressure in two dimensions. In the same way that gas will rapidly and spontaneously flow to achieve constant pressure, the surface active molecules will spread rapidly to achieve as low an area per molecule as possible, thereby reducing the surface tension of the entire surface covered by the monolayer [63, 80].

When the concentration of the surfactant is very low, monolayers of surface active materials will be of sufficiently low density that the molecules do not interact with each other. Such monolayers are thus often referred to as "gaseous" [81, 82]. The positively charged peptide molecules will also repel each other due to electrostatic forces, causing a further driving force for spreading [83].

Chapter 4 Peptides which inhibit neuronal nitric oxide synthase

4.1 Nitric oxide synthases

Nitric oxide is one of the most important chemical messengers in biological systems. It is, amongst other things, involved in cell signalling, host defence, memory formation and also acts as a vasodilator [84].

Nitric oxide is small, short-lived and easily dispersible through cell membranes and tissues. These properties negate the need for extra-cellular NO receptors and for degradation pathways targeted to this messenger. For these reasons levels of NO are moderated solely by the rate of its synthesis.

The three forms of nitric oxide synthase are therefore under very strict control, at the transcriptional, translational and post-translational levels. The major method of post-translational control is via protein-protein interactions, but phosphorylation events and lipid modification also play important roles [84, 85].

The three isoforms of nitric oxide synthase, neuronal NOS (nNOS, or NOS I), inducible NOS (iNOS, or NOS II) and endothelial NOS (eNOS, or NOS III) have quite different sequences but the same overall domain structures. The general structure of the three enzymes is illustrated in Figure 25.

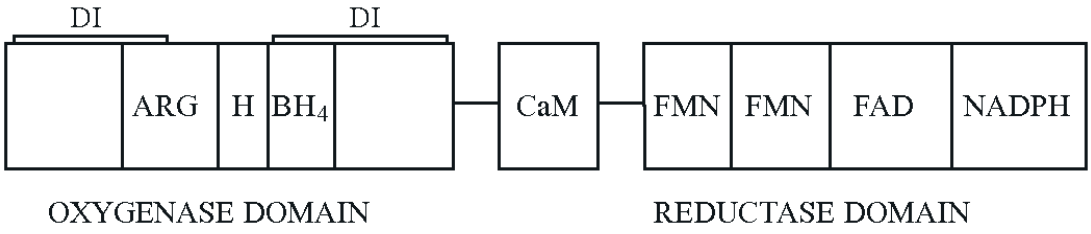

Figure 25: Box diagram of the general nitric oxide synthase structure. Variations occur in each of the three isoforms. (Adapted from Kone, 2003 [85].)

Each has an N-terminal oxidase domain, containing the binding sites for L-arginine (ARG), heme (H) and tetrahydrobiopterin (BH_4). The binding of these co-factors is required for homo-dimerisation of the monomer protein, at the dimerisation

interfaces (DI). The central region contains the calmodulin-binding site (CaM), and the C-terminal reductase domain contains binding sites for flavin mononucleotide (FMN), flavin adenine dinucleotide (FAD) and reduced nicotinamide adenine dinucleotide phosphate (NADPH) [85].

4.2 Calmodulin

Calmodulin is a highly conserved 148-residue protein which is primarily responsible for calcium transport in mammalian cells. It is produced by all eukaryotes, from the fly to the frog, cow to human, with very little sequence variability [86, 87].

Calmodulin is an allosteric modulator of all three isoforms of NOS. Binding to eNOS and nNOS is controlled by intra-cellular calcium concentration. Basal calcium levels are insufficient to cause binding; an influx of calcium is required to maintain calmodulin binding and activation of these enzymes. iNOS, however, binds to calmodulin irrespective of calcium concentrations and its activity is largely calcium independent [84].

Calmodulin is also required as a co-enzyme by a large number of other enzymes, and can bind over 100 different proteins [86]. Examples include calcineurin, myosin light chain kinase and cyclic AMP phosphodiesterase [[88]. Calmodulin can also act as an enzyme inhibitor, for example in the case of phosphofructokinase [89].

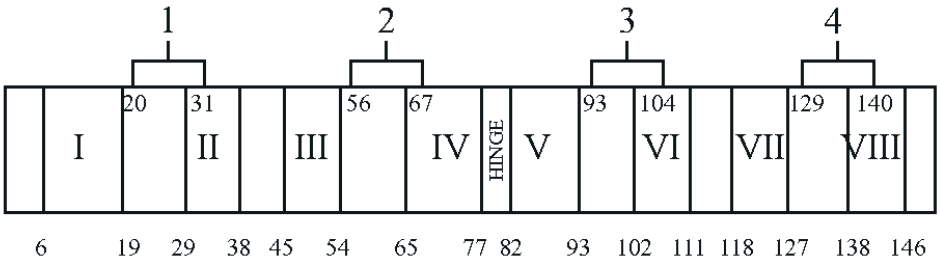

Figure 26: Box diagram of the calmodulin sequence, showing the eight helical regions and the four calcium binding loops.

Each calmodulin molecule binds four Ca^{2+} atoms, in four EF-hand helix-loop-helix domains, labelled 1 - 4 on Figure 26. Binding of calcium to these domains occurs in a stepwise manner. As each calcium atom binds, it effects changes in conformation of the protein to allow the subsequent ligands to bind.

The overall fold of Ca^{2+} calmodulin is a dumbbell shape, with two globular domains, each housing four helical regions, labelled with roman numerals on Figure 26. These comprise two EF-hand motifs in each domain. A large central helical region separates the two domains [90]. According to X-ray crystal structures, the helices IV and V and the region between form one large helix, spanning residues 65 - 92 [91, 92].

However according to NMR structures, the central hinge region is very flexible and is better represented as in Figure 26, with two helical regions and a central linker, or hinge [93]. This central linker can change conformation significantly in order to accommodate binding to calmodulin's many and varied binding partners [94].

There is a large hydrophobic region on each globular domain of calmodulin; these are surrounded by patches of negative electrostatic potential which are ideal binding sites for positively charged binding partners [95].

4.3 Peptides which bind to calmodulin – "baa" peptides

Calmodulin can bind many short, positively charged alpha helical protein sequences or "baa" peptides (basic amphipathic alpha helical peptides) [95] and there have been a number of studies in the past using both X-ray crystallography and NMR spectroscopy to determine the structures of these complexes [91].

A series of idealised peptides containing only leucine, tryptophan and lysine was constructed by DeGrado and co-workers in the mid-1980s, which was designed to bind very strongly to calmodulin under experimental conditions [96, 97]. An example is shown below in Figure 27.

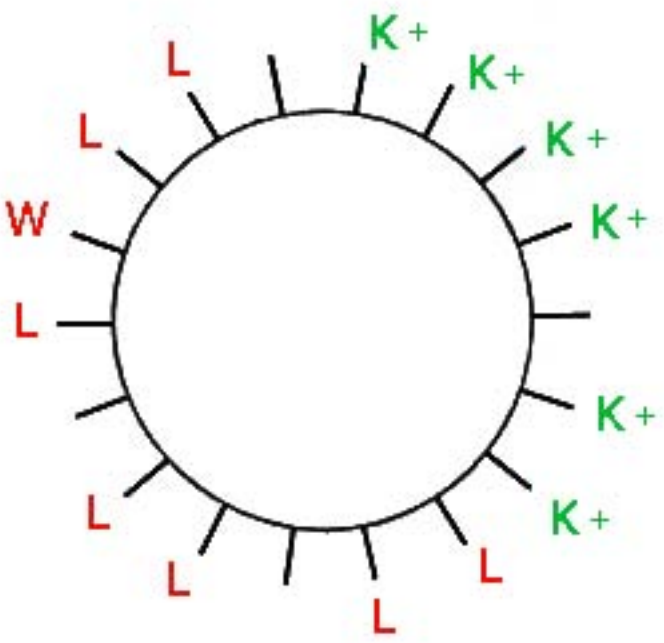

Figure 27: The model calmodulin binding peptide designed by DeGrado and co-workers with clearly defined amphipathicity and a high positive charge from basic lysine residues.

The positively charged, basic residues (shown in green on Figure 27) are clustered along one face of the peptide. These model peptides bind with high affinity to calmodulin. In other naturally occurring calmodulin binding sequences, the positively charged residues often sit on a curved trajectory around the body of the peptide. However these are also able to bind with high affinity due to the extremely flexible nature of calmodulin's binding site [95].

4.4 Peptides which bind to calmodulin – consensus hydrophobic residue sequences

There has also been considerable discussion that peptides which bind calmodulin must contain a general consensus sequence, with at least two long chain aliphatic

(Leu, Ile or Val) or aromatic residues positioned so that there are 7, 11 or 13 residues between them in the sequence in the binding region of the ligand [93, 98].

Positioning large aliphatic or aromatic amino acids 7 residues apart in the sequence places them along the same side of the peptide face, along the axis, when in an α-helical conformation, as discussed in section 1.5.

A study by Urbauer and co-workers showed that binding to calmodulin requires van der Waals interactions. The complex between calmodulin and the neuro-p peptide (the binding region of neuromodulin) was studied under high pressure conditions. High pressure conditions dissociate ionic interactions, but allow van der Waals interactions to remain intact. The midpoint dissociation pressure for ionic interactions is approximately a few hundred bar, the pressure required to dissociate van der Waals forces is ten-fold higher. The complex remained intact at kilobar pressure, indicating that van der Waals forces serve to maintain binding interactions even after ionic bonding has been disrupted [99].

The idealised peptides designed by DeGrado and co-workers also contain this consensus hydrophobic sequence, along the opposite axial face of the peptide to the basic residues [96, 97].

4.5 Binding modes of peptides to calmodulin

There are many binding modes of peptides or protein binding sequences to calmodulin. The protein can adopt either an extended or a collapsed conformation. In the former, a peptide ligand may interact with one half of the calmodulin molecule, binding on one lobe of the dumbbell only, or in the case of larger ligands, a trimer can form between the ligand and two calmodulin molecules [100].

Elshorst and co-workers showed in 1999 that the binding domain of the plasma membrane calcium pump (peptide C20W) binds only to the C-terminal domain of calmodulin. The structure of the complex was elucidated using heteronuclear NMR

experiments. This mode of binding is quite different from the majority of other published calmodulin-peptide complexes [101].

Another mode of binding involves the flexible central linker region wrapping around the ligand in order to form a globular spherical shaped complex. This mode is much more common and a number of examples of exist in the literature [100, 102].

A good example of this form of collapsed complex structure was elucidated by Ikura and co-workers in the early 1990s. The myosin light chain kinase binding region (peptide M13) from rabbit skeletal muscle light chain kinase was shown using 3- and 4-D NMR experiments to bind to both domains of calmodulin [98, 103].

The binding mode whereupon the central hinge of calmodulin wraps around the ligand has many slight variations. There are a number of overlapping sites in which different peptide and protein sequences are able to interact with calmodulin's binding regions on both domains. The inherent flexibility of calmodulin's binding specificity is what makes it such a centrally important and versatile protein [95]. It is therefore unsurprising that the sequence of calmodulin is so well conserved between so many species [104].

4.6 Litoria lesueuri

The stony creek frog, *Litoria lesueuri*, is unusual compared with other members of the *Litoria* genus in that it does not produce any anti-microbial peptides in its skin secretions. *L. lesuueri* only produces caerulein 1.1 (5), a neuropeptide, and lesueurin (6), a previously unknown peptide, which is unique to this species [27].

(5) Caerulein 1.1 pEQDY(SO_3)T GWMDF-NH_2

(6) Lesueurin GLLDI LKKVG KVA-NH_2

Screening of lesueurin for the common biological activities of other amphibian host defence peptides gave negative results. However, the synthesis of skin peptides is an

activity which requires great physiological input from the animals, so peptides which give no advantage to the animal are unlikely to be produced [105].

The properties of this peptide were therefore of great interest and a wider range of biological activities was screened for. This work and the subsequent testing of other previously uncharacterised peptides led to the discovery of three families of peptides which are active against neuronal nitric oxide synthase (nNOS).

4.7 nNOS active Australian amphibian peptides

The frog peptides which have been isolated by our group have only been tested against the calcium dependent neuronal isoform of NOS. Tests were performed in which radiolabelled arginine was allowed to be converted to citrulline by nNOS in the presence of calmodulin. Addition of various amphibian peptides to the test solution inhibited the conversion of arginine to citrulline with IC_{50} values in the range 1.7 – 41 μM.

By increasing the concentrations of calmodulin in these solutions the activity could be reinstated by up to 50%. The inhibition was determined to be non-competitive with respect to the arginine substrate and was therefore proposed to involve interaction with calmodulin, rather than direct interaction with the nNOS enzyme [27]. Selected nNOS active peptides are listed in Table 12.

Table 12: nNOS active peptides, their activity levels and species of origin. (Adapted from Apponyi et al, [10])

Name	Sequence	IC_{50}(μM)	Charge	Species
Group A				
Lesueurin	GLLDILKKVGKVA-NH_2	16.2	+3	*L. lesueuri*
Aurein 1.1	GLFDIIKKIAESI-NH_2	33.9	+1	*L. aurea*
Aurein 2.2	GLFDIVKKVVGALGSL-NH_2	4.3	+2	*L. aurea*
Aurein 2.3	GLFDIVKKVVGIAGSL-NH_2	1.8	+2	*L.aurea*
Aurein 2.4	GLFDIVKKVVGTLAGL-NH_2	2.1	+2	*L.aurea*
Citropin 1.1	GLFDVIKKVASVIGGL-NH_2	8.2	+2	*L. citropa*
Group B				
Dahlein 5.1	GLLGSIGNAIGAFIANKLKP-OH	3.2	+3	*L. dahlii*
Frenatin 3	GLMSVLGHAVGNVLGGLFKPKS-OH	6.8	+3	*L. infrafrenata*
Splendipherin	GLVSSIGKALGGLLADVVKSKGQPA-OH	8.5	+3	*L. splendida*
Group C				
Caerin 1.1	GLLGVLVSIAKJVLPHVVPVIAEHL-NH_2	36.6	+1	*L. splendida*
Caerin 1.6	GLFSVLGAVAKHVLPHVVPVIAEKL-NH_2	8.5	+2	*L. chloris*
Caerin 1.8	GLFKVLGSVAKHLLPHVVPVIAEKL-NH_2	1.7	+3	*L. chloris*
Caerin 1.9	GLFGVLGSIAKHVLPHVVPVIAEKL-NH_2	6.2	+2	*L.chloris*
Caerin 1.10	GLLSVLGSVAKHVLPHVVPVIAEKL-NH_2	41	+2	*L. chloris*

4.8 Aims:

To express ^{15}N labelled calmodulin using a bacterial expression system. To perform titration studies using ^{15}N-HSQC experiments in order to prove that the inhibition of nNOS by these peptides is *via* a binding interaction with calmodulin.

4.9 Bacterial protein expression systems

In the last two decades there has been a significant research effort put into perfecting the use of bacteria to over-express proteins of interest on a preparative scale. The basic principle involves inserting a DNA sequence which encodes the protein of interest into the bacterial cell thereby switching on expression of that gene. This is a very simplified view of the process, which is extremely elegant in its design.

Expression of a foreign gene in a bacterial host requires a number of other artificial genes, besides the gene of the expression target, to be inserted into the host cell. Collectively, these newly inserted genes are known as an expression system. The most commonly used expression system is the T7 system, which was also used in the current study [106].

4.10 Transcription of genes using the T7 promoter system

The first condition of use of the T7 system is that the T7 RNA polymerase gene be inserted into the cell's own chromosome, under the control of the lacUV5 promoter, as well as a lacI gene, which encodes the repressor protein for the lacUV5 promoter.

The insertion of this combination of genes is performed in such a way to cause the lacI gene to be constantly transcribed unless specifically switched off, so that the basal situation is that the T7 RNA polymerase gene is not transcribed.

Activation of transcription of the T7 RNA polymerase is possible by addition of isopropyl-β-D-thiogalactopyranoside (IPTG) to the growth medium. IPTG is an unnatural isomer of lactose which binds to and activates the lac UV5 promoter (usually activated by the presence of intracellular lactose) but which *E. coli* does not have the appropriate enzymes to break down in order to switch off the gene [107]. Therefore, lactose is not used, as the cells can break it down and halt expression of the desired gene product.

Once the cell has been set up to allow transcription of T7 RNA polymerase, the genes for the protein of interest must also be inserted. This is generally achieved by the insertion of a vector containing the appropriate gene, under control of a T7 promoter.

Thus, when IPTG is introduced to the cell, the repression of the polymerase is deactivated, and the polymerase is able to bind to the promoter controlling expression of the gene of interest. The T7 RNA polymerase is approximately five times more efficient at gene transcription than the *E. coli* RNA polymerase. Once the gene is switched on, it remains active until the cells are lysed or die due to the pressure from expressing the foreign protein, as they cannot switch the promoter off to revert to their normal cellular functions. Thus, the cell is rapidly forced to put all of its energies into expression of the chosen gene, often to the extent that all normal cellular processes are shut down [107].

As the T7 promoter consists of a DNA sequence rarely found anywhere else, this allows for specific control of gene expression, and as each gene inserted is followed by a T7 terminator sequence, no excess gene products are made.

Addition of 0.4 mM IPTG to a culture of *E. coli* BL21 DE3 cells, which have been transformed with a plasmid containing the T7 RNA polymerase gene, is sufficient to induce production of polymerase.

Obviously the expression of the inserted gene to the exclusion of other normal cellular genes is deleterious to the bacteria. In order to prevent them from simply ejecting the vector, antibiotic resistance genes are also inserted into the vector containing the gene of interest, so that only cells which contain the plasmid will exhibit antibiotic resistance. Therefore, when the cells are grown in a medium containing antibiotics (the most commonly used are kanamycin and ampicillin), only those containing the vector will survive [106].

4.11 Bacterial cell lines suitable for protein expression

The most commonly utilised cell line for bacterial protein expression is the *E. coli* BL21 DE3 strain. This strain has been specially developed to lack the *lon* protease and the *ompT* protease, both of which would otherwise degrade the over-expressed protein and significantly lower protein yields [106].

4.12 Fusion proteins

When the protein of interest is of a small size or prone to misfolding, it can be expressed as a fusion protein with a purification tag. This can aid in the folding of the protein and also assist with purification. An example is the glutathione S-transferase (GST) enzyme, a good example of a fusion partner which does both.

GST fusions are easily purified with a glutathione affinity column and cleaved using thrombin to give the expression partner. However cleavage with thrombin causes the addition of Gly-Ser sequence at the N-terminus of the protein so this may be unsuitable for the expression of some proteins, especially when the exact sequence is of importance [107, 108].

Another commonly used purification tag is the His-tag, in which a poly-histidine sequence is added at the N-terminus of the protein, allowing for purification using a nickel affinity column [108].

A number of different vectors are commercially available, each with slightly different optimisations and containing different purification tags and restriction sites. The restriction enzymes chosen to insert the gene of interest must be carefully chosen in order to avoid unintentional cleavage inside the gene sequence. Conveniently there are also a large number of restriction enzymes commercially available: finding one with an appropriate restriction site is generally not difficult [109, 110].

4.13 Bacterial expression of isotopically labelled proteins

Growth of bacteria is most rapid when using a rich growth media such as Luria broth, which essentially contains yeast extracts, sugars and vitamins and provides everything that growing bacterial cells require. Expression of proteins in rich media generally gives rapid expression and high yields [107].

When proteins are required for NMR studies and spin active isotopes are required to be present, bacteria must be grown in a minimal medium containing only the fundamental components necessary to enable cells to survive. The minimum requirements are a carbon source (generally glucose), a nitrogen source (generally ammonium chloride) and a series of vitamins and salts.

The disadvantage of using minimal medium is that cells being grown in a minimal medium are forced to synthesise, from starting materials, all of the molecules they require for growth. Therefore they grow much more slowly and gene expression is generally slower and of poorer yield than in a rich medium [111].

4.14 Preparation of ^{15}N labelled calmodulin for titration studies

In order to perform ^{15}N-HSQC titrations between our amphibian peptides and calmodulin, bacterial protein expression was employed to generate a ^{15}N-labelled sample of the protein.

As calmodulin is such a highly studied protein we were fortunate to be supplied by the authors of a previous study with a vector with the calmodulin sequence already inserted [101]. The vector was pET28a, the insert sequence was confirmed using PCR and is shown in Figure 28.

```
     Nco1/START                                                  10
TAT ACC ATG GCT GAC CAA CTG ACA GAA GAG CAG ATT GCA GAG TTC
     M   A   D   Q   L   T   E   E   Q   I   A   E   F
                             20
AAA GAA GCC TTC TCA TTA TTC GAC AAG GAT GGG GAC GGC ACC CTC
 K   E   A   F   S   L   F   D   K   D   G   D   G   T   I
         30                                          40
ACC ACA AAG GAA CTT GGC ACC GTT ATG AGG TCG CTT GGA CAA AAC
 T   T   K   E   L   G   T   V   M   R   S   L   G   Q   N
                             50
CCA ACG GAA GCA GAA TTG CAG GAT ATG ATC AAT GAA GTC GAT GCT
 P   T   E   A   E   L   Q   D   M   I   N   E   V   D   A
         60                                          70
GAT GGC AAT GGA ACG ATT GAC TTT CCT GAA TTT CTT ACT ATG ATG
 D   G   N   G   T   I   D   F   P   E   F   L   T   M   M
                             80
GCT AGA AAA ATG AAG GAC ACA GAC AGC GAA GAG GAA ATC CGA GAA
 A   R   K   M   K   D   T   D   S   E   E   E   I   R   E
         90                                         100
GCA TTC CGT GTT TTT GAC AAG GAT GGG AAC GGC TAC ATC AGC GCT
 A   F   R   V   F   D   K   D   G   N   G   Y   I   S   A
                            110
GCT GAA TTA CGT CAC GTC ATG ACA AAC CTC GGG GAG AAG TTA ACA
 A   E   L   R   H   V   M   T   N   L   G   E   K   L   T

         120                                         130
GAC GAA GAA GTT GAC GAA ATG ATA AGG GAA GCA GAT ATT GAT GGT
 D   E   E   V   D   E   M   I   R   E   A   D   I   D   G
                            140
GAC GGC CAA GTA AAC TAC GAA GAG TTT GTA CAA ATG ATG ACA GCA
 D   G   Q   V   N   Y   E   E   F   V   Q   M   M   T   A
    STOP                                    Not1
AAG TGA AGA GTC TAG AAT CGA TAA GCT TGC GGC CGC
 K
```

Figure 28: The protein encoding sequence of the inserted calmodulin gene.

The protein was expressed as a discrete unit with no fusion partner nor N- or C-terminal purification tags. The insert for calmodulin was inserted using Nco1 and Not1, thereby removing the His-tag functionality present in the pET28a+ vector, which is encoded in between these two restriction sites.

Following confirmation of the correct gene sequence using PCR, the vector was then transformed into the *E. coli* BL21 DE3 cell line for mass expression. Cells were grown in an overnight culture in Luria broth, (LB) then diluted 1/50 and grown to OD_{600} 0.8 in ^{15}N enriched minimal medium (min A [112]) containing 0.8g $^{15}NH_4Cl$ per litre.

Upon cell density reaching OD_{600} 0.8, the cells were induced with 50 mM isopropyl-β-D-thiogalactopyranoside (IPTG) and left to express for two hours before being harvested by centrifugation at 10,000 rpm for 15 minutes at 4˚C.

Upon harvest the cells were resuspended in 40 mL tris buffered saline (TBS) buffer containing 0.1% triton X-100. They were sonicated to induce lysis, during which phenylmethylsulphonyl fluoride (PMSF) was added to a final concentration of 1 mM to inhibit proteolytic degradation of the sample.

The lysate was then spun and filtered to remove cell debris and the resultant supernatant solution loaded onto a 50 mL anion exchange column packed with Q-sepharose (Sigma). A gradient of 0 - 100% buffer B over 8 column volumes was employed, where buffer A was 50 mM tris and buffer B was 50 mM tris plus 1 M sodium chloride: 4 mL fractions were collected, with calmodulin typically eluting in fractions 39 - 49, time 190 - 220 min post injection. A typical gel of the fractions containing calmodulin is displayed in Figure 29. There is still a significant quantity of high molecular weight contaminants present at this stage of purification.

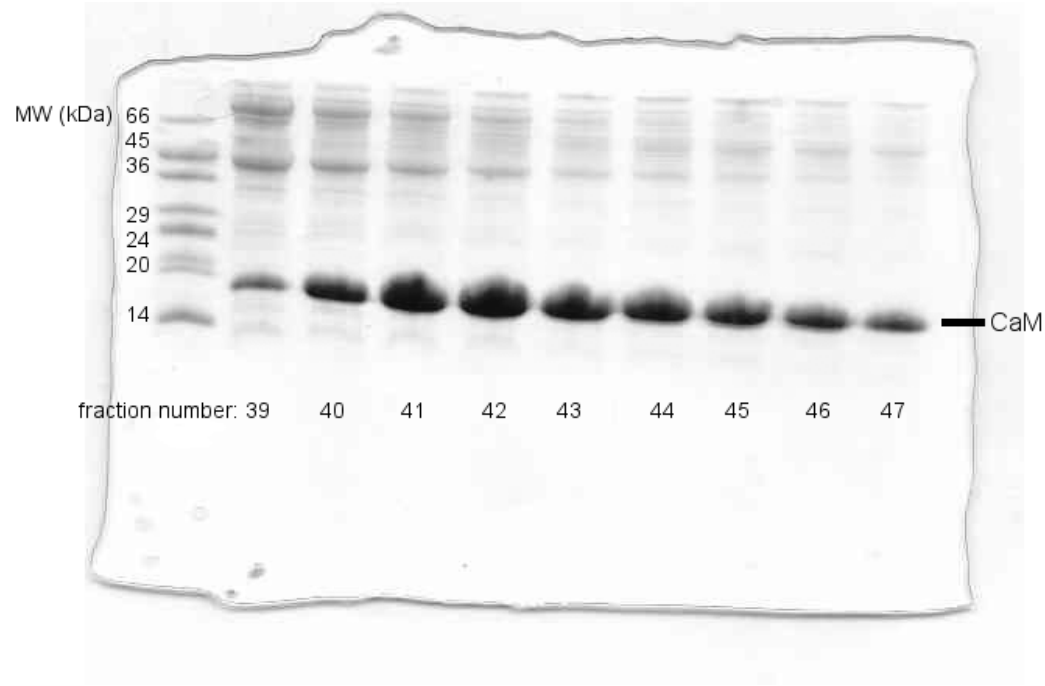

Figure 29: SDS-page gel of fractions 39 - 47 from a typical anion exhange column of unpurified calmodulin.

Following analysis of the column fractions using an SDS-PAGE gel, relevant fractions were combined and concentrated using an Amicon stirred cell for ultra filtration, fitted with a 10 kDa size limit filter. The concentrated solution was then eluted over 300 mL superdex 75 size exclusion chromatography resin, with tris buffered saline solution as the mobile phase [91]. 5 mL fractions were collected, with pure calmodulin eluting in fractions 41 – 46, 170 - 210 minutes post-injection.

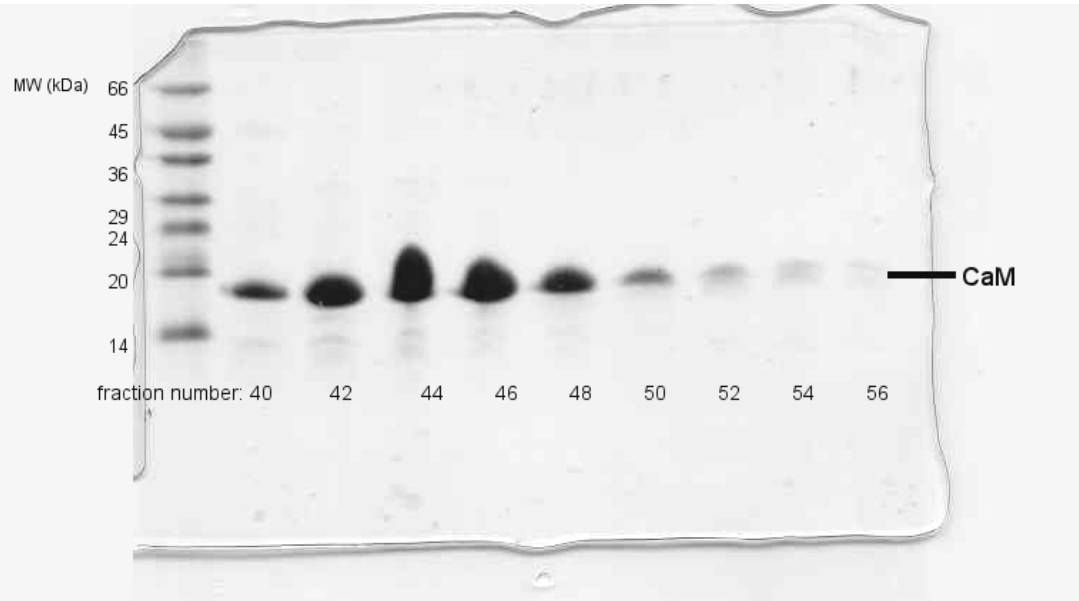

Figure 30: SDS gel of fractions 40 - 56 of a typical superdex 75 column of calmodulin.

The relevant fractions were identified using an SDS-PAGE gel. A typical gel of the fractions containing calmodulin is shown in Figure 30. At this stage the protein is now pure enough for NMR studies. The purified protein was then concentrated again using the Amicon stirred cell ultra filtration unit and a 10 kDa size exclusion filter. The buffer salts were removed using a PD-10 desalting column (Amersham Biosciences). Phosphate buffers co-precipitate with calcium and therefore could not be used, as the calmodulin requires calcium to be added to solution.

The calmodulin was concentrated by freeze-drying and the final concentration determined using the BCA method [113]. Each NMR sample contained 1.89×10^{-7} moles of calmodulin, or 3.159 mg in 500 µL total volume. The samples were adjusted to a pH of 6.3, potassium chloride added to a concentration of 31 mM and calcium chloride was added to a concentration of 6.3 mM, in a 10% D_2O solution. Sodium azide (0.02%) was added as a preservative. These are the same experimental conditions as were utilised for a previous study [114].

4.15 Titrations of Australian amphibian skin peptides with calmodulin

In order to prove the interaction between our nNOS active amphibian peptides and calmodulin, a series of ^{15}N-HSQC titrations has been performed. Increasing quantities of the unlabelled peptides were added into ^{15}N labelled calmodulin samples and a high resolution ^{15}N-HSQC spectrum was recorded after each addition.

The chemical shift perturbations were tracked by overlaying each new HSQC spectrum upon the previous ones. The HSQC spectrum is ideal for following the titration of a labelled protein with a peptide ligand. In this way it becomes clear immediately which residues are affected by the addition of the peptide [115].

4.16 Preparation of peptides for titration

In order to eliminate any possible unwanted effects on the chemical shifts due to changing concentrations or pH, the solvated peptides were adjusted to pH 6.3 [114] then aliquoted to appropriate portions prior to lyophilisation. Dried peptide portions were then added to the calmodulin in sequence with the pH being re-adjusted back to 6.3 as required after each addition by the addition of small quantities of hydrochloric acid or sodium hydroxide solutions. The volume of the sample was therefore kept relatively constant throughout the titration series. As previously discussed (section 4.14), phosphate buffers cannot be used due to the required calcium salts which precipitate as calcium phosphate in their presence.

The proportion of residues experiencing significant shifts (greater than 0.5 ppm in nitrogen and greater than 0.05 ppm in proton) was large in all cases, indicating that there is an overall change in conformation of calmodulin upon binding rather that localised structural changes at the binding interfaces.

4.17 Titration of calmodulin with splendipherin

The first titration was performed with splendipherin (3), the aquatic sex pheromone of *Litoria splendida*, a member of inhibitor group B which has an IC_{50} value of 8.5 μM and an overall charge of +3. In all titrations the quantity of calmodulin used was the same: 3.158 mg, equivalent to 1.89 x 10^{-7} moles.

(3) Splendipherin: GLVSS IGKAL GGLLA DVVKS KGQPA-OH

The Edmundson helical wheel representation of splendipherin, with positively charged residues displayed in green, is shown below in Figure 31.

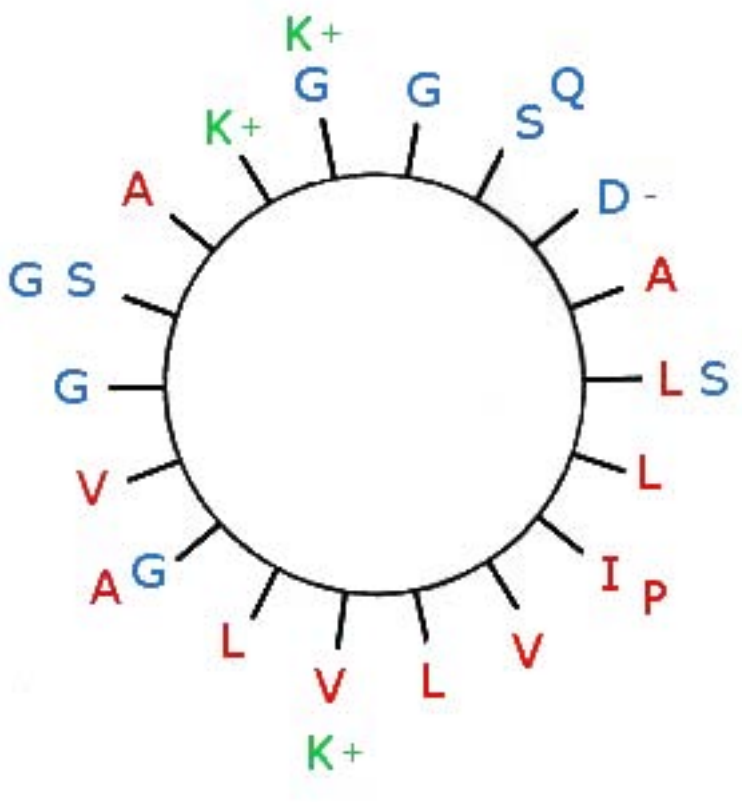

Figure 31: An Edmundson helical wheel representation of splendipherin.

The hydrophobic and hydrophilic regions are not particularly well defined over the length of the peptide, however when each helix is analysed separately, a much

clearer trend of delineation between the hydrophilic and hydrophobic zones is observed. This is particularly true of the N-terminal helix. The Edmundson helical wheel diagrams of the two separated helices are presented in Figure 32. Hydrophobic residues are shown in blue, hydrophilic residues in red and basic residues in green. The two central glycine residues are not included.

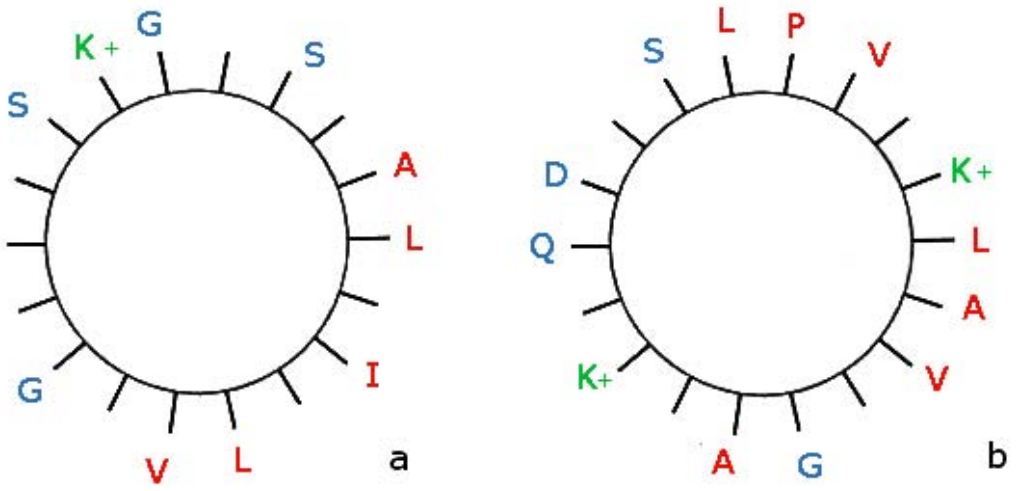

Figure 32: The two helices of splendipherin, presented as Edmundson helical wheel diagrams.

As can be seen in Figure 32a, the N-terminal helix of splendipherin fits the “baa” peptide model very well. The second helix is less clearly defined. Alanine 15 and lysine 16 are the only two residues which do not fit clearly into the amphipathic delineation. The quantities of splendipherin added during the titration are shown in Table 13.

Table 13: Quantities of splendipherin used for titration with calmodulin.

Step	Concentration (mM)	Splendipherin (mg)	Ratio of CaM to peptide
0	0	0	1:0
1	0.08	0.104	1:0.125
2	0.16	0.104	1:0.25
3	0.31	0.208	1:0.5
4	0.62	0.416	1:1
5	1.25	0.833	1:2
6	2.5	1.66	1:4

The chemical shift changes occurring in the ^{15}N-HSQC spectra of calmodulin upon addition of splendipherin indicate weak binding. Each nitrogen resonance which experiences a change in chemical shift is disrupted slowly, with approximately constant peak intensity. This is clearly indicative of a fast exchange regime, where both bound and unbound species of calmodulin are in rapid equilibrium, such that the chemical shifts displayed by a non-saturated sample arise from an average of the bound and unbound isoforms [29].

In particular, residues R90, D93 and Q135 clearly indicate a fast exchange binding, as indicated in Figure 33.

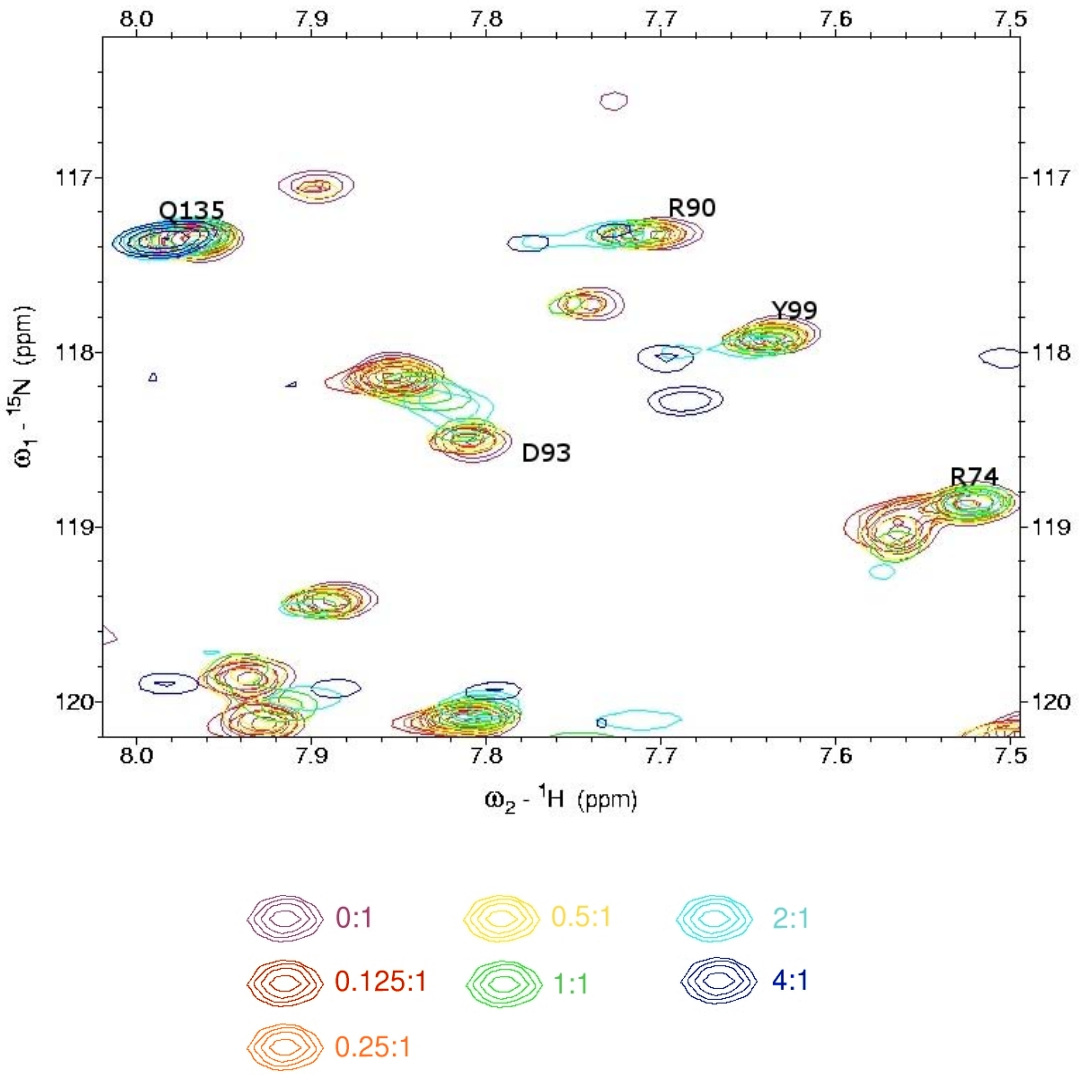

Figure 33: A section of the overlaid ^{15}N-HSQC spectra of the titration of calmodulin with splendipherin. Assigned residues in the unbound spectrum are labelled. The legend is shown below the spectrum.

The chemical shift perturbations experienced by the backbone amide atoms upon addition of splendipherin to calmodulin indicate that these two species do indeed bind. However, because splendipherin binds in fast exchange, it is not a suitable peptide to use for determination of a 3D NMR structure.

The interpretation of fast exchange spectra is inherently problematic, as stated eloquently by Lian in 1994 - "Interpretation of fast exchange spectra must of necessity be carried out in terms of a model and the conclusions will only be meaningful if the model is correct" [29]. As the mode of binding has not been determined yet, a suitable model cannot be proposed, especially because calmodulin can bind its partners in so many different conformations. Other peptides were therefore chosen for titration into calmodulin.

4.18 Titration of a citropin 1.1 analogue with calmodulin

The second peptide selected for titration was an analogue of citropin 1.1. (7)

(7) Citropin 1.1 analogue: GLFDV IAKVA SVIKK L-NH_2

This peptide is a member of inhibitor group A, and has a significantly lower IC_{50} value than splendipherin, indicating a stronger binding interaction. Citropin 1.1 itself (8) was not chosen as it has a much higher IC_{50} value, 8.2 μM, compared with that of the analogue, at 1.6 μM. This peptide (7) has an overall charge of +3.

(8) Citropin 1.1: GLFDV IKKVA SVIGG L-NH_2

Citropin 1.1 has very well defined amphipathicity along the entire length of the peptide, as presented in Figure 34. Hydrophobic residues are shown in red, hydrophilic residues are shown in blue and basic residues in green. Although citropin 1.1 has a higher IC_{50} value than the analogue (7), and also fits the "baa" peptide model (proposed by DeGrado and co-workers [96]) much more neatly, it also has a lower overall charge of +2, which may explain its weaker binding affinity.

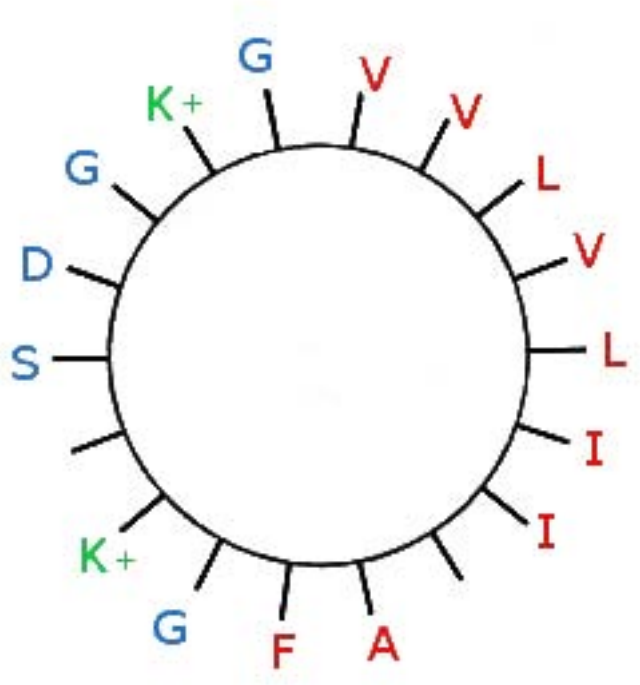

Figure 34: An Edmundson helical wheel projection of citropin 1.1 showing the good delineation between hydrophobic and hydrophilic zones.

The citropin analogue chosen is one of those studied in the work published by Doyle and co-workers in 2003 [35], in which a number of synthetic analogues of citropin 1.1 were produced and tested for their nNOS inhibition activity: (7) has the equal lowest IC_{50} value of any of the synthetic analogues.

The amphipathicity of the analogue peptide (7) is less well defined than that of citropin 1.1, with alanine 7 and lysine 14 overlapping between the hydrophilic and hydrophobic zones. However, these residues are well-separated along the length of the peptide. The hydrophobic and hydrophilic zones could therefore be considered to be curving along the length of the peptide as opposed to being regularly perpendicular to the axis. (Figure 35)

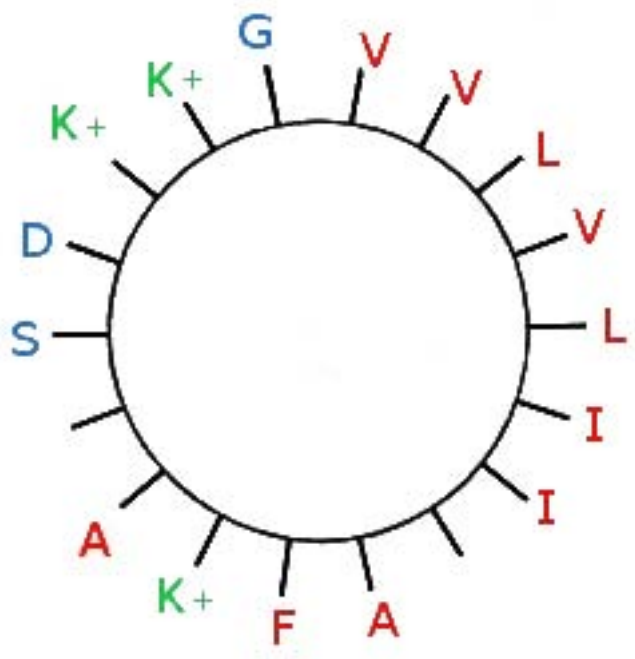

Figure 35: An Edmundson helical wheel projection of the citropin 1.1 analogue (7) used to titrate with calmodulin. Hydrophobic residues are shown in red, hydrophilic residues are shown in blue and basic residues in green.

Due to the low IC_{50} value and overall charge of +3, this peptide was expected to bind with good affinity for calmodulin. The quantities of peptide used in the titration are shown in Table 14.

Table 14: Quantities of the citropin 1.1 analogue used in the titration with calmodulin.

Step	Concentration (mM)	Citropin analogue (mg)	Ratio of CaM to peptide
0	0	0	1:0
1	0.0472	0.0402	1:0.125
2	0.0944	0.0805	1:0.25
3	0.189	0.1609	1:0.5
4	0.378	0.322	1:1
5	0.757	0.644	1:2
6	1.51	1.288	1:4
7	2.52	2.575	1:8

Again, the overlaid spectra of the titration of this peptide did not indicate a slow exchange regime. The chemical shifts of the majority of backbone amide nitrogen atoms are affected, but the binding mode qualifies as intermediate exchange, as the peak intensities are irregular. Some peaks experience an averaging and gradual change of chemical shift, whereas other peaks gradually disappear before reappearing at other coordinates.

Those peaks which appear to be in slow exchange often do not reappear with the same intensity as in the original spectrum. This is a classic case of intermediate exchange, described by Lian and co-workers as such: “if an existing protein resonance is sharp at very low concentrations, and broadens markedly as the ligand concentration increases, a signal reappears at high ligand concentration, and may shift somewhat as the concentration is further increased, then intermediate exchange is occurring.” [29]

Figure 36 shows a selected region of the titration spectra overlaid to show the irregularity of the peaks in this complex; assigned unbound peaks are labelled.

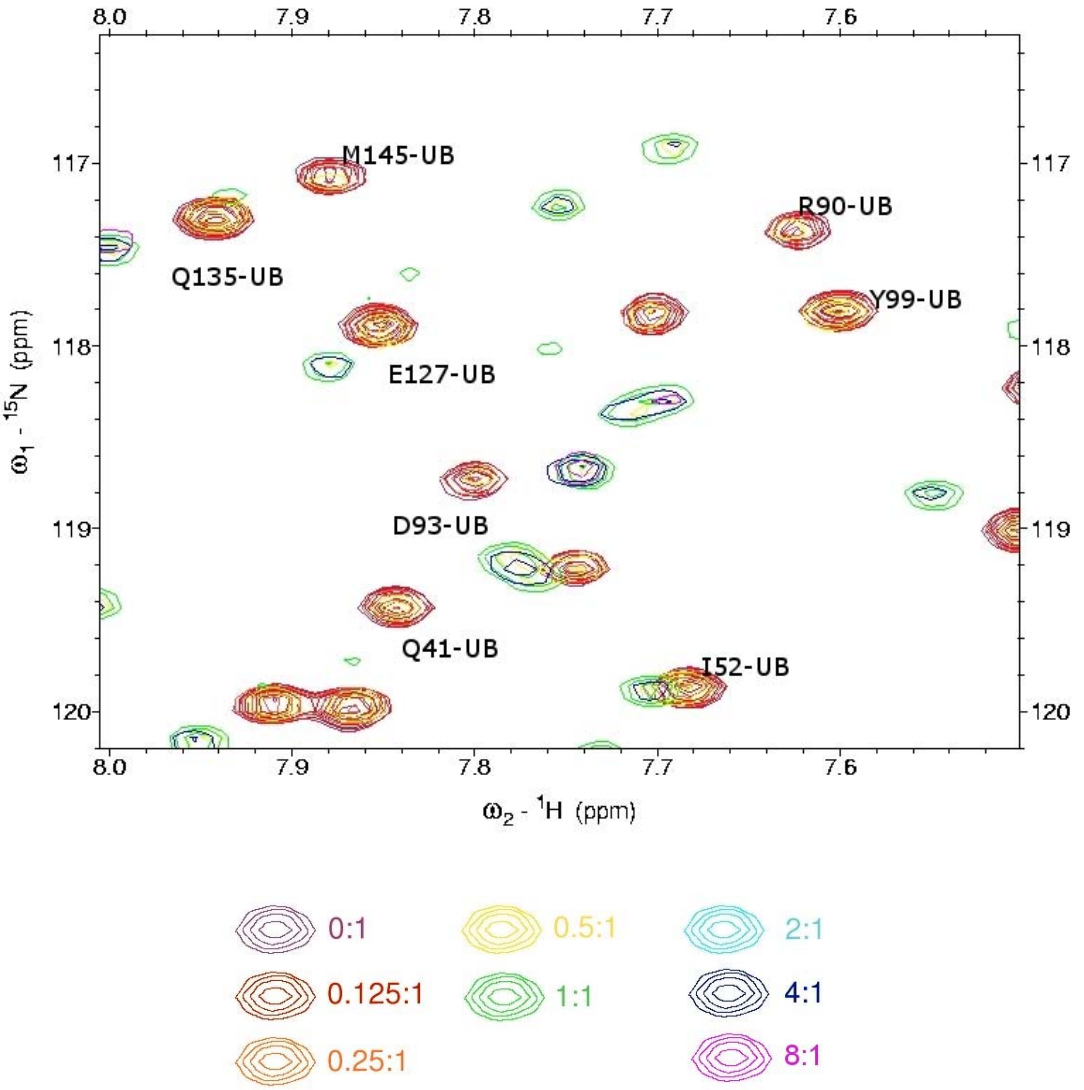

Figure 36: A region of the overlaid ^{15}N-HSQC spectra from the titration of calmodulin with the citropin analogue.

4.19 Titration of calmodulin with caerin 1.8

The third peptide chosen to titrate with calmodulin was the naturally occurring caerin 1.8 (9); its IC_{50} value is similar to that of the citropin 1.1 analogue, at 1.7 µM, but caerin 1.8 belongs to inhibitor group C, from which an example had not yet been studied, so it was chosen for this reason. Caerin 1.8 has an overall charge of +3, which also identified it as being a good candidate for binding studies.

(9) Caerin 1.8: GLFKV LGSVA KHLLP HVVPV IAEKL-NH_2

The Edmundson helical wheel diagram of the entire sequence of caerin 1.8 shows rather poor delineation between hydrophilic and hydrophobic zones, as presented in Figure 37.

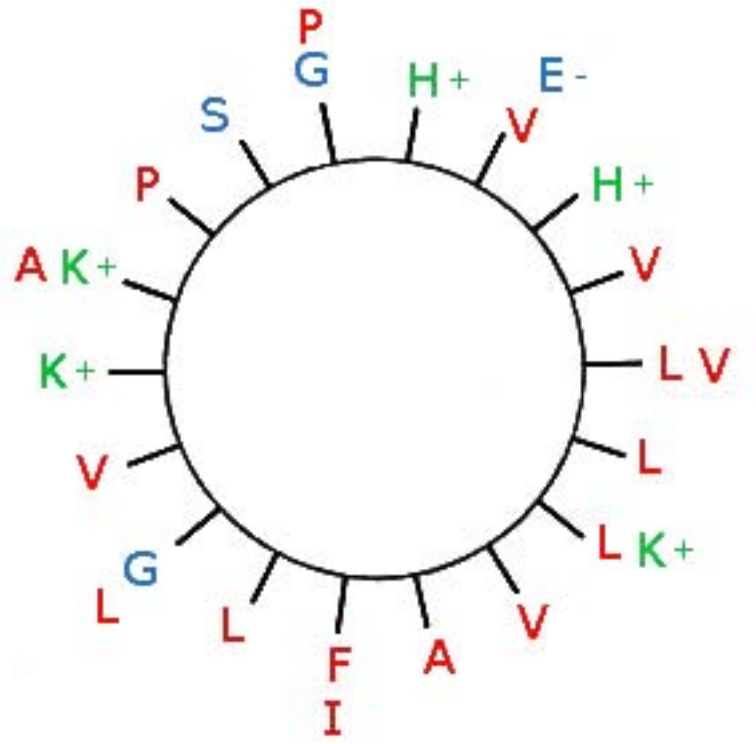

Figure 37: An Edmundson helical wheel projection of caerin 1.8. Hydrophobic residues are shown in red, hydrophilic residues in blue and basic residues in green.

However, dividing caerin 1.8 into two halves and generating an Edmundson helical wheel diagram for each half reveals much better separation, therefore it can be described as having its delineation curving along the peptide, rather than simply along the axis of its length. (Figure 38)

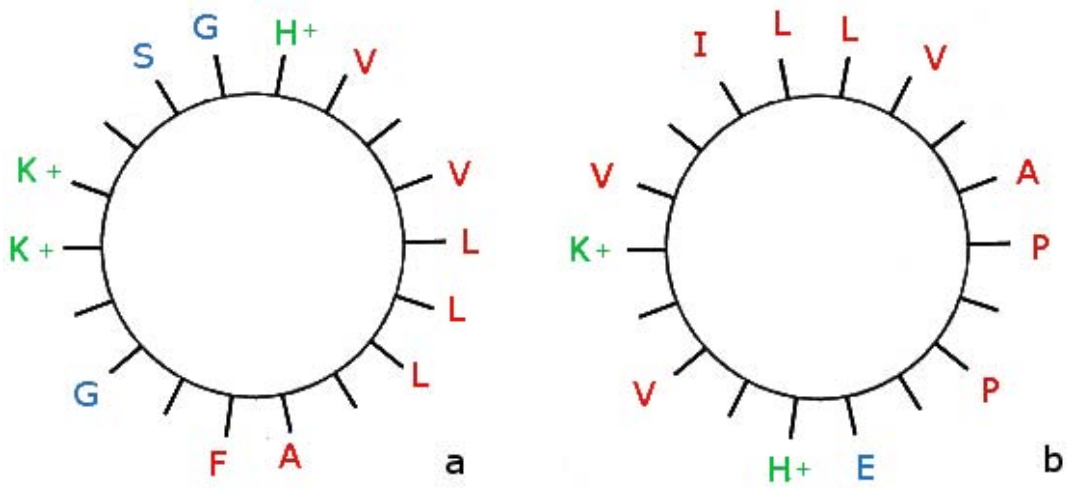

Figure 38: Edmundson helical wheel diagrams of the first half (a) and second half (b) of caerin 1.8.

In particular, the first half of caerin 1.8 has the potential to form an amphipathic helix (Figure 38a); the second half has its hydrophobic and basic residues clustered on one face, although the valine at position 20 is in the middle of the hydrophilic region. The quantities of caerin 1.8 which were used in the titration with calmodulin are shown in Table 15.

Table 15: Quantities of caerin 1.8 used in the titration with calmodulin.

Step	Concentration (mM)	Caerin 1.8 (mg)	Ratio of CaM to peptide
0	0	0	1:0
1	0.0756	0.10062	1:0.2
2	0.1134	0.20214	1:0.4
3	0.151	0.30187	1:0.6
4	0.189	0.4025	1:0.8
5	0.378	0.503	1:1
6	0.756	1.006	1:2
7	1.51	2.012	1:4

The titration series performed with caerin 1.8 showed consistent chemical shift changes and clearly indicates a slow exchange complex.

The resonances of the bound species begin to appear at low concentrations of the peptide, after the addition of only 0.4 equivalents of the peptide. The peak intensities of the bound and unbound forms at 0.6 equivalents of peptide are roughly equivalent; this indicates a 1:1 stoichiometry in the complex and is further evidence for the complex being in slow exchange.

The protein was fully bound and giving rise to completely new set of chemical shifts at a 1:1 concentration; saturation to 4:1 equivalents of peptide did not change the chemical shifts further [29].

Further, the peak intensities of the bound conformation attain the same intensity upon full saturation as the unbound protein had, further indicating that the complex is stable on the NMR timescale. The overlaid ^{15}N-HSQC spectra are illustrated in Figure 39.

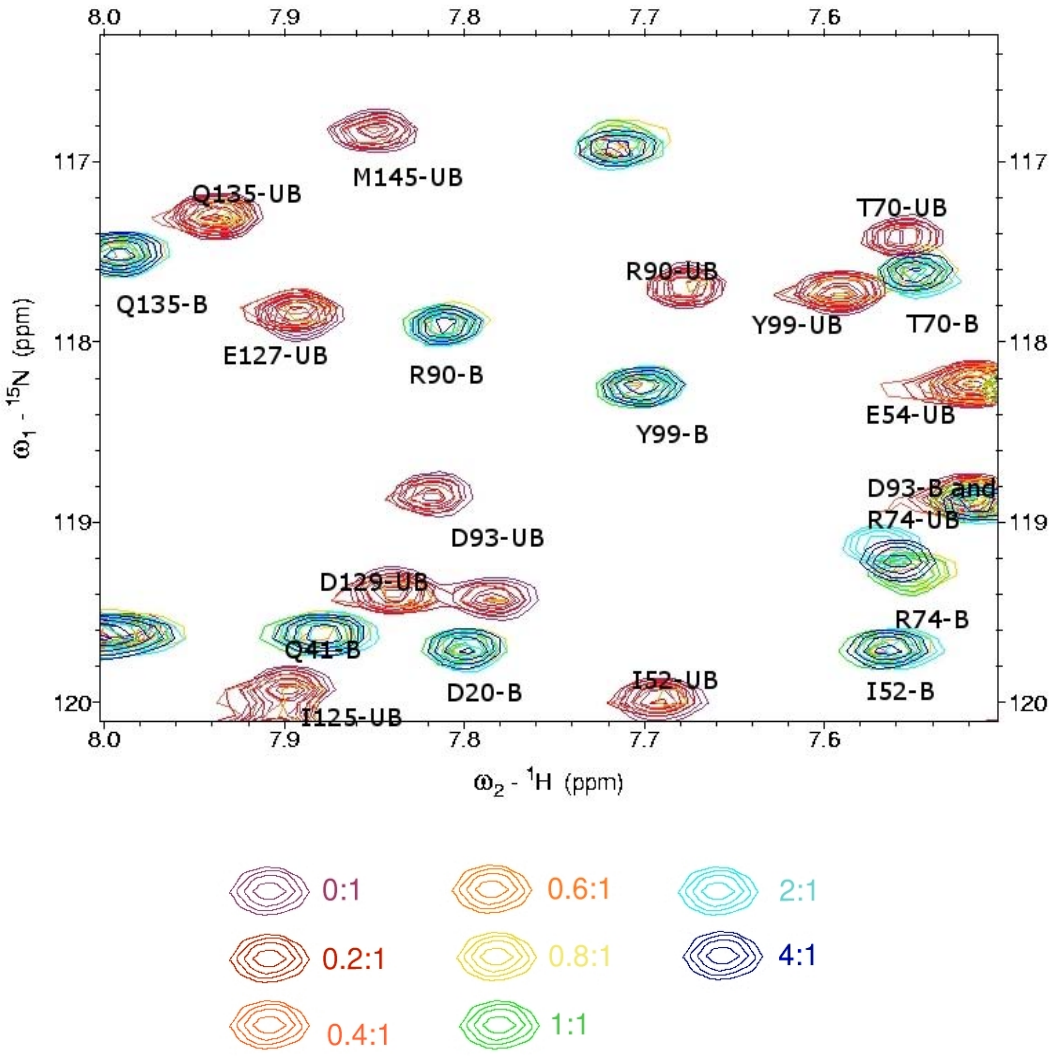

Figure 39: A region of the titration spectra of calmodulin bound to caerin 1.8.

The majority of chemical shifts in the bound and unbound spectra have been assigned, this involved the use of 3D NMR as discussed in Chapter 6. Here, the peaks are labelled with residue number and whether they belong to the bound conformation (denoted “B”) or the unbound conformation (denoted “UB”).

Residues such as D93, R90 and Y99 show clearly significant chemical shift changes upon binding. (Figure 39) The peak heights in the bound and unbound conformations are very similar, also indicating slow exchange.

4.20 Summary

Although splendipherin and the citropin analogue were expected to bind well to calmodulin, their binding was found to be reasonably weak under the conditions of the experiments.

Caerin 1.8 is the strongest binding partner for calmodulin of the three chosen for testing. All three of the peptides tested had a +3 charge, and so this difference alone cannot account for their different binding strengths [96]. Clearly, the binding affinity of calmodulin for its ligands is a complex balance between many different factors [87, 100].

Caerin 1.8 is expected to adopt an α-helical structure when in complex with calmodulin, in the same manner as the many other peptides capable of binding calmodulin which are unstructured in aqueous solution [102, 116].

However, this does not give any indication as to the kind of fold which calmodulin adopts during binding with the amphibian peptides. That the chemical shift changes occur throughout the calmodulin spectrum indicates that a significant change in conformation occurs [117].

Chapter 5 Expression of ^{15}N labelled caerin 1.8 peptide for NMR complex studies

5.1 Aims

To use a bacterial protein expression system to prepare doubly ^{13}C and ^{15}N-labelled caerin 1.8 as a fusion protein with glutathione S-transferase. To elucidate the conformation of the cleaved peptide when it is complexed with unlabelled calmodulin, using 3D heteronuclear NMR spectroscopy.

5.2 NMR studies of peptide-protein complexes

In order to fully study a complex between two binding partners, one species must be labelled with spin active isotopes and the other unlabelled. Changes in the structure of one partner in the presence of a ligand can therefore be studied without the distraction of correlations appearing due to the ligand itself, which may cause confusion with the changes in chemical shift occurring in the molecule of interest [118]. This is especially important when the complex is in slow exchange, as the new resonance positions often bear no relation to those of the unbound species [48].

Ideally, in our case where we wish to prove a binding interaction, labelling the peptide rather than the protein would be preferable. With only 25 residues, the study of the changes of conformation of the peptide could be achieved using only 2D NMR techniques. Studying the labelled 148-residue calmodulin protein is much less ideal, requiring 3D NMR as a minimum [119] and requiring much more intensive data analysis.

Commercial synthesis of uniformly ^{15}N and ^{13}C labelled peptides is prohibitively expensive. Therefore it was decided to express ^{15}N and ^{13}C labelled caerin 1.8 (9) using a bacterial expression system and a minimal labelled growth medium.

5.3 Construction of a vector to express caerin 1.8 as a fusion protein

Because of the small size of the peptide and to facilitate purification, we planned to express caerin 1.8 as a fusion protein with glutathione S-transferase (GST) using the pET32a+ vector (Novagen) and to cleave the fusion partner post-expression.

Expression as a GST fusion would allow for convenient purification also, using a glutathione affinity column, in a method similar to that used by Koenig and co-workers to express and purify the S2 peptide, which constitutes the binding sequence of bovine transductin [118].

Single stranded DNA synthesis is inherently error prone. This becomes more of a problem the larger the required gene product [120]. Due to the large size of the required insert (107 bp), the peptide encoding sequence was broken up into three smaller insert pairs. (Figure 40) The three pairs of oligonucleotides were annealed separately before being added to the overall ligation reaction.

```
5′ GATC CGA AAA TTT GTA TTT CCA GGG GCT GTT TG
        GCT TTT AAA CAT AAA GGT CCC CGA CAA AC CAC AAA 5′

5′ GTG TTT TAG GCA GCA TCG CCA AGC ACC TGC TTC
           ATC CGT CGT AGC GGT TCG TGG ACG AAG GCG TAC 5′

5′ CGC ATG TGG TCC CAG TAA TTG CAG AGA AAG CGT AG
           ACC AGG GTC ATT AAC GTC TCT TTC GCA TC TTAA 5′
```

Figure 40: The oligonucleotides encoding the caerin 1.8 sequence.

A TEV protease site was included between the GST and caerin 1.8 sequences, rather than the more routinely used thrombin site [108]. The use of thrombin would require the ideal recognition sequence LVPRGS, with cleavage occurring between the arginine and glycine residues and leaving an N-terminal sequence of GS on the passenger protein.

Maintaining the exact sequence of the peptide was considered to be of extreme importance as a previous mutation study shows that even slight changes in the sequences of these peptides can significantly alter activity levels [17]. For example, replacing the two lysine residues at positions 7 and 8 in citropin 1.1 with two alanine residues lowers the nNOS activity of the peptide from 13 μg/mL to 30 – 40 μg/mL [35].

The ideal recognition site for TEV protease is ENLYFQG, with cleavage occurring between the glutamine and glycine residues, [121, 122] leaving an N-terminal glycine residue on the passenger protein. This coincides with the N-terminal residue of the caerin 1.8 peptide.

The fully translated sequence of the insert is therefore as shown in Figure 41.

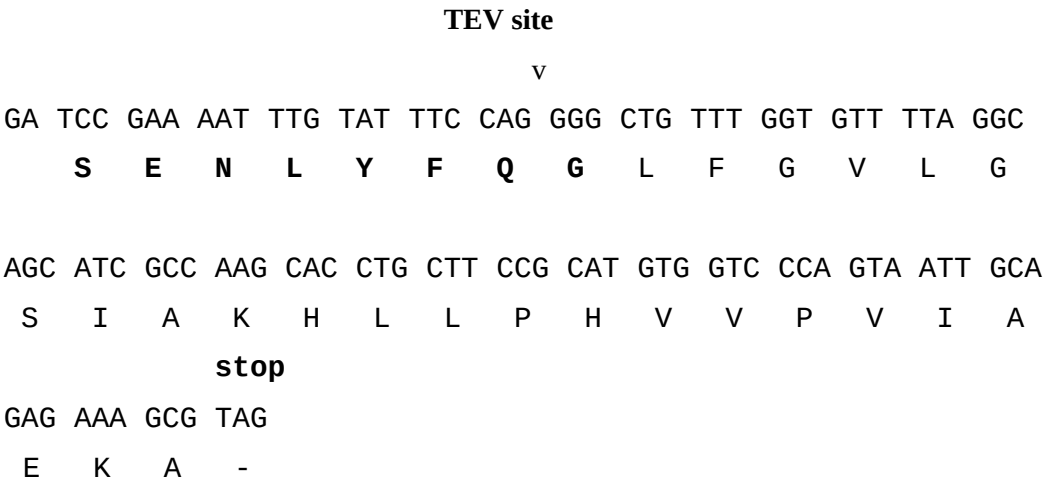

Figure 41: Translation of the oligonucleotide sequence inserted into the vector for expression of caerin 1.8.

5.4 Post-translational C-terminal amidation of synthetic caerin 1.8

The C-terminal leucine residue of caerin 1.8 was substituted with an alanine in the vector sequence in order to allow post-translational trans-peptidation with the carboxypeptidase Y enzyme. This enzyme cleaves the C-terminal residue of a protein or peptide and replaces it with a pre-amidated amino acid from solution. This process was necessary to achieve C-terminal amide functionality which is required for activity [123, 124].

Carboxypeptidase Y is most efficient at exchanging C-terminal residues when the leaving group is alanine or leucine, up to 98 or 41% respectively. Alanine was chosen because of the higher reported yields and also in order to make characterisation of the amidated product using mass spectrometry more simple by the subsequent larger difference in molecular weight between the reactant peptide and the amidated product [124, 125].

5.5 Expression tests with the caerin 1.8-GST fusion

The pET32a+ vector was expressed and purified, then cleaved with BamHI and EcoRI. After separately annealing the 3 insert pairs, a ligation reaction was performed overnight at 16º using T1 DNA ligase.

Transformation into *E. coli* strain DH5α of the newly constructed vector was unsuccessful on repeated attempts, with less than five colonies forming from each ligation reaction. The ligation of the vector was repeated and the products digested to check for correct insertion. The reaction products were run on 2% Agar gels, which showed correct size bands for both full vector and excised inserts. The transformation was therefore re-attempted with the pre-purified vector.

Upon eventual successful transformation and sequencing of the inserted vector, it was purified and transferred to the BL21 DE3 strain for expression tests but these yielded very poor results. Growth to induction density was very slow, taking

approximately 5 hours and growth essentially halted upon induction. Expression levels were also very poor, with the fusion protein appearing in both the supernatant and pellet fractions of lysed cells. The fusion protein was determined to be both insoluble and toxic to the cells.

Caerin 1.8 is active against gram positive bacteria at low concentrations, from 50 µg/mL against *B. cereus* down to 6 µg/mL against *S. aureus* [126]. Specifically it is active against *E. coli* at 100 µg/mL [127].

Although the pET32a+ vector is known to be somewhat leaky in its control of expression of encoded insert proteins, moderately toxic proteins are generally tolerated well enough by the cells to allow their expression. Levels of the peptide present in the cell culture were not expected to reach high enough concentration to negatively impact on the cells.

5.6 Summary

Unfortunately, the fusion protein of caerin 1.8 with GST must be toxic to the extent that the basal levels of expression of the anti-bacterial protein are enough to negatively impact on the cells [106, 128]. Therefore, expression of the peptide using this system is not possible. Structure determination of the peptide in the presence of calmodulin cannot be achieved using this method.

Chapter 6 Preparation and analysis of the calmodulin–caerin 1.8 complex

6.1 Aims

To prepare ^{15}N and ^{13}C doubly labelled calmodulin *via* a bacterial protein expression system. To assign the chemical shifts of the protein when bound with caerin 1.8, in order to determine the structure of the complex.

6.2 Preparation of ^{15}N and ^{13}C doubly labelled calmodulin

In order to study the caerin 1.8-calmodulin complex more thoroughly and to determine the mode of interaction between the two species, a series of 3D NMR spectra were recorded on a doubly ^{15}N and ^{13}C labelled sample of calmodulin in complex with caerin 1.8. The doubly labelled protein was purified as discussed in section 4.14, however there were significant changes employed in the expression method.

Overnight cultures of the bacteria containing the calmodulin vector grown in Luria broth were diluted 1/50 and allowed to grow until they reached OD_{600} 0.8. At this stage the cells were gently spun and the pellets were resuspended in ^{15}N and ^{13}C labelled minimal medium. The cells were allowed to recover from being harvested for one hour, then they were induced by adding IPTG to a concentration of 50 mM and left to express for two hours before being harvested.

This method, developed by Marley *et al* and others [111, 129], was used in order to allow cell bulk to form in unlabelled media so that only the protein of interest is expressed in labelled medium. This is much more efficient than growing cells to induction density in labelled media.

The cells do not need to be labelled themselves in order to produce labelled protein, and grow much more rapidly to inducible cell density in rich media. This also has the advantage of making the expression more efficient once it is induced. Rapidly growing cells are better at expressing protein; this is further enhanced by the addition of fresh media prior to the induction stage.

Furthermore, using this method, labelling efficiency is only reduced by 5 - 10%, whilst the amount of isotopically enriched starting materials required is greatly reduced, as the cells are resuspended in a much smaller volume of the minimal media. The cells are concentrated four times over the initial concentration, so that 2 L of initial LB culture can be resuspended in 0.5 L of minimal media to generate a similar amount of protein as would otherwise be gained from twice as much unlabelled media. This greatly lowers the cost and increases the efficiency of use of the isotopically labelled starting materials.

Once purified, the calmodulin and caerin 1.8 were mixed in a 1:4 ratio, as it was determined in the titration study that this was ample to achieve full saturation of the protein. The pH was adjusted to 6.3, with a final concentration in the sample of 31 mM potassium chloride, 6.3 mM calcium, 10% D_2O and 0.02% sodium azide, the same conditions as were used in the singly labelled titration experiments.

6.3 3D NMR spectroscopy of the calmodulin-caerin 1.8 complex

The following spectra were initially recorded on the complex: ^{15}N-HSQC, HNCACB and CBCA(CO)NH. Firstly, a sequential assignment strategy was attempted, however initial inspection of the HSQC spectrum indicated that there were a number of excess peaks. These were consistent between the HNCACB and CBCA(CO)NH spectra. There was a total of 210 separate peak strips, over fifty more than were expected. Further, many of the strips were broadened, indicating that they may have arisen from two very similar species. Calmodulin has 146 non-proline residues and so only 146 strips were expected to be present in the spectra.

Closer inspection of the chemical shifts of these strips indicated some duplication of chemical shift signatures in what should have been unique regions of the sequence. For example, there is only one occurrence of an alanine residue with a serine in the preceding position in the calmodulin sequence. This sequence occurs at positions 101 and 102. There were two strips with chemical shifts clearly indicative of this sequence, identifiable due to the distinctively low β-carbon shift of alanine at approximately 17 ppm and distinctively high β-carbon shift of serine at 65 ppm.

These two strips had ^{15}N shifts of 124.9 and 125.1 ppm. This is illustrated in Figure 42.

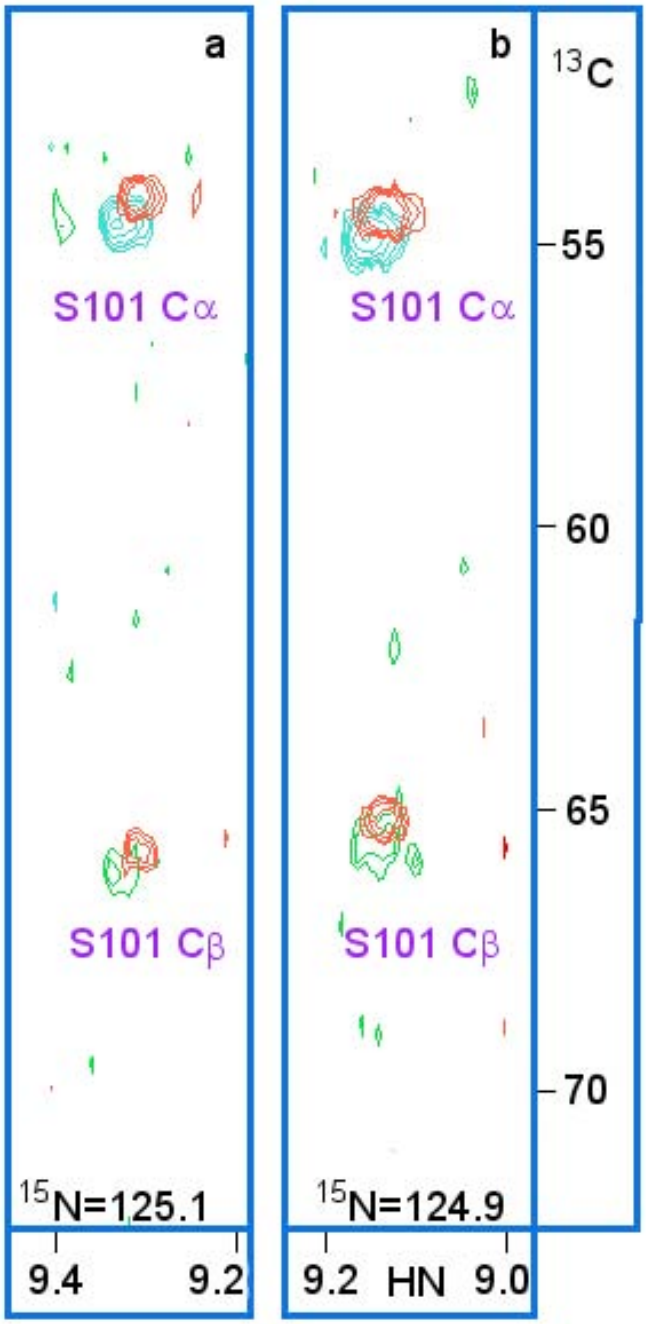

Figure 42: Strip plots of the overlaid HNCACB(blue (Cα) and green(Cβ)) and CBCA(CO)NH (red) spectra, showing the correlations between HN and N of A102 with S101, in the calmodulin-caerin 1.8 complex (a) and in free calmodulin (b).

Similarly, there is only one incidence of two adjacent threonine residues in the sequence, in positions 28 and 29. These residues are easy to identify due to their distinctive β-carbon shifts close to 70 ppm. Duplication of this sequence also occurs in the 3D NMR spectra: two strips with chemical shifts characteristic of a threonine preceded by another threonine appear with ^{15}N shifts of 114.6 and 113.8 ppm, these are shown in Figure 43.

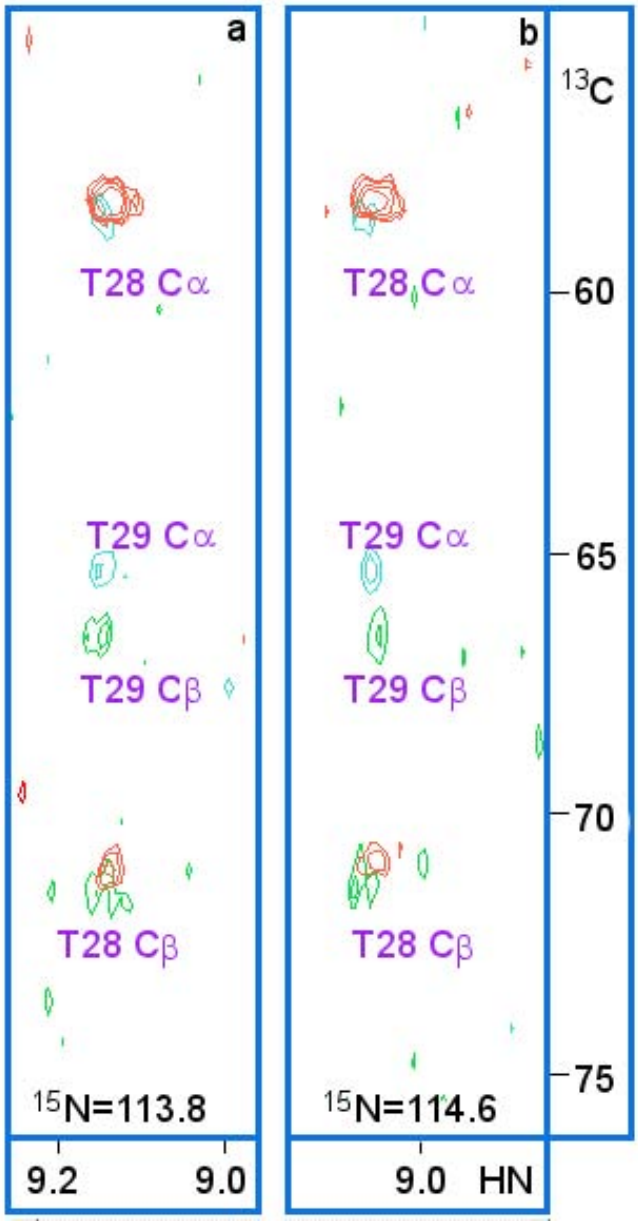

Figure 43: Strip plots of the overlaid HNCACB(blue (Cα) and green(Cβ)) and CBCA(CO)NH (red) spectra, showing the correlations between HN and N of T29 with T28, in the calmodulin-caerin 1.8 complex (a) and in free calmodulin (b).

Many other unique sequence regions with clearly identifiable chemical shift signatures were duplicated as well. These duplicated peaks generally had quite similar Cα and Cβ chemical shifts, but were separated to a greater degree on the nitrogen axis, by up to 3 ppm. A large number of the duplicated strips had very similar chemical shifts in the nitrogen axis and so had the appearance of one set of broadened peaks, indicating that two species were giving rise to very similar correlations. This is illustrated in Figure 44.

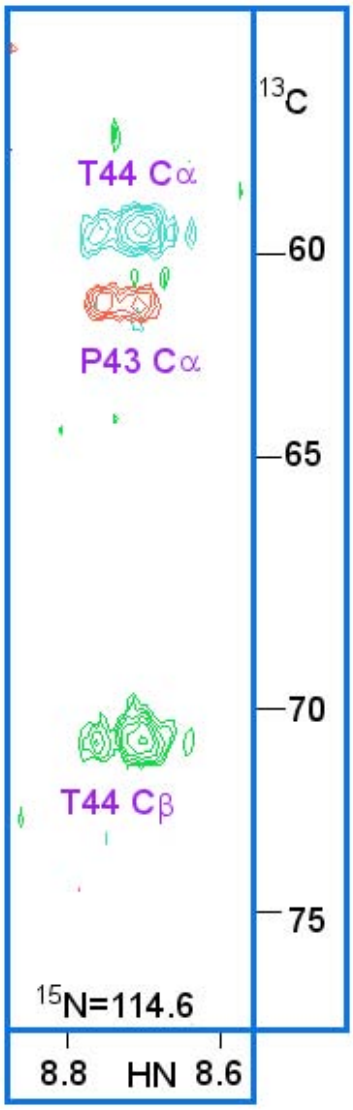

Figure 44: Strip plot of the overlaid HNCACB (blue and green) and CBCA(CO)NH (red) spectra showing the bound (left) and unbound (right) peaks for T44.

It was apparent that there were two conformational isomers of calmodulin present in the sample. A high resolution ^{15}N-HSQC spectrum of the complex sample was recorded at the conclusion of the collection of 3D experiments; this spectrum clearly has more than 280 backbone amide peaks, approximately double the expected 148 correlations.

Careful independent alignment of the final ^{15}N-HSQC spectrum recorded on the doubly labelled complex sample, with the ^{15}N-HSQC spectra recorded on both bound and unbound ^{15}N labelled calmodulin samples, showed that the two species present are the bound and unbound forms. Every peak in the spectra of the two singly labelled samples is represented in the final doubly labelled sample. A section of the overlaid spectra is shown in Figure 45.

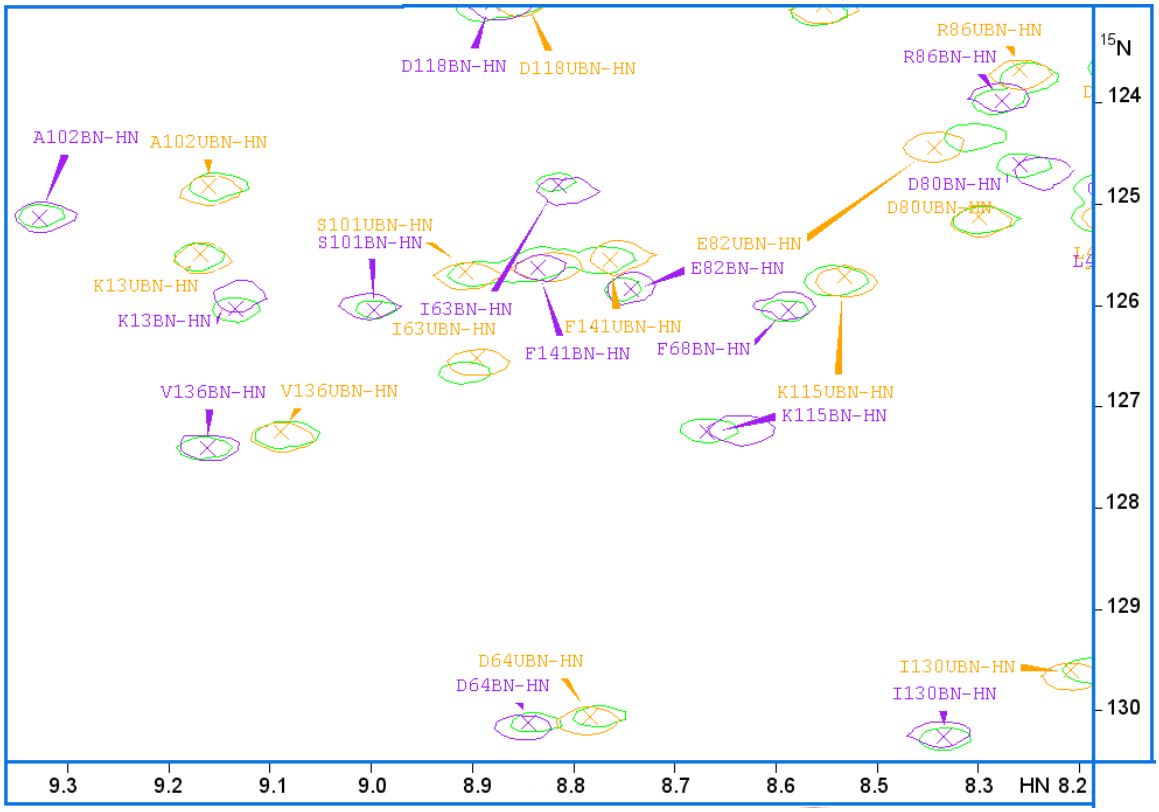

Figure 45: A region of the overlaid ^{15}N-HSQC spectra of singly ^{15}N labelled free calmodulin (orange), ^{15}N labelled calmodulin bound to caerin 1.8 (purple) and the ^{15}N and ^{13}C doubly labelled calmodulin in complex with caerin 1.8 (green).

One explanation for this phenomenon which can be ruled out is that a four-fold excess was not sufficient to fully complex the calmodulin. During the titration series with caerin 1.8 (section 4.16) it became clear that the protein-peptide complex had a 1:1 stoichiometry.

Therefore, the failure to achieve saturation is thought to be due either to the inherent inaccuracy with measurement of the concentration of calmodulin in the doubly labelled sample using the BCA method established by Walker and co-workers in 1994, [113] or because the peptide concentration was lower than it was calculated to be based on the dry weight of the peptide [104]. Therefore, a four-fold excess of peptide was not achieved as desired.

Although this situation was not ideal, it was decided to continue with assignment of the spectra, due to both time and spectrometer access restraints.

6.4 Co-assignment of the bound and unbound forms of calmodulin

In the ^{15}N-HSQC spectra, greater than 37% of the nitrogen chemical shifts and 62% of the proton chemical shifts had significant changes, when the thresholds were set at 0.25 and 0.025 ppm respectively. Even when placing the cut-offs at 0.5 and 0.05 ppm, greater than 40% of the proton chemical shifts and 30% of the nitrogen chemical shifts changed significantly upon addition of the peptide [130].

Chemical shift changes are expected to occur mainly about the active site of the enzyme undergoing a binding interaction [117, 131, 132]. Calmodulin experiences much larger chemical shift changes along its entire length upon binding of its ligands due to the global changes in fold which occur [100, 104].

This meant that the corresponding chemical shifts in the bound species could not be assigned directly by alignment with previously published data for free calmodulin. The 1991 study by Ikura and co-workers [104] provided a good starting point for the assignments of the free calmodulin resonances, especially when taken alongside the HNCACB and CBCA(CO)NH spectra recorded on the current sample which allowed

for identification of amino acid types, as discussed in section 2.18. Therefore the assignment of the spectra was simplified somewhat by comparison with these data.

That both bound and unbound calmodulin were present in the NMR sample allowed the determination of both the bound and unbound chemical shifts of calmodulin in exactly the same conditions. The majority of backbone HN, N, Cα and Cβ chemical shifts for free calmodulin and calmodulin in complex with caerin 1.8 have been co-assigned using standard methodology.

A combination of main-chain directed and sequential assignment strategies were employed [48]. The sequential approach was inadequate due to the duplication of each resonance, although classification according to amino acid type during the main-chain directed approach sped up the process somewhat.

Cross sections of the overlaid HNCACB and CBCA(CO)NH spectra illustrating sequential connectivities for the Cα resonances of residues D58 - T62 in the bound species are displayed in Figure 46.

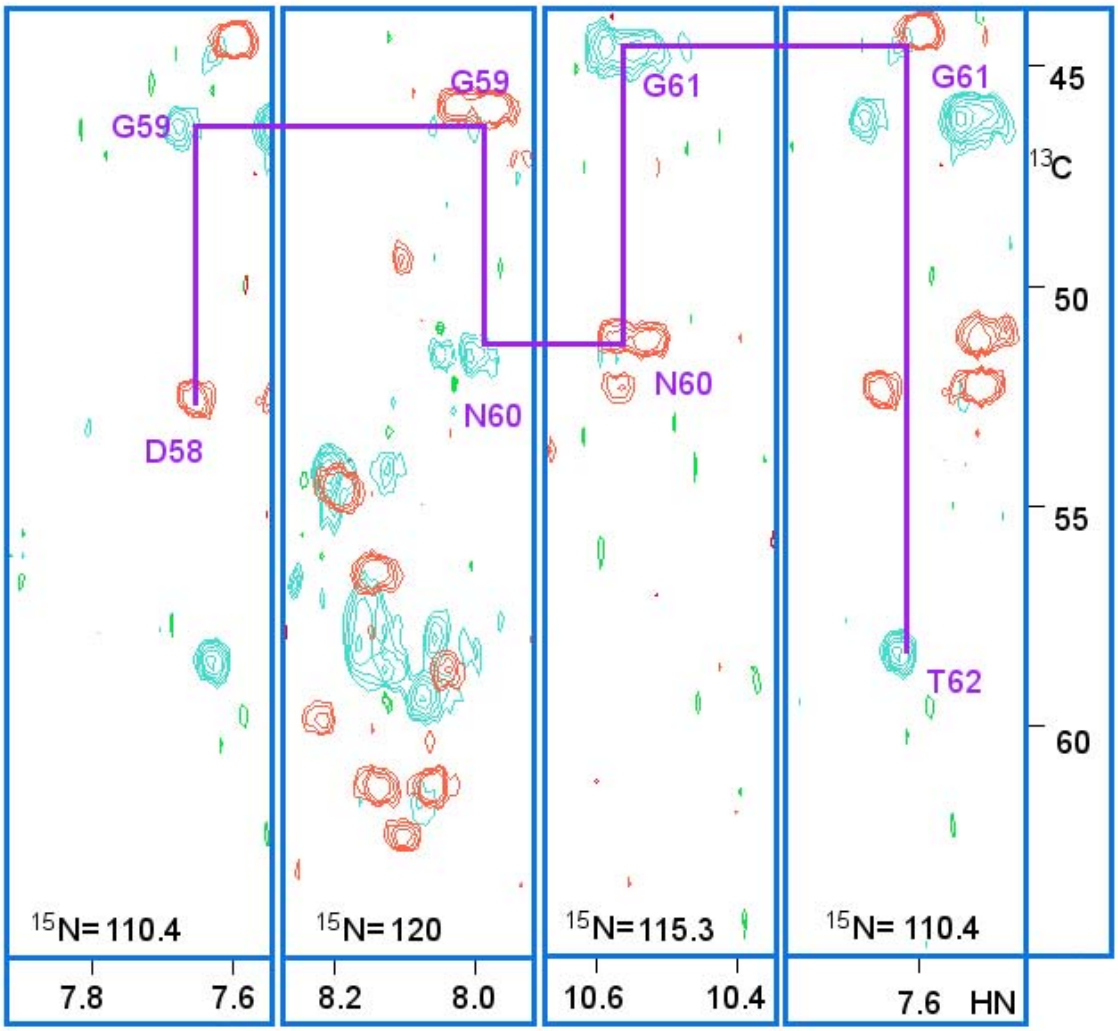

Figure 46: Cross sections of the HNCACB and CBCA(CO)NH spectra illustrating the sequential connectivites from residues D58 - T62 in the bound species. The HNCACB spectrum is shown in blue (Cα) and green (Cβ), the CBCA(CO)NH spectrum is shown in red.

Whilst the molecular weight of the complex with caerin 1.8 is higher by 2.6 kDa over free calmodulin, the levels of resolution of the ^{15}N-HSQC spectra of the two forms of protein are very similar. The increase in molecular weight does not cause any significant line broadening in the spectrum of the bound species. Both spectra contain mostly well-dispersed peaks with some overlap in the central region between 119 and 123 ppm in the nitrogen axis and 8.5 and 7.5 ppm in the proton axis. The same region in the doubly-labelled complexed sample is also less well resolved, due primarily to the higher number of peaks in this part of the spectrum.

For the unbound species, 81% of the backbone amide nitrogen and proton resonances are assigned and 95% of the Cα and Cβ chemical shifts have been identified. For the bound species, 79% of the backbone amide nitrogen and proton resonances and 95% of the Cα and Cβ shifts have been assigned.

The longest unbroken chains of assigned residues in free and bound forms of calmodulin are of 21 and 22 residues length respectively, from A15 - V35 in the free form and from F16 - R37 in the bound form. The longest stretch of unassigned residues in the free form is four residues, from M36 - L39. The next longest stretches are all of two residues' length, at F65 - P66, F68 - L69, K75 - M76, and E119 - E120. Of these, the Cα and Cβ chemical shifts can be obtained for the second residue from the subsequent residues' correlations in the CBCA(CO)NH spectra and so only eight residues in the 148 residue sequence are missing Cα and Cβ chemical shift information.

The longest stretches of unassigned residues in the bound form are only two residues in length, at positions E14 - A15, S38 - L39, F65 - P66, K75 - M76, E119 - E120, M124 - I25 and Q143 - M144. Extraction of the Cα and Cβ chemical shifts from the CBCA(CO)NH spectra leaves only seven residues in the bound form missing Cα and Cβ chemical shift information.

The distribution of these assignments with respect to amino acid types is summarised in Table 16. Full lists of the assigned N, HN, Cα and Cβ chemical shifts for both species are presented in Table 17 and Table 18.

Table 16: Distribution of assigned chemical shift residues of bound and unbound calmodulin.

		Assigned Residues	
Residue Type	Expected Residues	Free CaM	CaM-caerin 1.8
Ala	11	10	9
Arg	6	5	6
Asp/Asn	22	21	19
Cys	0	n/a	n/a
Glu/Gln	28	22	21
Gly	11	11	11
His	1	0	0
Ile	8	7	6
Leu	9	6	6
Lys	8	7	7
Met	9	4	5
Phe	8	5	6
Pro	2	0	0
Ser	4	3	3
Thr	12	11	11
Trp	0	n/a	n/a
Tyr	2	1	1
Val	7	7	7
Total	148	120	118

Table 17: N, HN, Cα, and Cβ chemical shifts for free calmodulin at pH 6.3, 25˚C, 31mM KCl and 6.3mM $CaCl_2$.

residue	amino acid	δN	δHN	δCα	δCβ
1	A				
2	D			53.35	40.3
3	Q	121.4	8.297	54.41	28.84
4	L	124.7	8.265	53.11	42.51
5	T	114.9	8.655	59.29	70
6	E	122.2	8.983	59.14	28.36
7	E	121.2	8.691	58.95	27.97
8	Q	122.4	7.719	58.06	28.43
9	I	121.5	8.343	65.21	37.13
10	A	123.2	7.691	54.35	16.76
11	E	121.5	7.74	58.24	28.6
12	F	122.1	8.545	58.06	36.61
13	K	125.3	9.163	59.15	30.91
14	E			57.91	28.21
15	A	123	7.834	54.28	16.43
16	F	120.7	8.492	60.96	38.03
17	S	114.5	7.91	60.55	62.17
18	L	122.4	7.377	56.16	40.73
19	F	116.7	7.213	58.36	40.6
20	D	119.5	7.773	51.4	37.99
21	K	126.2	7.635	57.42	31.52
22	D	115.7	8.122	51.84	38.75
23	G	111	7.747	46.06	n/a
24	D	122.4	8.383	52.37	39.44
25	G	115.1	10.59	44.19	n/a
26	T	114.8	8.111	58.81	71.66
27	I	128.7	9.672	59.17	38.58
28	T	118.3	8.397	58.47	58.47
29	T	114.6	9.065	65.3	66.46
30	K	122.8	7.622	58.08	31.5
31	E	123.4	7.637	58.45	28.86
32	L	122.5	8.667	57.05	41.75
33	G	108.8	8.639	47.47	n/a
34	T	120	7.878	65.71	67.5
35	V	124.1	7.594	65.19	30.44
36	M				
37	R				
38	S				
39	L			53.05	40.61
40	G	131.2	7.844	44.47	n/a

residue	amino acid	δN	δHN	δCα	δCβ
41	Q			53.06	29.39
42	N	118.5	8.672	50.25	69.58
43	P		n/a	61.02	
44	T	114.7	8.705	59.13	69.58
45	E	122.6	8.756	58.83	27.93
46	A	122.8	8.218	54.03	17.2
47	E	120.6	7.621	57.9	31.41
48	L	122	8.017	56.62	39.36
49	Q			57.52	28.43
50	D	122.3	8.139	56.64	39.4
51	M	121.2	7.798	58.35	32.38
52	I	120	7.656	63.65	36.37
53	N	119.3	8.553	54.81	37.02
54	E	118.2	7.506	57.94	29.32
55	V	110.9	7.134		
56	D			52.31	39.15
57	A	109.5	8.377	53.22	18.61
58	D	115.5	8.121	51.76	38.8
59	G	110.4	7.514	46.46	n/a
60	N	120	8.04	51.51	37.63
61	G	115.1	10.52	44.5	n/a
62	T	110.8	7.596	58.52	70.85
63	I			58.8	41.15
64	D	129.9	8.768	51.34	41.45
65	F				
66	P		n/a	65.19	29.45
67	E	119.6	7.933	57.69	29.45
68	F				
69	L			56.5	39.54
70	T	117.6	7.525	65.48	67.13
71	M	123.4	7.629	58.03	28.66
72	M			57.76	28.21
73	A	124	7.899	54.45	16.71
74	R	119.1	7.49	57.1	29.27
75	K				
76	M			55.42	31.93
77	K	122.6	7.804	55.42	31.93
78	D	123.6	8.254	53.68	39.97
79	T	116.1	8.057	61.24	68.7
80	D	125.3	8.398	53.62	40.29
81	S	119.3	8.392	58.63	62.67
82	E	124.1	8.397	57.37	28.58
83	E			58.64	27.83
84	E	122.1	7.714	57.65	28.99
85	I	123.8	7.939	63.59	36.56

residue	amino acid	δN	δHN	δCα	δCβ
86	R	123.9	8.344	59.09	28.6
87	E	119.8	8.04	57.74	27.92
88	A	122.9	8.011	54.01	17.43
89	F	121.3	8.769	60.92	30.14
90	R	117.6	7.806	57.59	38.02
91	V	120.2	7.495	64.68	30.55
92	F			57.88	39.22
93	D	118.9	7.803	51.27	37.32
94	K	127.5	7.682	57.67	32.25
95	D	115.4	8.019	51.88	38.62
96	G	111.1	7.612	46.17	n/a
97	N	121.6	8.325	51.7	37.01
98	G	115.3	10.58	44.2	n/a
99	Y	117.7	7.57	55	42.21
100	I	129	10.09	59.33	37.84
101	S	125.8	8.902	54.8	65.75
102	A	124.9	9.143	54.71	16.94
103	A	120.3	8.181	53.97	17.49
104	E	121.5	7.807	58.2	28.33
105	L	123	8.551	57.26	41.03
106	R	119.3	8.529	58.75	29.45
107	H			57.76	29.19
108	V	120.6	7.868	64.88	30.85
109	M	118.3	8.198	56.43	30
110	T			65.81	66.85
111	N	123.7	7.883	54.06	37.43
112	L			54.13	41.04
113	G	108.8	7.803	44.53	n/a
114	E	122	7.871	54.36	29.49
115	K	125.8	8.527	54.92	31.12
116	L	126.6	8.026	53.11	43.47
117	T	116.4	9.151	59.61	43.64
118	D	123.1	8.851	56.76	38.62
119	E				
120	E			58	29.28
121	V	123	8.041	66.05	30.41
122	D	121.4	8.023	56.55	39.41
123	E	121.6	7.935	57.99	
124	M			58.35	32.04
125	I	120	7.884	62.82	35.45
126	R	120.2	8.073	59.31	27.83
127	E	117.4	7.879	57.48	28.59
128	A	120.6	7.281	51.17	20.22
129	D	119.5	7.817	52.92	39.25
130	I	129.7	8.309	62.29	37.66

residue	amino acid	δN	δHN	δCα	δCβ
131	D	118.7	8.249	52.76	38.87
132	G	110.1	7.541	46.33	n/a
133	D	122.7	8.297	52.62	39.17
134	G	114.6	10.32	44.74	n/a
135	Q	117.2	7.897	52.27	31.23
136	V	127.3	9.074	60.45	32.71
137	N	123.4	7.561	52.69	39.21
138	Y			56.82	38.53
139	E	120.9	8.625	58.93	28.07
140	E	121.7	8.714	57.57	28.92
141	F	125.6	8.808	60.01	38.7
142	V	121.4	8.849	65.91	30.47
143	Q	119.6	7.118	57.74	27.18
144	M			57.09	32.33
145	M	116.7	7.795	54.25	30.93
146	T	113.8	7.53	61.5	69.15
147	A	128.6	7.717	51.81	18.06
148	K	127.7	7.683	56.72	32.69

Table 18: N, HN, Cα, and Cβ chemical shifts for calmodulin bound to caerin 1.8 at pH 6.3, 25˚C, 31mM KCl and 6.3mM $CaCl_2$.

residue	amino acid	δN	δHN	δCα	δCβ
1	A				
2	D			53.55	40.3
3	Q	121.2	8.252	54.41	28.92
4	L	125.3	8.275	53.38	42.66
5	T	114.8	8.708	59.36	70
6	E	122.3	8.96	59.21	27.97
7	E	121.5	8.687	58.89	28.63
8	Q	121.6	7.768	57.64	29
9	I	121.5	8.376	65.42	37.07
10	A	123	7.937	53.45	16.76
11	E	121.5	7.706	58.35	28.72
12	F			58.09	36.47
13	K	126.2	9.133	59.15	30.67
14	E				
15	A			53.89	17.29
16	F	120.5	8.672	61.18	38.61
17	S	113.6	7.882	60.34	62.18
18	L	122.4	7.304	56.16	40.73
19	F	116.7	7.389	56.19	38.85
20	D	119.6	7.784	51.46	37.91
21	K	126.9	7.5	57.43	31.38
22	D	115.9	8.229	52.08	38.57
23	G	111	7.706	46.18	n/a
24	D	122.8	8.277	52.23	39.17
25	G	114.9	10.56	44.56	n/a
26	T	114.8	8.06	58.81	71.66
27	I	128.8	9.8	59.17	38.58
28	T	119.3	8.273	58.51	67.56
29	T	113.8	9.151	65.17	66.52
30	K	123.2	7.553	58.03	31.41
31	E	122.9	7.522	57.98	29.15
32	L	122.4	8.101	56.77	41.44
33	G	109.1	8.726	47.34	n/a
34	T	120.4	7.794	65.76	67.63
35	V	124.1	7.229	65.43	30.44
36	M	120.2	8.443	58.05	28.3
37	R	120.8	8.429	58.5	28.3
38	S				
39	L			52.54	39.76
40	G	131.2	7.569	44.77	n/a

residue	amino acid	δN	δHN	δCα	δCβ
41	Q	119.2	7.562	52.39	29.73
42	N	117.9	8.692	50.37	38.26
43	P	114.8	n/a	60.95	30.98
44	T	114.8	8.764	59.48	70.13
45	E	123	8.758	59.03	27.77
46	A	122.3	8.194	53.94	17.23
47	E	120.6	7.649	57.93	28.78
48	L	121.9	8.056	56.54	39.24
49	Q			57.36	27.51
50	D	122.3	8.176	56.44	39.2
51	M	121.2	7.706	58.35	33.38
52	I	119.7	7.543	64.01	36.47
53	N	119.4	8.737	54.81	36.74
54	E	118.2	7.471	57.94	29.32
55	V	108.7	7.117	59.2	31.62
56	D			52.4	39.1
57	A	109.5	8.525	53.18	18.61
58	D	115.5	8.803	51.53	38.69
59	G	110.4	7.658	46.36	n/a
60	N	120	7.987	51.51	37.63
61	G	115.3	10.57	44.69	n/a
62	T	110.4	7.637	58.63	71.11
63	I	124.7	8.818	59.03	39.02
64	D	129.9	8.837	51.34	41.15
65	F				
66	P		n/a	65.44	29.62
67	E	119.4	7.94	57.65	28.59
68	F	125.8	8.447	61.4	39.24
69	L			57.65	39.77
70	T	117.4	7.507	65.33	67.13
71	M	123.11	7.579	58.03	31.41
72	M			58.19	28.08
73	A	124.6	7.949	54.31	17.1
74	R	119.1	7.561	57.1	29.51
75	K				
76	M			55.5	32.38
77	K	122.6	8.121	55.5	32.38
78	D			53.92	39.82
79	T	114.1	7.77	60.5	68.88
80	D	124.7	8.344	53.17	40.38
81	S	118.9	8.295	57.28	63.22
82	E	125.8	8.739	58.23	28.04
83	E			58.64	27.83
84	E	122.1	7.668	57.65	28.97
85	I			63.83	36.12

residue	amino acid	δN	δHN	δCα	δCβ
86	R	123.9	8.374	59.09	28.61
87	E	120.5	8.102	57.87	27.96
88	A	123.3	8.038	53.91	17.29
89	F	119.8	8.343	60.76	38.42
90	R	117.6	7.8	57.77	29.33
91	V	118.3	7.173	64.19	30.12
92	F	115.8	6.714	58.02	40.08
93	D	118.9	7.49	50.98	37.77
94	K	126.9	7.653	56.96	31.14
95	D	115.4	7.953	51.47	38.25
96	G	111.1	7.647	46.17	n/a
97	N	121.3	8.28	51.73	37.17
98	G	114.4	10.47	44.07	n/a
99	Y	117.9	7.678	55.33	41.69
100	I	129.7	10.13	60.34	37.66
101	S	126.2	9	54.65	66.08
102	A	125.1	9.321	54.5	16.91
103	A	120.3	8.208	53.96	17.49
104	E	122.5	7.865	58.44	27.31
105	L	122.1	8.174	56.58	39.18
106	R	120.3	8.244	56.67	28.86
107	H			58.43	28.78
108	V	121.2	7.568	65.48	31.12
109	M	118.3	8.218	56.43	30
110	T	116.8	8.117	64.36	67.92
111	N	125.6	7.948	55.02	36.55
112	L			54.5	41.17
113	G	108.4	7.829	44.41	n/a
114	E	121.9	7.973	53.49	30.16
115	K	127.3	8.65	54.42	31.15
116	L	126.6	8.048	53.11	43.64
117	T	116.4	9.228	59.61	43.34
118	D	123.1	8.886	56.89	38.62
119	E				
120	E			57.97	29.7
121	V	123	7.937	65.66	30.35
122	D	121.7	8.111	56.64	39.29
123	E	121	7.945	58.08	28.4
124	M				
125	I			61.44	41.24
126	R	120.2	8.159	58.24	27.3
127	E			58.51	29.57
128	A	117.4	7.921	49.64	22.91
129	D	119.7	8.105	54.23	40.02
130	I	130.1	8.433	61.88	38.25

residue	amino acid	δN	δHN	δCα	δCβ
131	D	119.3	8.229	53.06	38.63
132	G	110.1	7.495	46.33	n/a
133	D	122.3	8.296	52.39	39.46
134	G	113.8	9.88	44.99	n/a
135	Q	117.4	7.979	52.21	31.35
136	V	127.3	9.168	60.34	33.22
137	N	123.8	7.465	52.78	39.25
138	Y			56.51	38.46
139	E	121.5	8.641	58.56	27.9
140	E	122.3	8.736	57.87	28.33
141	F	125.8	8.847	60.13	38.87
142	V	121.4	8.78	66.14	30.47
143	Q				
144	M			57.32	30.75
145	M	115.8	7.712	54.42	29.83
146	T	112	7.665	60.97	69.31
147	A	129	7.485	51.99	18.24
148	K	128.6	7.949	56.49	32.86

6.5 Chemical shift analysis and discussion of structural implications

The Cα chemical shift index data for bound and free calmodulin are shown in Figure 47 and Figure 48. The α-helical and β-sheet regions are indicated by positive and negative shift changes, respectively. The exact placements of these structural motifs are listed in Table 19. Immediately obvious are the 8 helical regions of the protein, characterised by the positive α-carbon shift change. These α-helical regions are clearly visible on both graphs. Residues with no chemical shift information have been arbitrarily assigned a value of 0.5 to distinguish them from zero values.

It can also be seen that the central hinge in the bound form has less of a helical nature than in the free form, as evidenced by the higher density of –1 values in the region between residues 77 - 82. This loss of helicity indicates that there is a distinctive structural change occurring in the central hinge upon binding.

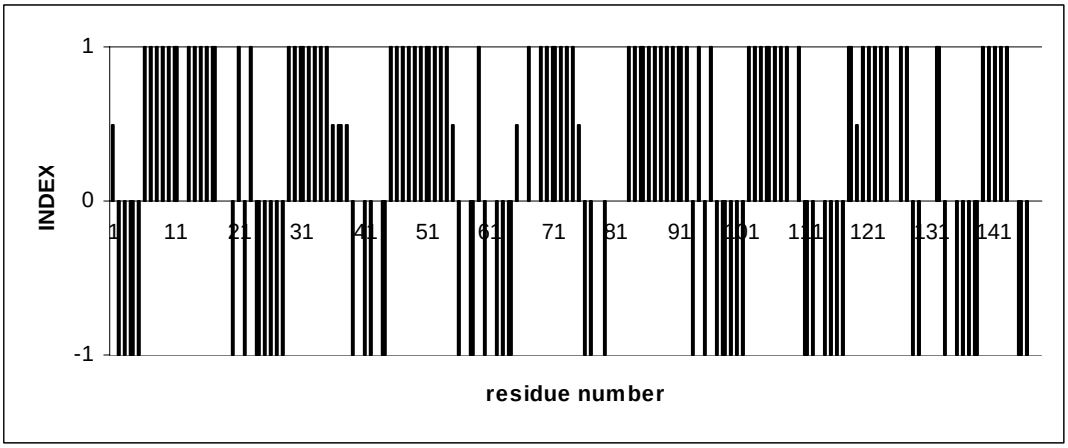

Figure 47: CSI plot derived from Cα chemical shifts of free calmodulin.

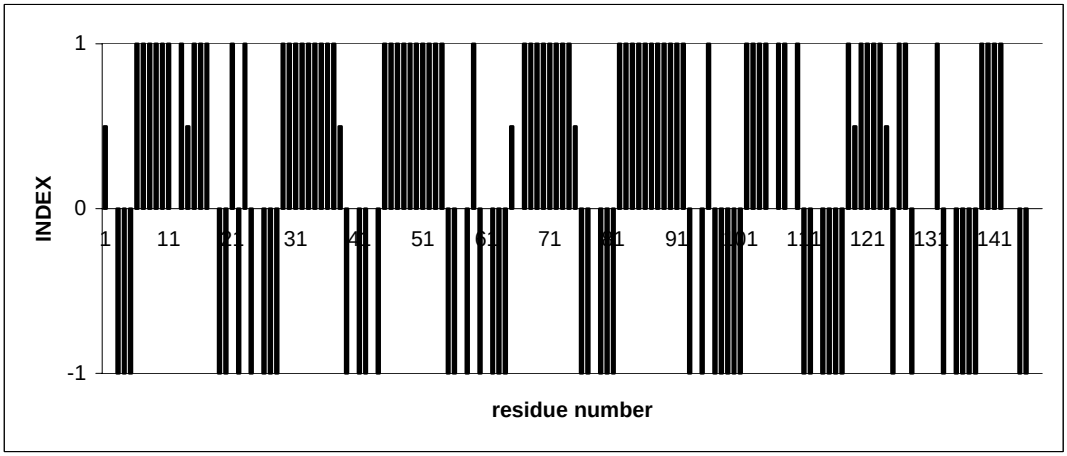

Figure 48: CSI plot derived from Cα chemical shifts of calmodulin bound to caerin 1.8.

Figures 1a and 2a have been constructed to demonstrate graphically the regions of calmodulin for which resonance assignments have been obtained, in both bound and unbound forms, respectively. Figures 1a and 2a also demonstrate which regions have defined secondary structure according to CSI data.

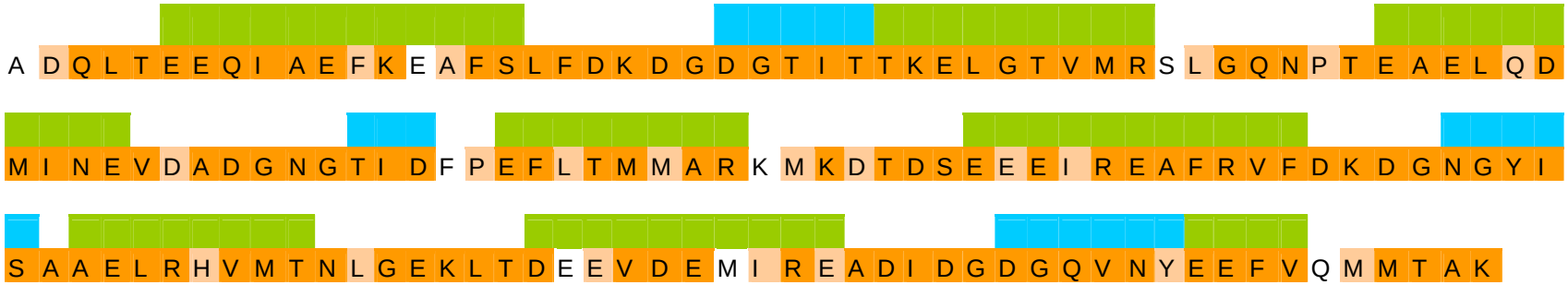

Figure 1a: Chemical shift assignments and structural motifs of calmodulin bound to caerin 1.8. Atoms with fully assigned backbone atoms are shown in dark orange, partially assigned atoms are shaded light orange. Green boxes indicate α-helical regions, blue boxes indicate β-sheet regions, as determined by CSI data.

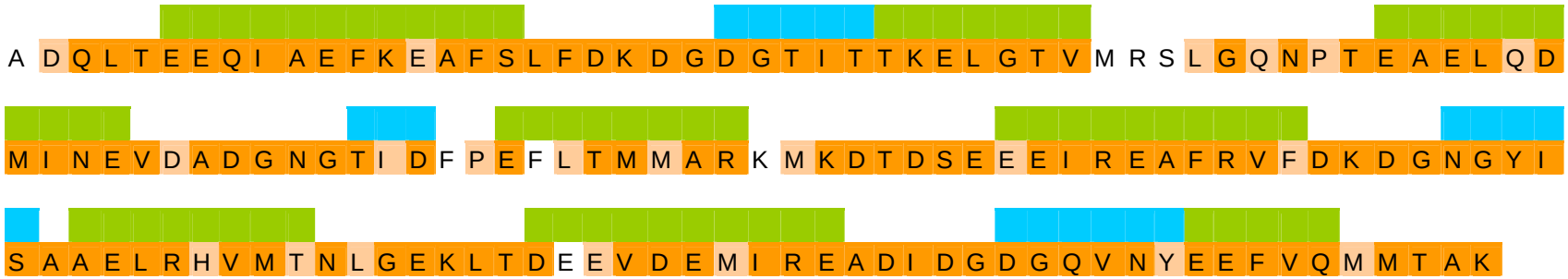

Figure 2a: Chemical shift assignments and structural motifs of free calmodulin. Atoms with fully assigned backbone atoms are shown in dark orange, partially assigned atoms are shaded light orange. Green boxes indicate α-helical regions, blue boxes indicate β-sheet regions, as determined by CSI data.

The Cα chemical shift index is the most indicative of secondary structural motifs [49]. However, the Cβ chemical shift index is very useful, to identify regions of β-sheet structure, as indicated by a positive β-carbon chemical shift change. These data are presented in Figure 49 and Figure 50 and the β-sheet regions are listed in Table 19. Again, residues with no chemical shift information have been arbitrarily assigned a value of 0.5 to distinguish them from zero values.

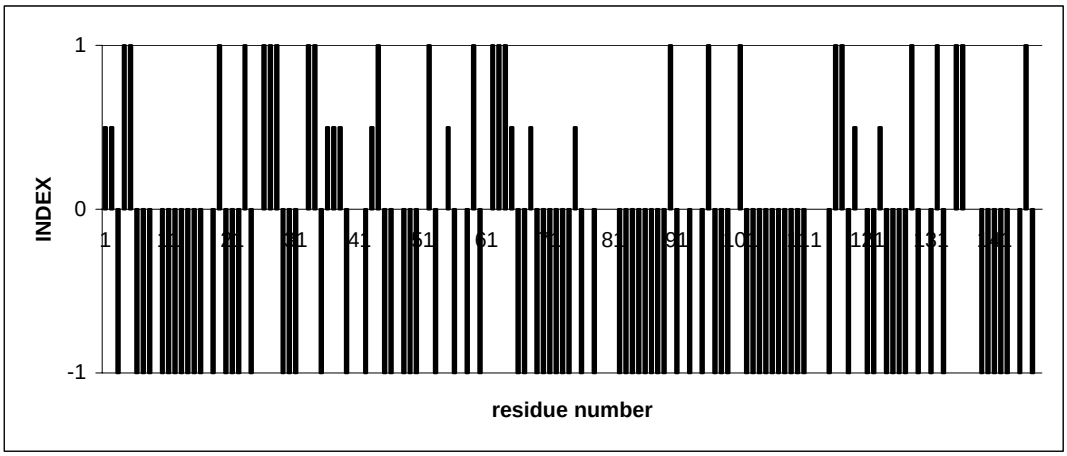

Figure 49: CSI plot derived from Cβ chemical shifts of free calmodulin.

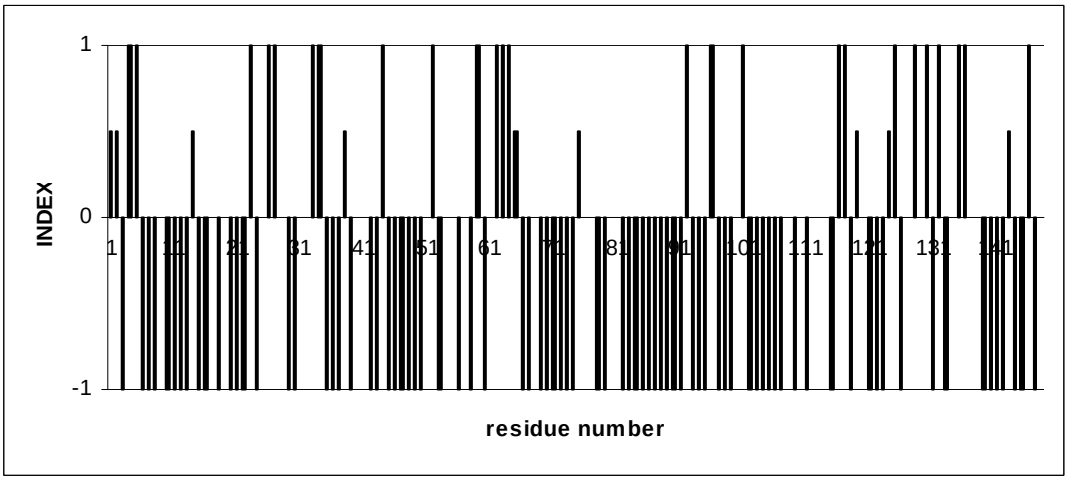

Figure 50: CSI plot derived from Cβ chemical shifts of calmodulin bound to caerin 1.8.

Chemical shift changes in the backbone of calmodulin are a good indicator of which parts of the protein undergo structural change upon binding to the peptide. However, full chemical shift assignment of the NOESY spectra for the sidechains of calmodulin in complex with caerin 1.8 is required in order to gain conclusive evidence for structural change [1]. Calmodulin is a highly plastic protein, and undergoes global structural changes upon binding to its ligands which are much larger than the changes experienced many other proteins [2, 3]. The CSI data obtained in this study indicates that there is less disruption to chemical shifts in the helical regions of the protein than in the inter-helical regions. Considering the large structural changes likely upon binding, this data can be seen as significant.

1. Wishart, D. S., Nip, A. M. (1998) Protein chemical shift analysis: a practical guide, *Biochem. Cell Biol. 76*, 153-163.

2. Wilson, M. A., Brunger, A. T. (2000) The 1.0A crystal structure of Ca^{2+}-bound calmodulin: an analysis of disorder and implications for functionally relevant plasticity, *J. Mol. Biol. 301*, 1237-1256.

3. Meador, W. E., Means, A. R., Quiocho, F. A. (1993) Modulation of calmodulin plasticity in molecular recognition on the basis of X-ray structures, *Science. 262*, 1718-1722.

Table 19: Location of α-helices and β-sheets in bound and free calmodulin determined by CSI methods.

	Unbound			Bound	
	Residue range			Residue range	
α-helix	Cα CSI		Ikura et al[133]	Cα CSI	
I	6 - 17		6 - 19	6 - 17	
II	29 - 35		29 - 38	29 - 37	
III	45 - 54		45 - 54	45 - 54	
IV	67 - 74		65 - 77	67 - 74	
V	83 - 92		82 - 93	82 - 92	
VI	102 - 110		102 - 111	102 - 110	
VII	118 - 127		118 - 127	118 - 127	
VIII	139 - 143		138 - 146	139 - 142	
β-sheet	Cα CSI	Cβ CSI	Ikura et al[133]	Cα CSI	Cβ CSI
I	24 - 28	26 - 28	27 - 29	24 - 28	26 - 27
II	62 - 64	62 - 64	62 - 64	62 - 64	62 - 64
III	97 - 101	101	99 - 101	97 - 101	101
IV	133 - 138	135 - 136	135 - 137	133 - 138	135 - 136

The regions of structure identified by the present study of free calmodulin agree well with those identified by Ikura et al [133]. The CSI method requires a dense grouping of four or more consecutive residues with the same value to define a region as having a particular structure [52]. Although the Cβ CSI values corresponding to the presence of a β-sheet only span up to two residues, their positioning is consistent with the published regions and so these data have been included in
Table 19.

Binding to caerin 1.8 does not affect the start and end points of the structured regions to a large extent. This indicates that the binding mode is likely to involve rearrangement of the α-helices of calmodulin in relation to one another, but in a manner so that the internal structure of the individual α-helices is not disturbed to a large degree.

In order to give a broad picture of the sequence regions whose chemical shifts are affected by binding, all of the assigned backbone atoms have been further analysed. The ^{15}N chemical shifts of the amide nitrogens are generally shifted downfield in a β-sheet region and upfield in an α-helical region. As such, the changes in chemical shift for ^{15}N would be expected to tend to the opposite direction as seen in the α-carbons. Although the changes in Figure 51 seem rather large when compared with those in Cα and HN, differences in ^{15}N shift up to ten fold higher in magnitude than those seen here are not uncommon and there are a number of other factors which also influence the ^{15}N chemical shifts.

The changes are in general more significant in the C-terminal domain than the N-terminal domain, indicating that the C-terminal domain undergoes a larger conformational change upon binding with the ligand than does the N-terminal domain. The changes in ^{15}N chemical shift experienced by calmodulin upon binding to caerin 1.8 are plotted in Figure 51.

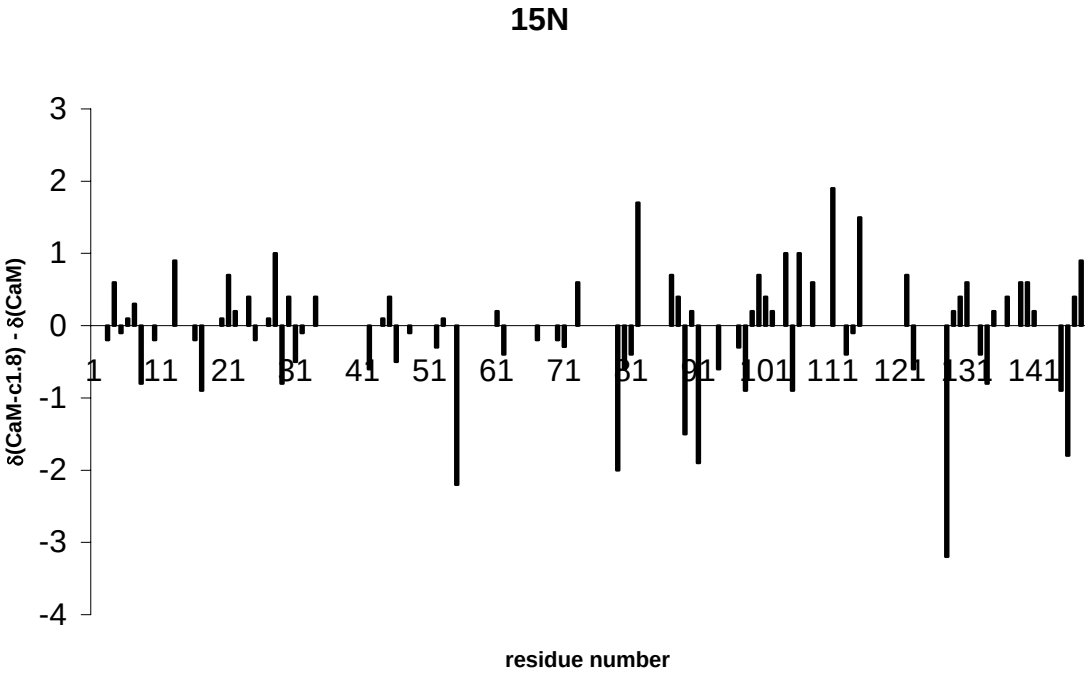

Figure 51: Plot of the changes in calmodulin chemical shift which occur upon complexation with caerin 1.8 for ^{15}N.

Cα also gives a good indication of the structural changes occurring. Again, the central helix is clearly disrupted by binding, as indicated by a consistent upfield chemical shift change across residues 79 - 81. This is also the case, although to a lesser extent, with helices II (residues 29 - 33) and VI (residues 93 - 95).

The changes in chemical shift of the α-carbons are of a larger magnitude in the C-terminal domain than the N-terminal domain, however they are not consistent in their sign. There is a particularly large change in calcium binding loop 1, but as it is isolated it can be considered as less significant than the clustered large changes in the C-terminal domain. These are more indicative that this region is involved in binding rather than of specific structural changes.

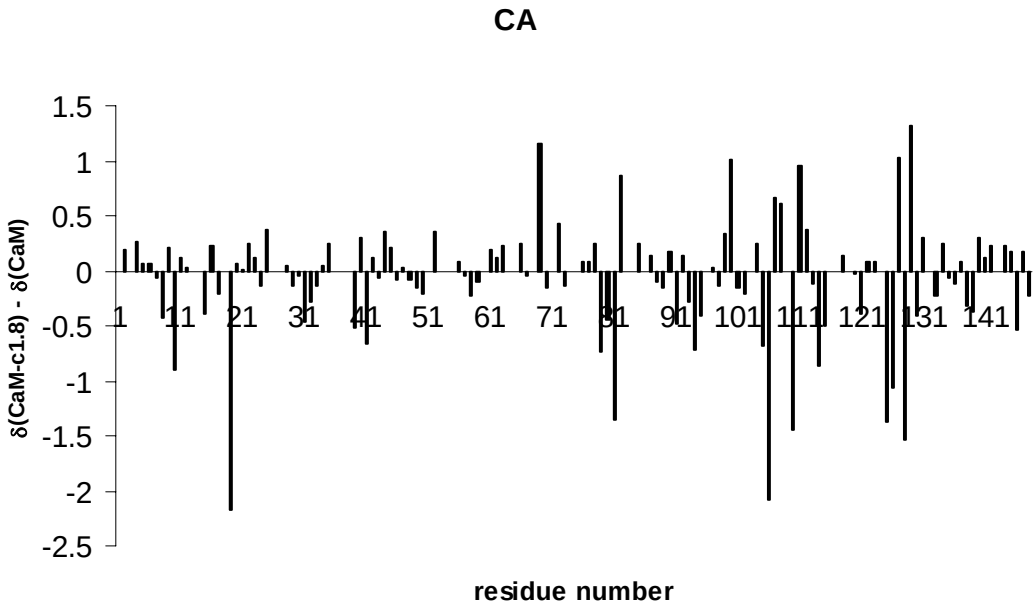

Figure 52: Plots of change in calmodulin chemical shift which occur upon complexation with caerin 1.8 for CA.

Changes in the HN chemical shift indicate differences in hydrogen bonding strength [134]. Again, these changes are more apparent in the inter-helical regions than inside

the α-helices themselves, as evidenced by the consistent changes of the same sign across sequential residues at positions 21 - 24, 78 - 80, 97 - 102 and 126 - 128.

These regions correspond to calcium binding loop I, the central hinge, and calcium binding loops III and IV respectively. The previous study by Ikura and co-workers also indicated that the calcium binding loops are disrupted by binding to a ligand [104]. The HN chemical shift changes which occur in calmodulin upon binding caerin 1.8 are plotted in Figure 53.

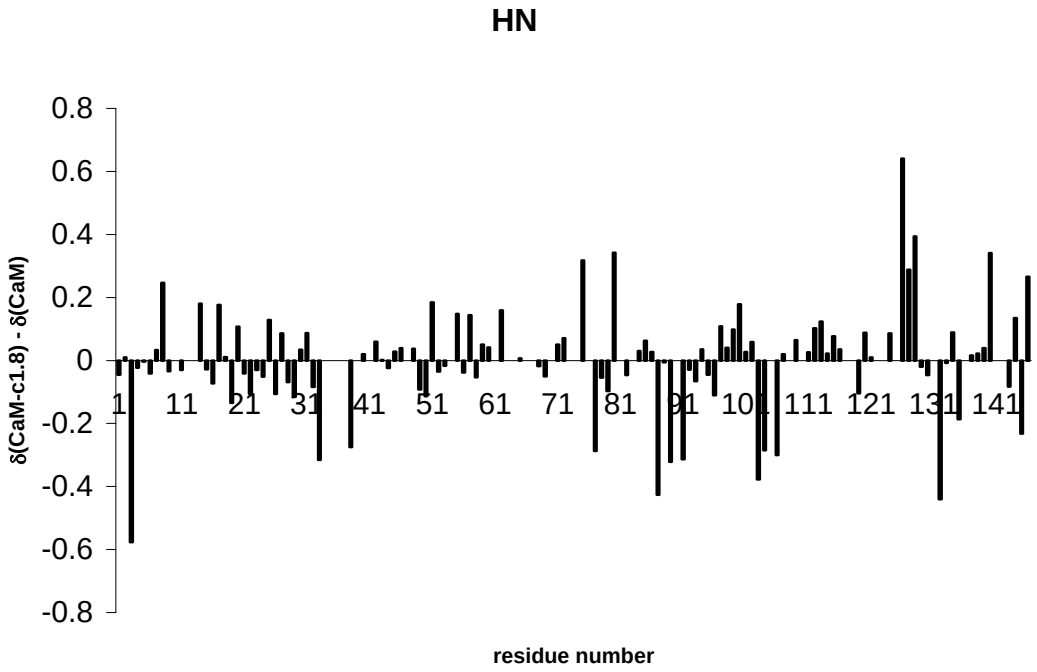

Figure 53: Changes in calmodulin HN chemical shift upon complexation with caerin 1.8.

The changes in HN chemical shift are also generally of a larger magnitude in the C-terminal domain. In the complex between calmodulin with the C20W peptide studied by Elshorst *et al* [101], the magnitude of changes in HN shift in the C-terminal domain is generally much larger than in the N-terminal domain. The C20W peptide interacts solely with the C-terminal domain of calmodulin. The situation in the present study is not so extreme but does imply a stronger interaction with the C-terminal domain.

The absolute values of the data published by Elshorst *et al* have been plotted against the data obtained in the current study for ease of comparison. The differences in temperature at which the data were recorded have not been accounted for as they can be expected to give rise to insignificant changes in chemical shift [101]. Absolute values were used in order to concentrate on the regions affected rather than the sign of the change. The regions of the sequence affected by binding in both data sets are quite similar. The changes occurring in helix VII are noticeably more intense in the Elshorst data set but generally elsewhere the trend of agreement between the regions which are affected is quite good. This is depicted in Figure 54.

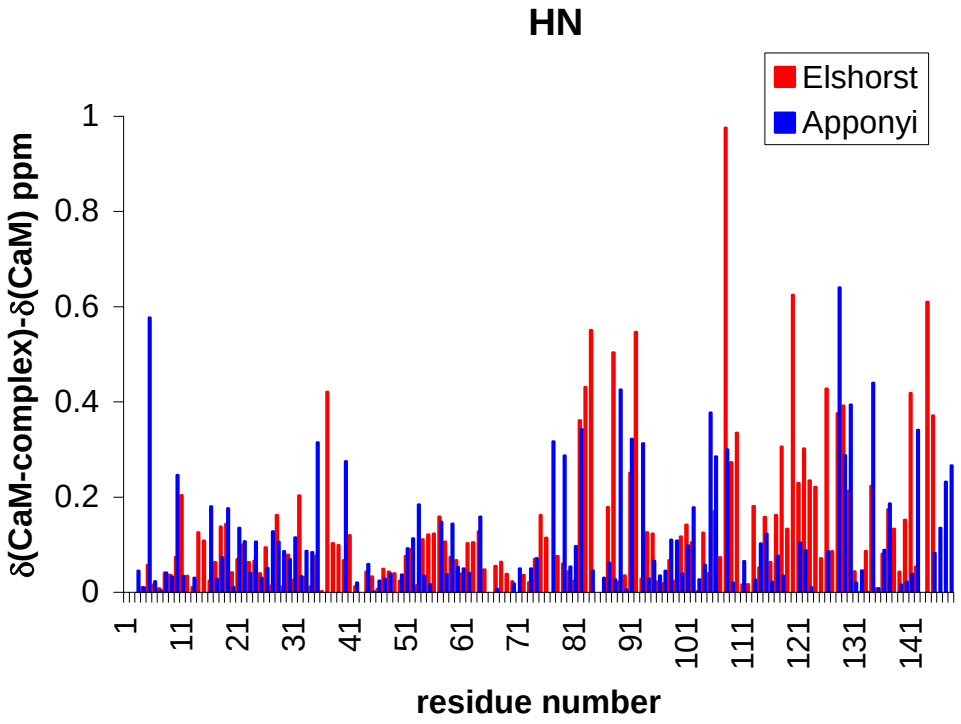

Figure 54: Changes in HN chemical shift experienced by calmodulin upon binding to caerin 1.8 and C20W peptide.

Comparison with the HN chemical shift changes in the complex of calmodulin with M13 peptide as studied by Ikura *et al* [104] also indicates that caerin 1.8 is likely to interact more strongly with the C-terminal domain. The complex with M13 has a tightly collapsed globular fold and the HN chemical shift changes are distributed evenly along the length of the protein, with changes in the central hinge of approximately two-fold higher intensity over the data obtained from the caerin 1.8 complex. This indicates that the disruption to the flexible hinge is much more significant in the complex with M13 than with caerin 1.8. The two binding modes give rise overall to significantly different chemical shift changes in HN. Again, the data published by Ikura have been plotted against the data obtained in the current study for ease of comparison. This is depicted in Figure 55.

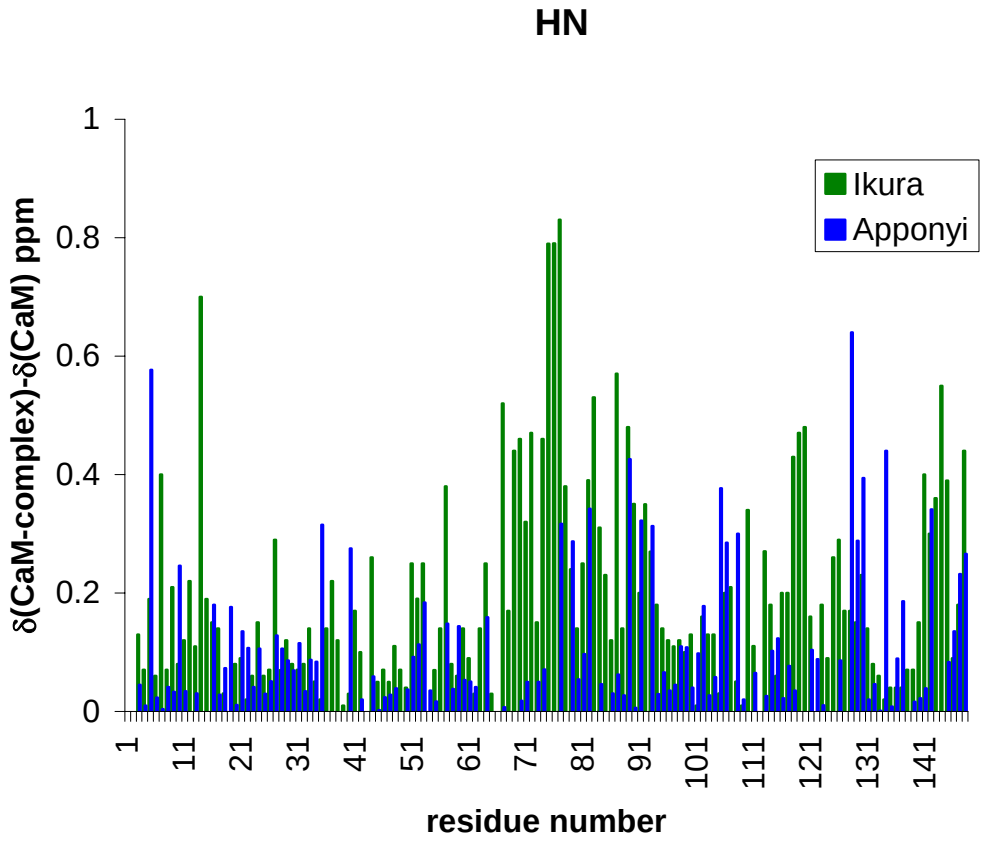

Figure 55: Changes in HN chemical shift experienced by calmodulin upon binding to caerin 1.8 and M13 peptide.

When the changes in all three atoms are combined, a good overall picture of the structural changes is given. A weighted average of the chemical shift changes which occur upon binding with caerin 1.8 was taken across the three backbone atoms and this is shown in Figure 56.

The chemical shift changes which occur in each atom type were averaged according to Equation 4, where, $\delta_{(CaM\text{-}c1.8)}$ are the chemical shifts of the complex, δ_{CaM} are the chemical shifts of unbound calmodulin and Δ_{max} is the largest chemical shift change in each residue type. This gives a better overall picture of the changes occurring in each residue, rather than just in each atom. Clearly, the changes are of a consistently larger magnitude in the C-terminal domain than in the N-terminal domain: the peptide must interact more strongly with the C-terminal domain.

$$\Sigma = | \delta_{(CaM\text{-}c1.8)} - \delta_{CaM} | / | \Delta_{max} |$$

Equation 4

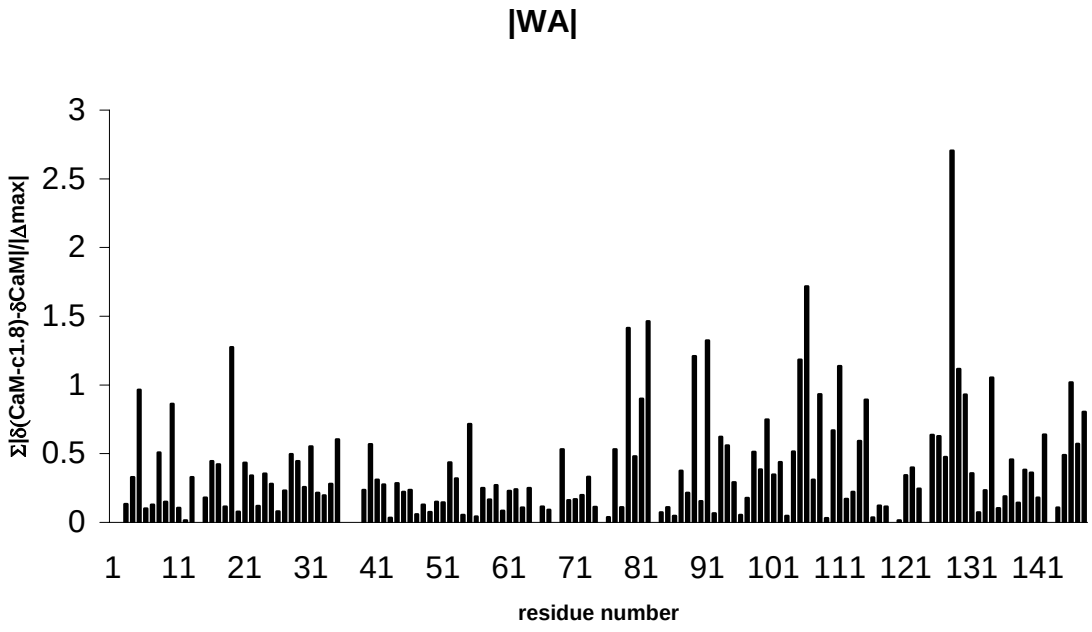

Figure 56:Weighted average of the chemical shift changes over all three backbone atoms.

6.6 Summary

Changes in chemical shift occur along the entire length of the protein, indicating that the whole protein is affected by binding the peptide ligand. The changes in the C-terminal domain are of greater magnitude than those in the N-terminal domain. These changes also indicate that a specific interaction is occurring, as opposed to a non-specific aggregation, which would be indicated by very small changes only [135].

By analysing the weighted average graph, it becomes clear that there are fewer significant changes occurring in the helical regions, particularly in the N-terminal end of the protein. The changes in the inter-helical regions are more significant, especially in the central hinge (residues 77 - 82) and in calcium binding loops numbers I and IV, between residues 19 - 29 and 127 - 138 respectively.

Combined, these data indicate that the rearrangement of the protein upon binding is more significant in the hinge region and in the inter-helical loops. The weighted average data also implies that binding to the peptide causes a greater conformational change in the C-terminal domain and so the binding interaction with the C-terminal domain is purported to be stronger than with the N-terminal domain.

This further supports the theory indicated by the CSI data that binding caerin 1.8 involves a rearrangement of the α-helices of calmodulin. The individual α-helices remain relatively undisturbed, especially in the N-terminal domain, whilst they move about in relation to one another.

Comparison with the shift difference plots from Elshorst's study [101] and Ikura's study [104] indicate that the N-terminal domain of calmodulin is affected to a greater degree when binding to caerin 1.8 than when in complex with the C20W peptide, but to a lesser degree than with the M13 peptide. The structure of the complex is therefore purported to lie in between the two.

Chapter 7 Summary and future directions

7.1 The structure and movement of splendipherin

The structure of splendipherin at an air-water interface was determined using 2D NMR spectroscopy methods. Splendipherin is an α-helical peptide with a central flexible hinge. The two glycine residues in the centre of the molecule are responsible for the lack of rigid structure in this region. The N-termimal α-helical region has well defined amphipathicity, whereas the C-terminal α-helical region does not.

In order to reach the mating partner of the male frog rapidly, the peptide travels across the surface of the water as a surfactant, *via* formation of a gaseous monolayer.

7.2 Titration of amphibian skin peptides with calmodulin

Three peptides have been shown definitively to bind to calmodulin, with differing binding strengths. Splendipherin, isolated from *Litoria splendida*, binds in fast exchange; the citropin 1.1 analogue modified from a native peptide isolated from *Litoria citropa* binds in intermediate exchange and caerin 1.8, isolated from *Litoria chloris*, binds in slow exchange.

It can therefore be concluded that it is *via* interaction with calmodulin that these peptides inhibit neuronal nitric oxide synthase. As they are not specifically able to interact with nNOS but rather with calmodulin, which is responsible for many cellular functions, they are not ideal candidates for future study as inhibitors of nNOS. However, calmodulin is such a pivotal protein that understanding its interactions with its binding partners is important.

Further titrations with other peptides would be useful to determine whether there is a regular relationship between the experimentally derived IC_{50} values and the binding strength with calmodulin, or whether the charge of the peptides has more of an effect. Peptides including members of the dahlein 5 family and members of the aurein 2 family would be of particular interest due to their low IC_{50} values, the dahleins have +3 charge [25], whereas the aureins have +2 charge [10, 20].

7.3 3D NMR studies of the complex between caerin 1.8 and calmodulin

The complex between caerin 1.8 and calmodulin was studied using 3D heteronuclear NMR methods. The majority of backbone HN, N, Cα and Cβ chemical shifts have been assigned.

Caerin 1.8 binds to calmodulin in a 1:1 stoichiometry. The C-terminal domain has a stronger binding interaction with the peptide than does the N-terminal domain.

Assignment of the side chain proton chemical shifts of calmodulin in complex with caerin 1.8 would be required in order to calculate an accurate structure for this complex. A series of 3D NMR experiments has been recorded on the sample in order to achieve this. Now that the majority of the backbone atom resonances have been identified, assignment of the sidechain protons will be relatively straightforward. This was not attempted during the current study because the full assignment of the side chain resonances, followed by structure determination calculations will require a significant amount of time.

Chapter 8 Experimental

8.1 Materials

All chemicals and reagents used were of analytical grade or of the highest purity available.

Peptides were commercially synthesized by Mimotopes (Clayton, Vic) *via* the standard N-α-Fmoc method, using L-amino acids. Details can be found in reference [136]. NMR peptide samples were greater than 90% pure by HPLC and electrospray mass spectrometric analysis.

All pH measurements were recorded using a Eutech Cyberscan pH 500 Meter with an AEP 331 Glass-body probe (183 - 4mm, thin stem).

8.2 Protein and peptide sample preparation

8.2.1 Buffers, solutions and growth media

All buffers and solutions were prepared using Milli-Q® water and sterilized either by autoclaving or filtration using a 0.45 µM filter. Ampicillin 100µg/mL or Kanamycin 25 µg/mL were added as required after sterilization of media. All percentages are listed as weight per volume.

Lurea broth (LB):	1% bacto-tryptone, 0.5% yeast extract, 1% sodium chloride, adjusted to pH 7.
LB agar plate:	LB medium supplemented with 1.5% bacto-agar.
Min A:	60 mM dipotassium phosphate, 33 mM potassium hydrogen phosphate, 1.7 mM sodium citrate, 15 mM ammonium chloride. Autoclave, then add 0.005% thiamine, 0.2% glucose, 0.8 mM magnesium sulphate [112].

Tris buffered saline (TBS):	25 mM tris pH 7.4, 137 mM sodium chloride, 2.7 mM potassium chloride
Coomassie blue stain:	0.1% coomassie blue, 30% methanol, 10% acetic acid
Destain solution:	50% methanol and 5% glacial acetic acid
Super Duper buffer:	33 mM tris pH 8.3, 62.5 mM potassium acetate, 10 mM magnesium acetate, 4 mM spermidine, 0.5 mM DTE
Ligase buffer:	50 mM tris pH 7.6, 10 mM magnesium chloride, 10 mM DTT, 50 mg/mL bovine serum albumin
Buffer A:	50 mM tris, filtered at 0.4 μm
Buffer B:	50 mM tris, 1 M sodium chloride, filtered at 0.4 μm

8.2.2 Protein gels

The Xcell sure lock mini cell system was used with pre-poured 4 - 12% gradient NuPage gels (Invitrogen) for protein analysis, along with MOPS running buffers, as per the manufacturer's instructions. SDS-7 protein molecular weight markers were purchased from Sigma. Coomassie blue stain was used to stain protein.

8.2.3 DNA analysis

Plasmids were purified using the Mo Bio Laboratories Ultraclean^{TM} miniprep kits according to the manufacturer's instructions. 2% agar gels and commercially available SPP1 markers (Geneworks) were used to analyse purified DNA. Ethidium bromide solution (5 μg/mL) was used to stain the gels which were then visualized under UV light. PCR reactions were undertaken as described in the literature [137]. Sequencing was performed at the Institute of Medical and Veterinary Science.

Restriction analysis of DNA samples was undertake by digesting approximately 4 - 5 µg of plasmid DNA with 2 - 4 units of restriction enzyme per µg DNA in a 20 µL volume of Super Duper buffer. (section 8.2.1) Restriction was performed at 37˚C for 2 - 6 hours and the resultant solutions analysed by gel electrophoresis.

DNA extraction from agar gels was performed using the Ultraclean^{TM} kit (Mo Bio) according to the manufacturer's instructions.

DNA ligation was performed using ligase buffer with 1 mM ATP and 1 unit of T4 DNA ligase in total 20 µL volume at 16˚C for at least eight hours. The inserts and vectors were included in a 3:1 ratio.

DNASIS (Hitachi Software Engineering America, San Francisco, CA) and Oligo^{TM} [138] software were used to edit and analyse DNA sequence data.

8.2.4 Bacterial cell lines

Stock cultures of *E. coli* strains and transformants were stored as glycerol stocks at –80˚C. The *E. coli* strain DH5α was used as a host for transformation and amplification of recombinant plasmids. The *E. coli* strain BL21(DE3) was used as a host for recombinant protein expression. The specific details of the genetic makeup of these strains have been reported [137].

8.2.5 Bacterial expression of calmodulin

A bacterial protein expression system was used to prepare high yields of soluble protein for NMR studies. A culture was prepared by inoculation of 10 mL LB medium with a single transformant *E. coli* BL21 (DE3) colony, containing the pET28 vector supplied by Krebs [101]. This was incubated overnight at 37˚C with shaking in a rotary shaker. A 2% subculture was made the following morning and allowed to grow until an optical density at 600 nm of 0.6 was reached. Protein

expression was induced by addition of IPTG to 0.1 mM and was allowed to continue for 2 hours (optimized by expression tests) at 37˚C with shaking. Cells were harvested via centrifugation at 10,000 rpm for 15 minutes, at 4˚C and either frozen until required at –18˚C or processed immediately.

Cell lysis was achieved by resuspending the cells in TBS buffer containing 0.1% Triton X-100 and lysed by four 30 seconds bursts of sonication in the presence of PMSF (1 mM final concentration). The lysate was centrifuged at 10,000 rpm for 30 min. The supernatant was filtered with a 0.45 µM filter and purified by anion exchange chromatography, concentrated with an Amicon stirred cell fitted with a 10 kDa cut-off filter and then further purified *via* size exclusion chromatography. The purification processes were monitored using SDS-page gel analysis of samples. Finally, the protein was desalted using a PD-10 desalting column (Pharmacia).

For ^{15}N labelled calmodulin, LB medium was substituted with Min A medium containing ^{15}N-enriched ammonium chloride., for ^{15}N and ^{13}C doubly labelled calmodulin, the Min A medium also contained ^{13}C-enriched glucose. Growth media were prepared as listed in section 8.2.1.

8.2.6 Anion exchange chromatography

0.45 µm filtered lysis supernatant was loaded onto a 50 mL column packed with Q-sepharose resin (Sigma) and unbound material was washed off with buffer A and collected. A gradient of 0 - 100% buffer B over 8 column volumes was employed. 5 mL fractions were collected with a flow rate of 5 mL/minute. Calmodulin typically eluted between fractions 39 - 49. The fractions were analysed using gel electrophoresis and those containing calmodulin were pooled and concentrated.

8.2.7 Size exclusion chromatography

Crude calmodulin in approximately 5 mL of TBS was loaded onto a 300 mL column containing superdex 75 resin (Sigma). The protein was eluted with TBS over 1

column volume at a flow rate of 1 mL/min. 4 mL fractions were collected, with calmodulin typically eluting in fractions 40 - 50.

8.3 NMR spectroscopy

All NMR spectroscopy was performed on a Varian Inova - 600 NMR spectrometer, fitted with a 5 mm inverse broadband triple resonance probehead and z-axis pulsed field gradients. All experiments were carried out at 25˚C. A ^{1}H frequency of 600 MHz, a ^{15}N frequency of 60 MHz and a ^{13}C frequency of 150 MHz were used in all experiments.

8.3.1 2D NMR Spectroscopy of splendipherin

The sample of splendipherin used to determine the 3D structure was prepared in a solution of 1:1 trifluoroethanol and water, with sodium 2,2-dimethyl-2-silapentane-sulphonate (DSS) as the internal standard. The pH was 2.11, 6.3 mg of peptide was used, giving a concentration of 3.89 mM.

Referencing in the splendipherin NMR spectra was to the methylene group of trifluoroethanol, 3.918 ppm for ^{1}H spectra and 60.975 ppm in the ^{13}C correlated spectra.

Processing of the spectra was performed on a Sun Microsystems Ultra Sparc 1/170 workstation using VNMR software (version 6.1A). Final 2D NMR matrices contained 4096 x 4096 data points, obtained by multiplying the original data matrices by a Gaussian function prior to zero-filling to 4096 data points in the F1 dimension followed by Fourier transformation.

8.3.2 Homonuclear NMR spectra of splendipherin

Pre-saturation was used for suppression of water in the NOESY and TOCSY spectra. This was achieved by applying low power pre-saturation to the appropriate resonance from the proton transmitter during a 1.5 second relaxation delay between each scan. Gradient suppression methods were employed for the COSY spectrum [139]. All ^{1}H experiments were obtained in phase sensitive mode, with time proportional phase incrementation in t_1 [140].

A total of 256 increments were collected per experiment, consisting of 32 time-averaged scans per increment. The FID in t_2 contained 2048 data points. The spectral width was 6999.7 Hz. The mixing time in the NOESY experiment was 150 ms.

8.3.3 Heteronuclear NMR spectra of splendipherin

For the heteronuclear experiments, 256 increments containing 32 scans each were acquired over 4096 data points, detected directly in the ^{1}H, F2 dimension. The spectral width for the ^{13}C F1 dimension was 24132.7 Hz. The inter-pulse delay was 3.6 ms, corresponding to 140 Hz.

8.3.4 Structure Calculations

Assignment of the NMR spectra was performed using a standard sequential assignment procedure, [47] and Sparky software (version 3.106).

The smaller peaks from each pair of symmetrical cross-peaks were integrated and converted to a distance restraints using the method of Xu and co-workers [53].

X-PLOR software (version 3.851) running on a Sun Microsystems Ultra Sparc 1/170 workstation was used to generate the structures. Floating stereo-specific assignments

were included [58] in the RMD and SA standard protocol [141], ambiguous restraints were treated with sum-averaging and refinement based on preliminary calculation results [57].

The All Hydrogen Distance Geometry (ALLHDG) force field (version 4.03) was used for the calculations [142]. For each calculation, 60 structures were generated with initial random backbone torsion angles and taken through 6500 steps (19.5 ps) of high temperature (2000 K) dynamics. The K_{noe} force constant was increased from 1000 to 5000 kcal.mol^{-1}.nm^{-2}. The K_{repel} force constant was increased from 200 to 1000 kcal.mol^{-1}.nm^{-4}. 2500 cooling steps (7.5 ps) were simulated to reach 1000 K. The K_{repel} force constant was increased to 40,000 kcal.mol^{-1}.nm^{-4} and the atomic radii decreased from 90% to 75% of those values in the ALLHDG parameter set during the cooling.

1000 steps (3 ps) of cooling then followed, decreasing the temperature of the system from 1000 K to 100 K. The resultant ensemble of 60 structures was subjected to 200 steps of gradient energy minimization following which the 20 lowest energy structures were selected for study.

3D structures were viewed using MOLMOL and INSIGHT II (version 95.0) software

8.3.5 NMR sample preparation for titration studies

Pre-weighed peptides were dissolved in water to known concentrations, adjusted to pH 6.3 then aliquoted to appropriate portions (as listed in sections 4.14 - 4.16) and lyophilised. Dried peptide portions were then added to the calmodulin sample in sequence. The pH was re-adjusted back to 6.3 with the addition of small quantities of 0.01 M hydrochloric acid or 0.01 M sodium hydroxide solutions as required after each addition.

The calmodulin samples used for the titrations contained calmodulin (1.89×10^{-7} moles), potassium chloride (6.3 mM), calcium chloride (31 mM) and 10% D_2O in aqueous solution at pH 6.3. Sodium azide (0.02%) was added as a preservative [114].

8.3.6 2D ^{15}N-HSQC titration experiments

Referencing in these experiments was to DSS, at 0 ppm in ^{1}H. The ^{15}N dimension carrier frequency was centered at 118.286 ppm.

The ^{15}N-HSQC experiments resulted in a matrix of 256 x 1024 data points. Each increment consisted of 16 scans. The spectral width was 7197.5 Hz in the proton dimension and 2200 Hz in the nitrogen dimension. Acquisition time was 2 hours 49 minutes. The standard gNhsqc pulse sequence from the vnmr library was used [143].

Processing of the spectra was performed on a Sun Microsystems Ultra Sparc 1/170 workstation using NMRPipe software [144]. Zero-filling was used to double the number of points in both dimensions and a sine-bell window function was applied. The conversion and processing files are shown in sections 8.3.7 and 8.3.8. The left half of the spectrum was extracted each time.

8.3.7 HSQC conversion file

```
#!/bin/csh

var2pipe -in ./fid -noaswap  \
  -xN              2048  -yN               512  \
  -xT              1024  -yT               256  \
  -xMODE        Complex  -yMODE      Rance-Kay  \
  -xSW         9000.900  -ySW         2200.000  \
  -xOBS         599.783  -yOBS          60.782  \
  -xCAR           4.773  -yCAR         118.286  \
  -xLAB              H1  -yLAB             N15  \
  -ndim               2  -aq2D          States  \
  -out ./test.fid -verb -ov

sleep 5
```

8.3.8 HSQC processing file

```
#!/bin/csh

nmrPipe -in test.fid -verb \
|nmrPipe -fn POLY -time \
|nmrPipe -fn SP -off 0.30 -end 1 -pow 1 \
|nmrPipe -fn ZF -auto\
|nmrPipe -fn FT \
|nmrPipe -fn SP -off 0.3 -end 1.0 -pow 1.0 -c 0.5 \
|nmrPipe -fn PS -p0 187.0 -p1 00.0 -di \
|nmrPipe -fn EXT -left -sw \
|nmrPipe -fn TP \
|nmrPipe -fn SP -off 0.3 -end 1 -pow 1 \
|nmrPipe -fn ZF -auto \
|nmrPipe -fn FT \
|nmrPipe -fn PS -p0 0.0 -p1 0.0 -di \
|nmrPipe -fn POLY -auto \
|nmrPipe -fn TP \
|nmrPipe -fn POLY -auto \
|nmrPipe -out hsqc.dat -ov –verb
```

8.3.9 3D NMR spectroscopy

All heteronuclear NMR experiments were performed at 25˚C on a Varian Inova-600 NMR spectrometer, using a ^{1}H frequency of 600 MHz, a ^{13}C frequency of 150 MHz and a ^{15}N frequency of 60 MHz. Referencing was by alignment with the chemical shifts of the previously published study by Ikura *et al* [133]. The standard pulse sequences ghn_cacb [145] and gcbca_co_nh [146] from the vnmr library were used.

The HNCACB experiment resulted in a matrix of 36 x 86 x 1024 data points. The spectral widths in F1, F2 and F3 were set to 7197.5 Hz for ^{1}H, 9049.5 Hz for ^{13}C and 1458.8 Hz for ^{15}N. Carrier frequencies for ^{1}H, ^{13}C and ^{15}N were set to 4.773, 47.362 and 118.861 ppm respectively. Each increment comprised 16 scans. The total acquisition time was 69 hours, 21 minutes and 15 seconds. The processing files for the HNCACB are shown in sections 8.3.10 and 8.3.11. Only the left hand side of the spectrum was extracted during processing. Zero-filling and a sine-bell window function were applied in all dimensions. Linear prediction was employed in the carbon and nitrogen dimensions.

8.3.10 HNCACB conversion file

```
#!/bin/csh

var2pipe -in ./fid -noaswap -aqORD 1 \
  -xN              2048  -yN               172  -zN                72  \
  -xT              1024  -yT                86  -zT                36  \
  -xMODE        Complex  -yMODE        Complex  -zMODE        Complex  \
  -xSW         7197.481  -ySW         9049.500  -zSW         1458.789  \
  -xOBS         599.796  -yOBS         150.825  -zOBS          60.784  \
  -xCAR           4.773  -yCAR          47.362  -zCAR         118.261  \
  -xLAB              H1  -yLAB             C13  -zLAB             N15  \
  -ndim               3  -aq2D          States                        \
  -out ./data/hncacb%03d.fid -verb -ov

sleep 5
```

8.3.11 HNCACB processing file

```
xyz2pipe -in data/hncacb%03d.fid -x -verb \
| nmrPipe -fn POLY -time \
| nmrPipe -fn SP -off 0.33 -end 0.98 -pow 2 -c 0.5 \
| nmrPipe -fn ZF -auto \
| nmrPipe -fn FT -auto \
| nmrPipe -fn PS -p0 180.0 -p1 0.0 -di -verb \
| nmrPipe -fn EXT -x1 11ppm -xn 5.5ppm -sw \
| pipe2xyz -out ft/cbcanh%03d.ft -x

xyz2pipe -in ft/cbcanh%03d.ft -z -verb \
| nmrPipe -fn SP -off 0.5 -end 0.98 -pow 1 -c 0.5 \
| nmrPipe -fn ZF -auto \
| nmrPipe -fn FT -auto \
| nmrPipe -fn PS -p0 0.0 -p1 0.0 -di -verb \
| pipe2xyz -out ft/cbcanh%03d.ft -z -inPlace

xyz2pipe -in ft/cbcanh%03d.ft -y -verb \
| nmrPipe -fn LP -x1 1 -xn 48 -ord 8 -fb -pred 48 -after \
| nmrPipe -fn SP -off 0.5 -end 0.98 -pow 1 -c 0.5 \
| nmrPipe -fn ZF -auto \
| nmrPipe -fn FT -auto \
| nmrPipe -fn PS -p0 0.0 -p1 0.0 -di -verb \
| nmrPipe -fn REV \
| pipe2xyz -verb -ov -out ft/cbcanh%03d.ft -y -inPlace
```

```
xyz2pipe -in ft/cbcanh%03d.ft -z -verb \
| nmrPipe -fn HT -auto \
| nmrPipe -fn PS -p0 0.0 -p1 0.0 -inv \
| nmrPipe -fn FT -inv \
| nmrPipe -fn ZF -inv \
| nmrPipe -fn SP -off 0.5 -end 0.98 -pow 1 -c 0.5 -inv \
| nmrPipe -fn LP -ps0-0 -ord 8 \
| nmrPipe -fn SP -off 0.5 -end 0.98 -pow 1 -c 0.5 \
| nmrPipe -fn ZF -size 128 \
| nmrPipe -fn FT \
| nmrPipe -fn PS -p0 0.0 -p1 0.0 -di -verb \
| pipe2xyz -out ft/cbcanh%03d.dat -z
```

The CBCA(CO)NH experiment results from a matrix of 36 x 53 x 2048 data points. The spectral widths in F1, F2 and F3 were set to 7197.5 Hz for ^{1}H, 9049.5 Hz for ^{13}C and 1458.8 Hz for ^{15}N. Carrier frequencies for ^{1}H, ^{13}C and ^{15}N were set to 4.773, 47.362 and 118.861 ppm respectively. Each increment comprised 16 scans. The total acquisition time was 69 hours, 21 minutes and 15 seconds. The processing files for the CBCA(CO)NH experiment are shown in sections 8.3.12 and 8.3.13. The left hand side of the spectrum was extracted during processing. Zero-filling and a sine-bell window function were applied in all dimensions. Again, linear prediction was employed in the carbon and nitrogen dimensions.

8.3.12 CBCA(CO)NH conversion file

```
#!/bin/csh

var2pipe -in ./fid -noaswap -aqORD 1 \
  -xN              2048  -yN               106  -zN                72  \
  -xT              1024  -yT                53  -zT                36  \
  -xMODE        Complex  -yMODE        Complex  -zMODE         Complex  \
  -xSW         7197.481  -ySW         9049.500  -zSW          1458.789  \
  -xOBS         599.796  -yOBS         150.825  -zOBS           60.784  \
  -xCAR           4.773  -yCAR          47.362  -zCAR          118.261  \
  -xLAB              H1  -yLAB             C13  -zLAB              N15  \
  -ndim               3  -aq2D          States                         \
  -out ./data/test%03d.fid -verb -ov

sleep 5
```

8.3.13 CBCA(CO)NH processing file

```
xyz2pipe -in data/test%03d.fid -x -verb \
| nmrPipe -fn POLY -time \
| nmrPipe -fn SP -off 0.33 -end 0.98 -pow 2 -c 0.5 \
| nmrPipe -fn ZF -auto \
| nmrPipe -fn FT -auto \
| nmrPipe -fn PS -p0 182.4 -p1 0.0 -di -verb \
| nmrPipe -fn EXT -x1 11ppm -xn 5.5ppm -sw \
| pipe2xyz -out ft/hcn%03d.ft -x

xyz2pipe -in ft/hcn%03d.ft -z -verb \
| nmrPipe -fn SP -off 0.5 -end 0.98 -pow 1 -c 0.5 \
| nmrPipe -fn ZF -auto \
| nmrPipe -fn FT -auto \
| nmrPipe -fn PS -p0 0.0 -p1 0.0 -di -verb \
| pipe2xyz -out ft/hcn%03d.ft -z -inPlace

xyz2pipe -in ft/hcn%03d.ft -y -verb \
| nmrPipe -fn LP -ps0-0 -ord 8 \
| nmrPipe -fn SP -off 0.5 -end 0.98 -pow 1 -c 0.5 \
| nmrPipe -fn ZF -auto \
| nmrPipe -fn FT -auto \
| nmrPipe -fn PS -p0 000.0 -p1 0.0 -di -verb \
| pipe2xyz -verb -ov -out ft/hcn%03d.ft -y -inPlace

xyz2pipe -in ft/hcn%03d.ft -z -verb \
| nmrPipe -fn HT -auto \
| nmrPipe -fn PS -p0 0.0 -p1 0.0 -inv \
| nmrPipe -fn FT -inv \
| nmrPipe -fn ZF -inv \
| nmrPipe -fn SP -off 0.5 -end 0.98 -pow 1 -c 0.5 -inv \
| nmrPipe -fn LP -ps0-0 -ord 8 \
| nmrPipe -fn SP -off 0.5 -end 0.98 -pow 1 -c 0.5 \
| nmrPipe -fn ZF -size 128 \
| nmrPipe -fn FT \
| nmrPipe -fn PS -p0 0.0 -p1 0.0 -di -verb \
| pipe2xyz -out ft/hcn%03d.dat –z
```

Assignment of the NMR spectra was performed using a combination of main-chain directed and standard sequential assignment procedure [47, 48] and Sparky software, version 3.111 for Windows XP [147]. Chemical shift analysis and graphing were performed using Microsoft Excel 2000.

References

1. Inglis, S. R., Jones, R., Fritz, D., Stojkowski, C., Booker, G. W., Pyke, S. M. (2005) Synthesis of 5-, 6- and 7-substituted-2-aminoquinolines as SH3 domain ligands, *Organic and Biomolecular Chemistry. 3*, 2543-2557.

2. Inglis, S. R., Stojkowski, C., Branson, K. M., Cawthray, J. F., Fritz, D., Wiadrowski, E., Pyke, S. M., Booker, G. W. (2004) Identification and specificity studies of small-molecule ligands for SH3 protein domains, *Journal of Medicinal Chemistry. 47*, 5405-5417.

3. Hiramatsu, K., Aritaka, N., Hanaki, H., Kawasaki, S., Hosoda, Y., Hori, S., Fukuchi, Y., Kobayashi, I. (1997) Dissemination in Japanese hospitals of strains of *Staphylococcus aureus* heterogeneously resistant to Vancomycin, *Lancet. 350*, 1670-1673.

4. Hancock, R. E. W. (1997) Peptide antibiotics, *Lancet. 349*, 418-422.

5. Zasloff, M. (1987) Magainins, a class of antimicrobial peptides from *Xenopus* skin: Isolation, characterisation of two active forms, and partial cDNA sequence of a precursor, *Proceedings of the National Academy of Sciences. 84*, 5449-5453.

6. Barra, D., Simmaco, M. (1995) Amphibian skin: A promising resource for antimicrobial peptides, *TIBTECH. 13*, 205-209.

7. Daly, J. W. (1998) Thirty years of discovering arthropod alkaloids in amphibian skin, *Journal of Natural Products. 61*, 162-172.

8. Cei, J. M., Erspamer, V., Rosechini, M. (1967) Taxonomic and evolutionary significance of biogenic amines and polypeptides occurring in amphibian skin I. Neotropical *leptodactylid* frogs, *Systematic Zoology. 16*, 328-342.

9. Zancanaro, C., Sbarbati, A., Bolner, A., Accordini, C., Piemonte, G., Osculati, F. (1995) Biogenic amines in the taste organ, *Chemical Senses. 20*, 329-335.

10. Apponyi, M. A., Pukala, T. L., Brinkworth, C. S., Maselli, V. M., Bowie, J. H., Tyler, M. J., Booker, G. W., Wallace, J. C., Carver, J. A., Separovic, F., Doyle, J., Llewellyn, L. E. (2004) Host-defence peptides of Australian anurans: structure, mechanism of actions and evolutionary significance, *Peptides. 2004*, 1035-1054.

11. Bowie, J. H., Wegener, K. L., Chia, B. C., Wabnitz, P. A., Carver, J. A., Tyler, M. J., Wallace, J. C. (1999) Host defence antibacterial peptides from skin secretions of Australian amphibians. The relationship between structure and activity, *Protein and Peptide Letters. 6*, 259-269.

12. Erspamer, V. (1994) Bioactive secretions of the amphibian integument. in *Amphibian Biology: The Integument.* (Heatwolde, H., ed) pp. 178-350, Surrey, Beatty and Sons, Norton, NSW.

13. Lazarus, L. H., Attila, M. (1993) The toad, ugly and venomous, wears yet a precious jewel in his skin, *Progress in Neurobiology. 41,* 473-507.

14. Jacob, L., Laszloff, M. (1994) Potential therapeutic applications of magainins and other antimicrobial agents of animal origin, *Ciba Foundation Symposium. 186,* 197-223.

15. Grenard, S. (1994) *Medical Herpetology*, Reptiles and Amphibian Magazine, Pottsville, PA.

16. Hancock, R. E. W., Chapple, D. S. (1999) Peptide antibiotics, *Antimicrobial Agents and Chemotherapy. 43*, 1317-1323.

17. Andreu, D., Rivas, L. (1998) Animal antimicrobial peptides: An overview, *Biopolymers (Peptide Science). 47,* 415-433.

18. Tyler, M. J. (1987) Frog and cane toad skin secretions in *Toxic plants and animals. A guide for Australia* (Covacevich, J., ed) pp. 329-339, Queensland Museum, Brisbane.

19. Anastasi, A., Erspamer, V. Endean, R. (1968) Isolation and amino acid sequence of caerulein, the active decapeptide of the skin of *Hyla caerulea, Archives of Biochemistry and Biophysics. 125*, 57-68.

20. Rozek, T., Wegener, K. L., Bowie, J. H., Olver, I. N., Carver, J. A., Wallace, J. C. (2000) The antibiotic and anticancer active aurein peptides from the Australian Bell frogs *Litoria aurea* and *Litoria raniformis*. The solution structure of aurein 1.2, *European Journal of Biochemistry. 267,* 5330-5341.

21. Wabnitz, P. A., Bowie, J. H., Tyler, M. J., Wallace, J. C., Smith, B. P. (2000) Differences in the skin peptides in male and female Australian tree frog *Litoria splendida, European Journal of Biochemistry. 267,* 269-275.

22. Stone, D. J. M., Waugh, R. J., Bowie, J. H., Wallace, J. C., Tyler, M. J. (1993) Peptides from Australian frogs. The structures of the caerins from *Litoria caerulea, Journal of Chemical Research, Synopses. 4*, 138.

23. Waugh, R., J., Stone, D. J. M., Bowie, J. H., Wallace, J. C., Tyler, M. J. (1993) Peptides from Australian frogs. The structures of the caerins and caeridins from *Litoria gilleni, Journal of Chemical Research, Synopses.*, 139.

24. Wegener, K. L., Wabnitz. P. A., Carver, J. A., Bowie, J. H., Chia, B. C. S., Wallace, J. C. (1999) Host defence peptides from the skin glands of the Australian Blue Mountains Tree frog *Litoria citropa*. Solution structure of the antibacterial peptide citropin 1.1, *European Journal of Biochemistry. 265*, 627-637.

25. Wegener, K. L., Brinkworth, C. S., Bowie, J. H., Wallace, J. C., Tyler, M. J. (2001) Bioactive dahlein peptides from the skin secretions of the Australian aquatic frog *Litoria dahlii*; sequence determination by electrospray mass spectrometry, *Rapid Communications in Mass Spectrometry. 15*, 1726-1734.

26. Raftery, M. J., Waugh, R. J., Bowie, J. H., Wallace, J. C., Tyler, M. J. (1996) The structures of the frenatin peptides from the skin secretion of the Giant Tree Frog *Litoria infrafrenata*, *Journal of Peptide Science. 2*, 117-24.

27. Doyle, J., Llewellyn, L. E., Brinkworth, C. S., Bowie, J. H., Wegener, K. L., Rozek, T., Wabnitz, P. A., Wallace, J. C., Tyler, M. J. (2002) Amphibian peptides that inhibit neuronal nitric oxide synthase, *European Journal of Biochemistry. 269*, 100-109.

28. Rozek, T., Wegener, K. L. Steinborner, S. T., Bowie, J. H., Tyler, M. J., Wallace, J. C. (1998) The maculatin peptides from the skin glands of the tree frog *Litoria genimaculata*- a comparison with the structures and antibacterial activities of maculatin 1.1 and caerin 1.1, *International Journal of Peptide and Protein Research. 4*, 111-115.

29. Steinborner, S. T., Gao, C. W., Raftery, M. J., Waugh, R. J., Blumenthal, T., Bowie, J. H. (1994) The structures of four tryptophillin and three rubellidin peptides from the Australian red tree frog *Litoria rubella*, *Australian Journal of Chemistry. 47*, 2099-2108.

30. Wegener, K. L. (2001) PhD thesis, Amphibian peptides: Their structures and bioactivity, University of Adelaide, Adelaide.

31. Epand, R. M., Vogel, H. J. (1999) Diversity of antimicrobial peptides and their mechanisms of action, *Biochimica et Biophysica Acta Biomembranes. 1462*, 11-28.

32. Sansom, M. S. P. (1991) The biophysics of peptide models of ion channels, *Progress in Biophysical Molecular Biology. 55*, 139-235.

33. Shai, Y. (1999) Mechanism of the binding, insertion and destabilization of phospholipid bilayer membranes by α-helical antimicrobial and cell non-selective membrane-lytic peptides, *Biochimica et Biophysica Acta. 1462*, 55-70.

34. Tossi, A., Tarantino, C., Romeo, D. (1997) Design of synthetic antimicrobial peptides based on sequence analogy and amphipathicity, *European Journal of Biochemistry. 250*, 549-558.

35. Doyle, J., Brinkworth, C. S., Wegener, K. L., Carver. J. A., Llewellyn, L. E., Olver, I. N., Bowie, J. H., Wabnitz, P. A., Tyler, M. J. (2003) nNOS inhibition, antimicrobial and anticancer activity of the amphibian skin peptide, citropin 1.1 and synthetic modfications. The solution structure of a modified citropin 1.1., *European Journal of Biochemistry. 270*, 1141-53.

36. Cruciani, R. A., Barker, J. L., Zasloff, M., Chen, H., Colamonici, O. (1991) Antibiotic magainins exert cytolytic activity against transformed cell lines through channel formation, *Proceedings of the National Academy of Sciences. 88*, 3792-3796.

37. Birch, M. C. (1974) *Pheromones*, North-Holland Publishing Co., Amsterdam.

38. Kikuyama, S., Toyoda, F., Ohmiya, Y., Matsuda, K., Tanaka, S., Hayashi, H. (1995) Sodefrin: A female-attracting peptide pheromone in newt cloacal glands, *Science. 267*, 1643-1645.

39. Yamamoto, K., Kawai, Y., Hayashi, T., et al. (2000) Silefrin, a sodefrin-like pheromone in the abdominal gland of the Sword-tailed Newt, *Cynops ensicauda*, *FEBS letters. 472*, 267-270.

40. Clore, G. M., Gronenborn, A. M. (1991) Structures of larger proteins in solution: Three- and four-dimensional heteronuclear NMR spectroscopy, *Science. 2*, 1390-1400.

41. Schiffer, M., Edmundson, A. B. (1967) Use of helical wheels to represent the structures of proteins and to identify segments with helical potential, *Biophysical Journal. 7*, 121-135.

42. Govil, G., Hosur, R. V. (1982) *Conformation of biological molecules : new results from NMR*, Springer-Verlag, New York.

43. Clore, G. M., Gronenborn, A. M. (1998) Determining the structures of large proteins and protein complexes by NMR, *TIBTECH. 16*, 22-34.

44. Evans, J. N. S. (1995) *Biomolecular NMR spectroscopy*, 2nd edn, Oxford University Press, Oxford.

45. Hore, P. J. (1995) *Nuclear magnetic resonance*, Oxford University Press, Oxford.

46. Silverstein, R. M., Webster, F. X. (1998) *Spectrometric identification of organic compounds*, 6th edn, John Wiley and Sons, Inc., New York.

47. Wuthrich, K. (1986) *NMR of proteins and nucleic acids*, 1st edn, Wiley-Interscience, New York.

48. Cavanagh, J., Fairbrother, W. J., Palmer, A. G., Skelton, N. J. (1996) *Protein NMR spectroscopy, principles and practice*, First edn, Academic Press, San Diego.

49. Wishart, D. S., Sykes, B. D. (1994) Chemical shifts as a tool for structure determination, *Methods in Enzymology. 239*, 363-392.

50. Pastore, A., Saudek, V. (1990) The relationship between chemical shift and secondary structure in proteins, *Journal of Magnetic Resonance. 90*, 165-176.

51. Wishart, D. S., Sykes, B. D., Richards, F. M. (1992) The chemical shift index: A fast and simple method for the assignment of protein secondary structure through NMR spectroscopy, *Biochemistry. 31*, 1647-1651.

52. Wishart, D. S., Sykes, B. D. (1994) The ^{13}C chemical shift index: A simple method for the identification of protein secondary structure using ^{13}C chemical shift data, *Journal of Biomolecular NMR. 4*, 171-180.

53. Xu, R. X., Word, J. M., Davis, D. G., Rink, M. J., Willard, D. H. Jr., Gampe, R. T. Jr. (1995) Solution structure of the human pp60c-src SH2 domain complexed with a phosphorylated tyrosine pentapeptide, *Biochemistry. 34*, 2107-2121.

54. Nilges, M., Clore, G. M., Gronenborn, A. M. (1988) Determination of three-dimensional structures of proteins from interproton distance data by hybrid distance geometry-dynamical simulated annealing calculations, *FEBS Letters. 229*, 317-324.

55. Clore, G. M., Brunger, A. T., Karplus, M., Gronenborn, A. M. (1986) Application of molecular dynamics with interproton distance restraints to three-dimensional protein structure determination, *Journal of Molecular Biology. 191*, 523-551.

56. Kaptein, R., Boelens, R., Scheek, R. M., van Gunsteren, W. F. (1988) Protein structures from NMR, *Biochemistry. 27*, 5389-5395.

57. Weber, P. L., Morrison, R., Hare, D. (1988) Determining stereo-specific ^{1}H nuclear magnetic resonance assignments from distance geometry calculations, *Journal of Molecular Biology. 204*, 483-487.

58. Folmer, R. H. A., Hilbers, C. W., Konings, R. N. H., Nilges, M. (1997) Floating stereospecific assignment revisited: Application to an 18 kDa protein and comparison with J-coupling data, *Journal of Biomolecular NMR. 9*, 245-258.

59. Ramachandran, G. N., Sasiskharan, V. (1968) Conformation of polypeptides and proteins, *Advances in Protein Chemistry. 23*, 283-437.

60. Hong, D. P., Hoshino, M., Kuboi, R., Goto, Y. (1999) Clustering of fluorine-substitued alcohols as a factor responsible for their marked effects on proteins and peptides, *Journal of the American Chemical Society. 121*, 8427-8433.

61. Rajan, R., Balaram, P. (1996) A model for the interaction of trifluoroethanol with peptides and proteins, *International Journal of Peptide and Protein Research. 48*, 328-336.

62. Schonbrunner, N., Wey, J., Engles, J., Georg, H., Kiefhaber, T. (1996) Native-like β-structure in a trifluoroethanol-induced partially folded state of the all β-sheet protein tendamistat, *Journal of Molecular Biology. 260*, 432-445.

63. Barnes, G., Gentle, I. (2005) *Interfacial science: an introduction*, Oxford University Press, Oxford.

64. Tanford, C. (1961) *Physical chemistry of macromolecules*, John Wiley and Sons, Inc., New York.

65. Ozawa, K., Headlam, M. J., Schaeffer, P. M., Henderson, B. R., Dixon, N. E., Otting, G. (2004) Optimization of an Escherichia coli system for cell-free synthesis of selectively ^{15}N-labelled proteins for rapid analysis by NMR spectroscopy, *European Journal of Biochemistry. 271*, 4084-4093.

66. Schon, O., Friedler, A., Freund, S., Fersht, A. R. (2004) Binding of p53-derived ligands to MDM2 induces a variety of long range conformational changes, *Journal of Molecular Biology. 336*, 197-202.

67. Di Stefano, D. L., Wand, A. J. (1987) Two-dimensional ^{1}H NMR study of human ubiquitin: a main chain directed assignment and structure analysis, *Biochemistry. 26*, 7272-7281.

68. Englander, S. W., Wand, A. J. (1987) Main-chain-directed strategy for the assignment of ^{1}H NMR spectra of proteins, *Biochemistry. 26*, 5953-5958.

69. Tyler, M. J., Davies, M., Martin, A. A. (1977) A new species of large green tree frog from northern Western Australia, *Transactions of the Royal Society of South Australia. 101*, 133-138.

70. Tyler, M. J., Davies, M. (1986) *Frogs of the Northern Territory*, 1st edn, G. L. Duffield, Darwin.

71. Tyler, M. J., Smith, L. A., Johnstone, R. E. (1994) *Frogs of Western Australia*, 2nd edn, Lamb Print, Perth.

72. Wabnitz, P. A., Bowie, J. H., Tyler, M. J., Wallace, J. C., Smith, B. P. (1999) Aquatic sex pheromone from a male tree frog, *Nature. 401*, 444-445.

73. Rollman, S., M., Houck, L. D., Feldhoff, R. C. (1999) Proteinaceous pheromone affecting female receptivity in a terrestrial salamander, *Science. 285*, 1907-1909.

74. Tinoco, I., Jr. (2002) Physical chemistry of nucleic acids, *Annual Reviews in Physical Chemistry. 53*, 1-15.

75. Richardson, J. S., Richardson, D. C. (1988) Amino acid preferences for specific locations at the ends of α-helices, *Science. 240*, 1648-1652.

76. Zhou, N. E., Zhu, B., Sykes, B. D., Hodges, R. S. (1992) Relationship between amide proton chemical shifts and hydrogen bonding in amphipathic α-helical peptides, *Journal of the American Chemical Society. 114*, 4320-4326.

77. Lee, S., Kwok, D. Y., Laibinis, P. E. (2002) Chemical influences on adsorption mediated self-propelled drop movement, *Physical Review E. 65*, 051602-1-9.

78. Suda, H., Yamada, S. (2003) Force measurements for the movement of a water drop on a surface with a surface tension gradient, *Langmuir. 19*, 529-531.

79. Yun, K., Cho, I., Bu, J., Kim, C. J., Yoon, E. (2002) A surface-tension driven micropump for low-voltage and low-power operations, *Journal of Microelectromechanical systems. 11*, 454-461.

80. Manning-Benson, S., Bain, C. D., Darton, R. C. (1997) Measurement of dynamic interfacial properties in an overflowing cylinder by ellipsometry, *Journal of Colloid and Interface Science. 189*.

81. Patil, G. S., Cornwell, D. G. (1978) Interfacial oxidation of α-tocopherol and the surface properties of its oxidation products, *Journal of Lipid Research. 19*, 416-422.

82. Cooper, S. (2005) Interfaces, colloids and gels, Accessed: 16/01/2006, http://www.dur.ac.uk/sharon.cooper/lectures/colloids/interfacesweb2.html#_Toc449417634.

83. Oshanin, G., De Coninck, J., Cazabat, A. M., Moreau, M. (1998) Microscopic model for spreading of a two-dimensional monolayer, *Journal of Molecular Liquids. 76*.

84. Kone, B. C. (2000) Protein-protein interactions controlling nitric oxide synthases, *Acta Physiol Scand. 168*, 27-31.

85. Kone, B. C., Kuncewicz, T., Zhang, W., Yu, Z. (2003) Protein interactions with nitric oxide synthases: controlling the right time, the right place, and the right amount of nitric oxide, *Am J Physiol Renal Physiol. 285*, F178-190.

86. Wikipedia. (2005) Calmodulin, Accessed: 19/12/2005, http://en.wikipedia.org/wiki/Calmodulin.

87. Hoeflich, K. P., Ikura, M. (2002) Calmodulin in action: Diversity in target recognition and activation mechanisms, *Cell. 108*, 739-742.

88. Klee, C. B., Newton, D. L., Ni, W. C., Haiech, J. (1986) Regulation of the calcium signal by calmodulin, *Ciba Foundation Symposium. 122*, 162-182.

89. Martin, S. R., Biekofsky, R. R., Skinner, M. A., Guerrini, R., Salvadori, S., Feeney, J., Bayley, P. M. (2004) Interaction of calmodulin with the phosphofructokinase target sequence, *FEBS letters. 577*, 284-288.

90. Biekofsky, R., R., Martin, S. R., Browne, J. P., Bayley, P. M., Feeney, J. (1998) Ca^{2+} coordination to backbone carbonyl oxygen atoms in calmodulin and other EF-hand proteins: ^{15}N chemical shifts as probes for monitoring individual-site Ca^{2+} coordination, *Biochemistry. 37*, 7617-7629.

91. Babu, Y. S., Bugg, C. E., Cook, W. J. (1988) Structure of calmodulin refined at 2.2 A resolution, *Journal of Molecular Biology. 204*, 191-204.

92. Meador, W. E., Means, A. R., Quiocho, F. A. (1992) Target enzyme recognition by calmodulin: 2.4 angstrom structure of a calmodulin-peptide complex, *Science. 257*, 1251-1255.

93. Meador, W. E., Means, A. R., Quiocho, F. A. (1993) Modulation of calmodulin plasticity in molecular recognition on the basis of X-ray structures, *Science. 262*, 1718-1722.

94. Chou, J. J., Li, S., Klee, C.B., Bax, A. (2001) Solution structure of Ca^{2+}-calmodulin reveals flexible hand-like properties of its domains, *Nature Structural Biology. 8*, 990-997.

95. O'Neil, K. T., DeGrado, W. F. (1990) How calmodulin binds its targets: Sequence independent recognition of amphiphathic α-helices, *Trends in Biological Sciences. 15*, 59-64.

96. DeGrado, W. F., Prendergast, F. G., Wolfe, H. R. Jr., Cox, J. A. (1985) The design, synthesis, and characterization of tight-binding inhibitors of calmodulin, *Journal of Cellular Biochemistry. 29*, 83-94.

97. Cox, J. A., Comte, M. Fitton, J. E., DeGrado, W. F. (1985) The interaction of calmodulin with amphiphilic peptides, *Journal of Biological Chemistry. 260*, 2527-2534.

98. Ikura, M., Clore, G. M., Gronenborn, A. M., Zhu, G., Klee, C. B., Bax, A. (1992) Solution structure of a calmodulin-target peptide complex by multidimensional NMR, *Science. 256*, 632-638.

99. Urbauer, J. L., Ehrhardt, M. R., Bieber, R. J., Flynn, P. F., Wand, A. J. (1996) High-resolution triple resonance NMR spectroscopy of a novel calmodulin-peptide complex at kilobar pressure, *Journal of the American Chemical Society. 118*, 11329-11330.

100. Vetter, S. W., Leclerc, E. (2003) Novel aspects of calmodulin target recognition and activation, *European Journal of Biochemistry. 270*, 404-414.

101. Elshorst, B., Hennig, M., Forsterling, H., Diener, A., Maurer, M., Schulte, P., Schwalbe, H., Griesinger, C., Krebs, J., Schmid, H., Vorherr, T., Carafoli, E.

(1999) NMR solution structure of a complex of calmodulin with a binding peptide of the Ca^{2+} pump, *Biochemistry. 38*, 12320-12332.

102. Seeholzer, S. H., Cohn, M., Putkey, J. A., Means, A. R., Crespi, H. L. (1986) NMR studies of a complex of deuterated calmodulin with melittin, *Proceedings of the National Academy of Sciences. 83*, 3634-3638.

103. Ikura, M., Barbato, G., Klee, C. B., Bax, A. (1992) Solution structure of calmodulin and its complex with a myosin light chain kinase fragment, *Cell Calcium. 13*, 391-400.

104. Ikura, M., Kay, L. E., Krinks, M., Bax, A. (1991) Triple-resonance multidimensional NMR study of calmodulin complexed with the binding domain of skeletal muscle myosin light-chain kinase: Indication of a conformational change in the central helix, *Biochemistry. 30*, 5498-5504.

105. Barra, D., Simmaco, M., Boman, H. G. (1998) Gene-encoded peptide antibiotics and innate immunity. Do "animacules" have defence budgets?, *FEBS letters. 430*, 130-134.

106. Studier, W. F., Rosenberg, A. H., Dunn, J. J., Dubendorff, J. W. (1990) Use of T7 RNA polymerase to direct expression of cloned genes, *Methods in Enymology. 185*, 60-89.

107. Studier, F. W., Moffat, B. A. (1986) Use of bacteriophage T7 RNA polymerase to direct selective high-level expression of cloned genes., *Journal of Molecular Biology. 189*, 113-130.

108. Jenny, R. J., Mann, K. G., Lundblad, R. L. (2003) A critical review of the methods for cleavage of fusion proteins with thrombin and factor Xa, *Protein Expression and Purification. 31*, 1-11.

109. Roberts, R. J. (1005) How restriction enzymes became the workhorses of molecular biology, *Proceedings of the National Academy of Sciences. 102*, 5905-5908.

110. Danna, K., Nathans, D. (1971) Specific cleavage of simian virus 40 DNA by restriction endonuclease of *Hemophilus Influenzae, Proceedings of the National Academy of Sciences. 2913-2917.*

111. Marley, J., Lu, M., Bracken, C. (2001) A method for efficient isotopic labeling of recombinant proteins, *Journal of Biomolecular NMR. 20*, 71-75.

112. Miller, J. H. (1972) *Experiments in molecular genetics*, Cold Spring Harbour Press, Cold Spring Harbour, N. Y.

113. Walker, J. M. (1994) The bicinchoninic acid (BCA) assay for protein quantiation, *Methods in Molecular Biology. 32*, 5-8.

114. Ikura, M., Kay, L. E., Bax, A. (1990) A novel approach for sequential assignment of ^{1}H, ^{13}C and ^{15}N spectra of larger proteins: Heteronuclear triple-resonance three-dimensional NMR spectroscopy. Application to calmodulin, *Biochemistry. 29*, 4659-4667.

115. Fisher, P. J., Prendergast, F. G., Ehrhardt, M. R., Urbauer, J. L., Wand, A. J., Sedarous, S. S., McCormick, D. J., Buckley, P. J. (1994) Calmodulin interacts with amphiphilic peptides composed of all D-amino acids, *Nature. 368*, 651-653.

116. Ikura, M., Bax, Ad. (1992) Isotope-filtered 2D NMR of a protein-peptide complex: Study of a skeletal muscle myosin light chain kinase fragment bound to calmodulin, *Journal of the American Chemical Society. 114*, 2433-2440.

117. Otting, G. (1994) Experimental NMR techniques for studies of protein-ligand interactions, *Current Opinion in Structural Biology. 3*, 760-768.

118. Koenig, B. W., Rogowski, M., Louis, J. M. (2003) A rapid method to attain isotope labeled small soluble peptides for NMR studies, *Journal of Biomolecular NMR. 26*, 193-202.

119. Ikura, M., Marion, D., Kay, L. E., Shih, H., Krinks, M., Klee, C. B., Bax, A. (1990) Heteronuclear 3D NMR and isotopic labeling of calmodulin, *Biochemical Pharmacology. 40*, 153-160.

120. Jayaraj, S., Reid, R., Santi, D. V. (2005) GeMS: an advanced software package for designing synthetic genes, *Nucleic Acids Research. 33*, 3011-3016.

121. Kapust, R. B., Tozser, J., Copeland, T. D., Waugh, D. S. (2002) The P1' specificity of the tobacco etch virus protease, *Biochemical and Biophysical Research Communications. 294*, 949-955.

122. Phan, J., Zdanov, A., Evdokimov, A. G., Tropea, J. E., Peters, H. K. III, Kapust, R. B., Li, M., Wlodawer, A., Waugh, D. S. (2002) Structural basis for the substrate specificity of the tobacco etch virus protease, *Journal of Biological Chemistry. 277*, 50564-50572.

123. Aasmul-Olsen, S., Christensen, K. A., Widmer, F. (1991) Carboxypeptidase mediated C-terminal amidation of polypeptide acids, *Biomedica Biochimica Acta. 10/11*, S106-S109.

124. Breddam, K., Widmer, F., Meldal, M. (1991) Amidation of growth hormone releasing factor (1-29) by serine carboxypeptidase catalysed transpeptidation, *International Journal of Peptide and Protein Research. 37*, 153-160.

125. Zhang, Z. Z., Yang, S. S., Dou, H., Mao, J. F., Li, K. S. (2004) Expression, purification, and C-terminal amidation of recombinant human glucagon-like peptide-1, *Protein Expression and Purification. 36*, 292-9.

126. Brinkworth, C. S., Bowie, J. H., Tyler, M. J., Wallace, J. C. (2002) A comparison of the host defence skin peptides of the New Guinea Tree frog (*Litoria genimaculata*) and the Fringed Tree frog (*Litoria eucnemis*). The link between the caerin and maculatin antibacterial peptides, *Australian Journal of Chemistry. 55*, 605-610.

127. Steinborner, S. T., Gao, C. W., Raftery, M. J., Waugh, R. J., Blumenthal, T., Bowie, J. H. (1998) New antibiotic caerin 1 peptides from the skin secretion of the Australian tree frog *Litoria chloris* - comparison of the activities of the caerin 1 peptides from the genus *Litoria*, *International Journal of Peptide and Protein Research. 51*, 121-6.

128. Dubendorff, J. W., Studier, F. W. (1991) Controlling basal expression in an inducible T7 expression system by blocking the target T7 promoter with lac repressor., *Journal of Molecular Biology. 219*, 45-59.

129. Cai, M., Huang, Y., Sakaguchi, K., Clore, G. M., Gronenborn, A. M., Craigie, R. (1998) An efficient and cost-effective isotope labeling protocol for proteins expressed in *Escherichia coli*, *Journal of Biomolecular NMR. 11*, 97-102.

130. Hensmann, M., Booker, G. W., Panatayou, G., Boyd, J., Linacre, G., Waterfield, M., Campbell, I. D. (1994) Phosphopeptide binding to the N-terminal SH2 domain of the p85a subunit of PI 3'-kinase: A heteronuclear NMR study, *Protein Sci. 3*, 1020-30.

131. Tsilikounas, E., Kettner, C. A., Bachovchin, W. W. (1992) Identification of serine and histidine adducts in complexes of trypsin and trypsinogen with peptide and nonpeptide boronic acid inhibitors by 1H NMR spectroscopy, *Biochemistry. 31*, 12839-12846.

132. Stanczyk, S. M., Bolton, P. H. (1992) Comparison of conformational features of staphylococcal nuclease in ternary complexes with pdTp, pdGp and nitrophenyl-pdTp, *Biochemistry. 31*, 6396-6401.

133. Ikura, M., Spera, S., Barbato, G., Kay, L. E., Krinks, M., Bax, A. (1991) Secondary structure and side-chain ^{1}H and ^{13}C resonance assignments of calmodulin in solution by heteronuclear multidimensional NMR spectroscopy, *Biochemistry. 30*, 9216-9228.

134. Wagner, G., Pardi, A., Wuthrich, K. (1983) Hydrogen bond length and ^{1}H NMR chemical shifts in proteins, *Journal of the American Chemical Society. 105*, 5948-5949.

135. El Thaher, T. S., Bailey, G. S., Wilson, M. T., Osborne, M., Moore, G. R. (1992) A ^{1}H NMR study of the interactions between rat tissue kallikrein and two peptide inhibitors, *Biochimica et Biophysica Acta. 1160*, 235-238.

136. Maeji, N. J., Bray, A. M., Valerio, R. M., Wang, W. (1995) Larger scale multipin peptide synthesis, *Peptide Research. 8*, 33-38.

137. Merkel, A. (2002) PhD thesis, Pleckstrin homology and tec homology domains link tec kinase signalling to the cytoskeleton, University of Adelaide, Adelaide.

138. Rychlik, W., Rhoads, R. E. (1989) A computer program for choosing optimal oligonucleotides for filter hybridization, sequencing and *in vitro* amplification of DNA, *Nucleic Acids Research. 17*, 8543-8551.

139. John, B. K., Plant, D., Webb, P., Hurd, R. E. (1992) Effective combination of gradients and crafted RF pulses for water suppression in biological samples, *Journal of Magnetic Resonance. 98*, 200-206.

140. Marion, D., Wuthrich, K. (1983) Application of phase sensitive two-dimensional correlated spectroscopy (COSY) for measurements of ^{1}H-^{1}H spin-spin coupling constants in proteins, *Biochemical and Biophysical Research Communications. 113*, 967-974.

141. Nilges, M. M., O'Donoghue, S. I. (1998) Ambiguous NOEs and automated NOE assignment, *Progress in Nuclear Magnetic Resonance Spectroscopy. 32*, 107-139.

142. Engh, R. A., Huber, R. (1991) Accurate bond and angle parameters for X-ray protein-structure refinement, *Acta Cryst. A47*, 392-400.

143. Kay, L., Keifer, P., Saarinen, T. (1992) Pure absorption gradient enhanced heteronuclear single quantum correlation spectroscopy with improved sensitivity, *Journal of the American Chemical Society. 114*, 10663-10665.

144. Delaglio, F., Grzesiek, S., Vuister, G. W., Zhu, G., Pfeifer, J., Bax, A. (1995) NMRPipe: a multidimensional spectral processing system based on UNIX pipes, *Journal of Biomolecular NMR. 6*, 277-293.

145. Wittekind, M., Mueller, L. (1993) A high sensitivity 3D NMR experiment to correlate amide proton and nitrogen resonances with the α-carbon and ß-carbon resonances in proteins, *Journal of Magnetic Resonance. 101B*, 201-205.

146. Grzesiek, S., Bax, A. (1992) Correlating backbone amide and side chain resonances in larger proteins by multiple relay triple resonance NMR, *Journal of the American Chemical Society. 114*, 6291–6293.

147. Goddard, T. G., Kneller, D. G. (2004) SPARKY, University of California, San Fransisco.

Available online at www.sciencedirect.com
SCIENCE DIRECT®
Peptides 25 (2004) 1035–1054
PEPTIDES
www.elsevier.com/locate/peptides

Host-defence peptides of Australian anurans: structure, mechanism of action and evolutionary significance

Margit A. Apponyi [a], Tara L. Pukala [a], Craig S. Brinkworth [a], Vita M. Maselli [a], John H. Bowie [a,*], Michael J. Tyler [b], Grant W. Booker [c], John C. Wallace [c], John A. Carver [d], Frances Separovic [e], Jason Doyle [f], Lyndon E. Llewellyn [f]

[a] *Department of Chemistry, The University of Adelaide, Adelaide, South Australia 5005, Australia*
[b] *School of Earth and Environmental Sciences, The University of Adelaide, Adelaide, South Australia 5005, Australia*
[c] *School of Molecular and Biomedical Sciences, The University of Adelaide, Adelaide, South Australia 5005, Australia*
[d] *Department of Chemistry, University of Wollongong, New South Wales, Wollongong 2522, Australia*
[e] *School of Chemistry, University of Melbourne, Melbourne, Vic. 3010, Australia*
[f] *Australian Institute of Marine Science, Townsville MC, Qld. 4810, Australia*

Received 11 December 2003; received in revised form 10 March 2004; accepted 11 March 2004

Available online 10 May 2004

Abstract

Host-defence peptides secreted from the skin glands of Australian frogs and toads, are, with a few notable exceptions, different from those produced by anurans elsewhere. This review summarizes the current knowledge of the following classes of peptide isolated and characterized from Australian anurans: neuropeptides (including smooth muscle active peptides, and peptides that inhibit the production of nitric oxide from neuronal nitric oxide synthase), antimicrobial and anticancer active peptides, antifungal peptides and antimalarial peptides. Other topics covered include sex pheromones of anurans, and the application of peptide profiling to (i) recognize particular populations of anurans of the same species and to differentiate between species, and (ii) investigate evolutionary aspects of peptide formation.

Keywords: Australian amphibians; Host-defence peptides; Bioactive peptides; Pheromones; Skin secretions; NMR; Mass spectrometry; Evolution

1. Introduction

Amphibians have rich chemical arsenals that form an integral part of their defence systems, and also assist with the regulation of dermal physiological action. In response to a variety of stimuli, host-defence compounds are secreted from specialized glands onto the dorsal surface and into the gut of the amphibian. Many of these peptides exhibit either potent vasodilator or antimicrobial activity [6,8,34,45]. Such peptides are secreted from the skin glands of metamorph and adult animals [25] but in at least one species (*Litoria splendida*) it has been shown that tadpoles contain the same host-defence peptides as the adult [103].

During the past decade we have isolated and identified peptides from the secretions of skin glands of 35 species of Australian frogs and toads from the genera *Litoria*, *Uperoleia*, *Limnodynastes*, *Cyclorana* and *Crinia*. The dorsal glands are best illustrated by *L. splendida* (Fig. 1: large parotoid and rostral glands on the head) [5], and *Litoria caerulea* (Fig. 2: granular glands over the whole dorsal surface) [5]. We obtain the secretions by electrical stimulation of the glands on the dorsal skin. This process, illustrated in Fig. 3, may be repeated at monthly intervals and does not harm the amphibians [95]. It is not unusual to be able to identify all of the major bioactive peptides using just one secretion from one animal. We have identified neuropeptides, membrane active peptides which exhibit antimicrobial, anticancer and sometimes antifungal activity, antimalarial peptides, and peptides which inhibit the formation of nitric oxide (NO) from neuronal nitric oxide synthase. Many of these peptides show multifaceted activity. The best examples of this are the caerin 1 peptides of Australian tree frogs of the genus *Litoria*, of which caerin 1.1 is an example (sequence shown below).

Caerin 1.1 GLLSVLGSVAKHVLPHVVPVIAEHL-NH_2

A major peptide of the glandular secretions of the tree frogs *L. splendida* and *L. caerulea*, has two amphipathic helices separated by a central flexible hinge region [109]. This peptide is a wide spectrum antibiotic (mainly against

* Corresponding author.
E-mail address: John.Bowie@adelaide.edu.au (J.H. Bowie).

0196-9781/$ – see front matter © 2004 Elsevier Inc. All rights reserved.
doi:10.1016/j.peptides.2004.03.006

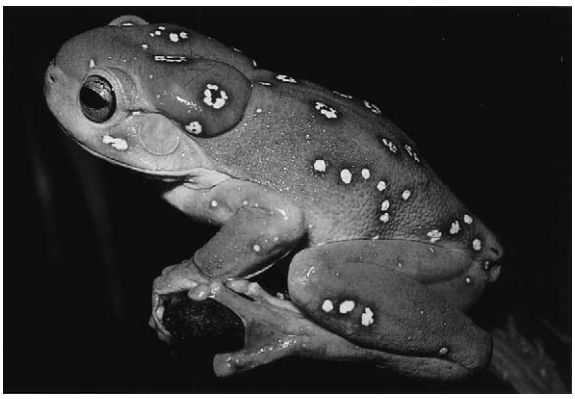

Fig. 1. *Litoria splendida*.

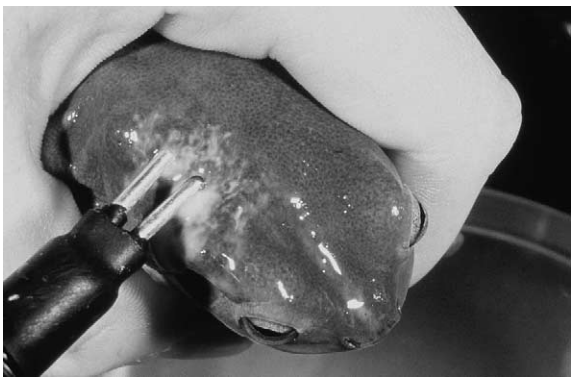

Fig. 3. Milking *Litoria caerulea*.

gram positive organisms but also against some gram negative organisms (MIC 1–100 μg/ml range)), shows IC_{50} in the 10^{-6} M range against all the major human cancer types, is active against some viruses (HIV and Herpes simplex 1 (MIC 20 and 24 μg/ml, respectively)), kills nematodes (at concentrations of 10^{-6} M), is active against the malaria parasite *Plasmodium falciparum* (MIC 10 μg/ml) and inhibits the formation of NO from neuronal nitric oxide synthase at an IC_{50} concentration of 37 μM. Caerin 1.1 lyses red blood cells at >250 μg/ml, a concentration greater than that required for the activities listed above. Some of these bio-activities are probably in excess of requirement as far as anurans are concerned, but tree frogs certainly use caerin 1 peptides as antimicrobials, and they may well use them to control the number of nematodes in the gut. Although there is currently little malaria in Australia, some anurans (e.g. species of the genus *Rana* [76]), are prone to infestation by *Plasmodium*, and caerin 1.1 can certainly deal with these parasites (for *L. caerulea* and *L. splendida*) if required to do so.

An earlier review [15] concentrated on antimicrobially active peptides from Australian anurans; this review will deal with all of the various types of peptide, and their activities, summarized above. In addition, the review will deal with (a) peptide sex pheromones of amphibians, and (b) the use of peptide profiling to assist with (i) the identification of different species of anuran, (ii) the identification of different populations of the same species, and (iii) the investigation of evolutionary trends of amphibians. The review will concentrate principally on the unique peptides of Australian anurans: bioactive peptides from anurans elsewhere have been dealt with by others [6,8,34,45]. The sequences of all peptides discussed in this article are listed (in alphabetical order of trivial names) in Table 1.

Fig. 2. *Litoria caerulea*.

2. Structure determination

2.1. Primary structure determination

Several methods have been utilized to determine the primary structure of the various host-defence peptides isolated from these secretions. These methods involve complementary use of mass spectrometry and automated Edman sequencing.

2.2. Positive ion mass spectrometry

The sequencing of peptides using positive ion mass spectrometry (MS) has been standard for some time and has been described extensively [9]. We have predominately used the B and Y + 2 fragmentations to elucidate the primary structure of peptides. The information provided by these fragmentations is summarized in Scheme 1. Briefly, B fragmentations provide sequencing information from the C-terminal end of the peptide while Y + 2 fragmentations provide sequencing information from the N-terminal end. In addition, the first B cleavage ion can be used to identify whether the peptide is a free carboxylic acid (loss of 18 Da from the MH^+ species) or has been post-translationally modified to the amide (loss of 17 Da from the MH^+ species). For other positive ion fragmentations of peptides, see Ref. [9].

MS coupled with enzymic digestion of the peptide can provide sequence information. For example, isobaric Lys and Gln are distinguished using Lys-C digestion. This enzyme cleaves at the C-terminal end of Lys.

Table 1
Alphabetical listing of selected amphibian peptides

Name	Sequence	MW	Species	Activity*
Aurein 1.1	GLFDIIKKIAESI-NH_2	1444	a	1, 2
Aurein 1.2	GLFDIIKKIAESF-NH_2	1478	a	1, 2
Aurein 2.1	GLLDIVKKVVGAFGSL-NH_2	1613	a	1, 2
Aurein 2.2	GLFDIVKKVVGALGSL-NH_2	1613	a	1, 2, 4
Aurein 2.3	GLFDIVKKVVGAIGSL-NH_2	1613	a	1, 2, 4
Aurein 2.4	GLFDIVKKVVGTLAGL-NH_2	1630	a	1, 2, 4
Aurein 2.5	GLFDIVKKVVGAFGSL-NH_2	1647	a	1, 2
Aurein 3.2	GLFDIVKKIAGHIASSI-NH_2	1766	a	1, 2
Aurein 4.1	GLIQTIKEKLKELAGGLVTGIQS-OH	2394	a	
Caeridin 1.1	GLLαDGLLGTGL-NH_2	1140	b, c, d, e, f	
Caeridin 1.2	GLLβDGLLGTGL-NH_2	1140	d	
Caeridin 1.4	GLLαDGLLGGLGL-NH_2	1096	e, f	
Caeridin 1.5	GLLβDGLLGGLGL-NH_2	1096	e, f	
Caeridin 2	GLLDVVGNLLGGLGL-NH_2	1408	c, d	
Caeridin 3	GLFDAIGNLLGGLGL-NH_2	1428	c, d	
Caeridin 4	GLLDVVGNVLHSGL-NH_2	1504	c	
Caerin 1.1	GLLSVLGSVAKHVLPHVVPVIAEHL-NH_2	2582	b, c, d	1, 2, 3, 4
Modification 1	GLLSVLGSVAKHVL**G**HVV**G**VIAEHL-NH_2	2502		1, 2
Modification 2	GLLSVLGSVAKHVL**A**HVV**A**VIAEHL-NH_2	2530		
Caerin 1.1.1	LSVLGSVAKHVLPHVVPVIAEHL-NH_2	2412	d	
Caerin 1.1.2	SVLGSVAKHVLPHVVPVIAEHL-NH_2	2299	d	
Caerin 1.1.3	VLPHVVPVIAEHL-NH_2	1420	b, c, d	
Caerin 1.1.5	GLLSVLGSVAKHVLPH-OH	1625	b, c, d	
Caerin 1.3	GLLSVLGSVAQHVLPHVVPVIAEHL-NH_2	2582	c	1, 2
Caerin 1.4	GLLSSLGSVAKHVLPHVVPVIAEHL-NH_2	2600	c, d	1
Caerin 1.5	GLLSVLGSVVKHVIPHVVPVIAEHL-NH_2	2610	c	1, 2
Caerin 1.6	GLFSVLGAVAKHVLPHVVPVIAEKL-NH_2	2591	e, f	1, 2, 4
Caerin 1.7	GLFKVLGSVAKHLLPHVAPVIAEKL-NH_2	2634	e, f	1, 2
Caerin 1.8	GLFKVLGSVAKHLLPHVVPVIAEKL-NH_2	2662	f	1, 2, 3, 4
Caerin 1.9	GLFGVLGSIAKHVLPHVVPVIAEKL-NH_2	2591	f	1, 2, 3, 4
Caerin 1.10	GLLSVLGSVAKHVLPHVVPVIAEKL-NH_2	2573	b	1, 2, 3, 4
Caerin 1.11	GLLGAMFKVASKVLPHVVPAITEHF-NH_2	2659	g	1
Caerin 2.1	GLVSSIGRALGGLLADVVKSKGQPA-OH	2392	b	1, 4
Caerin 2.2	GLVSSIGRALGGLLADVVKSKEQPA-OH	2464	c	1, 4
Caerin 2.4	GLVSSIGKALGGLLADVVKTKEQPA-OH	2450	c	4
Caerin 2.5	GLVSSIGRALGGLLADVVKSKEQPA-OH	2448	d	1, 4
Caerin 3.1	GLWQKIKDKASELVSGIVEGVK-NH_2	2382	b, c	1
Caerin 3.2	GLWEKIKEKASELVSGIVEGVK-NH_2	2397	c	1
Caerin 3.3	GLWEKIKEKANELVSGIVEGVK-NH_2	2424	c	1
Caerin 3.4	GLEWKIREKANELVSGIVEGVK-NH_2	2452	c	1
Caerin 4.1	GLWQKIKSAAGDLASGIVEGIKS-NH_2	2326	c	1
Caerin 4.2	GLWQKIKSAAGDLASGIVEAIKS-NH_2	2340	c	1
Caerin 4.3	GLWQKIKQAAGDLASGIVEGIKS-NH_2	2353	c	1
Caerulein 1.1	pEQDY(SO_3)TGWMDF-NH_2	1351	h	5
Caerulein 1.2	pEQDY(SO_3)TGWFDF-NH_2	1367	b, i	5
Caerulein 2.1	pEQDY(SO_3)TGAHMDF-NH_2	1373	i	5
Caerulein 2.2	pEQDY(SO_3)TGAHFDF-NH_2	1389	i	5
Caerulein 3.1	pEQDY(SO_3)GTGWMDF-NH_2	1408	i	5
Caerulein 3.2	pEQDY(SO_3)GTGWFDF-NH_2	1424	i	5
Caerulein 4.1	pEQDY(SO_3)TGSHMDF-NH_2	1389	i	5
Caerulein 4.2	pEQDY(SO_3)TGSHFDF-NH_2	1405	i	5
Citropin 1.1	GLFDVIKKVASVIGGL-NH_2	1613	i	1, 2, 3, 4
Modification 1	GLF**A**VIKKVASVIGGL-NH_2	1569		1, 2, 3, 4
Modification 2	GLFDVI**A**KVASVIGGL-NH_2	1556		1, 2, 3, 4
Citropin 1.2	GLFDIIKKVASVVGGL-NH_2	1613	i	1, 2, 3, 4
Citropin 1.3	GLFDIIKKVASVIGGL-NH2	1627	i	1, 2, 3, 4
Dahlein 1.1	GLFDIIKNIVSTL-NH_2	1430	j	1
Dahlein 1.2	GLFDIIKNIFSGL-NH_2	1434	j	1
Dahlein 4.1	GLWQLIKDKIKDAATGLVTGIQS-NH_2	2486	j	
Dahlein 5.1	GLLGSIGNAIGAFIANKLKP-OH	1952	j	4

Table 1 (*Continued*)

Name	Sequence	MW	Species	Activity*
Dynastin 1	GLVSNLGI-OH	729	k	
Dynastin 2	GLLSSLGLNL-OH	986	l	
Dynastin 3	GLVPNLLNNLGL-OH	1236	m	
Dynastin 4	GLVSNLGI-OH	772	n	
Dynastin 5	GLISNLGI-OH	786	n	
Dynastin 6	GAVSGLLTNL-OH	944	n	
Dynastin 7	GAVSGLLTNLGL-OH	1144	n	
Electrin 2.1	NEEEKVKWEPDVP-NH_2	1743	o	
Fletcherin	AGPVSKLVSGIGL-OH	1197	p	
Frenatin 1	GLLDALSGILGL-NH_2	1140	q	
Frenatin 2	GLLGTLGNLLNGLGL-NH_2	1423	q	
Frenatin 3	GLMSVLGHAVGNVLGGLFKPKS-OH	2180	q	4
Lesueurin	GLLDILKKVGKVA-NH_2	1352	r	4
Mactulatin 1.1	GLFGVLAKVAAHVVPAIAEHF-NH_2	2145	s	1, 2, 3, 4
Maculatin 1.2	GLFGVLAKVASHVVAAIAEHFQA-NH_2	2360	s	1, 2
Maculatin 1.3	GLLGLLGSVVSHVVPAIVGHF-NH_2	2068	g	1, 2
Maculatin 1.4	GLLGLLGSVVSHVLPAITQHL-NH_2	2121	g	1, 2
Maculatin 2.1	GFVDFLKKVAGTIANVVT-NH_2	1878	s	1, 2
Maculatin 3.1	GLLQTIKEKLESLAKGIVSGIQA-NH_2	2395	s	
Rubellidin 4.1	GLGDILGLLGL-NH_2	1039	t	
Rubellidin 4.2	AGLLDILGL-NH_2	883	t	
Rothein 2.1	AGGLDDLLEPVLNSADNLVHGL-NH_2	2230	u	
Rothein 3.1	ASAAGAVRAGGLDDLLEPVLNSADNLVHGL-NH_2	2964	u	
Signiferin 1	RLC*IPYIIPC*-OH (*indicates disulfide bridge)	1187	v	5
Splendipherin	GLVSSIGKALGGLLADVVKSKGQPA-OH	2364	b, c	4, 6
Tryptophyllin L 1.1	PWL-NH_2	414	t	
Tryptophyllin L 1.2	FPWL-NH_2	561	o, t	
Tryptophyllin L 1.3	pEFPWL-NH_2	672	t	
Tryptophyllin L 1.4	FPFPWL-NH_2	805	t	5
Tryptophyllin L 2.1	IPWL-NH_2	527	t	
Tryptophyllin L 3.1	FPWP-NH_2	545	o, t	
Tryptophyllin L 3.2	FPWP-OH	546	t	
Tryptophyllin L 3.3	pEFPWF-NH_2	706	t	
Tryptophyllin L 4.1	LPWY-NH_2	577	t	
Tryptophyllin L 4.2	FLPWY-NH_2	724	t	
Tryptophyllin L 5.1	pEIPWFHR-NH_2	965	t	
Uperin 1.1	pEADPNAFYGLM-NH_2	1208	w	5
Uperolein	pEPDPNAFYGLM-NH_2	1232	x	5

*Activity nomenclature: (1) antibiotic activity; (2) anticancer activity; (3) fungicide activity; (4) nNOS inhibitor; (5) neuropeptide, smooth muscle active; (6) aquatic sex pheromone.

Species: (a) *Litoria aurea*, *Litoria raniformis* [70]; (b) *Litoria splendida* [99]; (c) *Litoria caerulea* [89]; (d) *Litoria gilleni* [105]; (e) *Litoria xanthomera* [84,85]; (f) *Litoria chloris* [81]; (g) *Litoria eucnemis* [19]; (h) various species of the genus *Litoria* [34]; (i) *Litoria citropa* [107]; (j) *Litoria dahlii* [106]; (k) *Limnodynastes interioris* [60]; (l) *Limnodynastes dumerilii* [60]; (m) *Limnodynastes terraereginae* [60]; (n) *Limnodynastes salmini* [18]; (o) *Litoria electrica* [101]; (p) *Limnodynastes fletcheri* [18]; (q) *Litoria infrafrenata* [104]; (r) *Litoria lesueuri* [32]; (s) *Litoria genimaculata* [69]; (t) *Litoria rubella*[81,83]; (u) *Litoria rothii* [106]; (v) *Crinia signifera* [51] (w) *Uperoleia inundata* [1]; (x) many species of the genus *Uperoleia* [34].

2.2.1. Negative ion mass spectrometry

We also use negative ion mass spectrometry to assist in the primary sequencing of peptides. There are several cleavage processes that provide analogous information to that provided by the B and Y + 2 fragmentations in the positive ion mode. These cleavages are summarized in Scheme 2. The α cleavage process provides sequence information from the N-terminal end of the peptide while the β cleavage process provides information from the C-terminal end [13]. Generally, α fragmentation is more pronounced than β fragmentation [13].

Several other cleavages have been discovered that provide additional sequence information. These cleavages identify specific residues and/or the position of these residues in the peptide. The first set of cleavages identify the presence of specific residues by a characteristic loss of a neutral from the $(M–H)^-$ species, eg. CH_2O (Ser) [13], MeCHO (Thr) [13], H_2S (Cys) [11], H_2O (Asp, Glu) [13], NH_3 (Asn, Gln) [13].

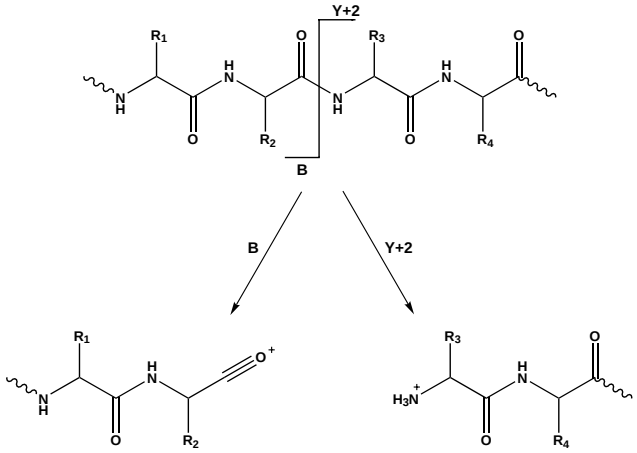

Scheme 1.

The second set of fragmentations involves backbone cleavages initiated from specific residues. The fragmentations result from cleavage of the bond between the NH and αC generating two possible ions depending on where the charge resides, namely δ (charge resides on the N-terminal fragment) and γ (charge resides on the C-terminal fragment) cleavage ions. Amino acid residues that undergo this type of fragmentation are Ser [13], Thr [13], Glu [13], Cys [11], Gln [13], Asp [13], Asn [13], and Phe [20]. A particular example is shown for Asp in Scheme 3. γ-Cleavage ions are generally more abundant than δ ions. For details of the other backbone cleavages see review [13].

Neither positive nor negative ion backbone fragmentations distinguish Leu and Ile. This is done by automated Edman degradation [13], which also confirms the total sequence.

The positive and negative ion spectra of a 16-residue peptide (1) are shown below for comparison. The collision induced mass spectrum of the MH^+ ion of (1) is shown in Fig. 4a. The B ions are drawn schematically above the spectrum while the Y + 2 ions are drawn below the spectrum. There are a total thirteen B ions and eleven Y + 2 ions, identifying the entire peptide sequence with the exceptions

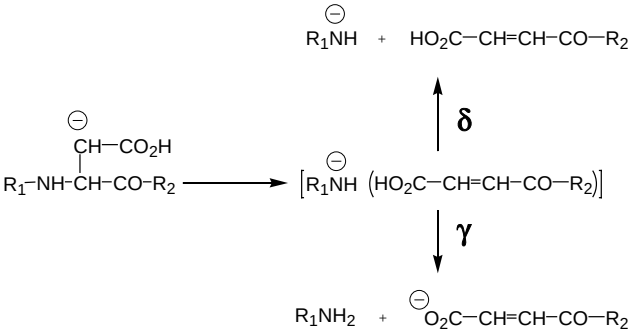

Scheme 3.

of the relative orientation of the first two residues (Gly Leu) and differentiation between isomeric Ile and Leu and isobaric Gln and Lys. The collision induced MS/MS data for the $(M–H)^-$ species of (1) is shown in Fig. 4b. The base peak in the spectrum is the $[(M–H)^–CH_2O]^-$ peak at *m/z* 1609 (loss of CH_2O is the side-chain cleavage of Ser) from which the majority of the remaining fragmentation results. Thirteen α ions and five β ions originate from this ion, identifying the peptide sequence with the exception of the relative orientation of the first two and last two residues. The lack of any γ fragmentation arising from residues 7 and 8 suggests that these residues are Lys rather than the isobaric Gln. Also the peaks at *m/z* 596 and 578 are backbone cleavage ions of Ser11 [13], identifying the position of this residue. The two spectra together identify the entire sequence of peptide (1) except for isomeric Ile and Leu and the relative orientation of the first two residues (Gly Leu).

(1) GLFAVIKKVASVIKGL(NH_2)

2.3. Three-dimensional structure determination

The elucidation of the three-dimensional (3D) structure of the various amphibian peptides is accomplished using a combination of two-dimensional (2D) nuclear magnetic resonance (NMR) experiments and computer modeling.

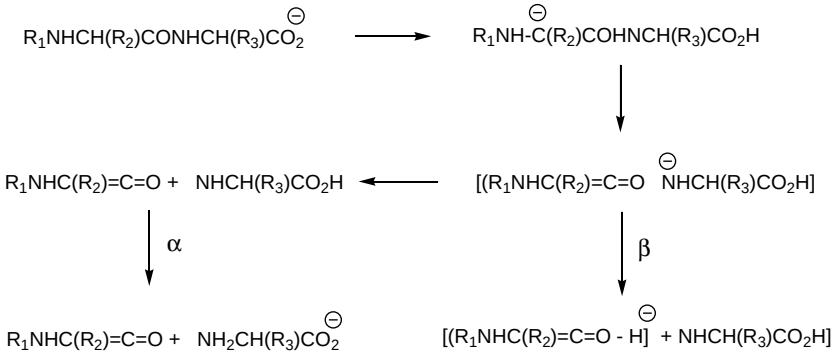

Scheme 2.

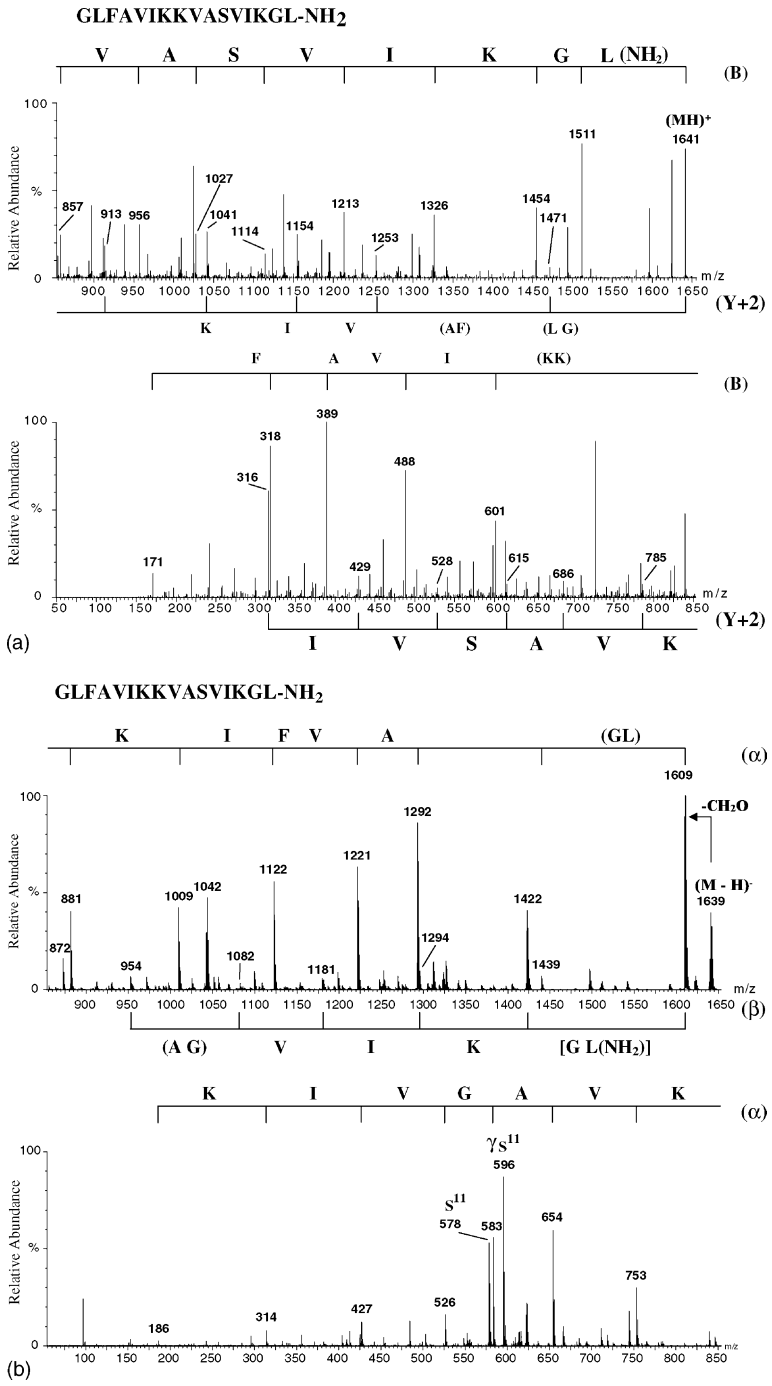

Fig. 4. (a) Collision induced MS/MS mass spectrum of the $(MH)^+$ ion of (1). B fragmentations are drawn schematically above the spectrum while Y + 2 fragmentations are shown below the spectrum. Magnification ranges: 495–1654 (2×). (b) Collision induced MS/MS mass spectrum of the $(M–H)^-$ ion of (1). The α and β fragmentation originating from the $[(M–H)^–CH_2O]^-$ ion are drawn above and below the spectrum, respectively. All other fragmentation is annotated on the spectrum. Magnification ranges: 58–597 (36×), 597–1432 (24×).

2.3.1. Solvent systems

The solvent system in which the NMR experiments are run is important. Solvent systems are chosen so as to mimic different conditions within the body. Three solvent systems have been used, viz. (i) varying mixtures of water and 2,2,2-trifluoroethanol (TFE) are used as a membrane mimicking solvent. TFE is known to disrupt intermolecular hydrogen bonds between the water and the peptide thus increasing the effectiveness of the intra-molecular bonds in the peptide responsible for the secondary structure [58,61]; (ii) a membrane mimicking solvent can also be generated using micelles. Micelles are spherical aggregates of amphiphilic

lipid molecules that form in water when the concentration of lipids is sufficiently high. For our investigations, the commonly used lipid is zwitterionic dodecylphospatidycholine (DPC). These lipids form stable micelles at concentrations of about 1 mM [53]; and (iii) NMR data were also obtained in water, allowing the structure of the peptides outside the membrane to be elucidated. In pure water, peptides often tend to form inter-molecular hydrogen bonds with the water, thereby disrupting the intra-molecular hydrogen bonding within the peptide responsible for the secondary structure.

2.3.2. ^1H NMR experiments

^{1}H 2D NMR experiments are used to assign the various proton resonances within the peptide under study. The experiments used include:

(i) Correlated spectroscopy experiments (COSY) indicate protons that are spin-spin coupled to each other (i.e. protons that are on adjacent nuclei) [37]. This is particularly useful for assigning proton resonances within specific spin systems (i.e. individual residues).

(ii) Total correlated spectroscopy experiments (TOCSY) provide additional information to that in a COSY spectrum by indicating all proton resonances in the same spin system. With respect to peptides and proteins, each amino acid residue constitutes a separate spin system [37].

(iii) Nuclear overhauser spectroscopy (NOESY) experiments indicate, via dipolar coupling, protons that are within 5 Å of each other in space. A spatial interaction is represented by a cross peak: the volume of the cross peak is inversely proportional to the sixth power of the distance between the two protons in question [37].

Citropin 1.1 GLFDVIKKAVASVIGGL(NH_2)

Sections of NOESY and TOSCY spectra of citropin 1.1 are shown in Fig. 5. The TOCSY spectrum shown on top indicates the through-bond connectivities within the spin systems of each residue. The NH region of the NOESY spectrum is shown below and depicts through-space NOE connectivities between sequential backbone NH protons.

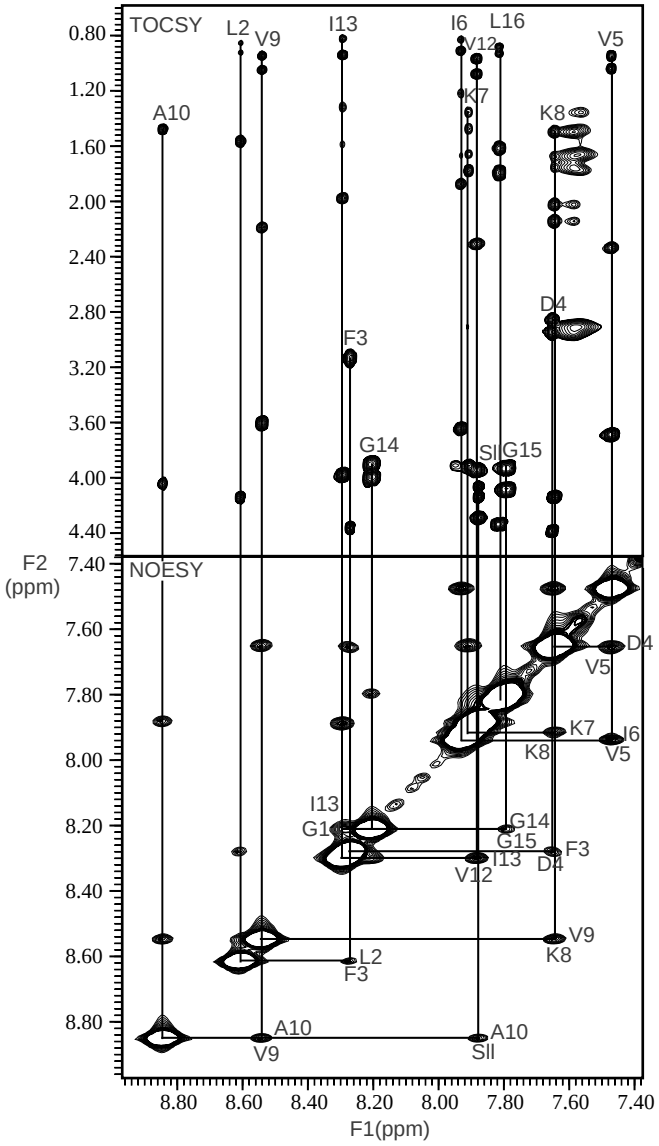

Fig. 5. Partial NOESY and TOCSY spectra of citropin 1.1 in TFE/water. Vertical lines connect the resonances in each spin system. These are labelled with the standard single-letter abbreviations for the residue type and a number indicating the sequential position of the residue. NOEs between sequential NH protons are indicated in the NOESY spectrum.

Having assigned the proton resonances in the peptide, the cross peaks in the NOESY spectrum are assigned accordingly. The best scenario is that each peak is uniquely assigned although this is usually improbable with systems as large as peptides. There are usually at least several peaks that have multiple assignments. The volume of each cross peak is determined and using the inverse sixth power relationship between volume and distance, a series of distance restraints is generated (i.e. a list of the distances between specific protons in the peptide) [110].

A series of dihedral restraints can also be generated from the $J^3_{NH\alpha H}$ spin–spin coupling constants measured from the high-resolution 1D ^{1}H NMR spectrum of the peptide [24]. These two restraint series are used in restrained molecular dynamics and simulated annealing calculations to generate the 3D solution structure of the peptide [110]. Beginning with an initial structure of poorly defined geometry [26], the system is manipulated such that all of the restraints are satisfied with the least number of violations. The most stable conformation (i.e. global minimum) is located by refining the distance restraints by removing the ambiguities in the assignments producing a representation of the peptide in solution [7,91]. The solution structures of six peptides (described in detail in this article) determined by the method described above are shown in Figs. 6–11. As an example, the solution structure of citropin 1.1 (derived in part from the data shown in Fig. 5) is shown in Fig. 7.

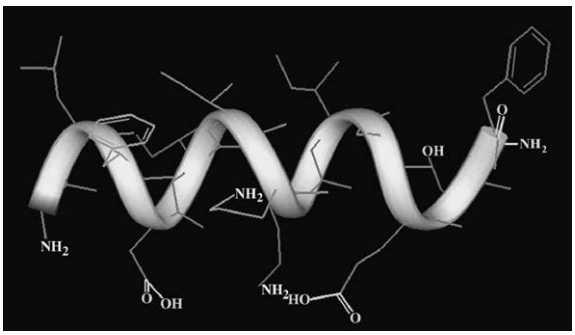

Fig. 6. The solution structure of aurein 1.2 as determined in TFE/water.

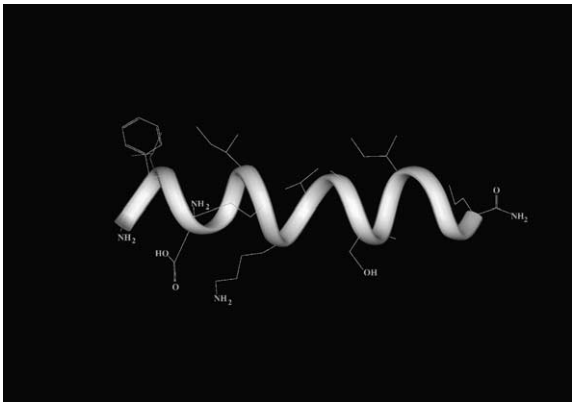

Fig. 7. The solution structure of citropin 1.1 as determined in TFE/water.

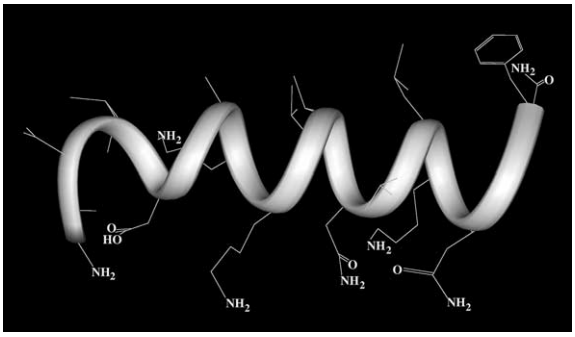

Fig. 8. The solution structure of uperin 3.6 as determined in TFE/water.

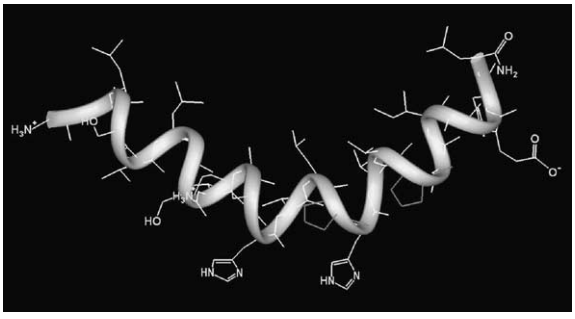

Fig. 9. The solution structure of caerin 1.1 as determined in TFE/water.

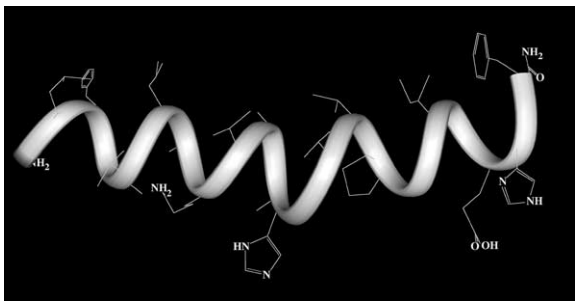

Fig. 10. The solution structure of maculatin 1.1 as determined in TFE/water.

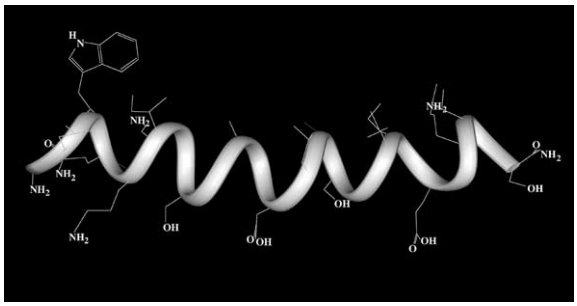

Fig. 11. The solution structure of caerin 4.1 as determined in TFE/water.

3. Antibacterial and anticancer peptides and fungicides

3.1. Antibacterial and anticancer active peptides

The dermal secretions of most Australian frog species contain at least one broad-spectrum antibiotic, and often a number of peptides with varied specificity to allow enhanced protection against a range of bacteria. Biological testing has revealed additional anticancer properties for a number of these peptides, with such coincident activity presumably due to a similar mechanism of action at both bacterial and cancer cells. The peptides are synthesized as a signal-spacer-peptide precursor, in which the signal directs the peptide to the gland before being cleaved by an endoprotease to give the spacer-peptide moiety, which is inactive and as such safe to store. Upon stimulation, the spacer is removed by a second endoprotease and the active peptide delivered onto the skin [38]. In the case of broad-spectrum antibiotics, a third endoprotease degrades and deactivates the peptide after a period of time on the skin (5–30 min depending on the species) [64].

Activity is thought to be mediated by disruption of either cancer or bacterial cell membrane integrity, since the all-D isomers have comparable activity with the natural L-form, ruling out interaction with specific chiral receptors [109]. A number of mechanisms have been proposed to rationalize membrane penetration by the peptide, the simplest of

which include the barrel-stave and carpet mechanisms. In the barrel-stave model, peptides aggregate at the membrane surface in α-helical form, driven by electrostatic attraction between charged residues and ionic sites on the bilayer. Subsequent insertion into the membrane then occurs via formation of a trans-membrane barrel-like pore, in which peptides are oriented perpendicular to the plane of the bilayer [33,72]. A minimum of 20 residues is required to span the membrane entirely although a modified model has been proposed whereby shorter peptides can dimerize end-on to effect complete penetration [2]. In contrast, the carpet mechanism is initiated as peptides assemble in α-helical form with their axis parallel to the membrane, forming a carpet-like monolayer on the surface. Above a critical concentration, transient holes are formed due to strain on the bilayer curvature, and the membrane degrades into micelle-like complexes [73,74]. Regardless of the mode of penetration, ultimately the disruption of normal membrane function results in excessive flux of ions and small molecules across the cytoplasmic membrane bilayer, in turn leading to cell lysis.

Amphibian peptides often have no mammalian counterpart, and display varying degrees of specificity for both bacterial and eukaryotic cells. For example, some exhibit broad-spectrum antibiotic activity while others are active against only selected micro-organisms [35]. In addition, other peptides are lethal to tumorigenic cells at concentrations that are harmless to normal cells [28]. This is thought to be a property of membrane construction, with factors including lipid composition, charge and potential influencing the peptides' binding and permeabilizing ability [52]. The efficacy of amphibian peptides, however, is modulated to a greater extent by structural properties of the peptide itself, with features including degree of helicity, charge state, amphipathicity and hydrophobicity being significant [29,93,108]. It is for this reason that both the primary and secondary structure of the peptides have a direct influence on the observed biological activity.

3.1.1. Short, linear, antibacterial and anticancer bioactive peptides (<20 residues): the aureins citropins, uperins and maculatin 2.1

One group of antibacterial and anticancer peptides that have been identified is a series of short peptides (<20 residues) isolated from various species of the *Litoria* and *Uperoleia* genera. This group contains the aureins 1–3 (from *Litoria aurea* and *Litoria raniformis* [70]), the citropins 1 (from *Litoria citropa* [107]), dahlein 1.2 (from *Litoria dahlii* [106]), maculatin 2.1 (from *Litoria genimaculata* [69]) and uperins 3.5 and 3.6 (from *Uperoleia inundata* [17] and *Uperoleia mjobergii* [16]). The sequences of these antibiotic peptides are listed in alphabetical order in Table 1. Their antibiotic activities together with those of some synthetic modifications of citropin 1.1 are recorded in Table 2 [31]. These peptides have also been tested by the National Cancer Institute (Washington) and have activities (IC_{50}) in the 10^{-5} to 10^{-6} M range against all classes of human cancers tested (viz. leukaemia, lung, colon, CNS, melanoma, ovarian, renal, prostate and breast cancers) [14,31,68].

There are several characteristics common to these peptides. First, they are all cationic, possessing at least two basic residues occurring at positions 7 and 8 and a free amine at the N-terminal end. Citropin 1.1 is a typical example, with sequence GLFDVIKKVASVIGGL-NH_2. With the exception of uperin 3.6 (which has an Arg at position 7) all the other peptides have the pattern of Lys7 Lys8. When one of these basic residues is replaced with Ala, the activity of the peptide is reduced remarkably (see citropin synthetic modification 2) but replacement of Asp4 with Ala (citropin synthetic modification 1) does not have any major influence on the activity. Replacement of both basic residues with Ala at positions 7 and 8 results in a lack of observable activity [31]. All the peptides are post-translationally modified to the C-terminal amide and this is vital for their observed activity. The size of the peptides also influences their activities. Sixteen or seventeen residues is the optimal length for these linear peptides (cf. aurein 2.1, citropin 1.1 and 1.2, and uperin 3.5 and 3.6). As the length decreases (cf. aurein

Table 2
The antibiotic activities of selected aurein (A) citropin (Ci), dahlein (D), maculatin (M) and uperin (U) peptides listed in Table 2

Organism	MIC (μg/ml)											
	A1.2	A2.1	A3.2	Ci1.1	Mod1	Mod2	Ci1.2	Ci1.3	D1.2	M2.1	U3.5	U3.6
Bacillus cereus	100	50		50	25	100	25	25	100	100	25	25
Leuconostoc lactis	12	6	6	6	3	25	3	6	25		3	3
Listeria innocua	100	6	100	25	25		100	25			25	50
Micrococcus luteus	100	100	100	12	12	100	12	12		100	12.5	25
Staphylococcus aureus	50		50	25	25	100	25	25	100	100	50	25
Staphylococcus epidermidis	50	50	50	12	12	100	25	25	100	50	12.5	12.5
Streptococcus uberis	50	100	50	25	25	100	12	25	100	25	12.5	12.5
*Escherichia coli**					100							
*Pasteurella multocida**	100											

*Gram-negative organism. Sequences are listed in Table 1. Antibiotic results are listed as MIC values (μg/ml). Where no figure is indicated, MIC is >100 μg/ml.

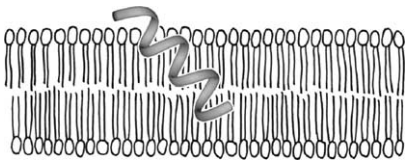

Fig. 12. Model proposed for the insertion of short amphibian peptides in DMPC membranes [49].

1.1, 1.2 and dahlein 1.2) or increases (cf. maculatin 2.1) the activity decreases.

The solution structures of the membrane active aurein 1.2 [70], citropin 1.1 [107] and uperin 3.6 [24] peptides have all been determined and have been shown to adopt well-defined amphipathic α-helical structures. The solution structures as determined in TFE/water are shown in Fig. 6 (aurein 1.2), Fig. 7 (citropin 1.1) and Fig. 8 (uperin 3.6). Solid-state NMR studies using both aurein 1.2 and citropin 1.1 indicate that the peptides first align themselves along the membrane and at higher concentrations tilt into the bilayer at an angle of about 40° (Fig. 12) [49]. This result is consistent with the peptides acting via the carpet mechanism.

3.1.2. Longer, hinged, antibacterial and anticancer peptides: caerins and maculatins

The largest group of antibacterial amphibian peptides isolated to date is that of the caerin peptides, with over 30 identified from more than six Australian frog species of the *Litoria* genus [79,80,84–86,88,89,105]. These can be further divided into four subgroups, with the caerin 1 broad-spectrum peptides the most common. All caerin 1 peptides have similar primary structures based on that of caerin 1.1 (Table 1), and are active mainly against Gram-positive bacteria. Caerins 1.1, 1.3, 1.4, 1.5 and 1.9 are typical of this group, and their activities are shown in Table 3. In addition to their antibiotic activities, these peptides have been tested by the National Cancer Institute (Washington) and have IC_{50} values in the 10^{-5} to 10^{-6} M range against all classes of cancers tested [14].

Until recently, nothing was known of the genes encoding these peptides. However, 3′-RACE analysis of skin mRNA from *L. caerulea* revealed a number of cDNAs encoding for caerin peptides, while also giving an insight into the structure of the pre-pro-peptide precursors [96]. A comparison of the amino acid sequences of the caerin precursors showed the acidic pro-piece is highly conserved, as is the N-terminal signal portion. In addition, these pre-pro-regions of the caerin precursors show significant identity with those from South American hylid frogs [96]. The sequences of the pre-pro-peptide for caerin 1.1 are given below. The C-terminal amide of the native peptide is formed by addition of a glycine residue to the end of the progenitor sequence which is post-translationally modified into an amide group [96].

Signal:	MASLKKSLFLVLLLGFVSVSIC
Spacer:	EEEKRQEDEDEHEEEGESQEEGSEEKR
Native peptide:	GLLSVLGSVAKHVLPHVVPVIAEHL-NH_2

Investigation into the solution structures of caerin 1.1 and related peptides suggests they form two amphipathic helices, separated by a more flexible hinge region initiated by Pro15 (Fig. 9) [106,109]. The hinge assists this peptide to interact effectively with the membrane, as optimal orientation of hydrophilic and hydrophobic zones are facilitated. This is supported by solid-state NMR studies in which it appears that at higher concentrations, the N-terminal helix sits on the surface of the membrane while the C-terminal helix penetrates the bilayer at an angle of approximately 40°, consistent with the carpet mechanism of action (Fig. 13) [49]. The molecules do not penetrate deeply into zwitterionic or positively charged membranes, which may explain why these positively charged peptides preferentially lyse bacterial rather than eukaryotic cells [49].

Synthetic modifications show that the antibacterial activity of caerin 1.1 (GLLGVLVSIAKHVLPHVVPVIAEHL-NH_2) is significantly reduced when Pro15 or Pro19 are replaced with Gly (modification 1, Table 3), and to a further

Table 3
The antibiotic activities of selected caerin (C) and maculatin (M) peptides

Organism	MIC (μg/ml)								
	C1.1	Mod 1	Mod 2	C1.3	C1.4	C1.5	C1.9	M1.1	M1.4
Bacillus cereus	50	50		50	50	50	100	25	100
Leuconostoc lactis	1.5	12	25	3	12	3	12	3	6
Listeria innocua	25	50		50	100	50	50	100	100
Micrococcus luteus	12	12		25	0.4	12	50	12	50
Staphylococcus aureus	3	25–50		6–12	100	25	12	6	50
Staphylococcus epidermidis	12	100		12	25	25	25	12	50
Streptococcus uberis	12	12		25	100	50	50	3	50
*Escherichia coli**		50			50				
*Pasteurella multocida**	25	100		50	25	25	50	50	

Sequences of the peptides together with those of the two synthetic modifications of caerin 1.1 are listed in Table 1. *Gram-negative organism. Antibiotic results are listed as MIC values (μg/ml). Where no figure is indicated, MIC is >100 μg/ml.

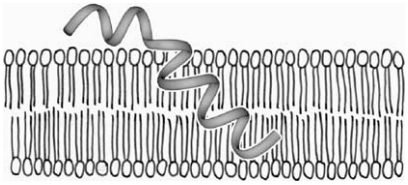

Fig. 13. Model proposed for the insertion of hinged amphibian peptides in DMPC membranes [49].

extent with Ala (modification 2, Table 3). This is thought to be a result of reduced conformational freedom, and demonstrates the importance of the flexible hinge in such peptides [59]. Since the positive charge of Lys11 may be involved in the interaction with anionic phospholipids in the membrane, it is not surprising that modification of this residue would affect the antibiotic activity. Substitution at this site with Gln gives the uncharged, naturally occurring caerin 1.3, which possesses markedly less activity than that of caerin 1.1.

The caerin 1 peptides are generally inactivated by enzymic cleavage of a number of residues from the N-terminus, giving degradation products such as caerin 1.1.1 and 1.1.2 (see Table 1). In addition, caerins 1.1.5 and 1.1.3 (Table 1) are made up of the residues from the first and second helices of caerin 1.1 respectively, and are found to be completely inactive [105]. Thus, it would seem the flexible hinge region and both helices are necessary for antibacterial activity. It was, therefore, surprising to find maculatin 1.1 (GLFGVLAKVAAHVVPAIAEHF-NH_2) from the skin secretion of *Litoria genimaculata* [69]. This molecule shows similar antibiotic activity compared with caerin 1.1 (Table 3), yet lacks four residues including Pro15. The solution structure of maculatin 1.1 has also been investigated, and forms a helix-bend-helix structure similar to that of caerin 1.1 in membrane-like media (Fig. 10) [23]. This molecule also displays similar interaction with model membranes in solid-state NMR studies [49]. In addition to maculatin 1.1, a number of similar peptides (maculatins 1.3 and 1.4 (Table 1)) have subsequently been isolated from *L. eucnemis* [19].

The caerin 2 peptides are the only caerin molecules to contain C-terminal CO_2H groups (Table 1), generally regarded as an indication of poor antibiotic activity. In fact, they show minimal activity against a range of bacteria (Table 4), and essentially no anti-cancer activity against the cell lines tested. However, the caerin 2 peptides inhibit the operation of nNOS (see Section 4.2.). The caerins 3 and 4 are related in that they all contain Trp3 and two or three Lys residues (Table 1). In addition, the caerins 3 and 4 are generally narrow spectrum antibiotics, commonly active only against a few of the species tested. For example, caerin 3.1 shows pronounced activity against *Micrococcus luteus*, while caerin 4.1 is active against *Pasteurella multocida* and *Escherichia coli* (Table 4). The solution structure of caerin 4.1 has been determined and shown to be a linear α-helix with well-defined hydrophobic and hydrophilic domains

Table 4
The antibiotic activities of selected caerin (C) 2–4 peptides

Organism	MIC (μg/ml)					
	C2.1	C2.2	C3.1	C3.2	C4.1	C4.3
Bacillus cereus						
Leuconostoc lactis						
Listeria innocua						
Micrococcus luteus		50	<0.4	3	12	25
Staphylococcus aureus						
Staphylococcus epidermidis						
Streptococcus uberis						
*Escherichia coli**					25	50
*Pasteurella multocida**	25	25				

*Gram-negative organism. Sequences are listed in Table 1. Antibiotic results are listed as MIC values (μg/ml). Where no figure is indicated, MIC is >100 μg/ml.

(Fig. 11) [22]. While the solution structures of members of the caerin 2 and 3 families have not yet been investigated, Edmundson projections suggest amphipathicity is not facilitated in an α-helical form, possibly explaining the poor antibacterial efficacy of these molecules. There are a number of peptides related to caerin 3 from other species of the genus *Litoria*; for example aurein 4.1 (Table 1, from *L. aurea* and *L. raniformis* [70]), dahlein 4.1 (Table 1, from *Litoria dahlii* [106]) and maculatin 3.1 (Table 1, from *Litoria genimaculata* [69]). These show no antibiotic activity and their role in the amphibian integument is not known at this time.

3.2. Antifungal peptides

Amphibians are prone to infection by fungi; the worst being the chytrid fungus (*Batrachochytrium dendrobatis*) which is affecting anuran populations worldwide [55,77]. It has already been shown that antibiotic peptides of some frogs from the northern hemisphere are active against the chytrid fungus (e.g. the temporins from *Rana* species and the magainins from *Xenopus laevis* [66]), and it thus seems likely that the membrane-active antimicrobial peptides of Australian anurans should similarly destroy the chytrid fungus. There is some anecdotal evidence for this in that frogs without the protection of skin antimicrobial peptides (e.g. species of the genus *Limnodynastes*) succumb more readily to the chytrid fungus than species from other genera that produce antimicrobial peptides. It has been shown recently that many membrane-active antibiotic peptides from Australian anurans kill the chytrid fungus, generally at concentrations in the micromolar range [65]: this includes the caerins 1, citropins 1, uperins, aureins, dahleins and so on. However, the situation is complex since species which have this apparent antifungal protection still succumb to the chytrid fungus. For example, those *Litoria* species that produce the caerin 1 antimicrobial (and antifungal) peptides may also be killed by the chytrid fungus [77]. The question is why do anurans that, in principle, have (apparently) adequate protection

against the chytrid fungus, still succumb to the fungus? Is the explanation the simple one that the zoospores of the fungus attach mainly to the underneath of the animal and this area is not effectively reached by the skin secretion from the back of the animal? Alternatively, perhaps the animal does not realize that the fungus is lethal, and does not engage its chemical arsenal. Or perhaps the fungus itself has an effective defence against the active peptides; for example a protease that cleaves and deactivates the antifungal peptide. The explanation for this strange phenomenon is not yet known.

4. Neuropeptides

4.1. Caeruleins and uperoleins

The majority of frogs of the genus *Litoria* and toadlets of the *Uperoleia* genus contain at least one neuropeptide of the caerulein and uperolein groups, respectively. The neuropeptide is often the major host-defence peptide in the glandular secretion. Such neuropeptides are both an integral part of the defence system, and also assist with the regulation of dermal physiological action [8,34,45]. The sequences of the caerulein and of uperolein and uperin 1.1 neuropeptides isolated from Australian anurans are listed in Table 1.

Caerulein, pEQDY(SO_3)TGWMDF-NH_2, (which we now call caerulein 1.1 to distinguish it from other caeruleins) is a common neuropeptide found in many frog species worldwide [34]. Caerulein 1.1 exhibits a spectrum of activity similar to that of the mammalian intestinal peptide hormones gastrin and cholecystokin (CCK): it contracts smooth muscle at better than nanomolar concentration, enhances blood circulation, modifies satiety, sedation and thermoregulation, is an analgesic several thousand times more potent than morphine, and has been used clinically during gall bladder operations [34].

The levels of caerulein 1.1, although identical for both male and female *L. splendida*, vary seasonally [102]. These seasonal changes may be involved in thermoregulation. During the spring to autumn period (in the southern hemisphere), which corresponds to the breeding period of *L. splendida*, caerulein 1.1 is the only smooth-muscle active neuropeptide present. During the winter period (June to August) the composition of the glandular skin secretion changes. There is a decrease in the concentration of caerulein 1.1, balanced by the formation of desulfated caerulein 1.1 (pEQDYTGWMDF-NH_2), and caerulein 1.2 [pEQDY(SO_3)TGWFDF-NH_2]. Both caerulein 1.1 and 1.2 show similar smooth muscle activity, but whereas caerulein 1.1 acts at a CCK site directly on smooth muscle, it appears that caerulein 1.2 elicits acetylcholine release, which initiates the smooth muscle activity. The Australian Blue Mountains Tree Frog (*Litoria citropa*) produces a variety of caerulein peptides (see Table 1) [98]: the reason for the presence of so many neuropeptides of the caerulein family in this species is not known at this time.

The hypertensive peptide uperolein [pEPDPNAFYGLM-NH_2] was first isolated from toadlets of the *Uperoleia* genus by Erspamer and colleagues [1]: uperolein is a member of the tackykinin family, exhibiting potent vasodilator and hypertensive action, together with intense spasmogenic activity of smooth muscle [34]. Ala2 uperolein (uperin 1.1, (pEADPNAFYGLM-NH_2) (from *Uperoleia inundata* [1,17])) has similar activity, exhibiting smooth muscle contraction of guinea pig ileum at 0.4 ng/kg (of body weight) and reduction of rabbit blood pressure at 5 ng/kg [17].

4.2. Nitric oxide synthase active peptides

The seemingly ubiquitous involvement of nitric oxide (NO) in biological systems has now resulted in an explosion of interest in the field. At high concentrations, NO behaves as a defensive cytotoxin against tumor cells and pathogens as the immune system utilizes the toxic properties of NO to kill or inhibit the growth of invading organisms. At low concentrations it serves as a cell-to-cell signalling agent, exerting its biological effects by reacting either directly or through other reactive nitrogen intermediates with a variety of targets. The diversity of this potential interaction is reflected in the large number of different systems that utilize NO as a mediator, including regulation of the circulatory and central nervous system, neurotransmission in contractile and sensory tissues, learning, and memory formation [10,62,90].

NO is notable among biological signals for its rapid diffusion, ability to permeate cell membranes and intrinsic instability, properties that eliminate the need for extracellular NO receptors or targeted NO degradation. Therefore, NO differs from most other neurotransmitters and hormones in that it is not regulated by storage, release or degradation, but rather solely by synthesis [62]. Nearly every cell type studied thus far has demonstrated the ability to synthesize NO by one of the three distinct isoforms of the nitric oxide synthase (NOS) enzymes isolated to date [10].

Nitric oxide synthases, expressed as neuronal NOS (nNOS, also called NOS1), inducible NOS (iNOS or NOS2), and endothelial NOS (eNOS or NOS3) isozymes, oxidize L-arginine (L-Arg) to NO and citrulline, thereby controlling NO distribution and concentration. The names reflect characteristics of the activity or the original tissues in which the enzymes were first described, but it is now known that each of these isoforms is expressed in a variety of tissues and cell types. All three isozymes are homodimers with subunits of 130–160 kDa. They differ in size, amino acid sequence (50–60% identity between any two isozymes), tissue distribution, transcriptional regulation, and activation by intracellular calcium, but they share an overall three-component construction [27], namely:

(i) An N-terminal catalytic oxygenase domain that binds heme (iron protoporphyrin IX), tetrahydrobiopterin (BH_4), and the substrate L-Arg;

(ii) A C-terminal reductase domain that binds flavin mononucleotide (FMN), flavin adenine dinucleotide (FAD), and NADPH; and
(iii) An intervening calmodulin-binding region that regulates electronic communication between the oxygenase and reductase domains. Occupation of this site facilitates electron transfer from the cofactors in the reductase domain to heme during NO production.

Calmodulin (CaM), a "dumbbell" shaped 148 residue protein, is required for activation of NOS. Calmodulin acts as an electron shuttle and is the cell's main intracellular calcium transporter. It appears that CaM is required to alter the conformation of the reductase domain, increase the rate of electron transfer into the flavins and increase the rate at which the reductase can transfer electrons to acceptors such as the active heme site [90].

Once NOS has been synthesized, its activity can then be regulated by post-translational mechanisms, and it is at this level that NO synthesis by nNOS and eNOS can be tightly controlled. At the normal resting level of Ca^{2+} in the cell, both nNOS and eNOS are inactive. However, when Ca^{2+} levels increase, the binding of calmodulin to these isoforms is triggered, resulting in the stimulation of catalytic activity [46]. The importance of this mechanism is that it allows NO synthesis to be coupled with known physiological stimuli such as neural depolarisation, shear stress, and second messenger systems such as cGMP which lead to rises in Ca^{2+} concentrations. In contrast, calmodulin is tightly bound to iNOS irrespective of the Ca^{2+} concentration, hence the regulation of iNOS occurs generally at the level of transcription.

The majority of frogs of the genus *Litoria* that we have studied contain at least one major peptide in their glandular secretions that inhibits the formation of NO by nNOS. These positively charged peptides fall into one of three categories: (a) peptides of the citropin 1 type, (b) caerin 1 peptides, particularly those with phenylalanine residues at position 3, and (c) the frenatin/splendipherin group of peptides. The most active of these are listed in Table 5 [31,32].

These peptides interfere with communication between Ca^{2+}CaM and nNOS. This is confirmed experimentally since: (i) addition of these peptides to nNOS during in vitro testing results in an inhibition of nNOS and decrease of NO production. Subsequent addition of CaM to these test solutions results in a partial recovery of nNOS activity, (ii) these peptides also inhibit the operation of calcineurin, another enzyme which requires Ca^{2+}CaM as a regulatory protein [32], and (iii) a preliminary 2D NMR study indicates that splendipherin (Table 5) forms a complex with CaM [3], as evidenced by chemical shift changes at significant residues [41].

That these nNOS active peptides interact with Ca^{2+}CaM rather than with the affected enzymes directly leads to the observation that any enzyme requiring Ca^{2+}CaM for function is a potential target of these host-defence peptides. Other examples of enzymes requiring Ca^{2+}CaM include myosin light chain kinase, phosphorylase kinase and adenylate cyclase [44]. Ca^{2+}CaM is also involved in regulation of the eukaryotic cytoskeleton [44] and is required by some protozoa for ciliate movement [57].

Although this means that peptides binding Ca^{2+}CaM probably do not act specifically on any one target enzyme, the probable advantage to the frog is the ability to interfere with many important cellular functions at once, causing maximum disruption to any attacker.

Table 5
nNOS inhibition activities of selected amphibian peptides

Name	Sequence	IC_{50} (μM)	Charge	Species
Inhibitor Group A				
Lesueurin	GLLDILKKVGKVA-NH_2	16.2	+3	a
Aurein 1.1	GLFDIIKKIAESI-NH_2	33.9	+1	b
Citropin 1.1	GLFDVIKKVASVIGGL-NH_2	8.2	+2	c
Aurein 2.2	GLFDIVKKVVGALGSL-NH_2	4.3	+2	b
Aurein 2.3	GFLDIVKKVVGIAGSL-NH_2	1.8	+2	b
Aurein 2.4	GLFDIVKKVVGTLAGL-NH_2	2.1	+2	b
Inhibitor Group B				
Dahlein 5.1	GLLGSIGNAIGAFIANKLKP-OH	3.2	+3	d
Frenatin 3	GLMSVLGHAVGNVLGGLFKPKS-OH	6.8	+3	e
Splendipherin	GLVSSIGKALGGLLADVVKSKGQPA-OH	8.5	+3	f
Inhibitor Group C				
Caerin 1.1	GLLGVLVSIAKHVLPHVVPVIAEHL-NH_2	36.6	+1	f
Caerin 1.10	GLLSVLGSVAKHVLPHVVPVIAEKL-NH_2	41	+2	g
Caerin 1.6	GLFSVLGAVAKHVLPHVVPVIAEKL-NH_2	8.5	+2	g
Caerin 1.8	GLFKVLGSVAKHLLPHVVPVIAEKL-NH_2	1.7	+3	g
Caerin 1.9	GLFGVLGSIAKHVLPHVVPVIAEKL-NH_2	6.2	+2	g

(a) *L. lesueuri* [32]; (b) *L. aurea* [70]; (c) *L. citropa*[100]; (d) *L. dahlii* [106]; (e) *L. infrafrenata* [15]; (f) *L. splendida* [99]; (g) *L. chloris* [15].

4.3. Cys containing neuropeptides from the genus Crinia

Although peptides containing Cys residues and disulfide bridges have been isolated from European and Indian frogs of the *Rana* genus [34,45,71,75], Cys containing peptides have only recently been discovered in Australian frogs. *Crinia signifera* has a number of antibiotic and nNOS active peptides in its glandular secretion, but no neuropeptides analogous to the caeruleins or uperoleins. Instead, the major component of the secretion, now called signiferin 1, has the structure shown below [51]. The nomenclature *C is used to indicate the presence of a disulfide bridge.

Signiferin 1	RL*CIPYIIP*C-OH
Tigerinin 2	RV*CFAIPLPI*CH-NH_2
Vasopressin	*CYFQN*CPRG-NH_2

The signiferin 1 sequence has some resemblance to the antibiotic tigerinins [71] (tigerinin 2 has the sequence shown above) and the human pituitary hormones oxytocin and vasopressin (vasopressin sequence shown above). Unlike tigerinin 2, signiferin 1 has no antibiotic activity: in preliminary experiments it has been shown to contract smooth muscle at the 10^{-9} M concentration [50].

4.4. Tryptophyllins

The Red Tree Frog *Litoria rubella* (Fig. 14) [5] is widespread throughout central and northern Australia and has evolved into a number of specific populations within this area [81,83]. It is a remarkable frog that can adapt to a range of climates from desert conditions to those of wet rain forests. There is a related frog called *Litoria electrica* found only in northern Australia in a specific region just below the Gulf of Carpentaria [101]. Both of these frogs produce abundant glandular secretions on the skin, but the secretions contain neither neuropeptides like caerulein nor antibacterial peptides. How then do these animals protect themselves from predators? The granular glands produce large amounts of small peptides related to the tryptophyllins, first discovered in the South American hylid frog *Phyllomedusa rohdei* by Erspamer et al. [36,39,54]. The tryptophyllin peptides from the two Australian frogs are listed together in Table 1.

Fig. 14. *Litoria rubella*.

Erspamer has found that neither his nor our tryptophyllins show significant smooth muscle activity (no effect below a concentration of 10^{-6} M), and we have shown that neither tryptophyllins L 1.2 (FPWL-NH_2), 1.3 (pEFPWL-NH_2) nor 3.1 (FPWP-NH_2) inhibit neuronal nitric oxide synthase [32]. One of Erspamer's tryptophyllins (FPPWM-NH_2) induces sedation and behavioral sleep in birds, and is also immunoreactive to a set of cells in the rat adenohypophysis [63]. Recently, the precursor cDNA for a novel tryptophyllin (LPHAWVP-NH_2) from the Mexican leaf frog (*Pachymedusa dacnicolor*) has been cloned and shown to contract smooth muscle at nanomolar concentrations [21]. It is also of interest that the tryptophyllin peptides show some sequence similarity to the human brain endomorphins (e.g. YPWF-NH_2 and YPWG-NH_2) that have a very high affinity for the γ-receptor [112]). At this time, the role of the tryptophyllins shown in Table 1 is still undetermined.

5. Amphibian pheromones

Pheromones are substances that are released to cause a behavioral response in a conspecific, and are commonly involved in mating and courtship. Although alarm responses had been characterized in *Bufo bufo* tadpoles upon exposure to crushed tadpole as early as 1949 [12], the first pheromone identified from a vertebrate was only discovered quite recently, in 1995 [43]. This female-attractant sex pheromone came from the Japanese fire-bellied newt, *Cynops pyrrhogaster*. Sodefrin, a 10-residue peptide was isolated in 1995 and was named for the Japanese word "to solicit" [43]. During species specificity testing, it was discovered that another newt species, *C. ensicauda*, also had a female attractant aquatic sex pheromone. This 10-residue peptide differs from sodefrin at positions 3 and 8, was isolated in 2000 and named silefrin [111].

Sodefrin	SIPSKDALLK-OH
Silefrin	SILSKDAQLK-OH

These peptide hormones are secreted from the abdominal glands through the cloacae of the animals and are both species-specific female attractants.

A 22-kDa proteinaceous courtship pheromone has also been discovered in a terrestrial salamander, *Plethodon jordani*. This protein hormone is deposited directly onto the skin of the female by the male from his mental glands, located under the chin. This pheromone is thought to shorten the courtship process [67].

The first anuran sex pheromone was isolated from *L. splendida* in 1997. *L. splendida*, also known as the Magnificent Tree Frog, was first identified in 1977 by Tyler et al. [94]. Monthly secretions were collected from male and female specimens over a period of three years using the surface electrical stimulation method [97]. The chromatograms of these secretions indicated a small component present in the male secretions only. Comparison of the

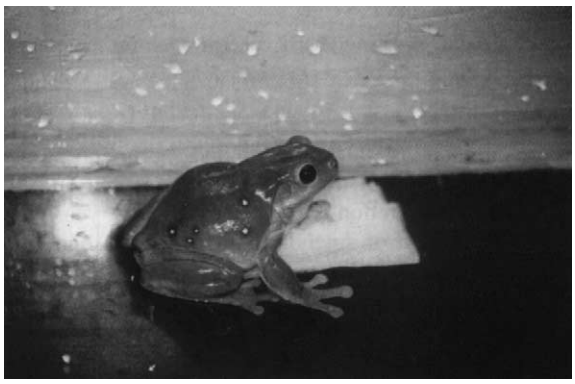

Fig. 15. Female *Litoria splendida* sitting on a pheromone sample during behavioral testing.

chromatograms from the three year period show that this compound, a 25-residue peptide, now named splendipherin, is produced in the highest levels during the mating season. Splendipherin GLVSSIGKALGGLLADVVKSKGQPA-OH

The peptide levels peak in February/March, at this point it constitutes up to 1% of the total secretion material, dropping to as low as 0.1% from June through to November, and was therefore investigated for a possible role in the breeding cycle of this species.

Behavioral tests were conducted in a 2-m glass tank containing a 2-cm depth of water. Females of the species exposed to the hormone at a concentration of ~10 pM, were attracted to the source with remarkably rapid response times [99]. Recognition of the peptide was apparent within twenty seconds of its introduction into the tank, and within an average of 6 min, female frogs would find and sit on the source of the pheromone (Fig. 15) [99] until physically removed. The tests were repeated with male *L. splendida* specimens and with *L. caerulea*, a related species of frog and showed that the pheromone is a species-specific female attractant with no effect on males or on other species.

As the peptide was not being moved toward the female by agitation of the water during the behavioral tests, as is the case with the newt hormones sodefrin and silefrin [43,111], nor being directly applied, as with the terrestrial salamander [67], we are interested in how the peptide moves through the aquatic environment. The structure of splendipherin has been determined using NMR and simulated annealing calculations; this structure is currently being employed in studies to determine the mode of action of splendipherin at the water surface [4].

6. Miscellaneous peptides

6.1. Antimalarial peptides

Anurans breed in aquatic environments that abound with insects, including mosquitoes. Even though malaria is rare in Australia, it is known that some European ranid frogs are prone to infestation by malaria parasites [76]. Perhaps anurans have evolved chemical protection against insects? Gas chromatographic separation of those components of the glandular secretion of *L. caerulea*, which are soluble in organic solvents, with mosquitoes enclosed in a container through which the effluent of the gas chromatogram passed, showed the presence of several volatile mosquito repellants. It was not possible to quantitatively reproduce the results of this experiment; the volatile components were present in trace amounts only, and some components were variable, differing from day to day. One of the insecticides was shown by GC/MS to be a methyl acetophenone (probably the *ortho*-isomer) [78].

Certain amphibian peptides kill the malaria parasite (*P. falciparum*). For example, the caerin 1 peptides are active at micromolar concentrations; caerin 1.8 (see Table 1 for the sequence) is the most potent. We are currently investigating the mode of action of the caerins 1 and other antimalarial peptides [92].

6.2. Inactive peptides

Marsh frogs of the genus *Limnodynastes* produce copious secretions from their dorsal granular glands, and in some cases from tibial glands on their legs. Only minute quantities of peptides are found in these secretions. We have named these peptides dynastins, and their sequences are listed in Table 1. An example is dynastin 1 (GLVSNLGI-NH_2, from *Limnodynastes interioris* [60]). The dynastins are all small anionic peptides, contain C-terminal CO_2H residues, and they exhibit no bio-activity in any of the test regimes that we now use. It is clear that this genus of frog has a very different defence mechanism to that of other animals that we have studied, and we do not know what that is.

Most of the tree frogs of the genus *Litoria* that we have studied produce inactive caeridin (e.g. caeridin 1, (GLLDGLLGTGL-NH_2) from various *Litoria* species [1]), frenatin (e.g. frenatin 1, (GLLDALSGILGL-NH_2) from *Litoria infrafrenata* [104]), or rubellidin (e.g. rubellidin 4.1 (GLGDILGLLGL-NH_2) from *L. rubella* [81,83]) peptides together with active peptides in their glandular secretions. These inactive peptides (see above and Table 1) show some structural resemblance to the dynastin peptides, but unlike the dynastins, they are all post translationally modified (C-terminal $CONH_2$). Their role in the amphibian integument is unknown.

Finally, there are peptides isolated from *L. electrica* and *Litoria rothii* that are unlike any other peptides obtained from Australian anurans. These include the anionic peptides electrin 2.1 (NEEEKVKWEPDVP-NH_2) from *L. electrica* [101] and the rotheins 2 and 3 (Table 1; e.g. rothein 2.1 (AGGLDDLLEPVLNSADNLVHGL-NH_2) from *L. rothii* [106]), which have shown no activity in any of our standard testing programs. They bear some resemblance to spacer peptides (e.g. the spacer peptides of the pre-pro-caerins

1 (see Section 3.3)) but most of these peptides from *L. electrica* and *L. rothii* are post translationally modified, containing C-terminal $CONH_2$ functionality.

7. Evolutionary implications

The recognition of taxa such as genera, species and subspecies was originally based entirely upon morphological characteristics. In the 1950s behavioral characteristics such as advertisement calls and other attributes were included in the definitions of taxa. With the development of biochemical techniques a new dimension was added [40].

A variety of tissue secretions has been used to determine the evolutionary relationships of frogs: e.g. *Bufo* parotoid gland toxins [47], skin alkaloids [56] and globin polypeptides [30].

With the development of a non-invasive technique to 'milk' dermal secretions from frog skin [95] it has become possible to study variations in individuals within species in Australia that have a broad geographic range, so demonstrating a divergence not suspected previously. An example is the Red Tree Frog, *L. rubella* (see Fig. 14), which occupies much of the northern half of the Australian continent as shown in Fig. 16. Specimens of *L. rubella* were examined from 15 localities. The peptide profiles differed in the majority of localities (see e.g. Fig. 17), the exceptions being from three adjacent localities in South Australia [81,83]. There is every indication that at least six populations of '*L. rubella*' can be recognized. What is required is a comparable study of pre-mating isolating mechanisms of *L. rubella* at these localities, to determine whether the populations have evolved isolating mechanisms separating them into distinct species. Preliminary data [48] of *L. rubella* taken at localities along the Stuart Highway from Marree (in South Australia) to Darwin (in the Northern Territory) (see Fig. 16), a distance of 2200 km, suggest

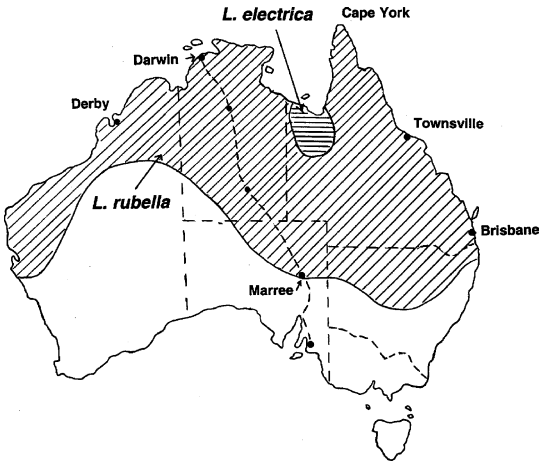

Fig. 16. Geographical distribution of *Litoria rubella* and *Litoria electrica* in Australia: (---) State boundaries; (---·---) Stuart Highway.

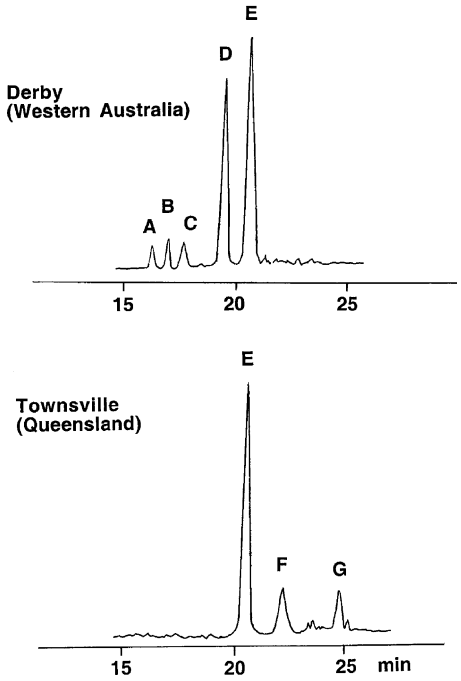

Fig. 17. HPLC peptide profiles of *Litoria rubella* [81,83] from Derby (Western Australia), and Townsville (Queensland). Peptides are as follows; (A) IEFFA-OH; (B) IEFFT-NH_2; (C) VDFFA-OH; (D) pEIPWFHR-NH_2; (E) FPWL-NH_2; (F) FPWP-NH_2; (G) FPFPWL-NH_2. For further information, including nomenclature of tryptophyllins, see Section 4.

that pre-mating data are consistent with peptide-profiling information.

To date, the only authenticated separation of a population from *L. rubella* is the recognition of *L. electrica* for individuals at localities south of the Gulf of Carpentaria in Queensland [42] (see Fig. 16). Peptide studies confirm the distinctness of this population as a separate species [101]. The peptide profile of *L. electrica* shows two tryptophyllins as the major components (the same as components E and F in Fig. 17), but it also contains six other peptides not produced by *L. rubella*. These data support the classification of *L. electrica* as a species separate from *L. rubella*, but also indicate the close relationship between the two species.

Of particular interest are the variations in the peptide profiles of *L. rubella* from the south (Brisbane) to the north (Cape York) of the Queensland eastern seaboard, a distance of 2300 km [82]. Fraction F (see Fig. 17) is minor compared with E in the south, but increases regularly to constitute the largest fraction in the north. Clinal variations in peptide profiles of this type can be interpreted as a progressive stage in evolution. Essentially, peptide studies provide an indication of genetic change.

The time scale of evolutionary change in peptide profiles may be short. Studies on the Green Tree Frog, *L. caerulea* [87] indicate significant differences in the peptide profiles of animals collected from different parts of Australia. There appear to be two major populations of *L. caerulea*, one in

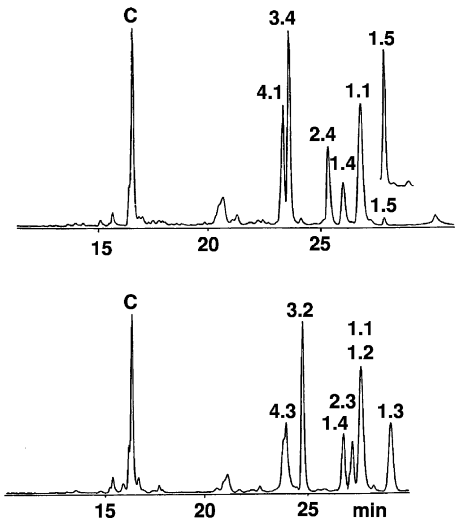

Fig. 18. HPLC peptide profiles of *Litoria caerulea* from (A) Proserpine (Queensland) and (B) Borroloola (Northern Territory). Peaks identified by numbers are caerin peptides: these numbers correspond to the sequences listed in Table 1. The peak designated by C is the neuropeptide caerulein 1.1 [pEQDY(SO_3)TGWMDF-NH_2].

the Northern Territory, the second along the Queensland eastern coastal region. The HPLC peptide profiles of animals obtained from these two areas are shown in Fig. 18. Whether these changes are predator or climate driven are not known at this time. Of particular interest are the differences in peptide profiles that have been noted between individuals at Darwin in the Northern Territory from those at Melville Island (off the coast from Darwin) [87]. These populations have been separated by the ocean for only 10,000 years.

We conclude that dermal peptide profiles of frogs provide a labile index of relationships that should be included in any evaluation of evolution of closely related species. The only proviso here is that the neuropeptide content of the peptide profile of an anuran may vary seasonally and this must be taken into account, e.g. the caerulein 1.1/1.2 variation of *L. splendida* (see Sections 4 and 5and [99]).

8. Conclusions

Australian amphibians have some of the most diverse yet simple host-defence peptides to be reported in the Animal Kingdom, ranging from neuropeptides with a wide range of activities to antibiotic, antiviral, antifungal, anticancer and antimalarial peptides. The range of 3D structures for the amphipathic antibiotic peptides (from simple amphipathic α helices to α helices with a central hinge) is spectacular, taking into account that most of these peptides have much the same spectrum of antibacterial activities. The modes of action of some of these active peptides are known (e.g. the smooth muscle activity of the caeruleins, and the membrane destroying power of the antimicrobial peptides), while others are currently under investigation (e.g. how structurally diverse peptides such as the frenatins 3, caerin 1 and citropin 1 peptides all inhibit the formation of NO from nNOS, and how the caerins 1 destroy the malaria parasite). The research that we carry out is primarily curiosity driven: we are fascinated by the host-defence chemistry of these primitive creatures. The impressive range of bio-activity of these peptides indicates that consideration of certain anuran peptides for pharmaceutical, clinical and/or agricultural use should be explored.

Acknowledgments

We thank the Australian Research Council, the South Australian Anticancer Foundation, and The University of Adelaide for providing the funding for this research.

References

[1] Anastasi A, Erspamer V, Endean R. Isolation and amino acid sequence of caerulein, the active decapeptide of the skin of *Hyla caerulea*. Arch Biochem Biophys 1968;125:57–68.
[2] Andreu D, Ubach J, Boman A, Wahlin B, Wade D, Merrifield RB, et al. Shortened cecropin A-melittin hybrids—significant size reduction retains potent antibiotic activity. FEBS Lett 1992; 296:190–4.
[3] Apponyi MA, Booker GW, Bowie JH. Unpublished observations.
[4] Apponyi MA, Bowie JH. Unpublished observations.
[5] Barker J, Grigg GC, Tyler MJ. A field guide to Australian frogs. NSW: Surrey Beatty and Sons; 1995.
[6] Barra D, Simmaco M. Amphibian skin: a promising resource for antimicrobial peptides. TIBTECH 1995;13:205–9.
[7] Barsukov IL, Lian L. Structure determination from NMR data. I. Analysis of NMR data. In: Roberts, GCK, editor. NMR of macromolecules: a practical approach. New York: Oxford University Press; 1993. p. 315–57.
[8] Bevins CL, Zasloff M. Peptides from frog skin. Annu Rev Biochem 1990;59:395–414.
[9] Biemann K, Martin SA. Mass spectrometric determination of the amino acid sequence of peptides and proteins. Mass Spectrom Rev 1987;6:1–76.
[10] Billiar TR. Nitric oxide, novel biology with clinical relevance. Ann Surg 1995;221:339–49.
[11] Bilusich D, Brinkworth CS, McAnoy AM, Bowie JH. The fragmentation of (M-H)-anions derived from underivatized peptides. The side chain loss of H2S from Cys. A joint experimental and theoretical study. Rapid Commun Mass Spectrom 2003;17:2488–94.
[12] Birch MC. Pheromones 32. Amsterdam: North-Holland; 1974.
[13] Bowie JH, Brinkworth CS, Dua S. Collision-induced fragmentations of the (M-H)-parent anions of underivatized peptides: an aid to structure determination and some unusual negative ion cleavages. Mass Spectrom Rev 2002;21:87–107.
[14] Bowie JH, Chia BCS, Tyler MJ. Host defence peptides from the skin glands of Australian amphibians: a powerful chemical arsenal. Pharmacol News 1998;5:16–21.
[15] Bowie JH, Wegener KL, Chia BCS, Wabnitz PA, Carver JA, Tyler MJ, et al. Host defence antibacterial peptides from skin secretions of Australian amphibians. The relationship between structure and activity. Protein Peptide Lett 1999;6:259–70.
[16] Bradford AM, Bowie JH, Tyler MJ, Wallace JC. New antibiotic uperin peptides from the dorsal glands of the Australian toadlet *Uperoleia mjobergii*. Aust J Chem 1996;49:1325–31.

[17] Bradford AM, Raftery MJ, Bowie JH, Tyler MJ, Wallace JC, Adams GW, et al. Novel uperin peptides from the dorsal glands of the Australian Flood Plain Toadlet *Uperoleia inundata*. Aust J Chem 1996;49:475–84.
[18] Bradford AM, Raftery MJ, Bowie JH, Wallace JC, Tyler MJ. Peptides from Australian frogs—the structures of the dynastins from *Limnodynastes salmini* and fletcherin from *Limnodynastes fletcheri*. Aust J Chem 1993;46:1235–44.
[19] Brinkworth CS, Bowie JH, Tyler MJ, Wallace JC. A comparison of the host defence skin peptides of the New Guinea Tree frog (*Litoria genimaculata*) and the Fringed Tree frog (*Litoria eucnemis*). The link between the caerin and the maculatin antimicrobial peptides. Aust J Chem 2002;55:605–10.
[20] Brinkworth CS, Dua S, McAnoy AM, Bowie JH. Negative ion fragmentations of deprotonated peptides: backbone cleavages directed through both Asp and Glu. Rapid Commun Mass Spectrom 2001;15:1965–73.
[21] Chen T, Orr DF, O'Rourke M, McLynn C, Biourson AJ, McLean S, et al. *Pachymedusa dacnocolor* tryptophyllin-1; structural characterization, pharmacological activity and cloning of precursor cDNA. Regulatory peptides, in press.
[22] Chia BCS, Carver JA, Lindner RA, Bowie JH, Wong H, Lie W. Caerin 4.1, an antibiotic peptide from the Australian tree frog *Litoria caerulea*. The NMR-derived solution structure. Aust J Chem 2000;53:257–65.
[23] Chia BCS, Carver JA, Mulhern TD, Bowie JH. Maculatin 1.1, an antimicrobial peptide from the Australian tree frog, *Litoria genimaculata*. Solution structure and biological activity. Eur J Biochem 2000;267:1894–908.
[24] Chia BCS, Carver JA, Mulhern TD, Bowie JH. The solution structure of uperin 3.6, an antibiotic peptide from the granular dorsal glands of the Australian toadlet, *Uperoleia mjobergii*. J Peptide Res 1999;54:137–45.
[25] Clark DP, Durell S, Maloy WL, Zasloff M. Ranalexin—a novel antimicrobial peptide from bullfrog (*Rana catesbeiana*) skin, structurally related to the bacterial antibiotic, polymyxin. J Biol Chem 1994;269:10849–55.
[26] Clore GM, Gronenborn AM. Determination of three-dimensional structures of proteins and nucleic acids in solution by nuclear magnetic resonance spectroscopy. Crit Rev Biochem Mol Biol 1989;24:479–564.
[27] Crane BR, Arvai AS, Gachhui R, Wu C, Ghosh DK, Getzoff ED, et al. The structure of nitric oxide synthase oxygenase domain and inhibitor complexes. Science 1997;278:425–31.
[28] Cruciani RA, Barker JL, Zasloff M, Chen H, Colamonici O. Antibiotic magainins exert cytolytic activity against transformed cell lines through channel formation. Proc Natl Acad Sci USA 1991;88:3792–6.
[29] Dathe M, Wieprecht T. Structural features of helical antimicrobial peptides: their potential to modulate activity on model membranes and biological cells. Biochim Biophys Acta Biomembr 1999;1462:71–87.
[30] Dessauer HC, Nevo E. Geographic variation of blood and liver proteins in cricket frogs. Biochem Genet 1969;3:171–88.
[31] Doyle J, Brinkworth CS, Wegener KL, Carver JA, Llewellyn LE, Olver IN, et al. nNOS inhibition antimicrobial and anticancer activity of the amphibian skin peptide, citropin 1.1 and synthetic modifications: the solution structure of a modified citropin 1.1. Eur J Biochem 2003;270:1141–53.
[32] Doyle J, Llewellyn LE, Brinkworth CS, Bowie JH, Wegener KL, Rozek T, et al. Amphibian peptides that inhibit neuronal nitric oxide synthase: the isolation of lesueurin from the skin secretion of the Australian Stony Creek Frog *Litoria lesueuri*. Eur J Biochem 2002;269:100–9.
[33] Epand RM, Shai YC, Segrest JP, Anantharamaiah GM. Mechanisms for the modulation of membrane bilayer properties by amphipathic helical peptides. Biopolymers 1995;37:319–38.
[34] Erspamer V. Bioactive secretions of the amphibian integument. In: Heatwole H, editor. Amphibian biology: the integument. vol. 1. Norton, NSW: Surrey, Beatty and Sons; 1994. p. 178–350.
[35] Erspamer V, Erspamer GF, Mazzanti G, Endean R. Active peptides in the skins of one hundred amphibian species from Australia and Papua New Guinea. Comp Biochem Physiol 1984;77C:99–108.
[36] Erspamer V, Melchiorri P, Erspamer GF, Montecucchi PC, de Castiglione R. Phyllomedusa skin: a huge factory and store-house of a variety of active peptides. Peptides 1985;6:7–12.
[37] Evans JNS. Biomolecular NMR spectroscopy. Oxford: Oxford University Press; 1995. p. 55–77.
[38] Ganz T. Biosynthesis of defensins and other antimicrobial peptides. In: Marsh J, Goode J, editors. Antimicrobial peptides. Ciba Foundation Symposium 186. London: John Wiley and Sons; 1994.
[39] Gozzini L, Montecucchi PC, Erspamer V, Melchiorri P. Tryptophyllins from extracts of *Phyllomedusa rhodei* skin: new tetra-, penta- and heptapeptides. Int J Peptide Protein Res 1985; 25:323–9.
[40] Guttman SI. Biochemical techniques and problems in anuran evolution. In: JL, V, editors. Evolutionary biology of the anurans. Contemporary research on major problems. Columbia: University of Missouri Press; 1973. p. 183–203.
[41] Hensmann M, Booker GW, Panayotou G, Boyd J, Linacre J, Waterfield M, et al. Phosphopeptide binding to the N-terminal SH2 domain of the p85-alpha subunit of PI 3′-kinase: a heteronuclear NMR study. Protein Sci 1994;3:1020–30.
[42] Ingram G, Corben C. *Litoria electrica*: a new tree frog from western Queensland. Mem Qld Mus 1993;28:475–8.
[43] Kikuyama S, Toyoda F, Ohmiya Y, Matsuda K, Tanaka S, Hayashi H. Sodefrin: a female-attracting peptide pheromone in newt cloacal glands. Science 1995;267:1643–5.
[44] Klee CB, Vanaman TC. Calmodulin. Adv Protein Chem 1982;35:213–321.
[45] Lazarus LH, Attila M. The toad, ugly and venomous, wears yet a precious jewel in his skin. Prog Neurobiol 1993;41:473–507.
[46] Lincoln J, Hoyle CHV, Burnstock G. Nitric oxide in health and disease. Cambridge: Cambridge University Press; 1997
[47] Low BS. Evidence from parotoid—gland secretions. In: Blair WF, editor. Evolution in the genus Bufo. Austin: University of Texas Press; 1972. p. 244–64.
[48] Low BS. Unpublished observations.
[49] Marcotte I, Wegener KL, Lam Y, Chia BCS, de Planque MRR, Bowie JH, et al. Interaction of antimicrobial peptides from Australian amphibians with lipid membranes. Chem Phys Lipids 2003;122:107–20.
[50] Maselli V, Musgrave I, Bowie JH, Tyler MJ. Unpublished observations.
[51] Maselli V, Pukala TL, Bowie JH, Tyler MJ. Unpublished observations.
[52] Matsuzaki K, Sugishita K, Fujii N, Miyajima K. Molecular basis for membrane selectivity of an antimicrobial peptide, magainin 2. Biochemistry 1995;34:3423–9.
[53] McDonnell PA, Opella SJ. Effect of detergent concentration on multidimensional solution NMR spectra of membrane proteins in micelles. J Magn Res B 1993;102:120–5.
[54] Montecucchi PC, Gozzini L, Erspamer V, Melchiorri P. The primary structure of tryptophan containing peptides from skin extracts of *Phyllomedusa rhodei* (tryptophyllins). Int J Peptide Protein Res 1984;24:276–85.
[55] Mutschmann F, Berger L, Zwart P, Gaedicke C. Chytridiomycosis in amphibians—first report in Europe http://www.ncbi.nlm.nih.gov/entrez/query.fcgi?cmd=Retrieve&db=PubMed&list_11084755&dopt=Abstract.
[56] Myers CW, Daly JW, Garroffo HM, Wisnieski A, Cover JFJ. Discovery of the Costa Rican poison frog *Dendrobates granuliferus* in sympatry with *Dendrobates pumilio*, and comments on taxonomic use of skin alkaloids. Am Mus Novit 1995;3144:1–21.

[57] Nakaoka Y, Tanaka H, Oosawa F. Ca^{2+}-dependent regulation of beat frequency of cilia in *Paramecium*. J Cell Sci 1984;65:223–31.
[58] Nelson JW, Kallenbach NR. Stabilization of the ribonuclease S-peptide a-helix by trifluoroethanol. Proteins Struct Funct Genet 1986;1:211–7.
[59] Pukala TL, Brinkworth CS, Carver JA, Bowie JH. Investigating the importance of the flexible hinge in caerin 1.1: the solution structures and activity of two synthetically modified caerin peptides. Biochemistry 2004;43:937–44.
[60] Raftery MJ, Bradford AM, Bowie JH, Wallace JC, Tyler MJ. Peptides from Australian frogs—the structures of the dynastins from the Banjo frogs *Limnodynastes interioris*, *Limnodynastes dumerilii* and *Limnodynastes terraereginae*. Aust J Chem 1993;46:833–42.
[61] Rajan R, Balaram P. A model for the interaction of trifluoroethanol with peptides and proteins. Int J Peptide Protein Res 1996;48:328–36.
[62] Rang HP, Dale MM, Ritter JM. Nitric oxide, editors. In: Pharmacology. Edinburgh: Churchill Livingstone; 1999. p. 188–97.
[63] Renda T, D'Este L, Buffa R, Usellini L, Capella C, Vaccaro R, et al. Tryptophyllin-like immunoreactivity in rat adenohypophysis. Peptides 1985;6:197–202.
[64] Resnick NM, Maloy WL, Guy HR, Zasloff M. A novel endopeptidase from *Xenopus* that recognizes a-helical secondary structure. Cell 1991;66:541–54.
[65] Rollins-Smith LA, Bowie JH, Tyler MJ. Unpublished observations.
[66] Rollins-Smith LA, Carey C, Conlon JM, Reinert LK, Doersam JK, Bergman T, et al. Antimicrobial activity of Temporin family peptides against the Chytrid fungus (*Batrachochytrium dendrobatidis*) associated with global amphibian declines. Agent Chemother 2003;47:1157–60.
[67] Rollman SM, Houck LD, Feldhoff RC. Proteinaceous pheromone affecting female receptivity in a terrestrial salamander. Science 1999;285:1907–9.
[68] Rozek T, Bowie JH, Wallace JC, Tyler MJ. The antibiotic and anticancer active aurein peptides from the Australian Bell Frogs *Litoria aurea* and *Litoria raniformis*. Part 2. Sequence determination using electrospray mass spectrometry. Rapid Commun Mass Spectrom 2000;14:2002–11.
[69] Rozek T, Waugh RJ, Steinborner ST, Bowie JH, Tyler MJ, Wallace JC. The maculatin peptides from the skin glands of the tree frog *Litoria genimaculata*—a comparison of the structures and antibacterial activities of maculatin 1.1 and caerin 1.1. J Peptide Sci 1998;4:111–5.
[70] Rozek T, Wegener KL, Bowie JH, Olver IN, Carver JA, Wallace JC, et al. The antibiotic and anticancer active aurein peptides from the Australian Bell Frogs *Litoria aurea* and *Litoria raniformis*. The solution structure of aurein 1.2. Eur J Biochem 2000;267:5330–41.
[71] Sai KP, Jagannadham MV, Vairaman M, Rajii NP, Devi AS, Nagaraj R. Tigerinins: novel antimicrobial peptides from the Indian frog *Rana tigerina*. J Biol Chem 2001;276:2701–7.
[72] Sansom MSP. The biophysics of peptide models of ion channels. Prog Biophys Mol Biol 1991;55:139–235.
[73] Shai Y. Mechanism of the binding, insertion and destabilization of phospholipid bilayer membranes by a-helical antimicrobial and cell non-selective membrane-lytic peptides. Biochim Biophys Acta 1999;1462:55–70.
[74] Shai Y, Oren Z. From "carpet" mechanism to de-novo designed diastereomeric cell-selective antimicrobial peptides. Peptides 2001;22:1629–41.
[75] Simmaco M, Mignogna G, Barra D. Antimicrobial peptides from amphibian skin: what do they tell us? Biopolymers 1998;47:435–50.
[76] Smith TG, Kim B, Hong H, Desser SS. Intraerythrocytic development of species of Hepatazoon infecting Ranid frogs: evidence for convergence of life cycle characteristics among Apicomplexans. J Parasitol 2000;86:451–8.
[77] Speare R, Berger L. Chytridiomycosis in amphibians in Australia http://www.jcu.edu.au/school/phtm/PHTM/frogs/chyspec.htm
[78] Steinborner ST, Bowie JH, Tyler MJ. Unpublished observations.
[79] Steinborner ST, Bowie JH, Tyler MJ, Wallace JC. An unusual combination of peptides from the skin glands of Ewings tree frog, *Litoria ewingi*—sequence determination and antimicrobial activity. Aust J Chem 1997;50:889–94.
[80] Steinborner ST, Currie GJ, Bowie JH, Wallace JC, Tyler MJ. New antibiotic caerin 1 peptides from the skin secretion of the Australian tree frog *Litoria chloris*—comparison of the activities of the caerin 1 peptides from the genus *Litoria*. Int J Peptide Protein Res 1998;51:121–6.
[81] Steinborner ST, Gao CW, Raftery MJ, Waugh RJ, Blumenthal T, Bowie JH, et al. The structures of four tryptophyllin and three rubellidin peptides from the Australian red tree frog *Litoria rubella*. Aust J Chem 1994;47:2099–108.
[82] Steinborner ST, Wabnitz PA, Bowie JH, Tyler MJ. The application of mass spectrometry to the study of evolutionary trends in amphibians. Rapid Commun Mass Spectrom 1996;10:92–5.
[83] Steinborner ST, Wabnitz PA, Waugh RJ, Bowie JH, Gao CW, Tyler MJ, et al. The structures of new peptides from the Australian Red Tree Frog *Litoria rubella*—the skin peptide profile as a probe for the study of evolutionary trends of amphibians. Aust J Chem 1996;49:955–63.
[84] Steinborner ST, Waugh RJ, Bowie JH, Wallace JC, Tyler MJ, Ramsay SL. New caerin antibacterial peptides from the skin glands of the Australian tree frog *Litoria xanthomera*. J Peptide Sci 1997;3:181–5.
[85] Steinborner ST, Waugh RJ, Bowie JH, Wallace JC, Tyler MJ, Ramsey SL. New caerin antibiotic peptides from the skin glands of the Australian tree frog *Litoria xanthomera*. Sequence determination by mass spectrometry. Rapid Commun Mass Spectrom 1997;11:997–1101.
[86] Stone DJM, Bowie JH, Tyler MJ, Wallace JC. The structure of caerin 1.1, a novel antibiotic peptide from Australian tree frogs. J Chem Soc Chem Commun 1992;72:1224–5.
[87] Stone DJM, Waugh RJ, Bowie JH, Wallace JC, Tyler MJ. Peptides from Australian frogs. The structures of the caerins from *Litoria caerulea*. J. Chem. Res. (S) 1993;138–9; (M) 1993;910–36.
[88] Stone DJM, Waugh RJ, Bowie JH, Wallace JC, Tyler MJ. Peptides from Australian frogs. Structures of the caerins and caeridin 1 from *Litoria splendida*. J. Chem. Soc. Perkin Trans. I 1992;3173–78.
[89] Stone DJM, Waugh RJ, Bowie JH, Wallace JC, Tyler MJ. Peptides from Australian frogs. The structures of the caerins from *Litoria caerulea*. J Chem Res (S) (M) 1993;138:910–36.
[90] Stuehr DJ, Ghosh S. Enzymology of nitric oxide synthases. In: Mayer B, editor. Nitric oxide. Handbook of experimental pharmacology. Berlin: Springer-Verlag; 2000:33–70.
[91] Sutcliffe MJ. Structure determination from NMR data II. Computational approaches. In: Roberts GCK, editor. NMR of macromolecules: a practical approach. New York: Oxford University Press; 1993:359–90.
[92] Tilley L, Maselli V, Bowie JH. Unpublished observations.
[93] Tossi A, Tarantino C, Romeo D. Design of synthetic antimicrobial peptides based on sequence analogy and amphipathicity. Eur J Biochem 1997;250:549–58.
[94] Tyler MJ, Davies M, Martin AA. A new species of large, green tree frog from Northern Western Australia. Trans R Soc S Aust 1977;101:133–8.
[95] Tyler MJ, Stone DJM, Bowie JH. A novel method for the release and collection of dermal, glandular secretions from the skin of frogs. J Pharm Toxicol Methods 1992;28:199–200.
[96] Vanhoye D, Brustion F, Nicolas P, Amiche M. Antimicrobial peptides from hylid and ranid frogs originated from a 150-million-year-old ancestral precursor with a conserved signal peptide but hypermutable antimicrobial domain. Eur J Biochem 2003;270:2068–81.
[97] Wabnitz PA. PhD thesis. Department of Chemistry, University of Adelaide, Adelaide; 1999.

[98] Wabnitz PA, Bowie JH, Tyler MJ. Caerulein-like peptides from the skin glands of the Australian Blue Mountains Tree Frog *Litoria citropa*. Part 1. Sequence determination using electrospray mass spectrometry. R Commun Mass Spectrom 1999;13:2498–502.

[99] Wabnitz PA, Bowie JH, Tyler MJ, Wallace JC, Smith BP. Differences in the skin peptides of the male and female Australian tree frog *Litoria splendida*—the discovery of the aquatic male sex pheromone splendipherin, together with Phe8 caerulein and a new antibiotic peptide caerin 1.10. Eur J Biochem 2000;267:269–75.

[100] Wabnitz PA, Bowie JH, Wallace JC, Tyler MJ. The citropin peptides from the skin glands of the Australian Blue Mountains Tree Frog *Litoria citropa*. Part 2: sequence determination using electrospray mass spectrometry. Rapid Commun Mass Spectrom 1999;13:1724–32.

[101] Wabnitz PA, Bowie JH, Wallace JC, Tyler MJ. Peptides from the skin glands of the Australian Buzzing Tree Frog *Litoria electrica*. Comparison with the skin peptides of the Red Tree Frog *Litoria rubella*. Aust J Chem 1999;52:639–45.

[102] Wabnitz PA, Bowie JH, Tyler MJ, Wallace JC, Smith BP. Differences in the skin peptides in male and female Australian tree frog *Litoria splendida*. Eur J Biochem 2000;267:269–75.

[103] Wabnitz PA, Walters H, Tyler MJ, Wallace JC, Bowie JH. First record of host defence peptides in tadpoles. The magnificent tree frog *Litoria splendida*. J Peptide Res 1998;52:477–81.

[104] Waugh RJ, Raftery MJ, Bowie JH, Wallace JC, Tyler MJ. The structures of the frenatin peptides from the skin secretions of the giant tree frog *Litoria infrafrenata*. J Peptide Sci 1996;2:117–24.

[105] Waugh RJ, Stone DJM, Bowie JH, Wallace JC, Tyler MJ. Peptides from Australian frogs. The structures of the caerins and caeridins from *Litoria gilleni*. J Chem Res (S) (M) 1993;139:937–61.

[106] Wegener KL, Brinkworth CS, Bowie JH, Wallace JC, Tyler MJ. Bioactive dahlein peptides from the skin secretions of the Australian aquatic frog *Litoria dahlii*: sequence determination by electrospray mass spectrometry. Rapid Commun Mass Spectrom 2001;15:1726–34.

[107] Wegener KL, Wabnitz PA, Carver JA, Bowie JH, Chia BCS, Wallace JC, et al. Host defence peptides from the skin glands of the Australian Blue Mountains Tree Frog *Litoria citropa*. Solution structure of the antibacterial peptide citropin 1.1. Eur J Biochem 1999;265:627–37.

[108] Wieprecht T, Dathe M, Schumann M, Krause E, Beyermann M, Bienert M. Conformational and functional study of magainin 2 in model membrane environments using the new approach of systematic double-D-amino acid replacement. Biochemistry 1996;35:10844–53.

[109] Wong H, Bowie JH, Carver JA. The solution structure and activity of caerin 1.1, an antimicrobial peptide from the Australian green tree frog, *Litoria splendida*. Eur J Biochem 1997;247:545–57.

[110] Xu RX, Word JM, Davis DG, Rink MJ, Willard DH, Gampe RT. Solution structure of the human pp60c-src SH2 domain complexed with a phosphorylated tyrosine pentapeptide. Biochemistry 1995;34:2107–21.

[111] Yamamoto K, Kawai Y, Hayashi T, Ohe Y, Hayashi H, Toyoda F, et al. Silefrin, a sodefrin-like pheromone in the abdominal gland of the sword-tailed newt, *Cynops ensicauda*. FEBS Lett 2000;472:267–70.

[112] Zadina JE, Hackler L, Ge L, Kastin AJ. A potent and selective endogenous agonist for the μ-opiate receptor. Nature 1997;386:499–502.